INVESTIGATING *C. ELEGANS* SMALL-MOLECULE SIGNALING PATHWAYS VIA 2D-NMR BASED COMPARATIVE METABOLOMICS

A Dissertation

Presented to the Faculty of the Graduate School

of Cornell University

In Partial Fulfillment of the Requirements for the Degree of

Doctor of Philosophy

By

Parag Mahanti

January 2014

INVESTIGATING *C. ELEGANS* SMALL-MOLECULE SIGNALING PATHWAYS VIA 2D-NMR BASED COMPARATIVE METABOLOMICS

PARAG MAHANTI, Ph.D.

Cornell University 2014

Molecular interactions provide the basis and structure of all life and living systems. Specifically, small molecules are principle mediators of essential processes across phyla, including signal transduction and metabolism, as well as inter-organismal chemical attraction and defense. Therefore, the knowledge of the identity of these molecules and their biosynthetic and degradation pathways is central to understand living systems. In this thesis, a comparative metabolomics approach will be discussed which is heavily based on 2D-NMR Spectroscopy but often requires LC/MS validation. Using this technique, two main small-molecule metabolic pathways have been investigated in the purview of this thesis using the model organism *C. elegans*.

The first one, the steroid biogenesis pathway, plays a central role in *C. elegans* metabolism by dictating its reproductive and developmental future and even its lifespan. Steroidal ligands have been proposed to bind to the Nuclear Hormone Receptor – DAF-12 and here using our approach we identify for the first time, the complete set of DAF-12 ligands in an unbiased and unambigious way. We then continue to investigate the biosynthetic pathway of these ligands and uncover

components of the network that were previously unrecognized, thus fundamentally revising the current viewpoint on this subject for future researchers to explore.

The second pathway, tryptophan degradation pathway, has increasingly become one of the most studied pathways in living organisms. In the context of this thesis we first identify anthranilic acids, metabolites of the tryptophan degradation pathway, as the fluorophore, that results in a striking blue fluorescence moments prior to the worm's death. This result is astounding since until now the origin of this fluorescence was considered to be something entirely different. Our findings reconfirm the importance of tryptophan catabolism across all organisms and provide us with a fantastic opportunity to explore and elucidate the roles of the non-small molecule components of a biosynthetic network, using metabolomics.

BIOGRAPHICAL SKETCH

The author was born in 1984 in Calcutta, India. He completed his schooling from St. Thomas' Boys' School, Kidderpore. In the year of 2003, he joined St. Stephen's College, Delhi affiliated under the Delhi University, to pursue a Bachelor's degree in Chemistry. After graduating with honors in 2006, he joined the University of Delhi, enrolling once again into St. Stephen's College to accomplish a Master's degree in Chemistry with an Organic Chemistry Specialization. In 2008, he came to Cornell University as a graduate student in the field of Chemistry and Chemical biology, and because of his interest in NMR Spectroscopy, started his research career at Prof. Frank Schroeder's research group. During this time he has devoted his efforts towards a better understanding of fundamental processes such as development, reproduction and death, using comparative metabolomics (2D-NMR and LC/MS based) as his analytical tool and the free living nematode, *Caenorhabditis elegans,* as his biological system.

Dedicated to my loving parents, Sukumar Mahanti and Arati Mahanti.

ACKNOWLEDGMENTS

This thesis and my journey from a graduate student to a PhD candidate would not have been possible without the help and support of a large number of people and I will be forever indebted to them for their support.

First and foremost, I would like to thank my advisor Frank Schroeder for his contribution. Without his constant guidance and support, many of the results I discuss today in this thesis would have been just a dream. I am quite proud and happy that I was able to work with someone like him during the early stages of my career irrespective of where my future leads me. I will definitely miss the scintillating discussions both within and outside the purview of Chemistry, Science and sometimes even reason! Thanks Frank!

I would also like to thank my other committee members, Prof. Linda Nicholson and Prof. Hening Lin. While I regret that I never got the opportunity to involve them more in my projects, I have always received fabulous insight from both and I am very thankful for their time, understanding and support.

Working on 5 different projects, that spanned almost 15 laboratories and more than 50 people, I cannot not thank my collaborators. I am extremely lucky that I had the opportunity to work with the likes of Josh Wollam, Cassandra Coburn, Kathlyn Dumas, Joshua Meisel and Ju-ling Liu. I would especially like to mention Josh W and Cassie who have been my primary collaborators and friends. It has been a pleasure answering questions about life and death across seas and continents and I am happy that in the end we succeeded! Also thanks to Prof. Adam Antebi, Prof. David Gems, and Prof. Patrick Hu for some amazing conversations about the steroid and tryptophan pathways.

That brings me to my lab members and anything I say about them is not going

to be enough. The Schroeder Lab is productive not because of our work ethic or extreme hours (!) but because of our camaraderie, something I couldn't have survived without. So, thanks a lot everyone, especially Josh Judkins and Neelanjan for their help with the steroid project, Inish, Ry and Josh B for just being there in the office, and Sarah and Zhihan for providing the best undergraduate support a grad student can want.

Spending five years in Ithaca requires a special kind of dedication and support system and I am extremely glad that I was blessed with an awesome group of friends such as Anandarup, Soumya, Aritro, Rachna, Siddharth and Angie. Ithaca will not be the same without them and thanks for being there all the time. An added vote of thanks to my support system in NYC – Anupam, Shivam, and Ushati. You know this would not be possible without you guys.

But really, none of this would matter if Debashree, my wife wasn't here. Most people don't understand what it is to be married to a PhD student and I think Debashree understood it much more than her share! Just saying thanks cannot ever do justice to you – but I will say it anyway – Thanks a lot DC!

And finally, I would love to thank my brother, Prasun and sister in law, Runali and my parents for their blessings and constant encouragement without which none of this would have ever been possible.

TABLE OF CONTENTS

LIST OF FIGURES

CHAPTER 1

CHAPTER 2

CHAPTER 3

CHAPTER 4

APPENDIX A

APPENDIX C

LIST OF TABLES

CHAPTER 1

PREFACE

This preface provides an introduction to the key concepts used in the subsequent chapters and the reasons behind pursuing these investigations. It also contains a brief description of each of the chapters.

C. elegans as a model organism for chemists to understand small molecule signaling pathways that regulate key biological processes

Molecular interactions provide the basis and structure of all life and living systems. Specifically, small molecules are principle mediators of essential processes across phyla, including signal transduction and metabolism, as well as inter-organismal chemical attraction and defense. Therefore, the identity of these molecules, their biosynthetic and degradation pathways, interaction with other biomolecules (protein, DNA, RNA) and associated networks of biotransformation and function, provides a much needed, deeper understanding of biological processes. In-depth knowledge about these small molecules and the associated networks, however will not alone answer higher level questions about life, behavior and disease. Molecules and networks are not alive, but the cross-talk between these networks and molecules, ultimately leading to a phenotype as a response to a change e.g. in the environment create what we perceive as "life", and we therefore need to understand small molecule metabolism in the context of whole organisms. Since the diversity of living organisms is enormous, it is necessary to focus on investigating a small number of simpler, representative organisms that are chosen for experimental convenience. A detailed and

holistic understanding of these organisms, termed as “model organisms” have provided, and will continue to provide, answers to key questions in biology, and unravel new questions and new directions for scientific research to move forward.

One of the most important model organisms for biomedical research is the roundworm, *Caenorhabditis elegans*, (1) because of its biological tractability and (2) because a large number of physiological pathways show analogies to similar pathways in higher animals, with intriguing implications for human health research*. C elegans* is a small, transparent, free-living nematode, which grows to an adult length of approximately 1.5mm (Riddle et al., 1997). It is found in microbe-rich habitats such as decaying plant matter (Felix and Branendle, 2010)**,** but can be easily grown on a bacterial lawn of *Escheria coli* in Petri dishes. It is highly differentiated yet small enough for high-throughput operations, has a short lifespan, can be easily grown in normal laboratory conditions without specialized training, equipment and stringent requirements of sterility, and experimentation with it is free of ethical concerns. These factors along with the significant additional advantage that *C. elegans* is one of the first organisms whose genomes were sequenced (*C. elegans* Sequencing Consortium, 1998), and can be genetically manipulated easily, provides chemists with a tractable platform for speedy verification of chemical hypothesis in a simple multicellular animal (Hulme and Whitesides, 2011). As a result, *C. elegans* has been extensively used in large-scale genetic screens (Sugimoto et al., 2004; Bazopoulao and Tavernarakis, 2009) and has had considerable impact on the understanding of neurodegenerative diseases (Dimitriadi et al., 2010; Wolozin et al., 2011), metabolic diseases (Hashmi et al., 2013**)** and infectious diseases and immunity (Powell et al., 2008, Marsh et al., 2012**)**. A fairly recent review (Kaletta and Hengartner,

2006) provides information about how important *C. elegans* has become in biomedical research, especially in understanding signaling pathways that regulate development and aging (Chapter 2 and 3) and neurodegeneration, immunity and death (Chapter 4).

Table P.1. *C. elegans* disease models. (adapted from Kaletta and Hengartner, 2006)

Disease	Pathway or genes (C. elegans orthologue)
Metabolic Syndrome	
Diabetes and obesity	Insulin/AKT (daf-2, ins-1, akt-1)
Aging	Caloric restriction; oxidative stress, e.g., Manganese superoxide dismutase (sod-3); Insulin receptor/PI3K (daf-2, age-1)
Oncology	
Cancer	EGF/RAS (let-23, let-60)
	DNA damage e.g., p53 (cep-1), BRCA1 (brc-1)
Neurodegeneration	
Alzheimer's disease	Presenilin (sel-12)
Parkinson's disease	α-Synuclein (no orthologue)
Huntington's disease	Huntington (no orthologue); polyglutamine (polyQ) aggregation
Neurobiology	
Depression	Serotonin
Pain, neuronal regeneration	Regeneration
Genetic Diseases	
ADPKD	PKD1 (lov-1), PKD2 (pkd-2)
Muscular dystrophy	Dystrophin (dys-1), emerin (emr-1)
Ionchannelopathies	Ion Channels
Innate Immunity	Bacillus thuringlensis toxin (Bt toxin)
	Host-pathogen interaction

Specifically, research efforts aimed at understanding aging have focused on one unique feature of nematode development – the dauer diapause. In favorable environments, which constitute optimum temperature (20-22 °C), high food (*E. coli*) availability and low local population density, the worm rapidly develops from an embryo to adult through four larval stages (L1-L4) in 3.5 days. This reproductive development ultimately leads to gravid hermaphrodites which reproduce over a 3-d to 5-d period and live for another 2-3 weeks. However, if exposed to higher temperatures (≥ 24 C), scarcity of food and overcrowded conditions, *C. elegans* will divert development to a specialized, alternative larval stage called the – "dauer diapause" (L3d), which is non-feeding and can persist under adverse conditions for several months (Cassada and Russell, 1975) (**Figure P.1**). This non-feeding dauer stage (from German "dauer" for enduring) is a unique example of developmental plasticity where life history traits are linked with changes in the environment. Genetic screens for mutants that either cannot attain the dauer stage or form dauer larvae constitutively have identified nearly 40 DAF (DAuer Formation) genes that are directly involved in dauer stage control (Riddle and Albert, 1997). Subsequent studies revealed a significant role for genes of the dauer pathway in the general regulation of lifespan, and orthologs of dauer genes in higher organisms appear to be involved in aging as well. (Kenyon et al., 1993; Tatar et al., 2003; Kenyon et al., 2001) Epistasis analysis of *daf* genes revealed a complex signalling network that regulates dauer diapause entry and exit and is connected with conserved pathways including steroid signaling, tryptophan degradation and serotonin signalling, cGMP, TGF-β and Insulin/IGF signalling. Furthermore, *C. elegans* genetic and RNAi screens have implicated a large number of additional genes with lifespan control (Hansen et al., 2005;

Hamilton, et al., 2005) many of which are also involved with fat storage regulation. (Ashrafi et al., 2003).

Despite its significance as a model organism and relevance as a disease model, the number of small-molecule signals and other metabolites that have been discovered from *C. elegans* is surprisingly, very small (Schroeder et. al., 2006). However this is not a reflection of the importance of small molecule mediated signaling in *C. elegans* and other nematodes, because the few *C. elegans* derived compounds identified so far are associated with strong phenotypes and are crucial in many physiological pathways. Therefore, investigation of small molecule signaling and biosynthesis in *C. elegans* provides a unique and untapped opportunity to significantly advance our current understanding of animal biology.

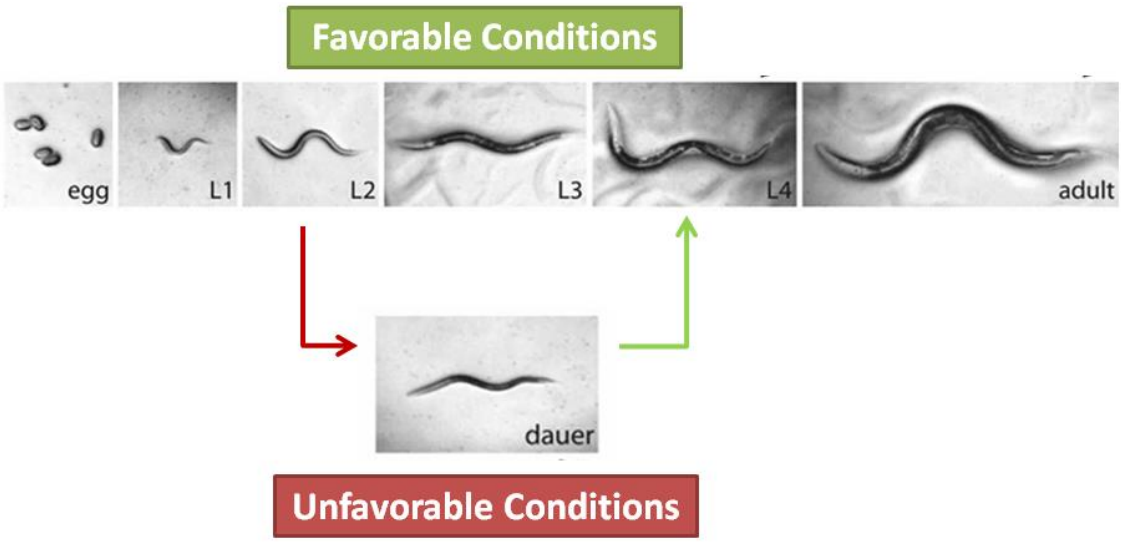

Figure P.1. *C. elegans* life cycle. Figure adapted from Fielenbach and Antebi, 2008.

Small-molecule signaling in the Dauer pathway in C. elegans.

In 1982, it was demonstrated by Riddle and Golden that then unknown small molecules released by *C. elegans* induce entry into and antagonize recovery from the dauer diapause. The subsequent identification of a mutant strain, *daf-22,* deficient of dauer-inducing activity (dauer pheromone) in its metabolite extracts, confirmed that this signal must be nematode-derived (Golden and Riddle, 1985). But it took more than 20 years after this initial discovery to finally reveal the chemical composition of the dauer pheromone. Several laboratories contributed to the discovery of the family of ascarosides (**Figure P.2**), hydrophilic glycosides of the di-deoxy sugar ascarylose, as major constituents of the dauer pheromone (Butcher et al., 2007; Jeong et al., 2005; Pungaliya et al., 2009). It also became clear that the dauer pheromone was not a single compound but a complex mixture of ascarosides in which certain components act synergistically in dauer induction.

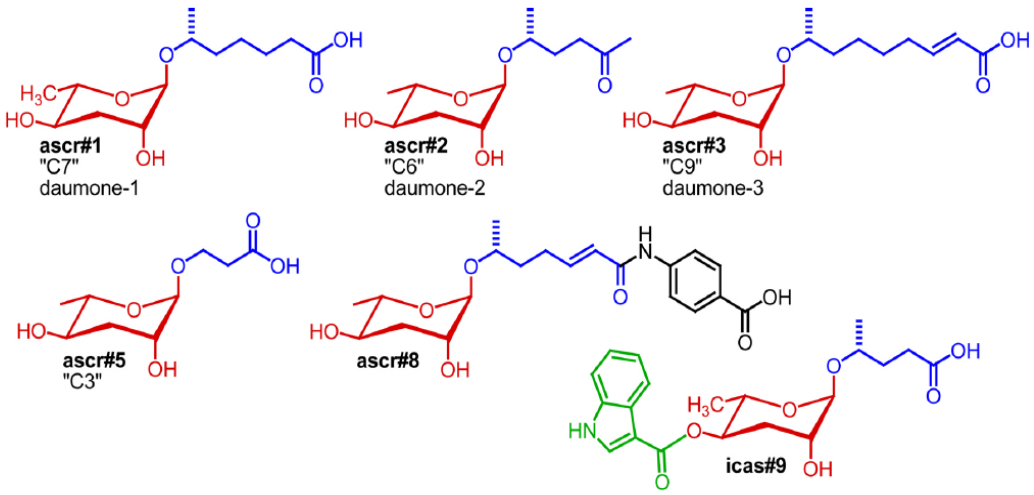

Figure P.2. Ascarosides that have been shown to induce dauer formation. Figure adapted from Ludewig and Schroeder, 2012.

Following their identification as constituents of the dauer pheromone, it was discovered that ascarosides serve additional major signaling functions. Srinivasan et. al found that specific concentrations and combinations of ascarosides can attract *C. elegans* sex-specifically (Srinivasan et al., 2012**)**. Macosko et al. unraveled the neuronal network that regulates hermaphrodite repulsion of ascarosides. More recently research from the Schroeder lab showed that indole ascarosides and p-hydroxybenzoyl ascarosides act as highly potent aggregation signals that attract both males and hermaphrodites (von Reuss et al., 2012), while ascaroside primarily produced by males attract hermaphrodites specifically (Izrayelit et al., 2012). The example of ascarosides is highly encouraging since the identification of chemical structures responsible for dauer induction led to the subsequent identification of more small molecules which in turn catalyzed a much broader understanding of pheromone mediated nematode behavior, providing an unique example of structure- and concentration-dependent differential activity of small molecules. More work is currently going on to understand the interaction of these small-molecules (ascarosides) with other biomolecules (their yet unidentified cognate receptors), and one can only imagine the possibilities of the information that may be obtained from such studies.

But the ascarosides are not the only small molecules that have been discovered to play key roles in the *C. elegans* dauer pathway. Using natural pheromone extracts, it has been shown that the dauer pheromone signal is detected and integrated by specific chemosensory neurons (Bargmann, 2006). When exposed to ascarosides, these neurons either initiate or block the production of secondary messengers such as TGF-β, cGMP, serotonin and insulin-like peptides. Downstream of these conserved neuroendocrine pathways, lies a nuclear hormone receptor, DAF-12 (**Figure P.3**).

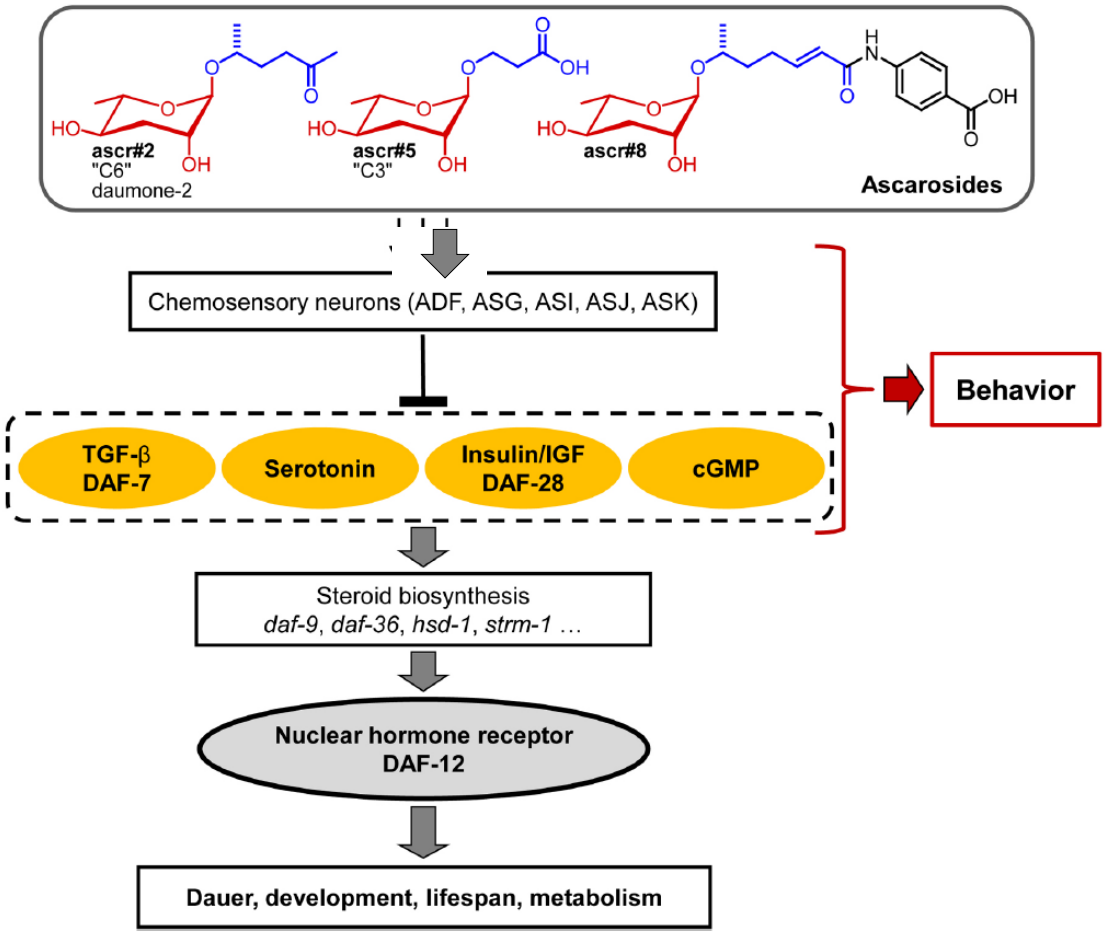

Figure P.3. Signaling network that regulates development, lifespan and metabolism in *C. elegans*. Figure adapted from Ludewig and Schroeder, 2012.

DAF-12, an ortholog of the human Vitamin-D receptor, represents a main switch in the signaling cascade controlling dauer formation and in recent years a large number of labs have reported the possible existence of small molecule hormone(s) in *C. elegans* as endogenous ligands for DAF-12 (Gerisch et al., 2001; Jia et al., 2002, Matyash et al., 2004). These molecules, possibly of steroidal origin, constitute the second major group of small molecule metabolites detected in *C. elegans* regulating fundamental

processes in nematodes, many of which are conserved in higher organisms, and determining the identity of these molecules is therefore a necessity.

The nuclear hormone receptor DAF-12 and steroid signaling in C. elegans

Nuclear Hormone Receptors (NHRs) constitute an ancient and probably the largest superfamily of ligand-dependent transcription factors, i.e. DNA-binding regulatory proteins that fine tune transcriptional pathways, in response to diverse signals e.g. developmental, environmental and nutritional. They are involved in every aspect of development, physiology and disease in humans (Sladek et al., 2010) and are highly ubiquitous in and unique to the animal kingdom. Because they can be pharmacologically manipulated by agonists or antagonists, NHRs represent a key mechanism for disease intervention.

NHRs share considerable amino acid sequence similarity in two, highly conserved domains – the DNA binding domain (DBD) and the ligand binding domain (LBD) (Renaud and Moras, 2000). Following ligand binding, an NHR undergoes a conformational change in which a C terminal activation helix, AF-2, folds back onto the LBD core, locking the NHR in an active confirmation, thus achieving transcriptional activation (Moras et al., 1998; Bledsoe et al., 2002; Cronet et al., 2001). NHRs having no ligand or for which no ligand(s) has been discovered, are termed orphans (Mangelsdorf et al., 1995) and efforts to identify cognate ligands for orphan receptors have contributed significantly to a deeper understanding of their physiological roles and mechanism. However identification of ligands for orphan receptors has often been based on random compound screens or other biased approaches, and in many cases it remains unclear if the reported ligands are true endogenous ligands.

When the *C. elegans* genome was completely sequenced (Consortium, 1998), one of the most surprising features was the enormously large family of 284 genes encoding for NHRs. It appears almost all of these genes produce proteins and are not pseudogenes (Miyabayashi et al., 1999) and therefore the *C. elegans* NHR family is far larger than its human (48 genes), mouse (49 genes), and fly (18 genes) counterparts (Maglich et al., 2001). This massive expansion of NHR genes in *C. elegans* provides an intriguing opportunity for biologists to study evolution and diversification of this family, as well for chemists to investigate the identity and biological roles of ligands of these NHRs. However, only a few *C. elegans* NHRs have known functions (Taubert et al., 2010). Currently mutation or suppression by RNA interference (RNAi) of 50 *C. elegans* NHRs are known to elicit detectable phenotypes (Harris et al., 2009) and only a few of these have been studied in any real depth.

DAF-12 is perhaps the most studied and best understood *C. elegans* NHR. As transcription factors that can both activate and repress, NHRs have the distinct ability to function as ligand-dependent switches that decide between several alternate organismal fates. Accordingly DAF-12 has a key role in the choice between the dauer diapause and reproductive development (Magner et al., 2008). Cellular and molecular genetic analysis studies suggest that environmental and physiological cues detected by sensory neurons in the head are integrated and transduced through guanylyl cyclase and various other signal transduction pathways (Fielenbach and Antebi, 2008; Antebi, 2013). These pathways in turn modulate two major conserved endocrine pathways, TGF-β and insulin/IGF signaling (IIS). In favorable environments, TGF-β and insulin/IGF peptide hormones are secreted from sensory neurons, and subsequently act on steroidogenic tissues to promote production of the DAF-12 ligands that were shown to be likely cholesterol-derived (Li, Kennedy

and Ruvkun, 2003; Ren et al., 1996). Binding of these steroidal ligands to DAF-12 is presumed to trigger recruitment of coactivator peptides, resulting normal developmental progression to adulthood. Conversely, in unfavorable environments, TGF-β and insulin/IGF peptides are downregulated, which results in repression of ligand biosynthesis. Unliganded DAF-12 then forms a complex with the DIN-1/SHARP corepressor and thereby specifies the long-lived dauer stage (Ludewig et al., 2004). Thus, DAF-12 and associated co-regulator complexes act as small-molecule hormone regulated molecular switches that specify two distinct life history modes, reproductive development and dauer diapause (**Figure P.4**). DAF-12 has also been implicated in regulation of fat metabolism, developmental timing and adult longevity (Fielenbach and Antebi, 2008) and together these reasons underline the importance of ascertaining the identity of the DAF-12 ligands.

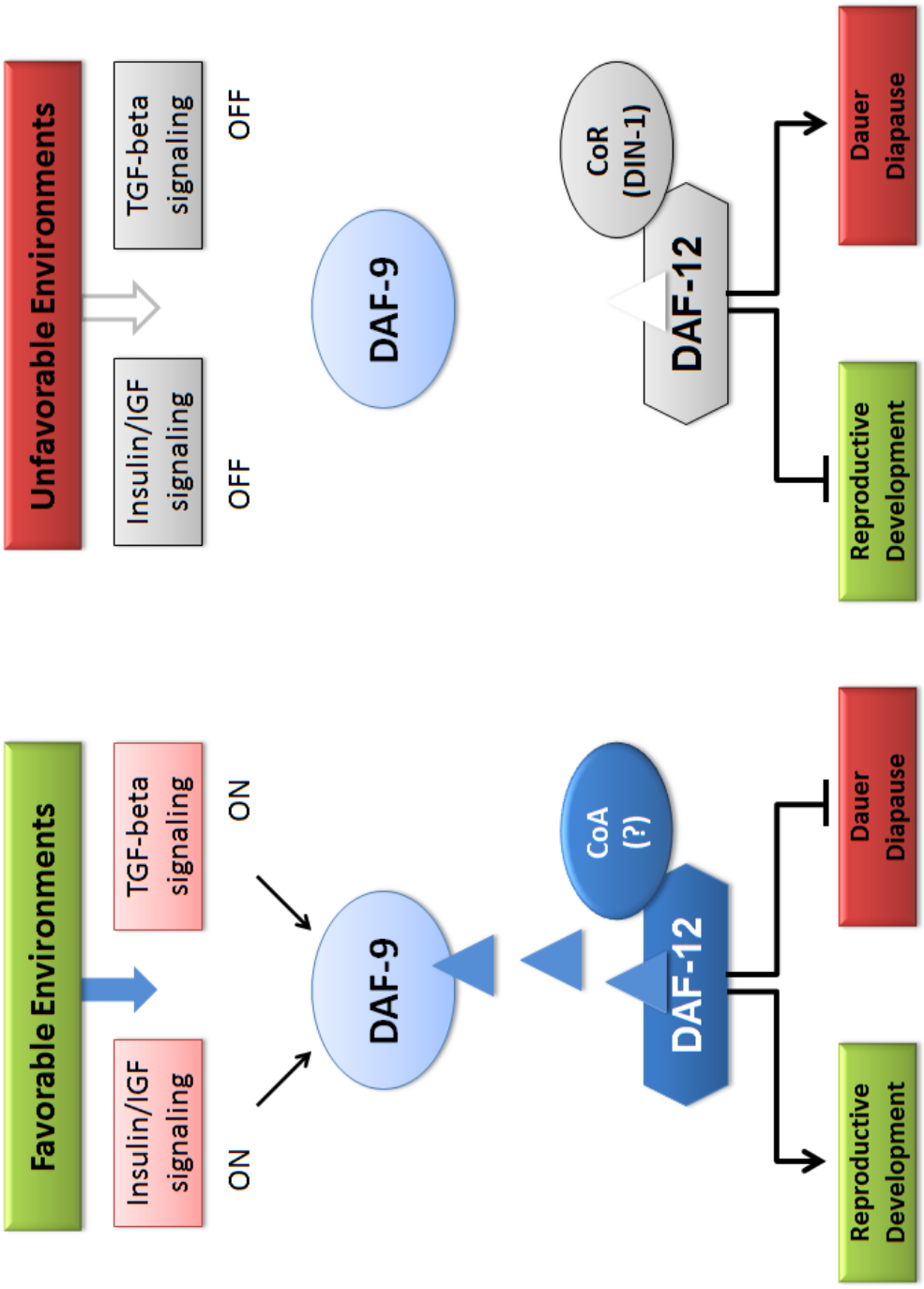

Figure P.4. Life history regulation by DAF-12. In favorable environments, uninhibited ligand production leads to liganded DAF-12 assembling with its putative coactivators to direct expression of genes involved in reproductive development. Under unfavorable conditions, unliganded DAF-12 together with its corepressor DIN-1 specify programs for dauer diapause.

That the DAF-12 ligands may be derived from cholesterol is suggested by multiple lines of evidence. *C. elegans*, being a cholesterol auxotroph, lacks the ability to synthesize cholesterol (Chitwood et al., 1999) and cholesterol deprivation produces Dauer constitutive (Daf-c) phenotypes (Gerisch et al., 2001, Jia et al., 2002, Matyash et al., 2004). Next, worms missing both homologs of the human Niemann-Pick type C1 gene, a glycoprotein involved in cholesterol transport, arrest constitutively as dauers (Li et al., 2004). Additionally weak alleles of *daf-9* mutant worms that are considered to be compromised in their ability to produce the DAF-12 ligand often show an enhanced dauer phenotype under cholesterol deprivation conditions (Gerisch et al., 2001; Jia et al., 2002). Furthermore, lipid extracts from wild-type worms can rescue *daf-9* phenotypes (Gill et al., 2004). Based on a large body of evidence implicating cholesterol derivatives, in 2006, Motola et al., reported the identification of two cholestenoic acids as endogenous ligands of DAF-12 (**Figure P.5**).

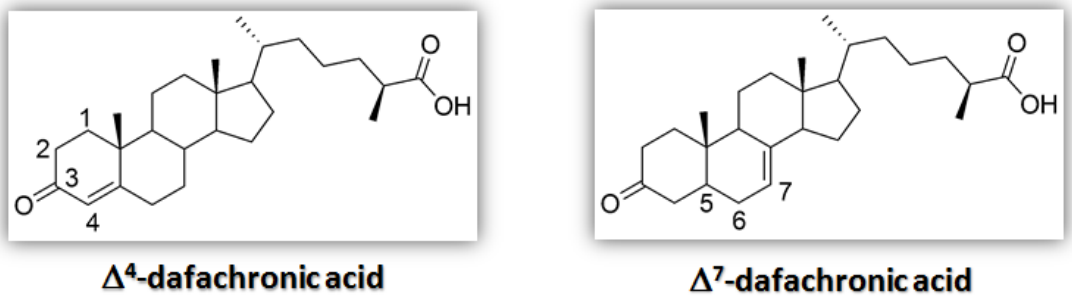

Δ^4-dafachronic acid Δ^7-dafachronic acid

Figure P.5. Putative ligands of DAF-12. Cholestenoic acid structures that were implicated as DAF-12 ligands by Motola et al. (2006) using genetic and biochemical techniques.

In order to identify the DAF-12 ligands, traditional natural products chemists might have resorted activity guided fractionation of the lipophilic worm extract with the objective of isolation of the active components in pure

form for complete spectroscopic structure determination (Schroeder, 2006). However Motola et al. pursued a different method originally based on screening a variety of commercially available steroids for DAF-12 binding using a cell-culture based transcriptional activation assay. The identified “hit” from this screen provided the clue that 3-keto functionality is essential for DAF-12 binding. Subsequently, utilizing DAF-9’s role as the last step of the ligand-biosynthetic pathway, two 3-keto steroids and known cholesterol metabolites known to be present in *C. elegans*, 4-cholesten-3-one and lathosterone, were hypothesized to be ligand precursors. Indeed, when incubated with DAF-9, the resultant product from both these precursors rescued *daf-9(-)* mutants. Based on these results and additional candidate screens, it was concluded that DAF-9, a CYP27A1 homolog, oxidizes cholesterol metabolites at the C-26/C-27 side chain, introducing a carboxylic acid moiety that was shown to be important for DAF-12 binding. While, the resultant molecules, termed dafachronic acids (DAs) (**Figure P.5**) are potently active at nM concentrations, Motola et al. and subsequent publications did not conclusively identify these compounds in *C. elegans* metabolite extracts, mainly because of the extremely low abundance of these molecules within the worms. Therefore, it ultimately remained unclear whether Δ^4- and Δ^7-dafachronic acid in fact represent the endogenous ligands of DAF-12. Apart from this oversight, this work is seminal especially since it is the first publication to report the de-orphanization of a *C. elegans* NHR and also provides evidence for the enzymatic activity of the cytochrome P-450, DAF-9.

Following the identification of DAF-9/CYP450 as a key steroid metabolizing enzyme and the description of putative structures of the endogenous DAF-12 ligands (Motola et al., 2006), a large number of publications have arisen in the last few years, speculating the biosynthetic

pathway of these cholesterol derived ligands. Dafachronic acids, due to their side chain carboxylation, structural modification in the C-7 position and the presence of an oxo-group at the 3-positions, are reminiscent of bile acids. Bile acids, like DAs, have been recently implicated in mammalian lifespan regulation, (Gems and Partridge, 2008; Amador-Noguez D et al., 2007).

Without comprehensive knowledge of the true structures of the endogenous ligands, any putative biosynthetic pathway will always be vulnerable to massive changes. Currently, many of the identified components (enzymes) of the DAF-12 ligand biosynthetic pathway are indeed homologous to proteins that are involved in the bile acid biosynthetic pathway of higher organisms (Wollam et al., 2011; Wollam et al., 2012; Yoshiyama-Yanagawa et al., 2011; Motola et al., 2006) and have therefore often drawn comparisons between the DAF-12 ligand biosynthetic pathway in *C. elegans* and bile acid biosynthetic pathways in higher organisms. However, several separate new publications have reported the ambiguity about the exact role of HSD-1 and its putative function towards the biosynthesis of Δ^4-DA (Dumas, 2010; Wollam, 2012) and the need for further detailed investigation for the complete characterization of this and other enzymes in terms of their sterol profile and role in the DAF-12-ligand biosynthesis, is evident.

Due to its central role in *C. elegans* development, metabolism and lifespan, unambiguous clarification of the identity of DAF-12 ligands is of central importance to the field, along with a detailed characterization of the associated biosynthetic machinery. But this will still leave us, the scientific community, with 283 other NHRs that are orphan. Consequently, a systematic, analytical approach needs to be developed for unambiguous identification of endogenous ligands for other orphan nuclear receptors in *C. elegans* and other higher organisms.

AHR-1 and the tryptophan degradation pathway in C. elegans

While there are 284 NHRs in *C. elegans*, of which only fifteen have clear homologs in other species, there are still other types of small-molecule-ligand mediated transcription factors that are conserved between *C. elegans* and higher animals. One such example is the Aryl Hydrocarbon Receptor (AhR) which belongs to the basic helix-loop-helix (bHLH)/PAS (Per/Arnt/Sim) family of transcription factors (Lindsey et al., 2012). Although structurally dissimilar from NHRs, AhR is well known for mediating transcriptional regulatory effects originating from environmental toxins. In fact, it was originally identified (Poland et al., 1976) in a study of dioxin toxicity as an intracellular receptor in mammalian cells that binds 2,3,7,8-tetrachlorodibenzo-*p*-dioxin (TCDD). More recently, dioxins and related compounds, including their interaction with the AhR, have been implicated in cancer, hepatotoxicity, birth defects, and immunological deficiencies in a variety of vertebrates, and all of these pathologies are due to defects in AhR activation (Schmidt and Bradfield, 1996; Whitlock et al., 1999). The mechanism of AhR action is similar to that described for other ligand-activated receptors and was determined by studies on AhR-mediated CYP1A1 gene expression (Ko et al., 1996). When not bound to a ligand, AhR is cytosolic and associated with heat shock proteins and prostaglandin E synthase 3, which together protects the receptor from proteolysis and prepares it for ligand binding (Kazlauskas et al., 2001). Upon ligand binding, the AhR translocates into the nucleus and forms a heterodimer with its partner, AhR nuclear translocator (ARNT). This complex then binds to specific response elements in target gene promoters to induce transcriptional activation in response to binding of specific ligands (Guyot et al., 2013). The appreciation that the AhR is important for development and the

finding that it can elicit different responses when bound to a diverse variety of ligands, has refueled interest in the search for bonafide “endogenous” ligands for AhR (Ngyuen et al., 2008). Therefore, chemical identification of the endogenous small-molecule modulators of this receptor will make a major contribution towards understanding development as well as immune and xenobiotic responses in higher organisms and will provide insights into the therapeutic potential that may arise from modulating this system.

While a large body of literature exists regarding the binding ability of exogenous molecules to AhR, search for endogenous activators of AhR has only just begun (Nguyen et al., 2008; Guyot et al., 2013). Heart and lung extracts (Chiaro et al., 2007) have been shown to contain AhR activators and several molecules such as arachidonic acid, leukotrienes, heme molecules, and UV photoproducts of tryptophan have been described as putative endogenous ligands (Nguyen et al., 2008). Among the most important studies, a tryptophan derivative, 6-formylindolo[3,2-b]carbazole (FICZ), with a high affinity for the AhR has been identified as an activator of CYP1A1 transcription. Another tryptophan metabolite, kynurenine, has been reported to bind the AhR and was implicated in the development of brain tumors (Optiz et al., 2011). More recently, indole 3-aldehyde was reported as an endogenous AhR ligand, regulating gut microbial immunity (Zelante et al., 2013).

However, no information is available about the endogenous ligands of AhRs for invertebrates. Specifically in *C. elegans,* where AhR has been shown to regulate neuronal development (Qin et al., 2004), it has been reported that TCDD does not bind to the AhR homolog, AHR-1. If AHR-1 does have an endogenous, small-molecule activator, its spectrum of ligands is potentially different from that of the mammalian receptor. From the point of view of chemists interested in small-molecule mediation of animal biology,

identification of AHR-1 ligands therefore provides an interesting challenge because of a) the diversity of ligand structures in mammals and b) the differences in functional outputs to AHR activation currently discovered in *C. elegans*. To address the first, a closer look at the structures of the putative mammalian ligands allows us to hypothesize that a deeper understanding of the tryptophan metabolites and their involvement in pathways that may be regulated by AhR is necessary.

Tryptophan, the rarest essential amino acid, exists as L-tryptophan in all proteins (Rongvaux et al., 2003) but has been shown to exist as D-tryptophan in certain secreted peptides (Gadupudi et al., 2011). There are three main pathways that catabolize L-tryptophan: the serotonin, indole and kynurenine pathways. These catabolic pathways are extremely important for the generation of multiple significant metabolites including the ubiquitous enzyme co-factor Nicotine Adenine dinucleotide (NAD), the neurotransmitter serotonin and the vitamin niacin (Stone et al., 2012)**.** In mammals, the kynurenine pathway catabolizes ~90% of L-tryptophan, and is controlled by two rate-limiting enzymes, tryptophan dioxygenase (TDO) and indoleamine-2,3 dioxygenase (IDO) (Gadupudi et al., 2011). Both IDO and TDO catalyze the same reactions, but TDO is highly substrate specific for L-tryptophan whereas IDO can also catalyze the D-isomer as well.

Since the discovery of NAD as a product of the kynurenine pathway many years ago, little attention has been paid to the biological functions of kynurenine pathway intermediates including kynurenine itself, one of the putative ligands of mammalian AhR. Only recently, several investigations have shown that kynurenine and its derivatives are both biologically active and significant, and may play important roles in multiple ageing and age-related diseases (**Figure P.6**) (van der Goot and Nollen, 2013).

Figure P.6. Tryptophan metabolism in health and disease. Tryptophan metabolism regulation is cell-type dependant and controlled both locally or systemically. Tryptophan metabolism plays a role in neuronal activity, immune regulation and behavior. (Figure adapted from van der Woot and Nollen, 2013)

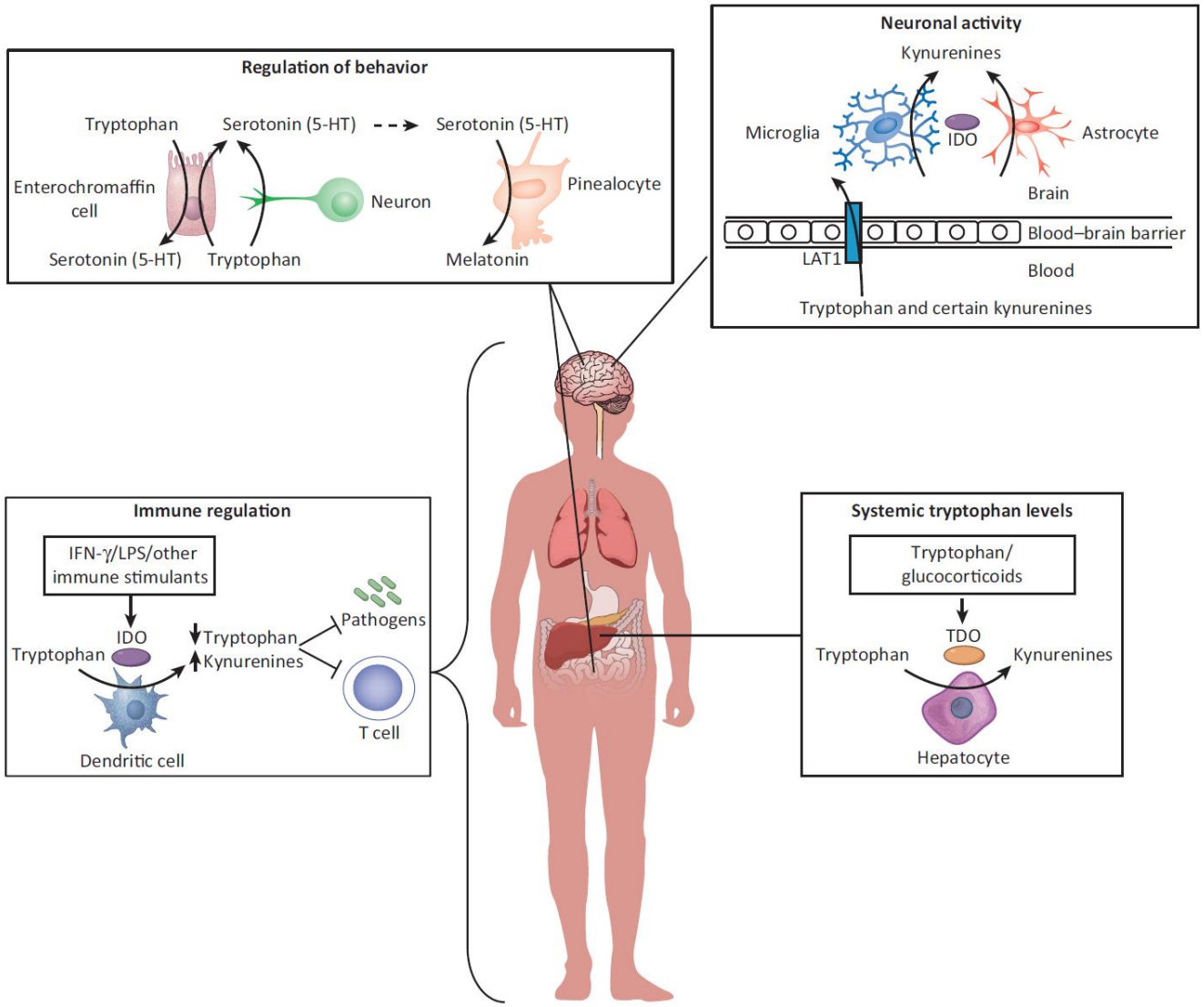
Regulation of behavior
Tryptophan
Serotonin (5-HT)
Serotonin (5-HT)
Enterochromaffin cell
Neuron
Pinealocyte
Serotonin (5-HT)
Tryptophan
Melatonin
Neuronal activity
Kynurenines
Microglia
IDO
Astrocyte
Brain
Blood–brain barrier
LAT1
Blood
Tryptophan and certain kynurenines
Immune regulation
IFN-γ/LPS/other immune stimulants
IDO
Tryptophan
Tryptophan
Kynurenines
Pathogens
T cell
Dendritic cell
Systemic tryptophan levels
Tryptophan/ glucocorticoids
TDO
Tryptophan
Kynurenines
Hepatocyte

While more recent work in model organisms has begun to examine the role of kynurenines in animal biology, very little work has been carried out in *C. elegans* on the kynurenine pathway. In 1970s a class of mutants was discovered, known as Flu mutants, due to their altered auto-fluorescent properties. The mutations have not been cloned and only provisionally mapped to different linkage groups, but enough information has been reported to unravel the functions of at least two of these genes, *flu-1* and *flu-2*, hypothesized to encode for the kynurenine-3-hydroxylase and kynureninase respectively (Nollen, 2012; Babu and Siddiqui, 1973) **(Figure P.7)**. The kynurenine pathway and the flu mutants therefore provide an excellent opportunity to utilize metabolomics approaches to understand how genetic changes can effect changes in the metabolome. Investigating the tryptophan pathway in *C. elegans* will not only provide a new opportunity to discover novel components of the tryptophan degradation pathway but this process will set the stage for a comprehensive screen for the presence of Ahr-1 ligand(s) within the *C. elegans* metabolome.

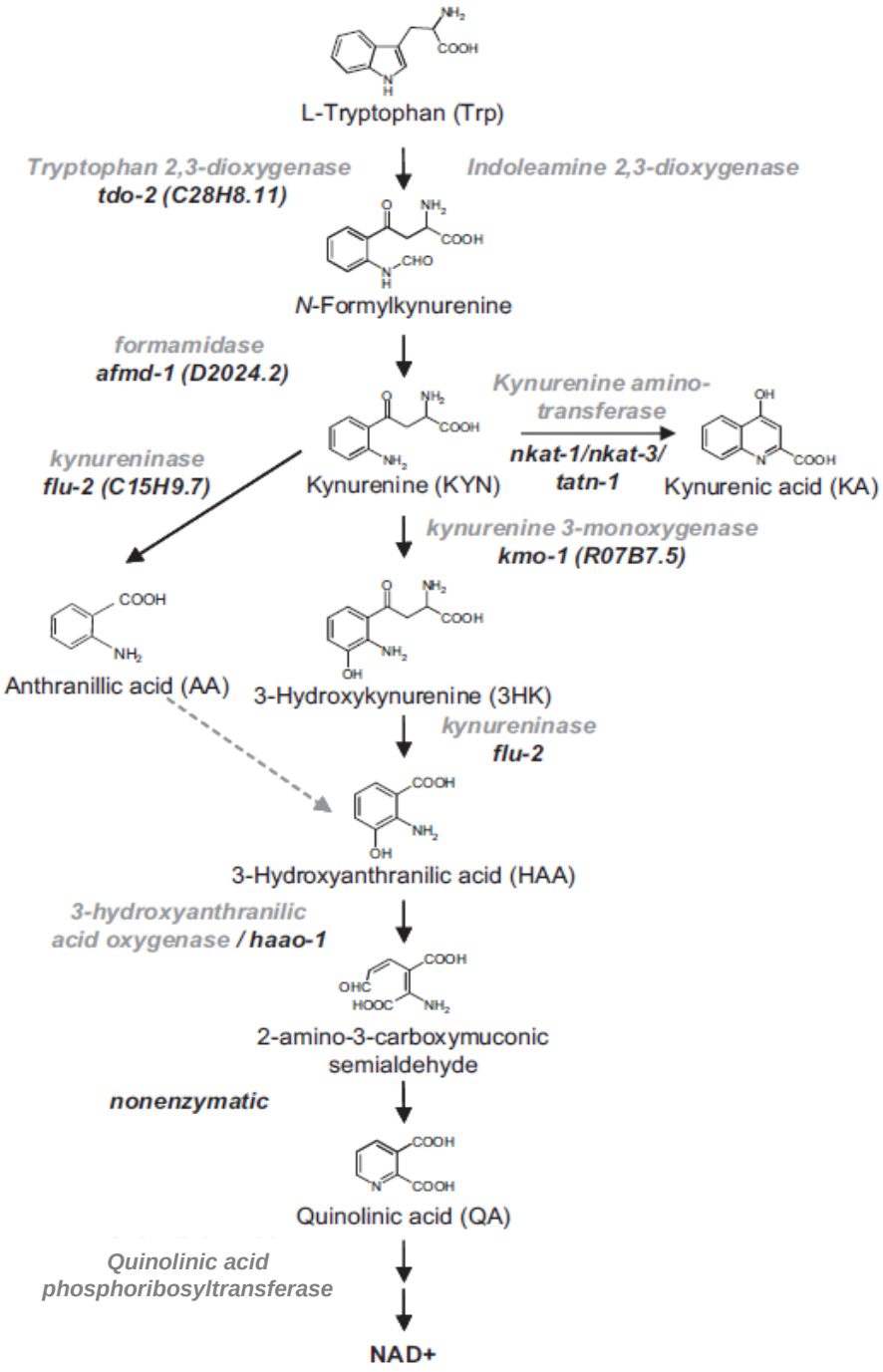

Figure P.7. Kynurenine Pathway. Schematic representation of the kynurenine pathway in *C. elegans* and humans. Human genes are shown in gray while ortholog *C. elegans* genes are shown in black. (Figure adapted from van der Goot et al., 2012)

2D-NMR Based Comparative Metabolomics as a new tool for understanding small molecule metabolism in living systems.

The study of diverse signaling pathways in *C. elegans* presents a fantastic opportunity to understand the role of small molecule signals and their biosynthesis in animal biology. However the common theme in all these investigations is the need to define the structural identities of the involved small-molecule ligands or metabolites. Therefore it is necessary to develop a largely unbiased technique that will allow us to unambiguously determine these structures from complex mixtures with minimal effort and time spent on isolation of pure natural product from the natural material. One of the techniques that has been developed in the Schroeder lab for this purpose is a comparative metabolomics approach named DANS or Differential Analysis by 2D NMR Spectroscopy. DANS allows for comparison of metabolomes derived from different genotypes and can greatly accelerate the identification of compounds whose production depends on a specific genomic background, because it reduces the need for extensive chromatographic fractionation; a major cause of compound loss due to degradation or decomposition in traditional structure elucidation schemes (Forseth and Schroeder, 2011).

2D-NMR can be conveniently used for the structural elucidation of several reactive, oligocyclic alkaloids derived from ants (Schroeder et al., 1996; Schroeder et al., 1996). More recently however, the DANS method has been used successfully in the elucidation of metabolites and biochemical pathways in fungi as well as *C. elegans* (Schroeder et al., 2007; Pungaliya et al., 2009; Forseth et al., 2011; Forseth et al., 2012; Robinnette et al., 2012). These examples have demonstrated the utility of a specific type of 2D-NMR spectrum (“dqfCOSY”) for compound identification via DANS, including the identification of synergistic components of the *C. elegans* dauer and mating

pheromones (Pungaliya et al., 2009, Srinivas et al., 2010, Forseth et al., 2011).

Encouraged by the success of this technique and intrigued by the important roles that nematode derived small-molecules play in regulating development, reproduction, life span and onset of death, this dissertation utilizes Differential Analysis by 2D NMR Spectroscopy to study the steroid signaling pathway and the tryptophan degradation pathway in *C. elegans***.**

In chapter 2, the author of this dissertation describes the development of a blueprint for the unambiguous identification of steroidal ligands of the *C. elegans* NHR, DAF-12. In collaboration with Neelanjan Bose (Schroeder Lab) and supported by other members of the Schroeder Lab, as well as our collaborators in the labs of Adam Antebi, (Max PIanck Institute for Biology of Aging, Cologne) and Patrick Hu (University of Michigan), the author describes the discovery of two novel endogenous activators of DAF-12, along with the identification of another steroidal ligand which had been previously proposed using biochemical investigations (Motola et al., 2006) (**Figure P.8**). This work is the first example of identification of endogenous NHR ligands from complex natural mixtures using NMR spectroscopic methods and provides a roadmap for similar studies to be carried out for other *C. elegans* and mammalian orphan NHRs.

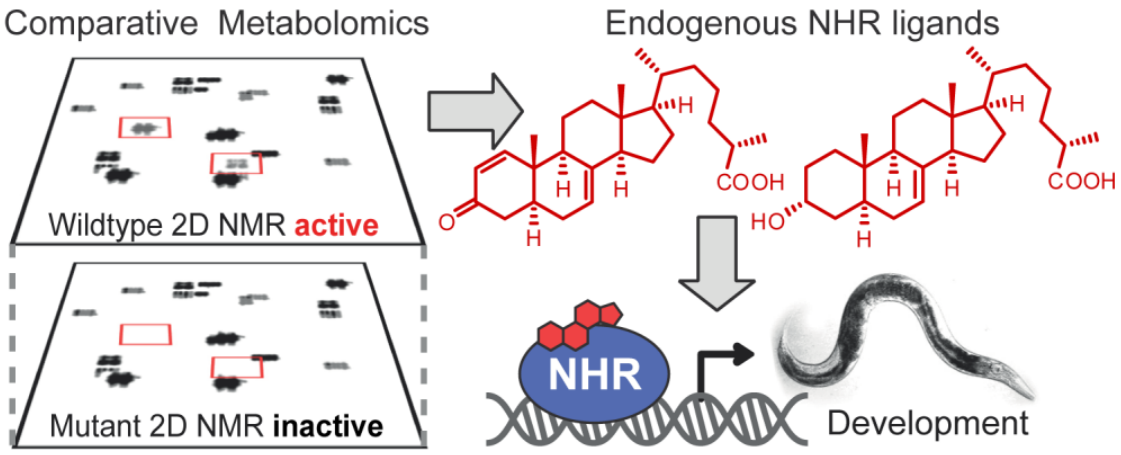

Figure P.8. Identification of novel steroid ligands for the NHR DAF-12.

In Chapter 3, the author in collaboration with Joshua Wollam (Adam Antebi Lab) and supported by members of the Schroeder and Antebi Labs, investigate the biosynthetic pathway of the identified endogenous DAF-12 ligands. This work provides evidence toward a major revision of the currently accepted ligand biosynthetic pathway and discovers new roles for previously proposed components of the pathway. Additionally this work also identifies the role of a novel cytochrome P450 in the DAF-12-ligand biosynthetic scheme, underlining the importance of investigating small-molecule signaling in living systems to uncover novel mechanisms or components.

In Chapter 4, the author describes the identification of a novel class of anthranilic acid derivatives (members of the tryptophan degradation pathway), which are responsible for a striking blue fluorescence that is emitted from intestinal cells of *C. elegans* and other nematodes, moments before death (**Figure P.9**). The identification of the "death fluorescence" phenomenon was carried out by Cassandra Coburn (David Gems Lab, University College London) and this work has been subsequently published in PLoS Biology earlier this year (Coburn et al., 2013). Additionally, this work has led to

preliminary investigations of the kynurenine pathway in *C. elegans* using DANS and initial results suggest the existence of previously unreported enzymatic components in this pathway.

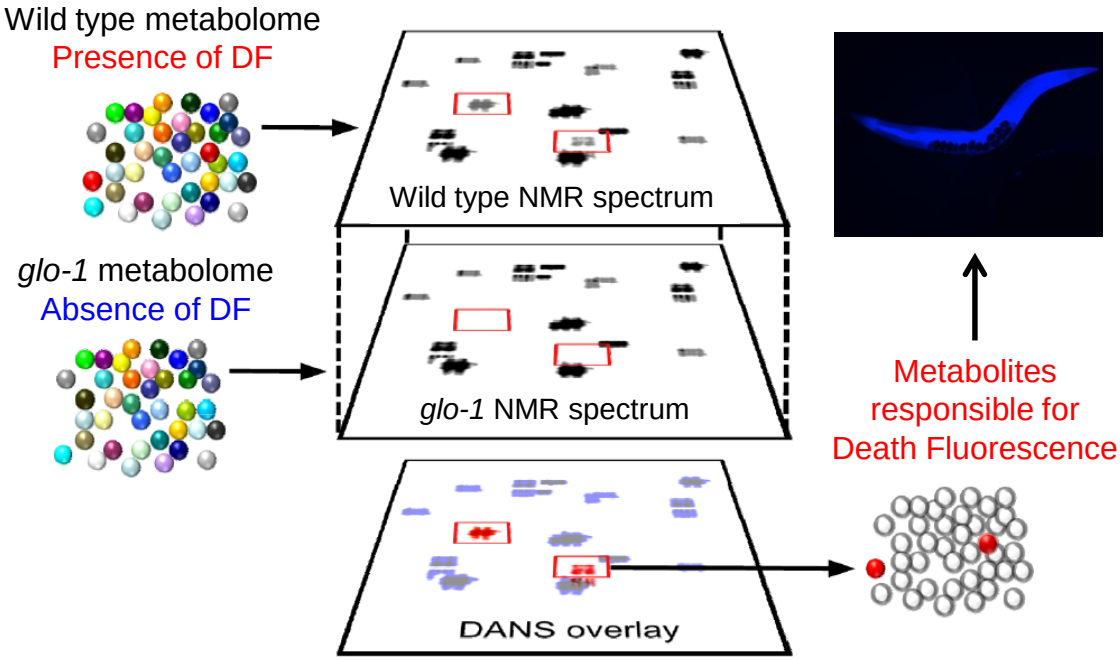

Figure P.9. Identification of death fluorescence in *C. elegans* using DANS methodology.

REFERENCES

Amador-Noguez, D., Dean, A., Huang, W., Setchell, K., Moore, D. and Darlington, G. (2007), Alterations in xenobiotic metabolism in the long-lived Little mice. Aging Cell *6*, 453–470.

Antebi, A. (2006). Nuclear hormone receptors in *C. elegans, WormBook*, ed. The *C. elegans* Research Community, WormBook

Antebi, A. (2013), Chapter Seven - Steroid Regulation of C. elegans Diapause, developmental Timing, and Longevity, In: Ann E. Rougvie and Michael B. O'Connor, Editor(s), Current Topics in Developmental Biology, Academic Press, *105*, 181-212, ISSN 0070-2153.

Arantes-Oliveira, N., Berman, J.R., and Kenyon, C. (2003). Healthy animals with extreme longevity. Science *302*, 611.

Ashrafi, K., Chang, F.Y., Watts, J.L., Fraser, A.G., Kamath, R.S. et al. (2003) Genome-wide RNAi analysis of *Caenorhabditis elegans* fat regulatory genes. Nature *421*, 268-272.

Babu P. (1974) Biochemical genetics of Caenorhabditis elegans. Mol. Gen. Genet. 135 39–44.

Bargmann, C.I. (2006). Comparative chemosensation from receptors to ecology. Nature *444*, 295–301.

Bazopoulou, D., Tavernarakis, N. (2009). The NemaGENETAG initiative: large scale transposon insertion gene-tagging in *Caenorhabditis elegans*. Genetica *137*, 39–46.

Bledsoe, R.K., Montana, V.G., Stanley, T.B., Delves, C.J., Apolito, C.J., et al. (2002). Crystal structure of the glucocorticoid receptor ligand binding domain reveals a novel mode of receptor dimerization and coactivator recognition. Cell *110*, 93–105.

Brenner, S. (2003). Nobel lecture. Nature's gift to science. Biosci Rep 23, 225–237.

Butcher, R.A., Schroeder, F.C., Fischbach, M.A., Straight, P.D., Kolter, R., Walsh, C.T., Clardy, J. (2007). The identification of bacillaene, the product of the PksX megacomplex in Bacillus subtilis. Proc Natl Acad Sci USA *104*, 1506–1509.

Butcher, R.A., Fujita, F., Schroeder, F.C., Clardy, J. (2007). Small-molecule pheromones that control dauer development in Caenorhabditis elegans. Nat Chem Biol *3*, 420-422.

C. elegans Sequencing Consortium, (1998). Genome sequence of the nematode C. elegans: a platform for investigating biology. Science *282*, 2012–2018.

Cassada, R. and Russell, R. (1975). The dauer-larva: A post-embryonic developmental variant of the nematode *C*. *elegans.* Dev Biol *46*, 326–342.

Chiaro, C.R., Patel, R.D., Marcus, C.B., Perdew, G.H. (2007). Evidence for an aryl hydrocarbon receptor-mediated cytochrome p450 autoregulatory pathway. Mol Pharmacol *72*,1369-79.

Chitwood, D.J. (1999). Biochemistry and function of nematode steroids. Crit Rev Biochem Mol Biol 34, 273–284.

Chung, K.-T. and Gadupudi, G. S. (2011). Possible roles of excess tryptophan metabolites in cancer. Environ Mol Mutagen *52*, 81–104.

Dimitriadi, M., Hart, A.C. (2010). Neurodegenerative disorders: insights from the nematode Caenorhabditis elegans. Neurobiol Dis *40*, 4-11.

Dumas, K.J., Guo, C., Wang, X., Burkhart, K.B., Adams, E.J., Alam, H., and Hu, P.J. (2010). Functional divergence of dafachronic acid pathways in the control of C. elegans development and lifespan. Dev Biol *340*, 605-612.

Félix, M.A., Braendle, C. (2010). The natural history of Caenorhabditis elegans. Curr Biol *20*, R965-R969.

Fielenbach, N., Antebi, A. (2008). C. elegans dauer formation and the molecular basis of plasticity. Genes Dev *22*, 2149-65.

Forseth, R.R., Fox, E.M., Chung, D., Howlett, B.J., Keller, N.P., and Schroeder F.C. (2011). Identification of cryptic products of the gliotoxin gene cluster using NMR-based comparative metabolomics and a model for gliotoxin biosynthesis. J Am Chem Soc 133, 9678-81.

Forseth, R.R., and Schroeder, F.C. (2011). NMR-spectroscopic analysis of mixtures: from structure to function. Curr Opin Chem Biol *15*, 38-47.

Gems, D., Partridge, L. (2008). Stress-response hormesis and aging: "that which does not kill us makes us stronger”. Cell Metab *7*, 200–203;

Gerisch, B., and Antebi, A. (2004). Hormonal signals produced by DAF-9/cytochrome P450 regulate C. elegans dauer diapause in response to environmental cues. Development *131*, 1765-1776.

Gerisch, B., Rottiers, V., Li, D., Motola, D.L., Cummins, C.L., Lehrach, H., Mangelsdorf, D.J.,and Antebi, A. (2007). A bile acid-like steroid modulates Caenorhabditis elegans lifespan through nuclear receptor signaling. Proc Natl Acad Sci U S A *104*, 5014-5019.

Gerisch, B., Weitzel, C., Kober-Eisermann, C., Rottiers, V., and Antebi, A. (2001). A hormonal signaling pathway influencing C. elegans metabolism, reproductive development, and life span. Dev Cell *1*, 841-851.

Gill, M.S., Held, J.M., Fisher, A.L., Gibson, B.W., and Lithgow, G.J. (2004). Lipophilic regulator of a developmental switch in *C. elegans*. Aging Cell *6*, 413–421.

Golden JW, Riddle DL (1984). A *C. elegans* dauer-inducing pheromone and an antagonistic component in the food supply. J. Chem. Ecol*. 10*, 1265-1280.

Guyot, E., Chevallier, A., Barouki, R., Coumoul, X. (2013). The AhR twist: ligand-dependent AhR signaling and pharmaco-toxicological implications. Drug Discov Today 18, 479-86.

Hamilton, B., Dong, Y., Shindo, M., Liu, W., Odell, I., Ruvkun, G., Lee, S.S. (2005). A systematic RNAi screen for longevity genes in *C. elegans*. Genes &Dev *19*, 1544-1555.

Hannich, J.T., Entchev, E.V., Mende, F., Boytchev, H., Martin, R., et al. (2009). Methylation of the sterol nucleus by STRM-1 regulates dauer larva formation in Caenorhabditis elegans. Dev Cell *16*, 833-843.

Hansen, M., Hsu, A.L., Dillin, A., Kenyon, C. (2005). New Genes Tied to Endocrine, Metabolic, and Dietary Regulation of Lifespan from a *Caenorhabditis elegans* Genomic RNAi Screen, PLoS Genetics *1*, 119-128.

Harris, T.W., Antoshechkin, I., Bieri, T., Blasiar, D., Chan, J., Chen, W.J., De La Cruz, N., Davis, P., Duesbury, M., Fang, R., Fernandes, J., Han, M., Kishore, R., Lee, R., Müller, H.M., Nakamura, C., Ozersky, P., Petcherski, A., Rangarajan, A., Rogers, A., Schindelman, G., Schwarz, E.M., Tuli, M.A., Van Auken, K., Wang, D., Wang, X., Williams, G., Yook, K., Durbin, R., Stein, L.D., Spieth, J., Sternberg, P.W., 2010 Jan. WormBase: a comprehensive resource for nematode research. Nucleic Acids Res. 38 (Database issue), D463–D467

Hashmi, S., Wang, Y., Parhar, R.S. (2013) A *C. elegans* model to study human metabolic regulation. Nutr Metab [Lond.] *10*, 31.

Held, J.M., White, M.P., Fisher, A.L., Gibson, B.W., Lithgow, G.J., and Gill, M.S. (2006). DAF-12-dependent rescue of dauer formation in Caenorhabditis elegans by (25S)-cholestenoic acid. Aging Cell *5*, 283-291.

Hulme, S.E., and Whitesides, G.M. (2011). Chemistry and the worm: Caenorhabditis elegans as a platform for integrating chemical and biological research. Angew Chem Int Ed Engl *50*, 4774-4807.

Jeong, P.Y., Jung, M., Yim, Y.H., Kim, H., Park, M. et al. (2005) Chemical structure and biological activity of the *Caenorhabditis elegans* dauer-inducing pheromone. Nature *433*, 541-545.

Jia, K., Albert, P.S., Riddle, D.L. (2002). DAF-9, a cytochrome P450 regulating *C. elegans* larval development and adult longevity. *Development* 129, 221-31.

Kazlauskas, A., Sundstrom, S., Poellinger, L., Pongratz, I. (2001). The hsp90 chaperone complex regulates intracellular localization of the dioxin receptor. Mol Cell Biol *21*, 2594–2607.

Kenyon, C. (2001). A conserved regulatory system for aging. Cell *105*, 165-8.

Kenyon, C., Chang J., Gensch, E., Rudner, A., Tabtiang R. (1993). A *C. elegans* mutant that lives twice as long as wild type. *Nature 366*, 461-4.

Kenyon, C. (2010). A pathway that links reproductive status to lifespan in Caenorhabditis elegans. Ann N Y Acad Sci *1204*, 156-162.

Ko, H. P., Okino, S. T., Ma, Q., Whitlock, J. P. (1996). Dioxin-induced CYP1A1 transcription in vivo: the aromatic hydrocarbon receptor mediates transactivation, enhancer-promoter communication, and changes in chromatin structure. Mol. Cell. Biol. *16*, 430–436.

Li, W., Kennedy, S.G., Ruvkun, G. (2003) daf-28 encodes a C. elegans insulin superfamily member that is regulated by environmental cues and acts in the DAF-2 signaling pathway. Genes & Dev *17*, 844–858.

Li, B., Forseth, R.R., Bowers A.A., Schroeder F.C., and Walsh CT. (2012) A backup plan for self-protection: S-methylation of holomycin biosynthetic intermediates in Streptomyces clavuligerus. Chembiochem *13*, 2521-6.

Lindsey, S. and Papoutsakis, E.T. (2012). The evolving role of the aryl hydrocarbon receptor (AHR) in the normophysiology of hematopoiesis. Stem Cell Rev *8*, 1223-35.

Ludewig, A.H., Kober-Eisermann, C., Weitzel, C., Bethke, A., Neubert, K., Gerisch, B., Hutter, H., and Antebi, A. (2004). A novel nuclear receptor/coregulator complex controls C. elegans lipid metabolism, larval development, and aging. Genes Dev *18*, 2120-2133.

Ludewig, A.H. and Schroeder, F.C. (2013). Ascaroside signaling in *C. elegans*, *WormBook*, ed. The *C. elegans* Research Community, WormBook,

Magner, D.B., Antebi, A. (2008) Caenorhabditis elegans nuclear receptors: insights into life traits. Trends Endocrinol Metab.*19*, 153-60.

Marsh, E.K., May, R.C. (2012) Caenorhabditis elegans, a model organism for investigating immunity. Appl Environ Microbiol *78*, 2075–2081.

Matyash, V., Entchev, E.V., Mende, F., Wilsch-Brauninger, M., Thiele, C., Schmidt, A.W. et al. (2004). Sterol-derived hormone(s) controls entry into

diapause in *C. elegans* by consecutive activation of DAF-12 and DAF-16. PLoS Biol. *2*, e280.

Motola, D.L., Cummins, C.L., Rottiers, V., Sharma, K.K., Li, T., Li, Y. et al. (2006). Identification of ligands for DAF-12 that govern dauer formation and reproduction in C. elegans. Cell *124*, 1209-1223.

Nguyen, L.P., Bradfield, C.A. (2008).The search for endogenous activators for the aryl hydrocarbon receptor. Chem Res Toxicol *21*, 102–116.

Olsen A., Vantipalli, M.C., Lithgow G.J. (2006). Using Caenorhabditis elegans as a model for aging and age-related diseases. Ann NY Acad Sci *1067*, 120-8.

Opitz C.A., Litzenburger U.M., Sahm F., Ott M., Tritschler I., et al. (2011). An endogenous tumour-promoting ligand of the human aryl hydrocarbon receptor. Nature. *478*, 197-203.

Poland, A. and Kende, A. (1976). 2,3,7,8-Tetrachlorodibenzo-p-dioxin: environmental contaminant and molecular probe. *Fed Proc 35*, 2404–2411.

Powell, J.R. and Ausubel, F.M. (2008). Models of Caenorhabditis elegans infection by bacterial and fungal pathogens. Methods Mol Biol *415*, 403-27.

Patel, D.S., Fang, L.L., Svy, D.K., Ruvkun, G., and Li, W. (2008). Genetic identification of HSD-1, a conserved steroidogenic enzyme that directs larval development in Caenorhabditis elegans. Development *135*, 2239-2249.

Pungaliya, C., Srinivasan, J., Fox, B.W., Malik, R.U., Ludewig, A.H., Sternberg, P.W., and Schroeder, F.C. (2009). A shortcut to identifying small molecule signals that regulate behavior and development in Caenorhabditis elegans. Proc Natl Acad Sci USA *106*, 7708-7713.

Qin, H.T. and Powell-Coffman, J.A. (2004). The *Caenorhabditis elegans* aryl hydrocarbon receptor, AHR-1, regulates neuronal development. Dev Biol *270*, 64–75.

von Reuss, S.H., Bose, N., Srinivasan, J., Yim, J.J., Judkins, J.C., Sternberg, P.W., and Schroeder, F.C. (2012). Comparative metabolomics reveals biogenesis of ascarosides, a modular library of small molecule signals in C. elegans. J Am Chem Soc *134*, 1817–1824.

Ren, P., Lim, C.S., Johnsen, R., Albert, P.S., Pilgrim, D., et al. (1996). Control of C. elegans larval development by neuronal expression of a TGF-beta homolog. Science *274*, 1389–1391.

Renaud, J.P., Rochel, N., Ruff, M., Vivat, V., Chambon, P., Gronemeyer, H., and Moras, D. (1995). Crystal structure of the RAR- *γ* ligand-binding domain bound to all-trans retinoic acid. Nature *378*, 681–689.

Riddle, D.L., Albert, P.S. (1997). In *C. elegans* II, D.L. Riddle, T. Blumenthal, B.J. Meyer, and J. R. Priess, eds. (Cold Spring Harbor, NY: Cold Spring Harbor Laboratory Press), 739–768.

Robinette, S.L., Bruschweiler, R., Schroeder, F.C., Edison, A.S. (2012). NMR in metabolomics and natural products research: two sides of the same coin. Acc Chem Res *45*, 288–297.

Rongvaux, A., Andris, F., Van Gool, F., Leo, O. (2003) Reconstructing eukaryotic NAD metabolism. Bioessays *25*, 683–690.

Rottiers, V., Motola, D.L., Gerisch, B., Cummins, C.L., Nishiwaki, K., Mangelsdorf, D.J., and Antebi, A. (2006). Hormonal control of C. elegans dauer formation and life span by a Rieske-like oxygenase. Dev Cell *10*, 473-482.

Schmidt, J.V., Bradfield, C.A. (1996). Ah receptor signaling pathways. Annu Rev Cell Dev Biol *12*, 55–89.

Sladek, F. (2011). What are Nuclear Receptor Ligands? Mol Cell Endocrinol *334*, 3–13.

Schroeder, F.C. (2006). Small molecule signaling in *Caenorhabditis elegans*. ACS Chem Biol *1*, 198-200.

Schroeder, F.C., Gibson, D.M., Churchill, A.C.L., Wursthorn, E.J., Krasnoff, S.B., Clardy, J. (2007). Differential Analysis of 2D NMR Spectra: New Natural Products from a Pilot-Scale Fungal Extract Library. Differential Analysis of 2D NMR Spectra: New Natural Products from a Pilot-Scale Fungal Extract Library. Angew Chem Int Ed *46*, 901–904.

Siddiqui, S.S. and Babu, P. (1980) Kynurenine hydroxylase mutants of the nematode Caenorhabditis elegans. Mol Gen Genet 179, 21–24

Sluder, A.E. and Maina, C.V. (2001). Nuclear receptors in nematodes: themes and variations. Trends Genet. *17*, 206–213.

Srinivasan, J., Kaplan, K., Ajredini, R., Zachariah, C., Alborn, H., Teal, P., et al. (2008). A synergistic blend of small molecules differentially regulates both mating behavior and population density in *Caenorhabditis elegans*. Nature *454*, 1115-8.

Srinivasan, J., von Reuss, S.H., Bose, N., Zaslaver, A., Mahanti, P., et al. (2012). A Modular Library of Small Molecule Signals Regulates Social Behaviors in Caenorhabditis elegans. PLoS Biol *10*, e1001237.

Stone, T.W., Forrest, C.M., Stoy, N., Darlington, L.G. (2012). Involvement of kynurenines in Huntington's disease and stroke-induced brain damage. J Neur Trans *119*, 261–274.

Sugimoto, A. (2004). High-throughput RNAi in Caenorhabditis elegans: Genome-wide screens and functional genomics. Differentiation *72*, 81–91.

Tatar, M., Bartke, A., Antebi, A. (2003). The endocrine regulation of aging by insulin-like signals. Science *299*, 1346-51.

Taubert, S., Ward, J.D., and Yamamoto, K.R. (2010). Nuclear hormone receptors in nematodes: evolution and function. Mol Cell Endocrinol *334*, 49-55.

Kaletta T., and Hengartner, M.O. (2006). Finding function in novel targets: C. elegans as a model organism. Nat Rev Drug Discov *5*, 387-399.

van der Goot, A.T., and Nollen, E.A.A. (2013). Tryptophan metabolism: entering the field of aging and age-related pathologies. Trends Mol Med *19*, 336 – 344.

Whitlock, J. P. (1999). Induction of cytochrome P4501A1. Annu Rev Pharmacol Toxicol *39*, 103–125.

Williams, T.W., Dumas, K.J., and Hu, P.J. (2010). EAK proteins: novel conserved regulators of C. elegans lifespan. Aging *2*, 742-747.

Wollam, J., and Antebi, A. (2011). Sterol regulation of metabolism, homeostasis, and development. Annu Rev Biochem *80*, 885-916.

Wollam, J., Magner, D.B., Magomedova, L., Rass, E., Shen, Y., Rottiers, V., Habermann, B., Cummins, C.L., and Antebi, A. (2012). A Novel 3-Hydroxysteroid Dehydrogenase That Regulates Reproductive Development and Longevity. PLoS Biol *10*, e1001305.

Wollam, J., Magomedova, L., Magner, D.B., Shen, Y., Rottiers, V., Motola, D.L., Mangelsdorf, D.J., Cummins, C.L., and Antebi, A. (2011). The Rieske oxygenase DAF-36 functions as a cholesterol 7-desaturase in steroidogenic pathways governing longevity. Aging Cell *10*, 879-884.

Wolozin, B., Gabel, C., Ferree, A., Guillily, M., Ebata, A. (2011). Watching worms whither: modeling neurodegeneration in C. elegans. Prog Mol Biol Transl Sci *100*, 499-514.

Yoshiyama-Yanagawa, T., Enya, S., Shimada-Niwa, Y., Yaguchi, S., Haramoto, Y., Matsuya, T., *et al.* (2011). The conserved Rieske oxygenase DAF-36/Neverland is a novel cholesterol-metabolizing enzyme. J Biol Chem *286*, 25756-25762.

Zelante, T., Iannitti, R.G., Cunha, C., De Luca, A., Giovannini, G., Pieraccini, G., Zecchi, R., D'Angelo, C., Massi-Benedetti, C., Fallarino, F., et al. (2013). Tryptophan Catabolites from Microbiota Engage Aryl Hydrocarbon Receptor and Balance Mucosal Reactivity via Interleukin-22. Immunity *39*, 372–385.

CHAPTER 2

COMPARATIVE METABOLOMICS REVEALS ENDOGENOUS LIGANDS OF DAF-12: A NUCLEAR HORMONE RECEPTOR REGULATING *C. ELEGANS* DEVELOPMENT AND LIFESPAN

Introduction:

Nuclear hormone receptors (NHRs) are DNA-binding proteins that regulate gene expression in response to environmental, nutritional and developmental signals. The activity of a large proportion of these evolutionarily conserved, transcription factors is selectively and reversibly modulated by small-molecule ligands. Even very small changes in ligand structures may result in dramatic changes of transcriptional activity and specificity (Brown and Slatopolsky, 2008; Singarapu 2011) and therefore, precise knowledge of the structure of these small-molecule NHR ligands is essential for understanding their role in controlling diverse aspects of metazoan metabolism, cell differentiation, development and aging. However, despite this need for a comprehensive understanding of ligand structures and their biosynthetic pathways to understand NHR function (Mangelsdorf, 1995; Wollam and Antebi, 2011), the endogenous ligands of many NHRs have remained poorly characterized, often due to very low abundance of these molecules in highly complex animal metabolomes (Schupp and Lazar, 2010).

The free living nematode *C. elegans* has 284 NHRs, allows easy genetic manipulation, and can be grown in substantially large quantities, providing an unique opportunity to investigate structures, biosynthesis, and functions of NHR ligand in a relatively simple model system (Hulme and Whitesides, 2011; Taubert et. al., 2010). In *C. elegans*, DAF-12, a homolog of

vertebrate Vitamin D (VDR) and liver X receptors (LXR), functions as a ligand-dependent switch that control both adult lifespan and larval development (Antebi, 2000; Fielenbach, 2008; Kenyon, 2010; Shen, 2012). The biosynthesis of the ligands of DAF-12, hypothesized to be of steroidal origin (Matyash, 2004; Gerisch, 2001; Jia, 2002), is controlled by a complex endocrine signaling network, many components of which, appear to be highly conserved between *C. elegans* and mammals (Fielenbach and Antebi, 2008). Perception of environmental stimuli by chemosensory neurons regulates signaling via the conserved insulin/IGF and TGF-β pathways, which converge on genes implicated in DAF-12-ligand biosynthesis (**Figure 2.1**). Under unfavorable conditions such as overcrowding or scarcity of food, ligand biosynthesis is suppressed, and unliganded DAF-12 interacts with its co-repressor DIN-1 (Ludewig et al., 2004). The resulting transcriptional repression of DAF-12 target genes causes developmental arrest and entry into a highly stress-resistant larval stage called the dauer diapause (Gems et al., 1998; Larsen et al., 1995; Schaedel et al., 2012) (**Figure 2.1**). In contrast, favorable environmental conditions trigger upregulation of DAF-12 ligand biosynthesis. DAF-12 ligand binding then results in dissociation of the corepressor DIN-1 to allow expression of DAF-12 target genes, promoting rapid developmental progression from larvae to reproductive adults (Fielenbach and Antebi, 2008; Ludewig et al., 2004) (**Figure 2.1**). Additionally, ligand-dependent activation of the DAF-12 target genes *mir-84* and *mir-241*, two microRNAs of the conserved *let-7* family (Bethke et al., 2009; Hammell et al., 2009), is required for lifespan regulation in response to signals from reproductive tissues (Kenyon et al., 2010; Yamawaki et al., 2010). These findings suggest that metazoan lifespan is coupled to the gonad via NHR signaling (Shen et al., 2012).

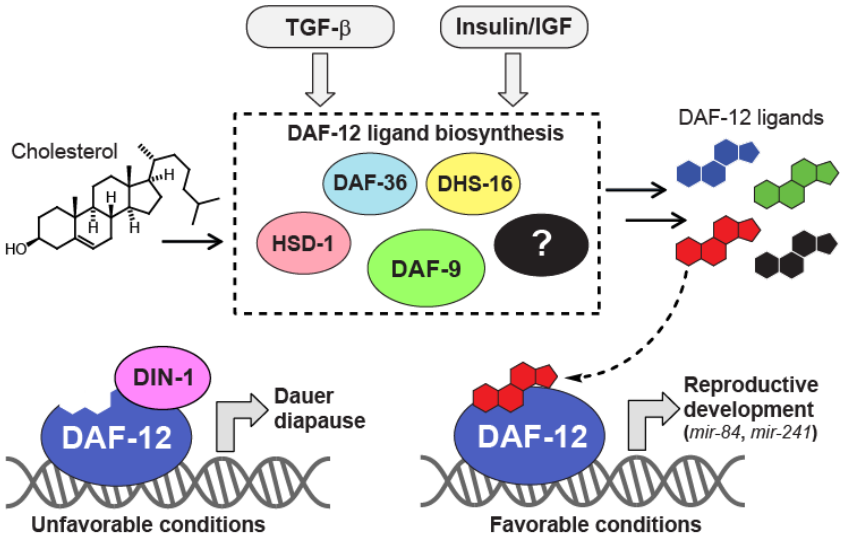

Figure 2.1. Role of DAF-12 in the dauer pathway. Under favorable conditions, signaling via the insulin/IGF and TGF-β pathways drive biosynthesis of steroidal DAF-12-ligands. Liganded DAF-12 promotes development, in part via transcription of the *let-7*-family microRNA's *mir-84* and *mir-241*. Under unfavorable conditions, ligand biosynthesis is inhibited, resulting in interaction of unliganded DAF-12 with its co-repressor DIN-1 and target gene repression (Ludewig et al., 2004)

Based on extensive biochemical studies, two bile acid-like steroids named Δ^4- and Δ^7-dafachronic acid were proposed as endogenous ligands of DAF-12 (**Figure 2.2**) (Motola et al., 2006). Central to the identification of these steroids named as dafachronic acids (DAs), as DAF-12 ligand candidates were precursor studies in which a variety of 3-keto steroids were identified as substrates for the cytochrome P450, DAF-9, which had been shown to act upstream of DAF-12 in DAF-12-ligand biosynthesis (Gerisch et al., 2001; Jia et al., 2002; Motola et al., 2006). DAF-9 was further shown to act on the sidechain in these cholestenones introducing a terminal carboxyl group

(**Figure 2.2**) (Motola et al., 2006). In a separate study, a DAF-12-activating isomer of 3β-hydroxy cholest-5-enoic acid was detected in *C. elegans* metabolite extracts (Held et al., 2006). However, given the very low concentrations of the putative DAF-12-ligands in *C. elegans*, isolation and full spectroscopic characterization of these compounds was not pursued (Motola et al., 2006).

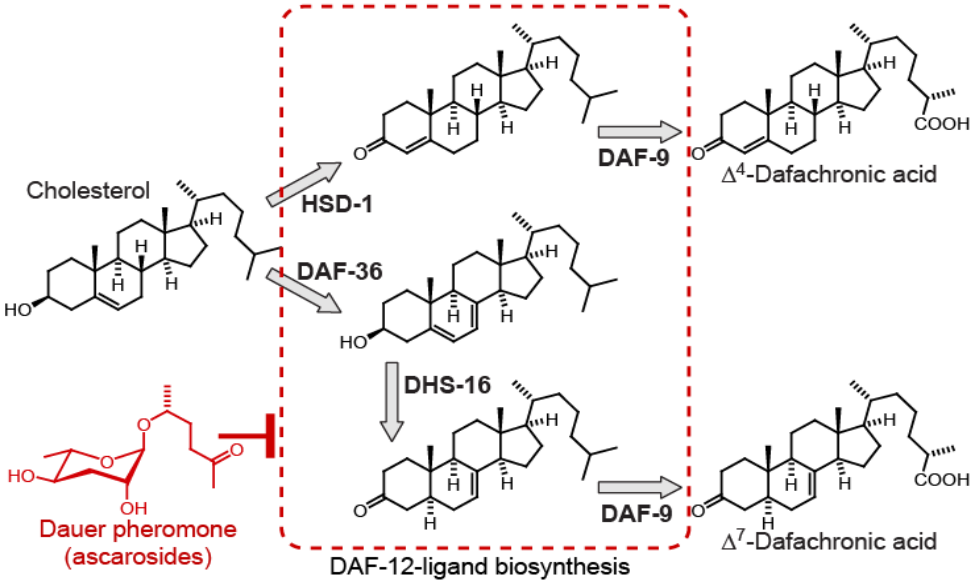

Figure 2.2. Previously described DAF-12-ligands and proposed biosynthetic pathway - (Dumas et al., 2010; Gerisch et al., 2007; Patel et al., 2008; Rottiers et al., 2006; Williams et al., 2010; Wollam et al., 2011; Yoshiyama-Yanagawa et al., 2011). DAF-12-ligand biosynthesis is downregulated in response to dauer pheromone (Schaedel et al., 2012), a blend of ascarosides, e.g. the shown ascr#2 (red).

In this chapter, the author shows how by developing an unbiased, comparative metabolomics approach to specifically address the problems created by low abundance of the target molecule in a complex animal metabolome, several novel and endogenous steroidal ligands of DAF-12 are identified. This approach utilizes the Differential Analysis by 2D-NMR Spectroscopy (DANS) technique to compare metabolomes of 'ligand-deficient' and 'ligand-rich' animals and provides a blue-print for the systematic identification of ligands of other *C. elegans* and mammalian NHRs.

This work was done in collaboration with Neelanjan Bose (Frank Schroeder Lab, Cornell University). Synthetic compounds were provided by Joshua Judkins and some of the bio-assays were carried out in collaboration with Dr. Joshua Wollam (Adam Antebi Lab, MPI Cologne) Dr. Axel Bethke (Frank Schroeder Lab, Cornell University) and Dr. Kathlyn J. Dumas (Patrick Hu Lab, University of Michigan).

Developing a systematic blueprint for identification of endogenous DAF-12 ligands:

Since all of the earlier body of work associated with finding the identity of DAF-12 ligands relied on classical genetics and biochemical experiments, our first objective was to identify the endogenous ligands of DAF-12 based on direct and unambiguous spectroscopic evidence obtained from analysis of the *C. elegans* metabolome. For this purpose we employed a combination of activity-guided fractionation and NMR-based comparative metabolomics via DANS (Differential Analyses by 2D NMR Spectroscopy) (**Figure 2.3**). 2D NMR spectroscopy provides a largely unbiased overview of metabolome composition, and comparing 2D NMR spectra of different mutant backgrounds via DANS often allows the detection and partial identification of very minor

metabolites such as signaling molecules (Pungaliya et al., 2009; Forseth and Schroeder, 2011). DANS relies on correlating changes in the metabolome with perturbations made in the genome, for compound identification and thereby reduces the need for extensive fractionation, which frequently results in loss of activity or the introduction of artifacts (Forseth and Schroeder, 2011). We envisioned that this approach could be applied to identify DAF-12-ligands if one compared a *C. elegans* mutant metabolome lacking DAF-12-ligands with the metabolome of animals that produces DAF-12-ligands abundantly.

For this DANS-based ligand identification, we chose *daf-9;daf-12* double mutants as the ligand-deficient strain and *daf-22* mutants as a ligand-rich reference strain. Even though *daf-9;daf-12* double mutants do not produce DAF-12-ligands, they bypass the dauer stage, because lack of DAF-12 prevents the execution of genetic programs required for dauer formation (Gerisch et al., 2004) and therefore can be grown in large volumes that allows NMR spectroscopic analyses of less abundant metabolites. *daf-22* mutant worms develop normally to adulthood, but are defective in the biosynthesis of the dauer-inducing ascarosides (Butcher et al., 2009; von Reuss et al., 2012), which we hypothesized may adversely affect DAF-12-ligand production in wild-type liquid cultures (**Figure A.1**)**.** Downregulation of DAF-12-ligand biosynthesis by ascarosides is also suggested by the finding that exposure to high concentrations of dauer pheromone abolished expression of DAF-9, one of the key enzymes in the proposed biosynthetic pathway of DAF-12-ligands (Schaedel et al. 2012).

In preparation for DANS analysis, metabolome extracts obtained from large scale, mixed stage, liquid cultures of the wild-type, *daf-9;daf-12* and *daf-22* strains were fractionated using an automated, highly reproducible chromatography system (Appendix A). The resulting parallel sets of

metabolome fractions were assessed for DAF-12-ligand content using both *in vivo* and *in vitro* bioassays (**Figure 2.3**). The *in-vivo* assay used *daf-9(dh6)* worms, which are defective in DAF-12-ligand production. In the absence of exogenously added DAF-12-ligand or a suitable precursor, developing *daf-9(dh6)* worms arrest as dauer larvae, because DAF-12 constitutively interacts with its corepressor DIN-1 (Gerisch et al., 2004; Gerisch et al., 2007; Ludewig et al., 2004). The assay scored the ability of added metabolome fractions to rescue the arrested dauer larvae and promote development to adulthood, providing a measure for the presence of a DAF-12 ligand or suitable precursor in the exogenously added fractions that would dissociate the DAF-12/DIN-1 corepressor complex. The *in-vitro* assay measured DAF-12 transcriptional activation of a luciferase reporter in HEK-293T cells that were co-transfected with full-length DAF-12 and the reporter construct (Bethke et al., 2009). This assay provided a measure for ligand-dependent interaction of DAF-12 with mammalian coactivator(s) endogenous to the cell line. Both of these assays consistently showed activity for three groups of *daf-22* and wild type metabolome fractions (regions I-III in **Figure 2.3**), suggesting the presence of DAF-12-ligands or precursors, whereas all *daf-9;daf-12* fractions were inactive in both assays, as expected based on previous work (Gerisch et al., 2004; Gerisch et al., 2007; Motola et al; 2006). As anticipated, *daf-22* fractions were significantly more active in both assays than the corresponding wild-type fractions, suggesting much higher production of DAF-12-ligands in *daf-22* mutants (**Figure 2.3, Figure A.1**).

Figure 2.3. Detection of DAF-12-ligands in *C. elegans* mutant metabolomes. (A) Fractionation of active, ligand-rich daf-22 and inactive daf-9;daf-12 metabolomes is followed by 2D-NMR-based comparative metabolomics of active fractions. (B) Assessment of DAF-12-ligand content using (**Top**) an in vitro luciferase assay in HEK-293T cells transfected with full-length DAF-12 and a mir84p-luciferase reporter vector and (**Bottom**) in vivo daf-9(dh6) dauer rescue assays. (C) daf-9;daf-12 metabolome fractions are inactive in the luciferase assay. 100 nM Δ^7-DA is used as a positive control.(D) Luciferase assays of daf-22 metabolome fractions reveal three active regions.(E) Daf-9(dh6) dauer rescue assays of daf-22 metabolome fractions show activity in the same three regions. For worm images of scored phenotypes and additional activity data see **Figure A.1**.

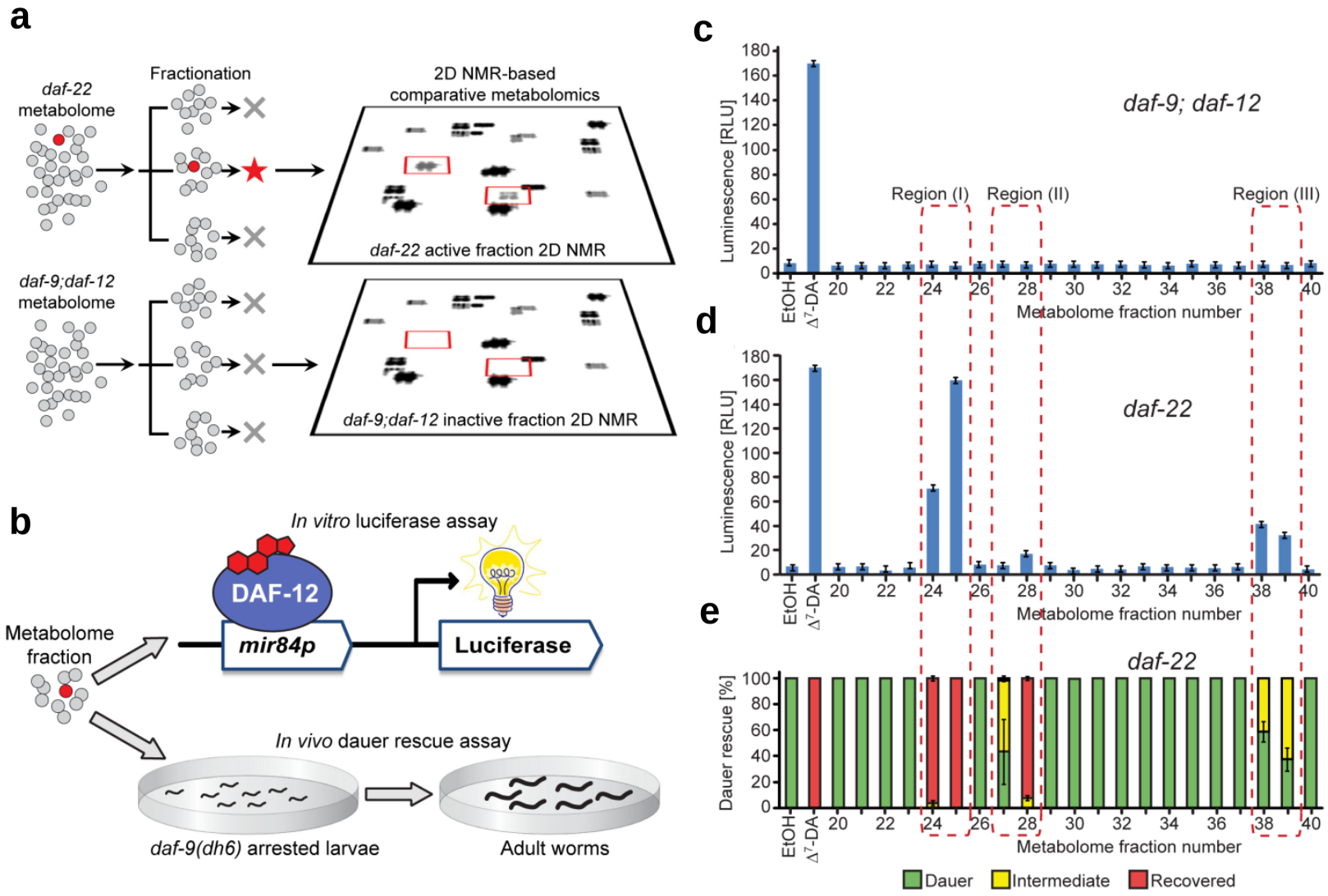
a
daf-22
metabolome
Fractionation
2D NMR-based
comparative metabolomics
daf-22 active fraction 2D NMR
daf-9;daf-12
metabolome
daf-9;daf-12 inactive fraction 2D NMR
b
In vitro luciferase assay
DAF-12
mir84p
Luciferase
Metabolome
fraction
In vivo dauer rescue assay
daf-9(dh6) arrested larvae
Adult worms
c
daf-9; daf-12
Luminescence [RLU]
Region (I)
Region (II)
Region (III)
EtOH
Δ7-DA
Metabolome fraction number
d
daf-22
Luminescence [RLU]
Metabolome fraction number
e
daf-22
Dauer rescue [%]
Metabolome fraction number
Dauer
Intermediate
Recovered

DANS reveals steroids with unexpected structural features:

Two-dimensional (2D) NMR spectra of the most active group of *daf-22* fractions, active region I, revealed the presence of long-chained ascarosides (Pungaliya et al., 2009), in addition to a complex mixture of fatty acids, glycerides, other lipids, and several epidioxy sterol derivatives, (**Figure A.2**) (Gunatilaka et al., 1981; Sera et al., 1999), all of which were also present in similar concentrations in corresponding *daf-9;daf-12* metabolome fractions. However, a more rigorous inspection of region I 2D NMR spectra revealed several sets of signals that were consistently absent in *daf-9;daf-12*, and thus appeared to be *daf-9*-dependent (**Figure 2.4**). Subsequent analysis of these differential signals strongly suggested steroidal structures. Because of their extremely low concentrations, detailed characterization of the putative *daf-9*-dependent steroids required additional fractionation via HPLC, which resulted in two active samples each containing 1-2% of *daf-9*-dependent components (**Figure 2.5**).

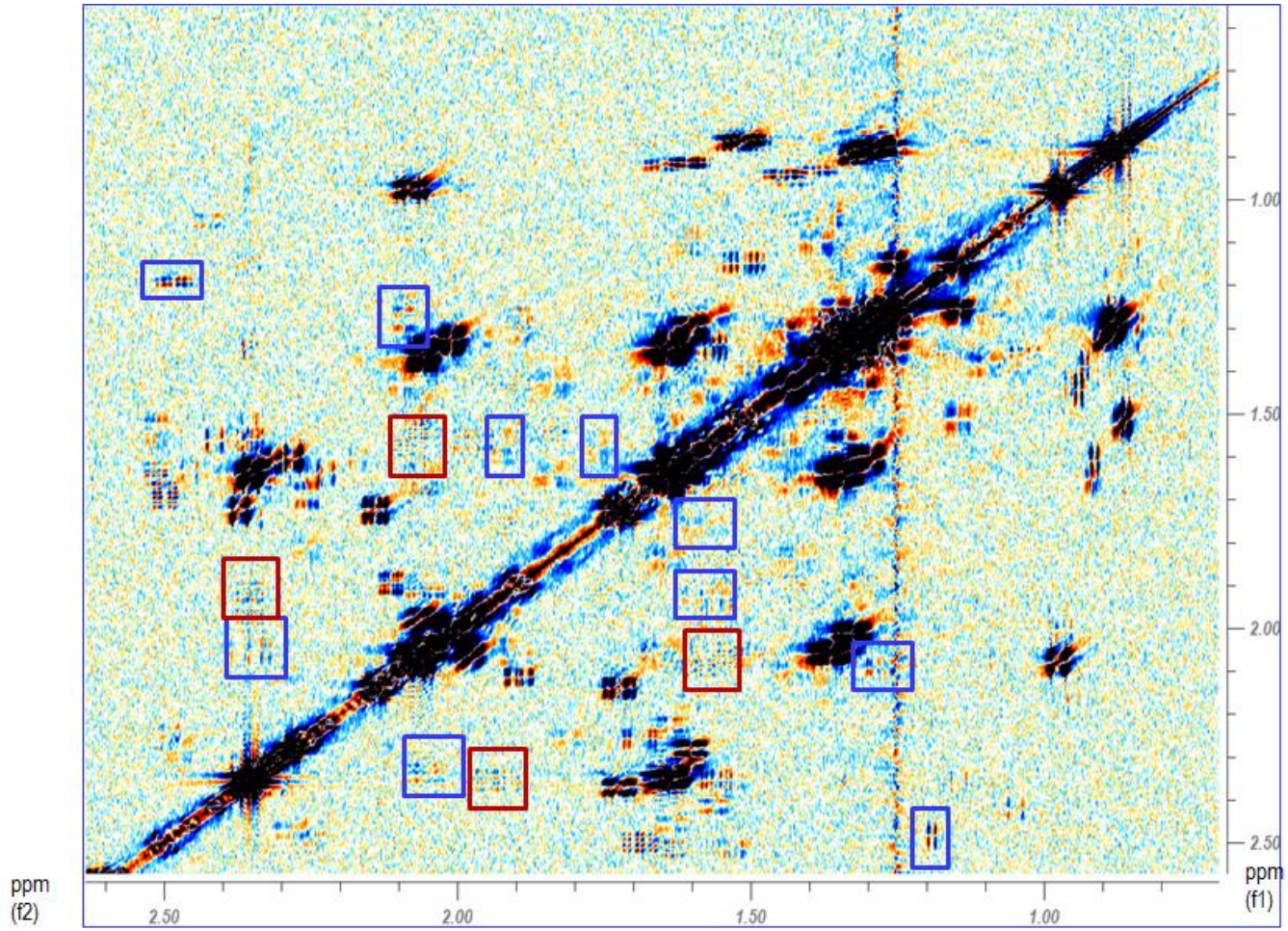

Figure 2.4. Detection of daf-9-dependent signals using 2D-NMR Spectroscopy. *Daf-22* active metabolome fraction (F25) contained both *daf-9* dependent cross peaks (blue boxes) and *daf-9* independent cross peaks (red boxes).

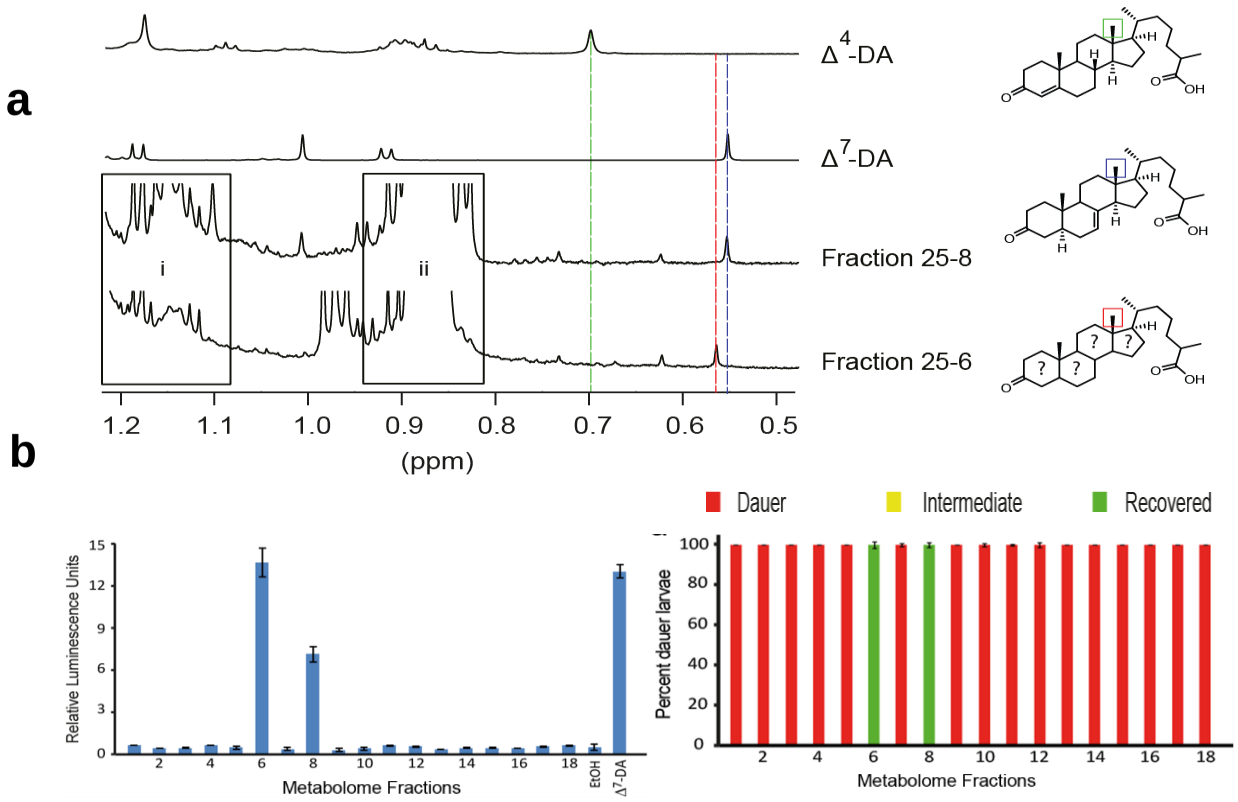

Figure 2.5. Analysis of active fractions. (a) Comparison of representative sections of ^{1}H-NMR spectra of active HPLC-enriched fractions with the proposed DAF-12 ligands[3] revealed the presence of Δ^{7}-DA in fraction 25-8, and an unknown steroid ligand in fraction 25-6 that is distinctly different from Δ^{7}- and Δ^{4}-DA. ^{1}H-NMR spectra of the natural fractions also show that *C. elegans* derived lipids (i, ii) constitutes the majority of the active fractions. **(b)** Assessment of DAF-12 transcriptional activation in the *in vitro* luciferase assay in HEK-293T cells (left) and dauer rescue activity in *daf-9(dh6)* worms (right) with HPLC-enriched fractions 25-6 and 25-8 obtained from *daf-22* active metabolome fraction 25.

NMR-spectroscopic analysis of the most active fractions showed a distinct set of *daf-9*-dependent signals at 5.9 and 7.0 ppm with a coupling constant of 10 Hz, which strongly suggested the presence of an unusual Δ^1-unsaturated 3-keto steroid (**Figure 2.6**). Comparison with literature data suggested 3-oxocholesta-1,7-dienoic acid ("$\Delta^{1,7}$-DA"), which had not previously been described from worms, in addition to smaller amounts of the known Δ^7-DA (**Figure 2.6**) (Motola et al., 2006). Δ^1-unsaturated steroids are rare in nature, and we are aware of only one other example in animals, the identification of (25*S*)-3-oxocholesta-1,4-dienoic acid from the Indonesian soft coral, *Minabea* sp. (Wang et al., 2009).

Figure 2.6. Detection of endogenous DAF-12-ligands via DANS and subsequent confirmation by SIM-GC/MS. dqfCOSY spectrum of inactive *daf-9;daf-12* metabolome fraction corresponding to active region I. Enlarged section (upper left) compares *daf-9;daf-12* with corresponding *daf-22* section, showing one of the differential crosspeaks (red) that led to identification of $\Delta^{1,7}$-DA, next to non-differential signals representing a metabolite present in both *daf-9;daf-12* and *daf-22*, an epidioxy sterol (blue). Enlarged section (lower right) shows example crosspeaks from the comparison of the *strm-1* (*vide infra* Chapter 2) and *daf-9;daf-12* metabolomes, showing signals (green) characteristic for Δ^{7}-DA in the *strm-1* spectrum but not the *daf-9;daf-12* spectrum.

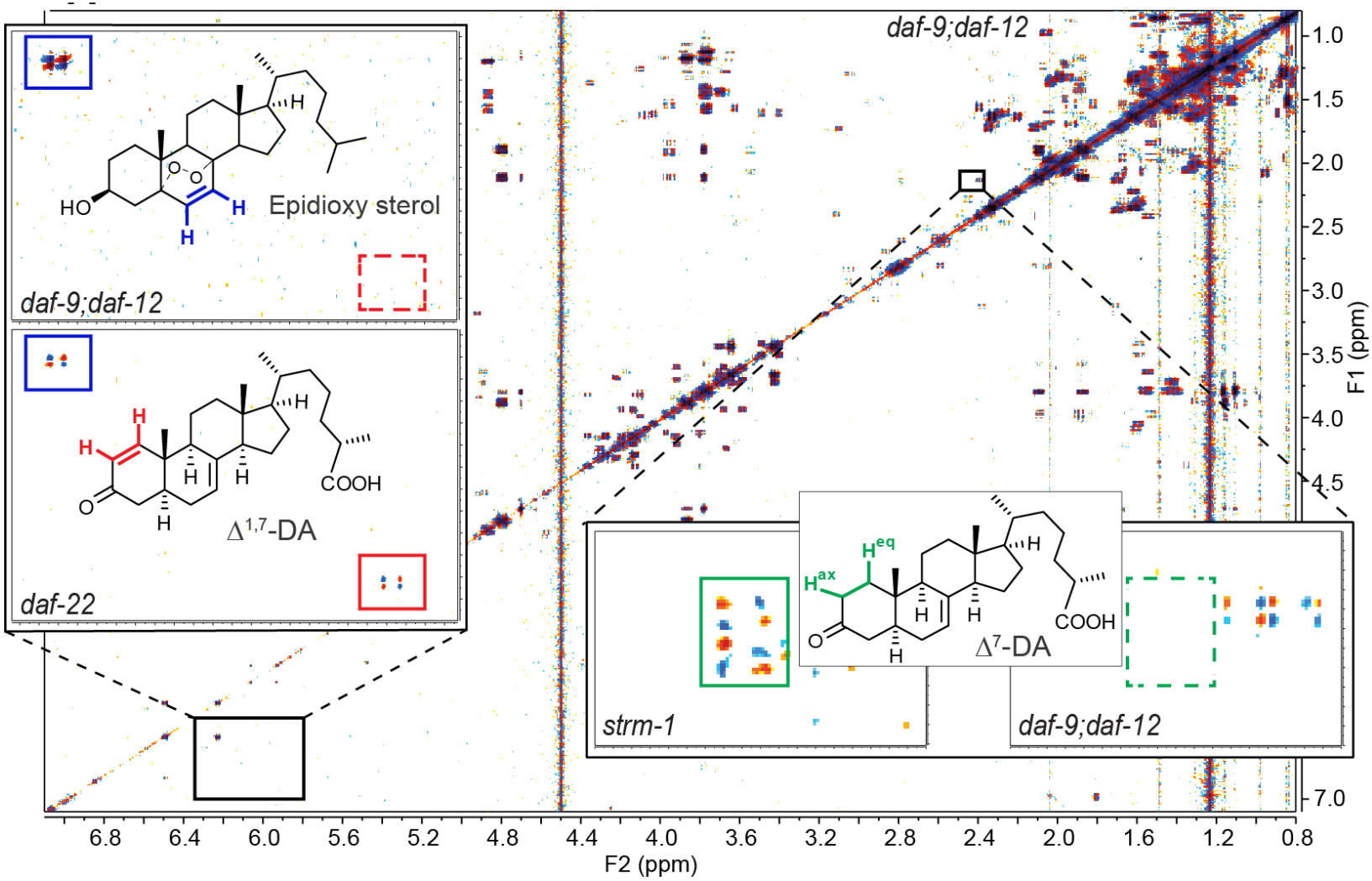
daf-9;daf-12
Epidioxy sterol
HO
daf-9;daf-12
Δ1,7-DA
COOH
daf-22
Δ7-DA
Hax
Heq
COOH
strm-1
daf-9;daf-12
F2 (ppm)
F1 (ppm)
6.8
6.4
6.0
5.6
5.2
4.8
4.4
4.0
3.6
3.2
2.8
2.4
2.0
1.6
1.2
0.8
1.0
1.5
2.0
2.5
3.0
3.5
4.0
4.5
7.0

Authentic synthetic samples of $\Delta^{1,7}$- and Δ^{7}-DA were synthesized *de novo* in our lab by Joshua Judkins and the structural assignments were confirmed by comparison of spectroscopic data and GC/MS chromatographic retention times with those of the synthetic samples (**Figure A.3**). Previous work had also suggested the specificity of the relative configuration at C-25 of the side chain and to determine the relative configuration of the chiral centers at position 25 in the sidechains of Δ^{7}-DA and $\Delta^{1,7}$-DA, we carried out an NMR spectra based titration experiment using synthetic samples of (25*S*)- and (25*R*)-diastereomers with those of the natural samples. These analyses unambiguously established the configuration of natural Δ^{7}-DA and $\Delta^{1,7}$-DA as (25*S*) (**FIGURE** 2.8).

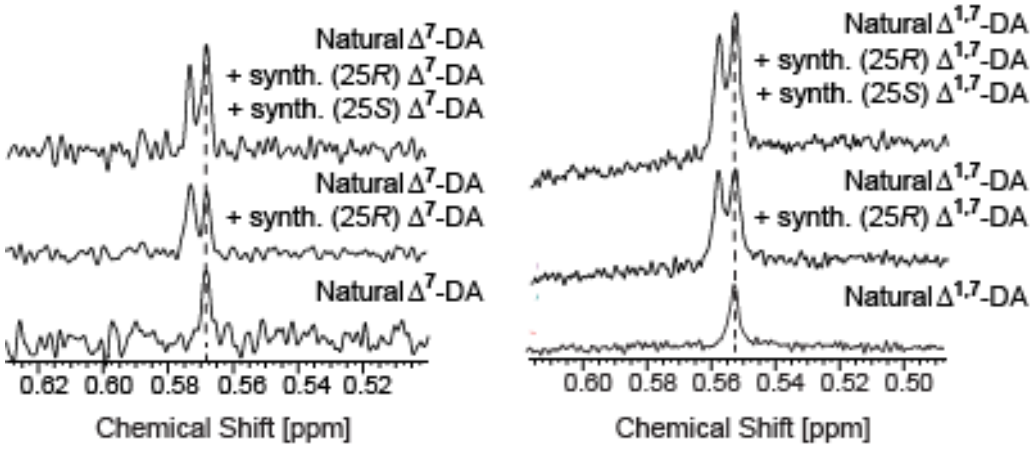

Figure 2.7. Absolute configuration of dafachronic Acids. (Left) NMR-spectroscopic determination of the absolute configuration at C-25 in natural Δ^{7}-DA. C-18 singlet region of ^{1}H NMR spectra (600 MHz, pyridine-d_5) of natural Δ^{7}-DA and mixtures with synthetic (25*R*)-Δ^{7}-DA and (25*S*)-Δ^{7}-DA. **(Right)** NMR-spectroscopic determination of the absolute configuration at C-25 in natural $\Delta^{1,7}$-DA. C-18 singlet region of ^{1}H NMR spectra (600 MHz, pyridine-d_5) of natural $\Delta^{1,7}$-DA and mixtures with synthetic (25*R*)-$\Delta^{1,7}$-DA and synthetic (25*S*)-$\Delta^{1,7}$-DA

Comparative analysis of active region II using a similar workflow showed that this region contained yet another novel steroid in much lower quantities. To conclusively identify the extremely low abundant, active component in this region, we had to acquire a 900 MHz 2D-NMR Spectrum for additional sensitivity, which led us to identify the presence of another novel *daf-9*-dependent cholestenoic acid derivative, featuring a rather unusual 3α-hydroxylation: (25*S*)-3α-hydroxy cholest-7-enoic acid ("3α-OH-Δ^7-DA") (**Figure 2.8**).

Figure 2.8. Detection of 3α-OH-Δ^7-DA in active region II. (a) Section of dqfCOSY spectrum (900 MHz, $CDCl_3$) indicating the presence of 3α-OH-Δ^7-DA in HPLC-enriched fraction of active region II. **(b)** Section of dqfCOSY spectrum (600 MHz, $CDCl_3$) of synthetic 3α-OH-Δ^7-DA. Characteristic crosspeaks of 3α-OH-Δ^7-DA are boxed red; signals from other metabolites are boxed blue.

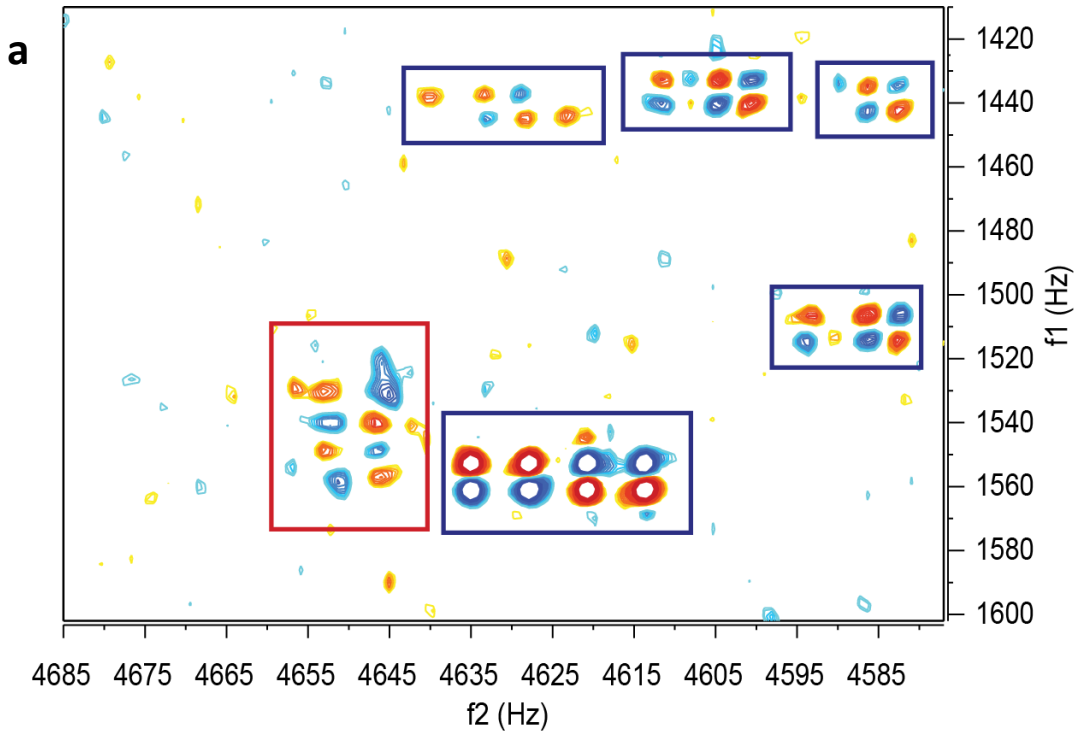
a
1420
1440
1460
1480
1500
1520
1540
1560
1580
1600
f1 (Hz)
4685 4675 4665 4655 4645 4635 4625 4615 4605 4595 4585
f2 (Hz)

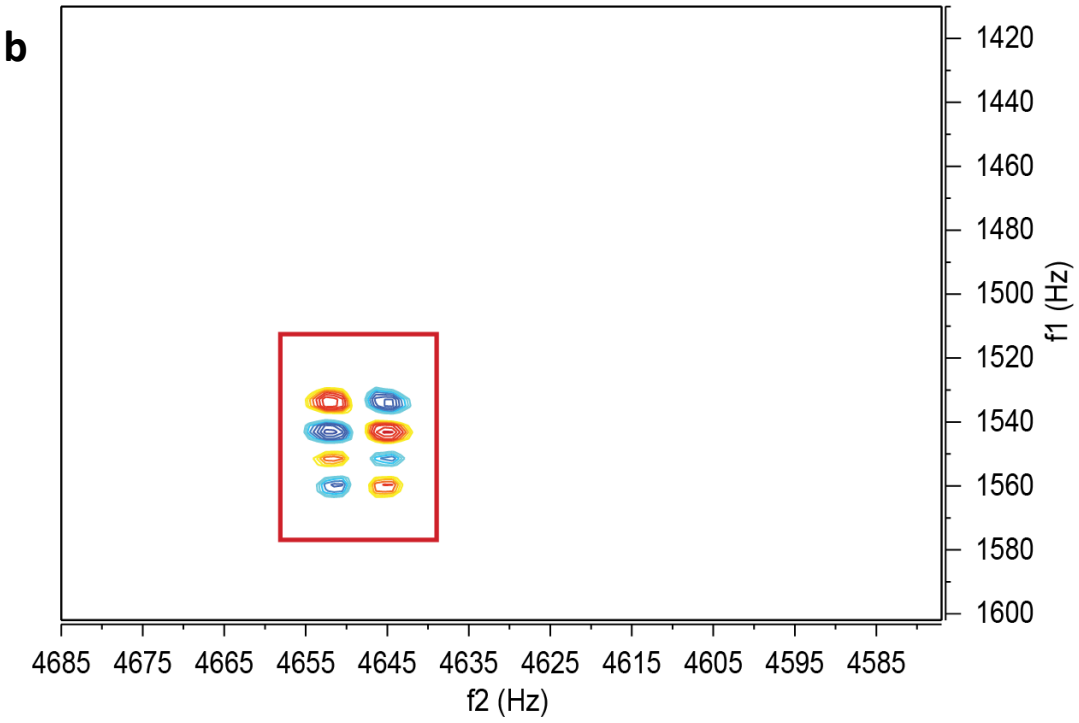
b
1420
1440
1460
1480
1500
1520
1540
1560
1580
1600
f1 (Hz)
4685 4675 4665 4655 4645 4635 4625 4615 4605 4595 4585
f2 (Hz)

Once again the comparison of 2D-NMR spectra of the natural material to that of the synthetic sample confirmed the structural assignments and the GC/MS fragmentation pattern of 3α-OH-Δ^7-DA strongly suggests that it is identical to the heretofore unidentified isomer of (25*S*)-cholest-3β-enoic acid previously reported as a DAF-12-ligand by Held et al. (**Figures A.7 and A.8**) (Held et al., 2006). As all 3-hydroxylated steroids previously described from *C. elegans* feature 3β-configuration, the identification of 3α-OH-Δ^7-DA is very surprising and suggested novel enzymatic activities in the biosynthetic scheme of DAF-12 Ligands (Chapter 3). We subsequently inspected both active and inactive *C. elegans* metabolome fractions for the presence of the corresponding 3β-stereoisomer, 3β-OH-Δ^7-DA (**Figure 2.9**); however, 3β-OH-Δ^7-DA could not be detected in either wild-type or *daf-22* mutant metabolomes, indicating that production of 3α-OH-Δ^7-DA is highly selective.

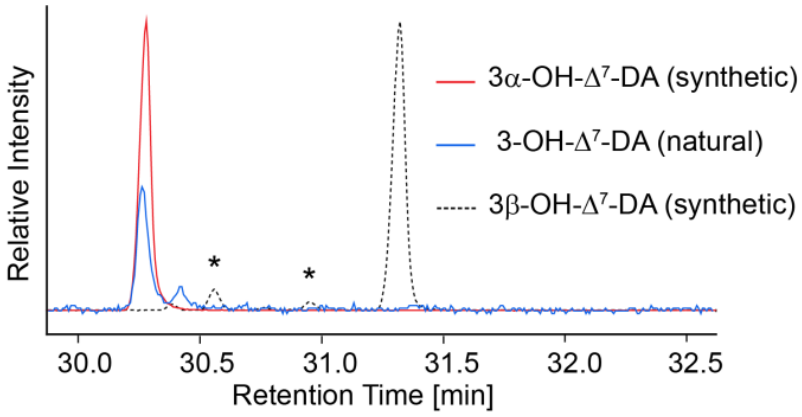

Figure 2.9. Identification of 3α-OH-Δ^7-DA in active region II. GC/MS total ion chromatograms (TIC) of synthetic 3α-OH-Δ^7-DA, synthetic 3β-OH-Δ^7-DA, and natural 3-OH-Δ^7-DA TMS derivatives. The GC retention times for the natural compound matches precisely with that of synthetic 3α-OH-Δ^7-DA and is distinctly different from that of the 3β-isomer. (*) indicates small amounts of impurities in the synthetic 3β-OH-Δ^7-DA sample.

Active region III, representing a series of metabolome fractions with comparatively low *daf-9(dh6)* dauer rescue activity, revealed trace quantities of glucosides of $\Delta^{1,7}$-DA and Δ^{7}-DA that were not characterized further as part of this study. However, future investigations on this active region would be extremely informative especially with the recent findings of multiple glycosylated derivatives of other C. elegan derived small molecules.

Using both 2D-NMR spectroscopy and SIM-GC/MS, we also checked the *daf-22* mutant and wild-type metabolomes for the presence of the previously reported Δ^{4}-DA. We were unable to detect Δ^{4}-DA in any of the analyzed *C. elegans* metabolome samples, whereas metabolome fractions spiked with trace quantities of synthetic Δ^{4}-DA confirmed the sensitivity of our MS based detection methods (**Figure 2.10**). We then considered the possibility that our growth conditions may have affected the production of the putative precursor of Δ^{4}-DA, 4-cholesten-3-one (Motola et al., 2006; Patel et al., 2008). However, analysis of wild-type metabolome samples by GC-MS and NMR spectroscopy revealed that 4-cholesten-3-one is as abundant as lathosterone (**Figure 2.11**, **Figure A.11**), a putative precursor of Δ^{7}-DA (Motola et al., 2006, Wollam et al., 2012), suggesting that absence of Δ^{4}-DA is not the result of a lack of suitable precursors. Therefore, it appears that Δ^{4}-DA may not play a significant physiological role as a DAF-12 ligand, although its transient or very low-level production cannot be excluded.

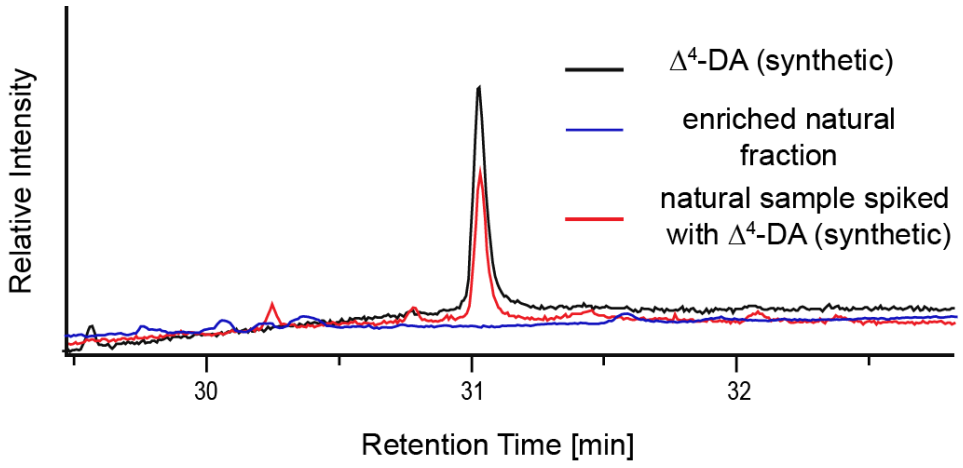

Figure 2.10. SIM-GC/MS analysis did not reveal Δ^4-DA as a significant *C. elegans* metabolite. SIM-GC/MS total ion chromatograms (TIC) of synthetic Δ^4-DA methyl ester, 1% injection of methylated inactive fraction 26 from *daf-22* to which trace amounts of synthetic Δ^4-DA (100 ng, ~20-fold less than Δ^7-, $\Delta^{1,7}$-DAs in active metabolome fractions) had been added, and 100% injection of a methylated and HPLC-enriched natural fraction matching the LC retention time of synthetic Δ^4-DA**.**

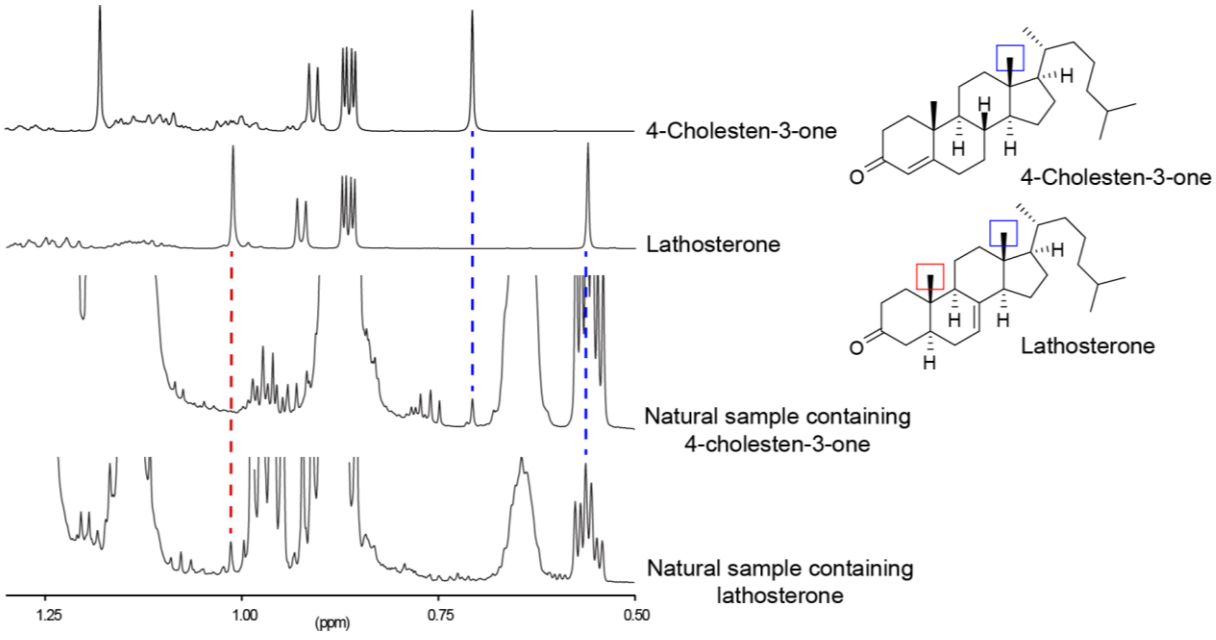

Figure 2.11. Identification of 4-cholesten-3-one and lathosterone from *daf-22*. Comparison of representative sections of ^{1}H-NMR spectra of enriched fractions from *daf-22* with synthetic 4-cholesten-3-one and lathosterone revealed the presence of the 3-keto-steroids in the natural sample.

Newly identified steroids are biologically active:

In order to confirm that the newly identified endogenous steroid molecules were indeed physiologically relevant DAF-12 ligands, we next investigated the biological properties of synthetic samples of the identified *daf-9*-dependent steroids (**Figures 2.12**). Bioassays with synthetic samples of $\Delta^{1,7}$-DA showed that this compound activates DAF-12 in mammalian cells (EC_{50} = 146 nM) and that its potency in the *daf-9(dh6)* dauer rescue assay is similar (EC_{50} = 2 nM) or slightly higher than that of Δ^{7}-DA (**Figure 2.12** and **Table A.1**). Similarly, 3α-OH-Δ^{7}-DA was active in both the *in vivo* and *in vitro* assays, whereas its 3β-stereoisomer did not activate DAF-12 in mammalian cells at any of the concentrations tested and rescued the *daf-9(dh6)* dauer phenotype only at very high concentrations (**Figure 2.12**).

We also tested the two most abundant *daf-9*-dependent compounds for their effect on lifespan in germline-deficient *glp-1* mutant worms. Germline-deficient *glp-1* mutant worms live up to 60% longer than wild-type; however, this lifespan extension has been shown to depend on functional DAF-12 and DAF-12-ligand biosynthetic enzymes (Arantes-Oliviera et al., 2003; Yamawaki et al., 2010) . Correspondingly, ligand-deficient *glp-1;daf-36* double mutant worms lack the *glp-1* lifespan extension phenotype (Gerisch et al., 2007). We found that both Δ^{7}-DA and $\Delta^{1,7}$-DA fully restore *glp-1*-dependent lifespan extension in *glp-1;daf-36* double mutants (**Figure 2.12** and **Figure A.9**).

For quantification of the identified *daf-9*-dependent steroids, we employed highly sensitive SIM-GC/MS detection of characteristic mass spectrometric fragments of volatile methylated or silylated derivatives (Extended Experimental Procedures). SIM-GC/MS showed that $\Delta^{1,7}$-DA is slightly more abundant than Δ^{7}-DA in *daf-22* worms, whereas in wild-type animals $\Delta^{1,7}$-DA is more than twice as abundant as Δ^{7}-DA, with concentrations

(averaged over the worm bodies) of 40 nM and 130 nM for Δ^7-DA and $\Delta^{1,7}$-DA, respectively (**Figure 2.12, Table A.1**). 3α-OH-Δ^7-DA occurs at about 3-5-fold lower concentrations than Δ^7-DA in both wild-type and *daf-22* mutants. Based on the specific activities determined for synthetic samples of Δ^7-DA, $\Delta^{1,7}$-DA, and 3α-OH-Δ^7-DA it appears that these three compounds can account for all of the activity in regions I and II in both wild-type and *daf-22* metabolomes.

To test whether the identified *daf-9*-dependent compounds constitute *bona-fide* ligands of DAF-12, we measured ligand dependent binding of DAF-12 with the SRC1-4 peptide containing the nuclear receptor box ("NR box") motif of mammalian coactivator SRC-1 (Motola et al., 2006; Fukuyama et al., 2006), using the Alphascreen technology. The Alphascreen is a proximity based biomolecular screening strategy commonly used for assessing direct binding ability of small molecules with nuclear hormone receptors (Glickman et al., 2002; Xu et al., 2002) among other interactions, and has been previously used for assessing binding affinity of dafachronic acids with DAF-12 (Motola, et al., 2006; Wang et al., 2009; Zhi et al., 2012). We found that Δ^7-DA, $\Delta^{1,7}$-DA and 3α-OH-Δ^7-DA effect concentration-dependent recruitment of SRC1-4, with EC_{50} values of 8 nM and 15 nM for Δ^7-DA and $\Delta^{1,7}$-DA, respectively, whereas affinity of 3α-OH-Δ^7-DA was lower (EC_{50} = 200 nM, **Figure 2.12** and **Table A.1**). These relative potencies of Δ^7-DA, $\Delta^{1,7}$-DA and 3α-OH-Δ^7-DA are similar to relative activities observed in the luciferase assay (**Figure 2.12, Table A.1**).

Figure 2.12. Biological activity of dafachronic acids. (A) Assessment of DAF-12 transcriptional activation in HEK-293T cells by the identified endogenous DAF-12-ligands. Luciferase assays were measured in triplicates and are shown with SD. (B) *Daf-9(dh6)* dauer rescue with the identified endogenous DAF-12-ligands at 27 °C. For each data point there were two replicates with 100 animals per replicate, error bars SD. (C) Both Δ^{7}-DA (100 nM) and $\Delta^{1,7}$-DA (100 nM) restore lifespan extension to *glp-1* animals in *daf-36* null background. (D) Alphascreen assay for ligand-dependent recruitment of SRC1-4 peptide by DAF-12, showing fold activation of DAF-12 with different ligand candidates over control (ethanol).

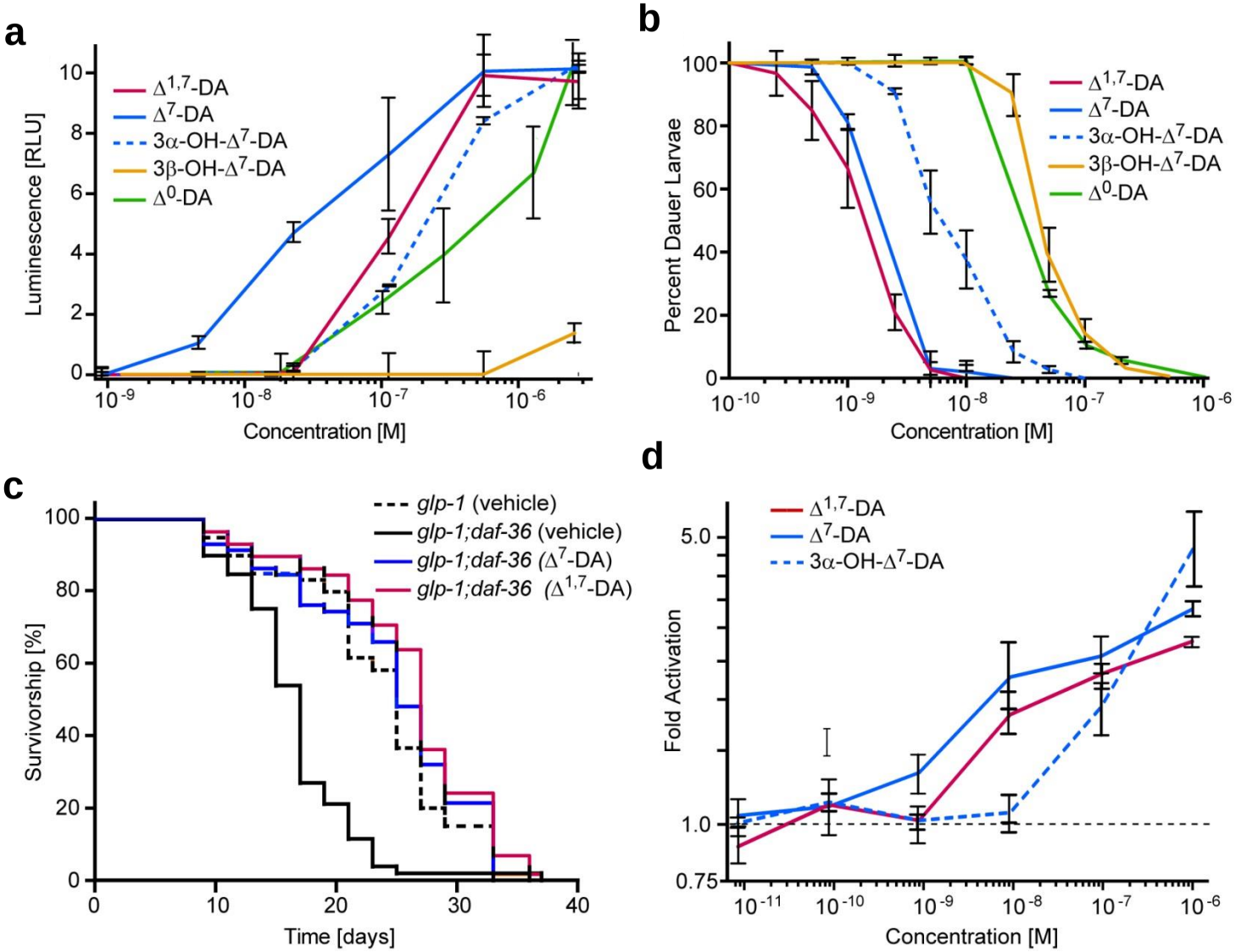
a
Luminescence [RLU]
Concentration [M]
Δ1,7-DA
Δ7-DA
3α-OH-Δ7-DA
3β-OH-Δ7-DA
Δ0-DA
b
Percent Dauer Larvae
Concentration [M]
c
Survivorship [%]
Time [days]
glp-1 (vehicle)
glp-1;daf-36 (vehicle)
glp-1;daf-36 (Δ7-DA)
glp-1;daf-36 (Δ1,7-DA)
d
Fold Activation
Concentration [M]

Taken together, these results indicate that $\Delta^{1,7}$-DA and Δ^{7}-DA are high-affinity ligands of DAF-12 that promote reproductive development and adult longevity, whereas 3α-OH-Δ^{7}-DA is of lower potency in promoting these phenotypes and Δ^{4}-DA is not present at physiologically relevant concentrations. These findings indicate a) that previous hypotheses about DAF-12-ligand structures must be revised and b) that there exists at least two novel enzymes in the biosynthetic pathway of DAF-12 ligands that have not been identified.

Conclusions and Discussion

In this chapter, the author has shown how, using 2D-NMR based comparative metabolomics changes in the metabolome can be analyzed and correlated with perturbations in the genome. This study, utilizing *C. elegans* as a model organism, has provided a systematic blue print to identify small molecule ligands of NHRs, which control key life processes in metazoans. Unique among of the 284 NHRs in *C. elegans*, DAF-12 plays a central role in regulating reproduction, development, lifespan, fat-metabolism and other essential programs in nematodes, and therefore has been the object of a large number of studies in recent years. In contrast to earlier work that was primarily based on screening candidate structures our approach has finally revealed the real, endogenous ligands of this essential transcriptional regulator in *C. elegans*.

The newly identified, $\Delta^{1,7}$-DA, is not only the most abundant ligand in wild-type worms, but also more potent, and interestingly incorporates an unsaturation in the 1,2 position in the A-ring of the steroid moiety. 1,2 unsaturated steroids are not common in animals and only one other example of the existence of this moiety in metazoans is known (Wang et al., 2009).

However, it is well known that the introduction of Δ^1 unsaturation in natural 3-keto steroids, e.g. testosterone and corticosteroids, can have pronounced effects on their biological properties (Counsell and Klimstra, 1962; Goulding and Flower, 2001). Analysis of X-ray structures of the DAF-12 ligand binding domain complexed with DAs have demonstrated that small structural changes in the A and B rings of the bound steroid have significant effects on ligand affinity to DAF-12 (Wang et al., 2009b; Zhi et al., 2012), suggesting that specific modifications in the steroid A-ring may serve to fine-tune DAF-12 transcriptional regulation. Identification of the enzyme(s) introducing the Δ^1-double bond will play an important role in elucidating functional differences between $\Delta^{1,7}$- and Δ^7-DA and may motivate re-analysis of mammalian metabolomes for the presence of endogenous Δ^1-steroids.

The additional identification of the 3α-OH-Δ^7-DA creates a striking parallel to mammalian bile acid metabolism, which produces almost exclusively sterols with 3α configuration **(Figure 2.13)** (Russell, 2003). Given its stereoselective biosynthesis by an as-yet unknown enzyme, it is likely that 3α-OH-Δ^7-DA serves specific functions in DAF-12 signaling. Notably, 3β-OH-Δ^7-DA, which is absent in wild type worms is much less active in both the *in vivo* and *in vitro* assays. However, it should be noted that both the transcriptional activation assay in mammalian cell-culture and the Alphascreen assay (**Figure 2.12**) have limited cogency for judging the relative potency of different DAF-12 ligands *in vivo*, as both assays depend on recruitment of mammalian coactivators such as SRC-1, whereas *in-vivo* function of DAF-12 is thought to involve ligand-dependent dissociation of the endogenous *C. elegans* corepressor DIN-1 followed by binding of yet unidentified co-activators (Ludewig et al., 2004). The identification of multiple endogenous small molecule regulators of DAF-12 in this study will accelerate the pursuit of yet

elusive DAF-12 interactors and other components of DAF-12-dependent dauer and lifespan regulation.

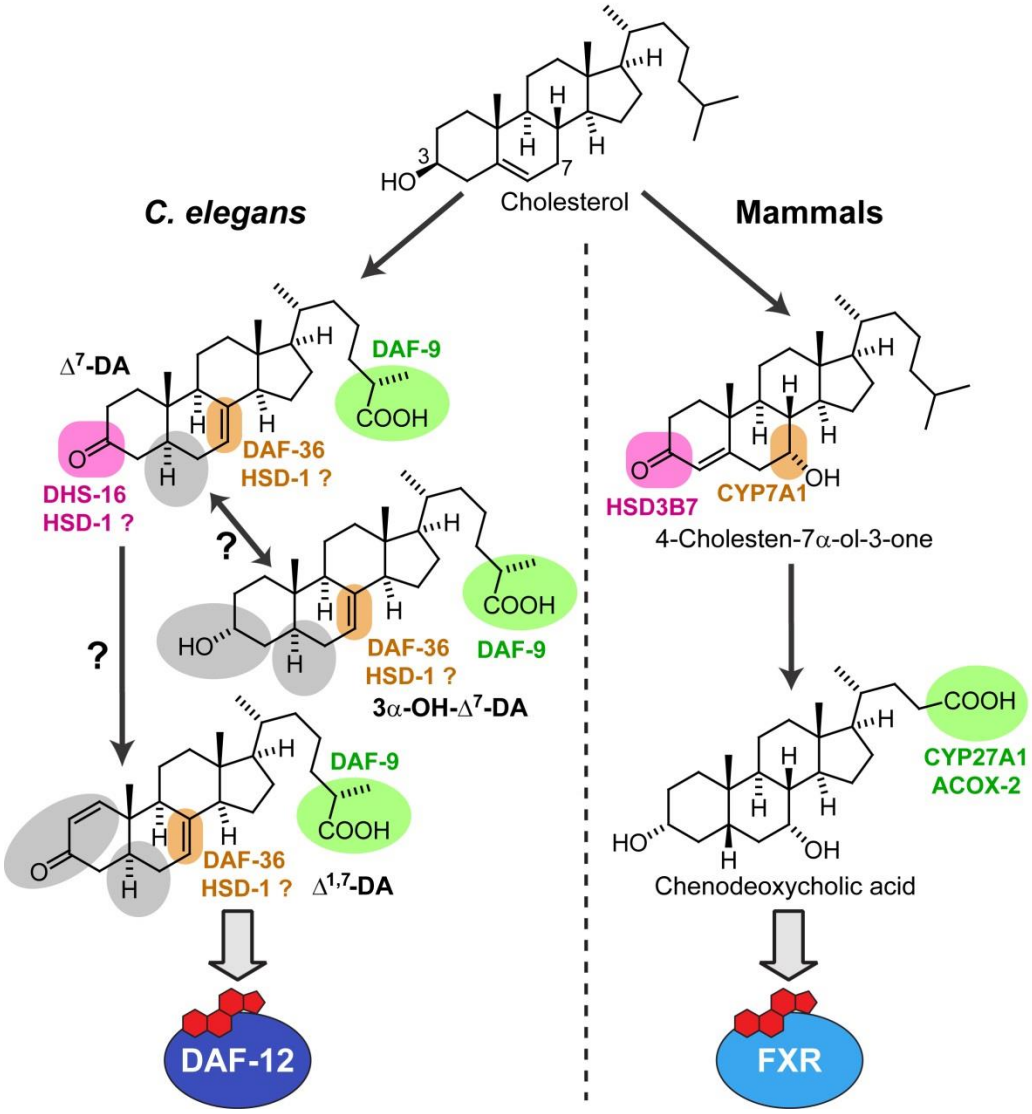

Figure 2.13. Comparison of NHR signaling in nematodes and mammals. In nematodes, oxidation/epimerization in position 3, oxidation in position 7, and side chain oxidation produces ligands of the NHR DAF-12, whereas similar modification of the steroid skeleton in mammals produces bile acids that serve as ligands of farnesoid X receptor (FXR) (Russell, 2003). Although DAF-9 has often been assumed to act directly upstream of DAF-12, our results suggest that DAF-9 may act on a variety of different substrates,E including both 3-keto and 3-hydroxy sterols. Enzymes introducing the structural features highlighted in gray are not known.

REFERENCES

Antebi, A., Yeh, W.H., Tait, D., Hedgecock, E.M., and Riddle, D.L. (2000). daf-12 encodes a nuclear receptor that regulates the dauer diapause and developmental age in C. elegans. Genes Dev *14*, 1512-1527.

Arantes-Oliveira, N., Berman, J.R., and Kenyon, C. (2003). Healthy animals with extreme longevity. Science *302*, 611.

Arda, H.E., Taubert, S., MacNeil, L.T., Conine, C.C., Tsuda, B., Van Gilst, M., Sequerra, R. Doucette-Stamm, L., Yamamoto, K.R., and Walhout, A.J. (2010). Functional modularity of nuclear hormone receptors in a Caenorhabditis elegans metabolic gene regulatory network. Mol Syst Biol *6*, 367.

Bethke, A., Fielenbach, N., Wang, Z., Mangelsdorf, D.J., and Antebi, A. (2009). Nuclear hormone receptor regulation of microRNAs controls developmental progression. Science *324*,95-98.

Brown, A.J., and Slatopolsky, E. (2008). Vitamin D analogs: therapeutic applications and mechanisms for selectivity. Mol Aspects Med *29*, 433-452.

Butcher, R.A., Ragains, J.R., Li, W., Ruvkun, G., Clardy, J., and Mak, H.Y. (2009). Biosynthesis of the Caenorhabditis elegans dauer pheromone. Proc Natl Acad Sci U S A *106*, 1875-1879.

Counsell, R.E., and Klimstra, P.D. (1962). Anabolic Agents: Derivatives of 2-Halo 5alpha-Androst-1-Ene. J Med Pharm Chem *91*, 477-483.

Dumas, K.J., Guo, C., Wang, X., Burkhart, K.B., Adams, E.J., Alam, H., and Hu, P.J. (2010). Functional divergence of dafachronic acid pathways in the control of C. elegans development and lifespan. Dev Biol *340*, 605-612.

Fielenbach, N., and Antebi, A. (2008). C. elegans dauer formation and the molecular basis of plasticity. Genes Dev *22*, 2149-2165.

Forseth, R.R., and Schroeder, F.C. (2011). NMR-spectroscopic analysis of mixtures: from structure to function. Curr Opin Chem Biol *15*, 38-47. 23

Fukuyama, M., Rougvie, A.E., and Rothman, J.H. (2006). C. elegans DAF-18/PTEN mediates nutrient-dependent arrest of cell cycle and growth in the germline. Curr Biol *16*, 773-779.

Gems, D., Sutton, A.J., Sundermeyer, M.L., Albert, P.S., King, K.V., Edgley, M.L., Larsen, P.L. and Riddle, D.L. (1998). Two pleiotropic classes of daf-2 mutation affect larval arrest, adult behavior, reproduction and longevity in Caenorhabditis elegans. Genetics *150*, 129-155.

Gerisch, B., and Antebi, A. (2004). Hormonal signals produced by DAF-9/cytochrome P450 regulate C. elegans dauer diapause in response to environmental cues. Development *131*, 1765-1776.

Gerisch, B., Rottiers, V., Li, D., Motola, D.L., Cummins, C.L., Lehrach, H., Mangelsdorf, D.J.,and Antebi, A. (2007). A bile acid-like steroid modulates Caenorhabditis elegans lifespan through nuclear receptor signaling. Proc Natl Acad Sci U S A *104*, 5014-5019.

Gerisch, B., Weitzel, C., Kober-Eisermann, C., Rottiers, V., and Antebi, A. (2001). A hormonal signaling pathway influencing C. elegans metabolism, reproductive development, and life span. Dev Cell *1*, 841-851.

Glickman J.F., Wu X, Mercuri R, Illy C, Bowen BR, He Y, Sills M. (2002). A comparison of ALPHAScreen, TR-FRET, and TRF as assay methods for FXR nuclear receptors. J Biomol Screen. 7(1), 3-10

Goulding N.J. and Flower R.J. (2001). Glucocorticoids (Milestones in Drug Therapy). BirkHouser Publishing House.

Gunatilaka, A.A.L., Gopichand, Y., Schmitz, F.J., and Djerassi, C. (1981). Minor and Trace Sterols in Marine-Invertebrates. Isolation and Structure Elucidation of 9 New 5-Alpha,8-Alpha-Epidioxy Sterols from 4 Marine Organisms. J Org Chem *46*, 3860-3866.

Hammell, C.M., Karp, X., and Ambros, V. (2009). A feedback circuit involving let-7-family miRNAs and DAF-12 integrates environmental signals and developmental timing in Caenorhabditis elegans. Proc Natl Acad Sci U S A *106*, 18668-18673.

Hannich, J.T., Entchev, E.V., Mende, F., Boytchev, H., Martin, R., Zagoriy, V., Theumer, G., Riezman, I., Riezman, H., Knolker, H.J.*, et al.* (2009). Methylation of the sterol nucleus by STRM-1 regulates dauer larva formation in Caenorhabditis elegans. Dev Cell *16*, 833-843.

Held, J.M., White, M.P., Fisher, A.L., Gibson, B.W., Lithgow, G.J., and Gill, M.S. (2006). DAF-12-dependent rescue of dauer formation in Caenorhabditis elegans by (25S)-cholestenoic acid. Aging Cell *5*, 283-291.24

Hulme, S.E., and Whitesides, G.M. (2011). Chemistry and the worm: Caenorhabditis elegans as a platform for integrating chemical and biological research. Angew Chem Int Ed Engl *50*, 4774-4807.

Jia, K., Albert, P.S., and Riddle, D.L. (2002). DAF-9, a cytochrome P450 regulating C. elegans larval development and adult longevity. Development *129*, 221-231.

Kenyon, C. (2010). A pathway that links reproductive status to lifespan in Caenorhabditis elegans. Ann N Y Acad Sci *1204*, 156-162.

Larsen, P.L., Albert, P.S., and Riddle, D.L. (1995). Genes that regulate both development and longevity in Caenorhabditis elegans. Genetics *139*, 1567-1583.

Ludewig, A.H., Kober-Eisermann, C., Weitzel, C., Bethke, A., Neubert, K., Gerisch, B., Hutter, H., and Antebi, A. (2004). A novel nuclear receptor/coregulator complex controls C. elegans lipid metabolism, larval development, and aging. Genes Dev *18*, 2120-2133.

Mangelsdorf, D.J., Thummel, C., Beato, M., Herrlich, P., Schutz, G., Umesono, K., Blumberg, B., Kastner, P., Mark, M., Chambon, P.*, et al.* (1995). The nuclear receptor superfamily: the second decade. Cell *83*, 835-839.

Motola, D.L., Cummins, C.L., Rottiers, V., Sharma, K.K., Li, T., Li, Y., Suino-Powell, K., Xu, H.E., Auchus, R.J., Antebi, A.*, et al.* (2006). Identification of ligands for DAF-12 that govern dauer formation and reproduction in C. elegans. Cell *124*, 1209-1223.

Ogawa, A., Streit, A., Antebi, A., and Sommer, R.J. (2009). A conserved endocrine mechanism controls the formation of dauer and infective larvae in nematodes. Curr Biol *19*, 67-71.

Patel, D.S., Fang, L.L., Svy, D.K., Ruvkun, G., and Li, W. (2008). Genetic identification of HSD-1, a conserved steroidogenic enzyme that directs larval development in Caenorhabditis elegans. Development *135*, 2239-2249.

Pungaliya, C., Srinivasan, J., Fox, B.W., Malik, R.U., Ludewig, A.H., Sternberg, P.W., and Schroeder, F.C. (2009). A shortcut to identifying small molecule signals that regulate behavior and development in Caenorhabditis elegans. Proc Natl Acad Sci USA *106*, 7708-7713.

Robinette, S.L., Bruschweiler, R., Schroeder, F.C., and Edison, A.S. (2011). NMR in Metabolomics and Natural Products Research: Two Sides of the Same Coin. Acc Chem. Res.

Rottiers, V., Motola, D.L., Gerisch, B., Cummins, C.L., Nishiwaki, K., Mangelsdorf, D.J., and Antebi, A. (2006). Hormonal control of C. elegans dauer formation and life span by a Rieske-like oxygenase. Dev Cell *10*, 473-482.

Russell, D.W. (2003). The enzymes, regulation, and genetics of bile acid synthesis. Annu Rev Biochem *72*, 137-174.

Schaedel, O.N., Gerisch, B., Antebi, A., and Sternberg, P.W. (2012). Hormonal Signal Amplification Mediates Environmental Conditions during Development and Controls an Irreversible Commitment to Adulthood. PLoS Biol *10*, e1001306.

Schupp, M., and Lazar, M.A. (2010). Endogenous ligands for nuclear receptors: digging deeper. J Biol Chem *285*, 40409-40415.

Sera, Y., Adachi, K., and Shizuri, Y. (1999). A new epidioxy sterol as an antifouling substance from a palauan marine sponge, lendenfeldia chondrodes. J Nat Prod *62*, 152-154.

Shen, Y., Wollam, J., Magner, D., Karalay, O., and Antebi, A. (2012). A steroid receptor microRNA switch regulates life span in response to signals from the gonad. Science *338*, 1472-1476.

Singarapu, K.K., Zhu, J., Tonelli, M., Rao, H., Assadi-Porter, F.M., Westler, W.M., DeLuca, H.F., and Markley, J.L. (2011). Ligand-specific structural changes in the vitamin D receptor in solution. Biochemistry *50*, 11025-11033.

Taubert, S., Ward, J.D., and Yamamoto, K.R. (2010). Nuclear hormone receptors in nematodes: evolution and function. Mol Cell Endocrinol *334*, 49-55.

Theofilopoulos, S., Wang, Y., Kitambi, S.S., Sacchetti, P., Sousa, K.M., Bodin, K., Kirk, J., Salto, C., Gustafsson, M., Toledo, E.M.*, et al.* (2013). Brain endogenous liver X receptor ligands selectively promote midbrain neurogenesis. Nature chemical biology *9*, 126-133.

von Reuss, S.H., Bose, N., Srinivasan, J., Yim, J.J., Judkins, J.C., Sternberg, P.W., and Schroeder, F.C. (2012). Comparative metabolomics reveals biogenesis of ascarosides, a modular library of small molecule signals in C. elegans. J Am Chem Soc *134*, 1817–1824.

Wang, W., Lee, J.S., Nakazawa, T., Ukai, K., Mangindaan, R.E., Wewengkang, D.S., Rotinsulu, H., Kobayashi, H., Tsukamoto, S., and Namikoshi, M. (2009a). (25S)-cholesten-26-oic acid derivatives from an Indonesian soft coral Minabea sp. Steroids *74*, 758-760.

Wang, Z., Zhou, X.E., Motola, D.L., Gao, X., Suino-Powell, K., Conneely, A., Ogata, C., Sharma, K.K., Auchus, R.J., Lok, J.B.*, et al.* (2009b). Identification of the nuclear receptor DAF-12 as a therapeutic target in parasitic nematodes. Proc Natl Acad Sci U S A *106*, 9138-9143.

Williams, T.W., Dumas, K.J., and Hu, P.J. (2010). EAK proteins: novel conserved regulators of C. elegans lifespan. Aging (Albany NY) *2*, 742-747.

Wollam, J., and Antebi, A. (2011). Sterol regulation of metabolism, homeostasis, and development. Annu Rev Biochem *80*, 885-916.

Wollam, J., Magner, D.B., Magomedova, L., Rass, E., Shen, Y., Rottiers, V., Habermann, B., Cummins, C.L., and Antebi, A. (2012). A Novel 3-Hydroxysteroid Dehydrogenase That Regulates Reproductive Development and Longevity. PLoS Biol *10*, e1001305.

Wollam, J., Magomedova, L., Magner, D.B., Shen, Y., Rottiers, V., Motola, D.L., Mangelsdorf, D.J., Cummins, C.L., and Antebi, A. (2011). The Rieske oxygenase DAF-36 functions as a cholesterol 7-desaturase in steroidogenic pathways governing longevity. Aging Cell *10*, 879-884.

Xu H.E., Stanley T.B., Montana V.G., Lambert M.H., Shearer B.G, Cobb J.E.,. McKee D.D., Galardi C.M., Plunket K.D., Nolte R.T., Parks D.J., Moore J.T., Kliewer S.A., Willson T.M., Stimmel J.B. (2002). Structural basis for antagonist-mediated recruitment of nuclear co-repressors. Nature 415, 813-7

Yamawaki, T.M., Berman, J.R., Suchanek-Kavipurapu, M., McCormick, M., Gaglia, M.M., Lee, S.J., and Kenyon, C. (2010). The somatic reproductive tissues of C. elegans promote longevity through steroid hormone signaling. PLoS Biol *8*.

Yoshiyama-Yanagawa, T., Enya, S., Shimada-Niwa, Y., Yaguchi, S., Haramoto, Y., Matsuya, T., Shiomi, K., Sasakura, Y., Takahashi, S., Asashima, M.*, et al.* (2011). The conserved Rieske oxygenase DAF-36/Neverland is a novel cholesterol-metabolizing enzyme. J Biol Chem *286*, 25756-25762.

Zhi, X., Zhou, X.E., Melcher, K., Motola, D.L., Gelmedin, V., Hawdon, J., Kliewer, S.A., Mangelsdorf, D.J., and Xu, H.E. (2012). Structural conservation of ligand binding reveals a bile acid-like signaling pathway in nematodes. J Biol Chem *287*, 4894-4903.

CHAPTER 3

COMPARATIVE METABOLOMICS ANALYSIS OF DA BIOSYNTHESIS MUTANTS REVEAL NOVEL PATHWAYS OF STEROID HORMONE PRODUCTION

Introduction:

Prior to this study, none of the structures of the proposed DAF-12 ligands had been confirmed based on comprehensive spectroscopic analysis and the previous chapter described how this study achieves the identification of endogenous DAF-12 ligands. However, based on the putative ligand structures (Motola, 2006; Δ^4- and Δ^7-dafachronic acids) a biosynthesis model has been developed (**Figure 3.1**) and the biochemical roles of genes proposed to function upstream of DAF-9 in DAF-12-ligand biosynthesis have been studied extensively (Dumas et al., 2010; Patel et al., 2008; Rottiers, 2006; Williams et al., 2010; Wollam et al., 2011; Yoshiyama-Yanagawa et al., 2011; Hannich et al., 2009).

In each of these studies it has been assumed that there are two distinct, parallel pathways emanating from exogenous cholesterol that leads to the biosynthesis of Δ^4- and Δ^7-dafachronic acid. DAF-12-ligand biosynthesis begins with oxidation of cholesterol by the Rieske-like oxygenase DAF-36 yielding 7-dehydrocholesterol (Gerisch et al., 2007; Rottiers et al., 2006; Wollam et al., 2011; Yoshiyama-Yanagawa et al., 2011). 7-dehydrocholesterol is converted by an as yet unidentified enzyme to lathosterol, which is subsequently oxidized to the corresponding ketone, lathosterone, by the short-chain dehydrogenase, DHS-16 (Wollam et al., 2012). Lathosterone is then converted to Δ7-DA by DAF-9 (Gerisch and Antebi, 2004; Gerisch et al., 2007;

Motola et al., 2006). In addition, a parallel pathway for the biosynthesis of Δ4-DA involving the putative hydroxysteroid dehydrogenase, HSD-1, has been proposed (Dumas et al., 2010; Patel et al., 2008), although recent evidence suggests that HSD-1 has no role in the production of the putative precursor of Δ4-DA, 4-cholesten-3-one (Wollam et al., 2012), leaving its role in DAF-12 ligand biosynthesis undetermined (**Figure 3.1**). However, with our recent findings in Chapter 2 that a) Δ^4-dafachronic acid is not present in whole worm extracts in physiologically relevant concentrations; b) $\Delta^{1,7}$ -dafachronic acid is the most abundant dafachronic acid endogenously produced in *C. elegans*; and c) *C. elegans*, and presumably other nematodes (Zhi, 2012), possess the enzymatic machinery to manipulate the 3-position in the steroid A-ring as corroborated by the identification of 3α-OH-Δ^7-DA it becomes imperative to reinvestigate the role of these putative steroid biosynthetic enzymes in the context of DAF-12-ligand biosynthesis.

More recent work has shown that the proposed DAF-12 ligands do not explain all DAF-12 associated functions and has suggested a functionally divergent biosynthetic network with the possibility of alternative DAs (Dumas, 2010), a hypothesis confirmed by the results reported in the previous chapter. These results taken together indicate that the DAF-12-ligand biosynthetic pathway is more complex than originally thought and the identities of several enzymes, which likely constitute important regulatory nodes controlling DAF-12 activity, still remain unknown,.

In this chapter, the author describes how utilizing a multidisciplinary and collaborative approach combining chromatographic separation; NMR Spectroscopy and GC/MS analysis (in collaboration with Neelanjan Bose, Frank Schroeder Lab and Daniel Magner, Adam Antebi Lab); chemical syntheses (in collaboration with Joshua Judkins, Frank Schroeder Lab);

genetic screening and biochemical methods (in collaboration with Joshua Wollam, Adam Antebi Lab), the sterol metabolome of *C. elegans* was analyzed. In the process, several striking pieces of evidence, including the identity of a novel cytochrome p450 involved in the biotransformation of DAF-12 ligands were discovered, which reveal several novel pathways for DAF-12-ligand production strongly suggesting that the accepted ligand-biosynthetic pathway require substantial revision.

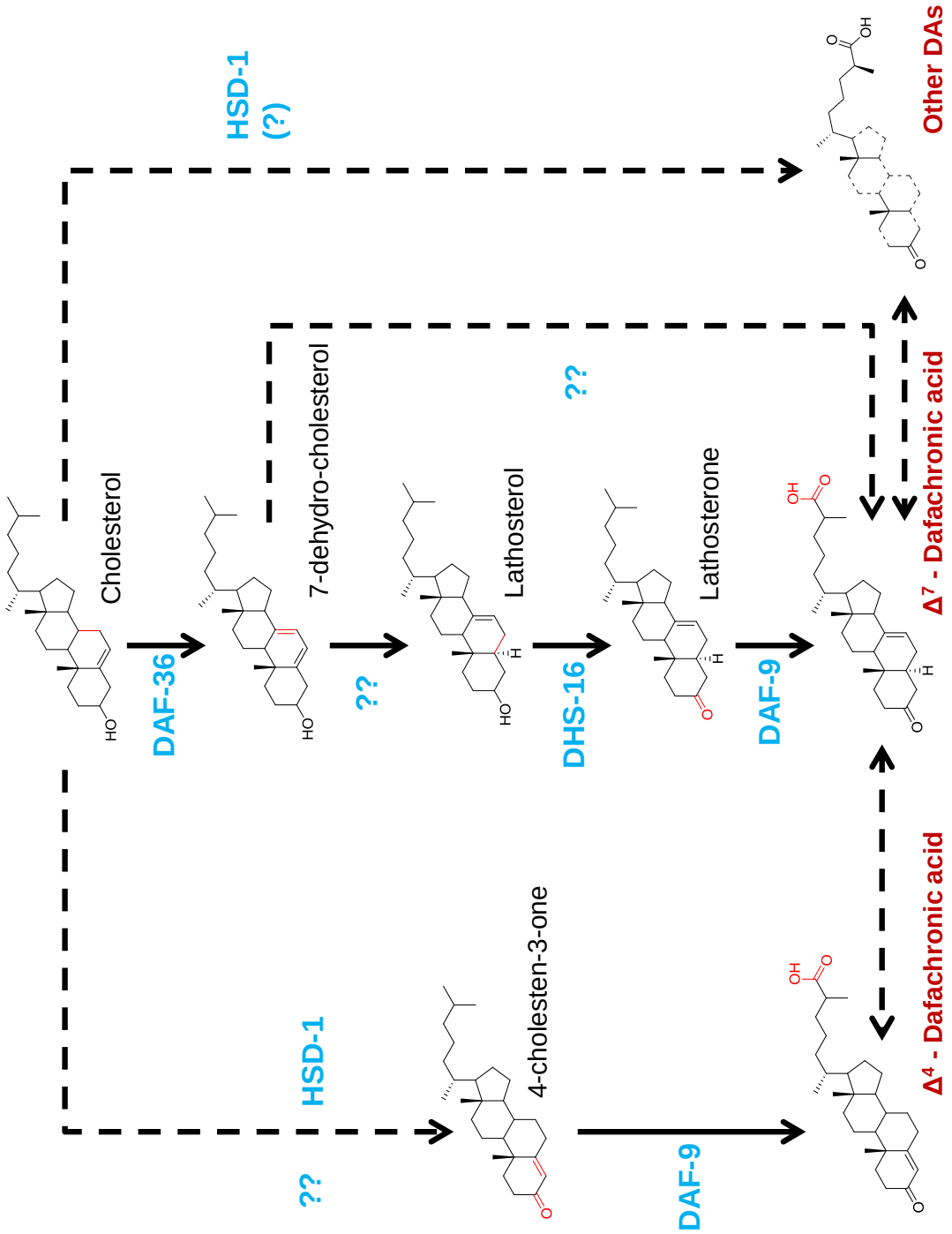

Figure 3.1 Putative Biosynthetic Pathway of Dafachronic Acids. Figure adapted from Wollam, 2012; Patel, 2008, Rottiers, 2006, Dumas, 2010 and this work (Chapter 2).

Comparative Metabolomics Suggest Tissue Specific Ligand Biosynthesis:

Intrigued by the extremely low abundance of the previously proposed DAF-12-ligand Δ^4-dafachronic acid in *C. elegans* whole worm extracts we began our biosynthetic analysis analysis with profiling *hsd-1*mutants and *hsd-1;daf-22* double mutants, since HSD-1 has been proposed to be enzymatically responsible for the conversion of cholesterol to Δ^4-cholestenone. Whereas *hsd-1* fractions contained only very small amounts of dauer rescuing activity, the activity profile of *hsd-1;daf-22* fractions was very similar to that of *daf-22* single mutant fractions, consistent with the hypothesis that production of dauer pheromone via DAF-22 downregulates DAF-12-ligand production (**Figure 3.2**).

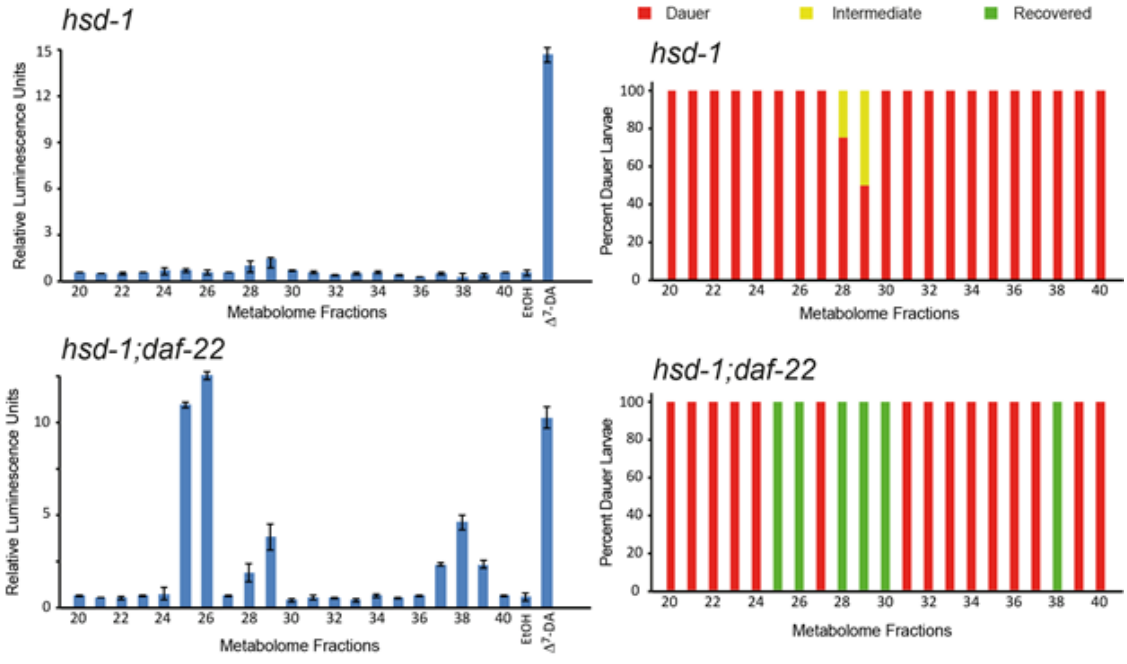

Figure 3.2 Bioactivity of hsd-1 metabolome fractions. Assessment of DAF-12 ligand content using the *in vitro* luciferase assay in HEK-293T cells (left) and the *in vivo daf-9(dh6)* dauer rescue (right) with metabolome fractions from **(Top)** *hsd-1*, **(Bottom)** *hsd-1;daf-22*

However, comparative metabolomic analysis of *hsd-1;daf-22* region I revealed production of large quantities of an additional steroid in *hsd-1;daf-22* worms that is not produced in either *daf-22* or *daf-9;daf-12* mutants. Subsequent NMR spectroscopic analysis and comparison with a synthetic sample led to the identification of this *hsd-1*-specific steroid as (25*S*)-3-keto-cholestanoic acid ("Δ^0-DA", **Figure 3.3**). This fully saturated DA derivative is active in both the DAF-12 luciferase assay and the *daf-9(dh6)* dauer rescue assay, although its activity is lower than that of $\Delta^{1,7}$-and Δ^7-DA (**Figure 3.4**). Δ^0-DA was absent in wild-type and *daf-22* metabolomes, as determined by NMR spectroscopy and SIM-GC/MS. Analysis of *hsd-1;daf-22* activity region II revealed a second *hsd-1*-specific steroid, 3β-OH-Δ^7-DA (**Figure B.1**). In *hsd-1;daf-22* mutants, 3β-OH-Δ^7-DA is as abundant as the 3α-isomer, whereas 3β-OH-Δ^7-DA is absent in both wild-type and *daf-22* mutants. GC/MS analysis of *hsd-1;daf-22* activity region I further revealed that amounts of both $\Delta^{1,7}$- and Δ^7-DA are slightly reduced compared to *daf-22* worms, whereby production of Δ^7-DA may be more strongly affected than that of $\Delta^{1,7}$-DA (**Figure 3.5**). The identification of 3β-OH-Δ^7-DA and Δ^0-DA in *hsd-1;daf-22* mutant worms suggests that HSD-1 may directly or indirectly participate in the biosynthesis of Δ^7-DA and possibly $\Delta^{1,7}$-DA. HSD-1 has homology to mammalian 3β-hydroxysteroid dehydrogenases (Patel et al., 2008), which suggested its participation in introducing the 3-keto functionality in Δ^4-DA. The absence of Δ^4-DA and our identification of Δ^0-DA as a shunt metabolite in *hsd-1;daf-22* mutants may indicate that the *hsd-1* pathway includes introduction of the 7,8-double bond in a saturated precursor, for example cholestanol, 3β-OH-Δ^0-DA, or Δ^0-DA, by an as-yet unknown enzyme, or that HSD-1 itself has 7-dehydrogenase activity. Notably, HSD-1 is expressed mainly in the neuron-like XXX cells, which lack expression of the Rieske-like oxygenase, DAF-36, required for biosynthesis of

most 7,8-unsaturated steroids in *C. elegans (*Wollam et al., 2011; Yoshiyama-Yanagawa et al., 2011) . Taken together, our results suggest that HSD-1 contributes to Δ^7-DA biosynthesis in the XXX cells, but that Δ^7-DA and $\Delta^{1,7}$-DA are produced via a separate pathway in other tissues.

Figure 3.3. Identification of Δ^0-DA in active region I of *hsd-1;daf-22*. Sections of dqfCOSY spectra (600 MHz, $CDCl_3$) used for identification of Δ^0-DA. **(a)** HPLC-enriched fraction from *hsd-1;daf-22* mutant. **(b)** Synthetic Δ^0-DA. Crosspeaks characteristic for Δ^0-DA are boxed blue.

a

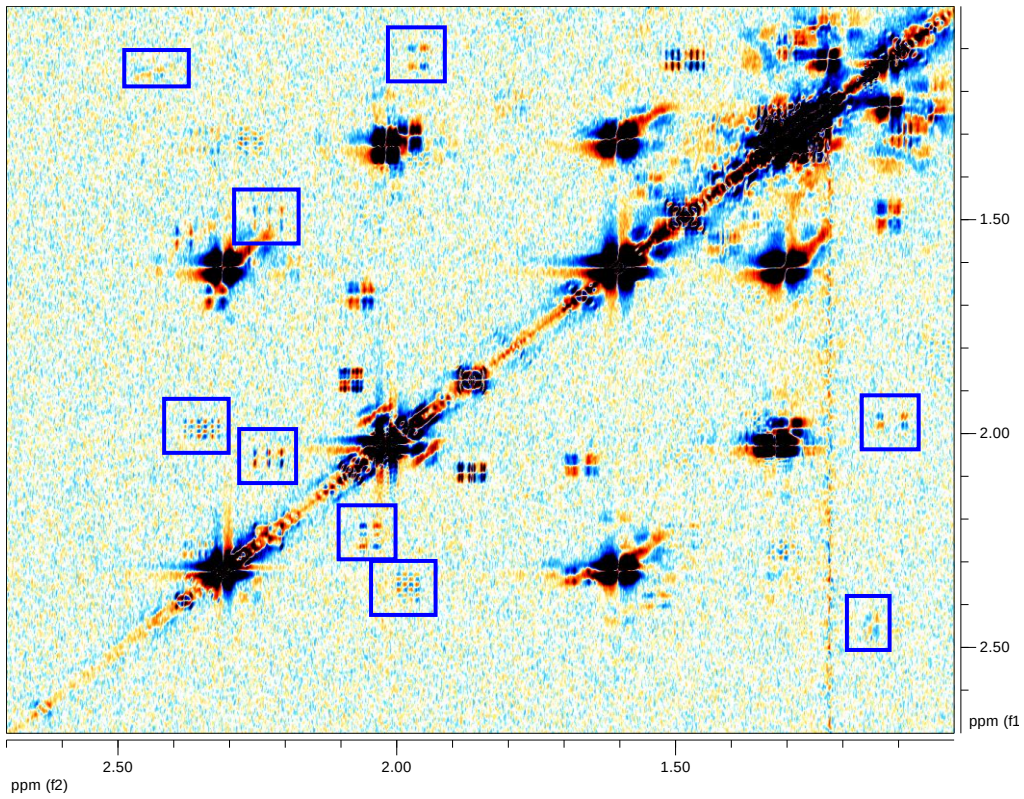
1.50
2.00
2.50
ppm (f1
2.50
2.00
1.50
ppm (f2)

b

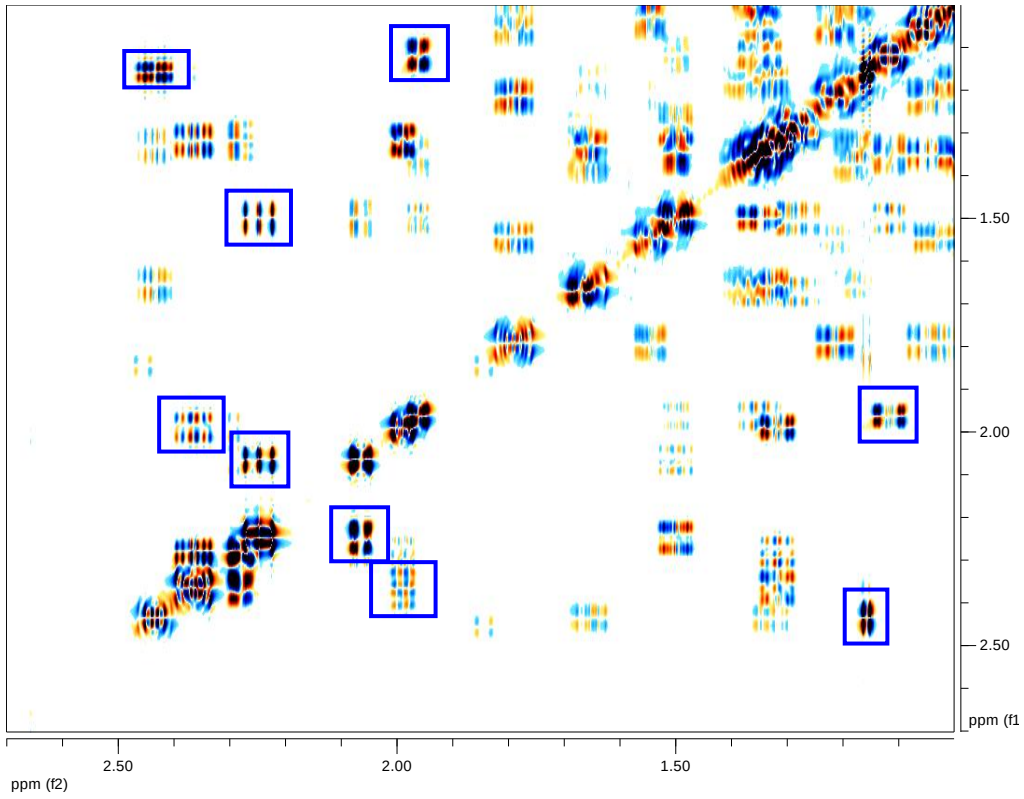
1.50
2.00
2.50
ppm (f1
2.50
2.00
1.50
ppm (f2)

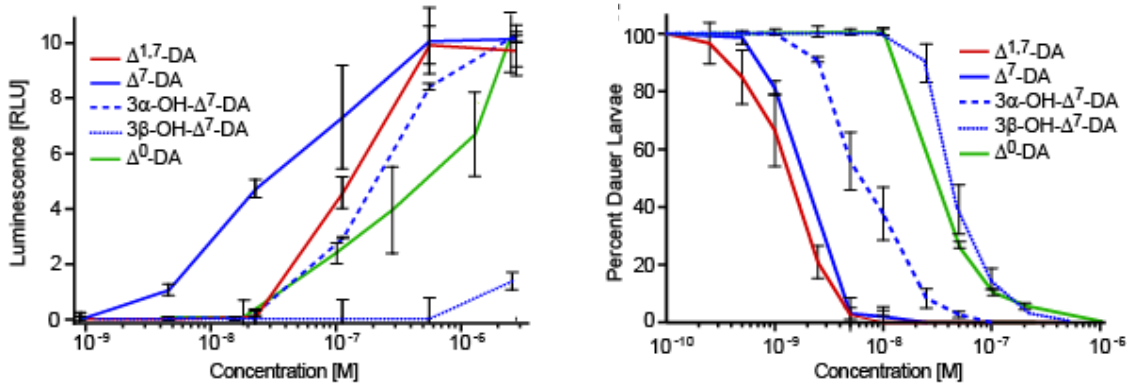

Figure 3.4. Biological acitivity of DAs identified in this study. **(Left)** Assessment of DAF-12 transcriptional activation in HEK-293T cells by the identified endogenous DAF-12-ligands. Luciferase assays were measured in triplicates and are shown with SD. **(Right)** *Daf-9(dh6)* dauer rescue with the identified endogenous DAF-12-ligands at 27 °C. For each data point there were two replicates with 100 animals per replicate, error bars SD.

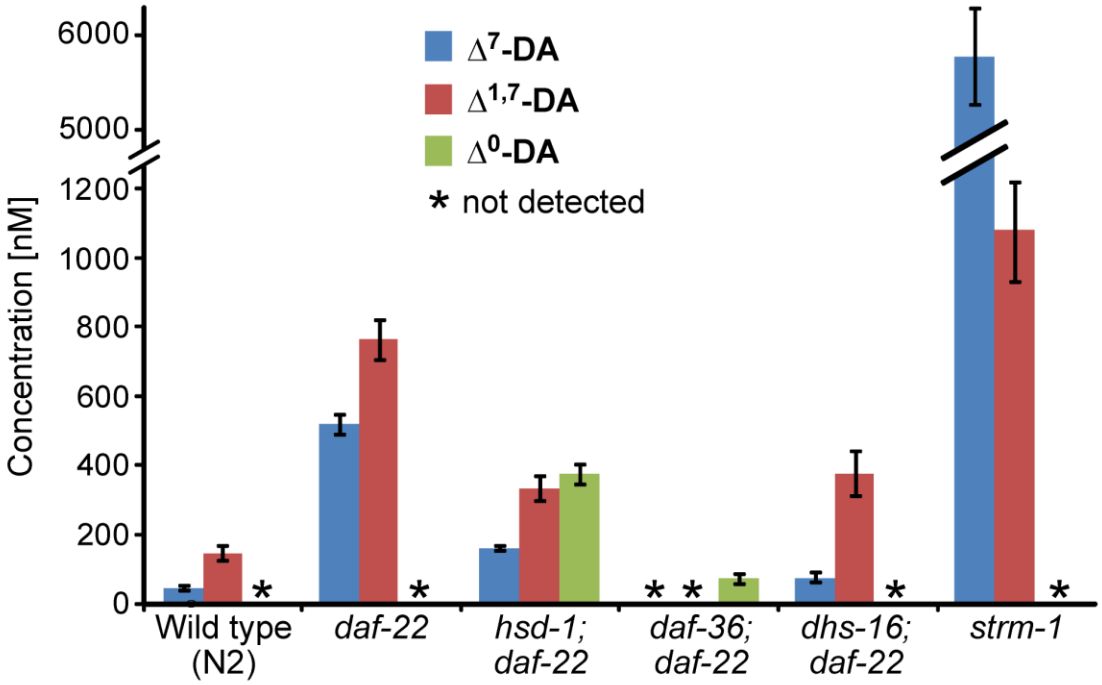

Figure 3.5. Endogenous concentrations of DAs. *In vivo* concentrations of Δ^7-DA, $\Delta^{1,7}$-DA, and Δ^0-DA derived from SIM-GC/MS-based quantification in wild-type (N2), *daf-22*, and steroid metabolism mutants (error bars, SD).

Next, we investigated the DAF-12-ligand profile of mutants of the Rieske-like oxygenase, DAF-36 [2-3]. Mutants of *daf-36*, which is expressed primarily in the worm intestine, exhibit phenotypes consistent with strongly reduced DAF-12-ligand biosynthesis, such as a higher tendency to enter dauer (Rottiers et al., 2006). As in the case of *hsd-1* mutants, we found *daf-36* mutant metabolome fractions to be largely inactive in the dauer rescue and luciferase assays, whereas *daf-36;daf-22* double mutants produced significant dauer rescue activity in region I (**Figure 3.7**). GC/MS analysis revealed the presence of saturated Δ^0-DA in this region (**Figure B.2**), which we had previously found only in *hsd-1;daf-22* mutants. In contrast to *hsd-1;daf-22* mutants, Δ^0-DA appears to be responsible for all of the activity observed in *daf-36;daf-22* region I, since neither Δ^7- nor $\Delta^{1,7}$-DA were detectable in this mutant. Total DAF-12-ligand amounts were much lower in the *daf-36;daf-22* metabolome than in *hsd-1;daf-22* (**Figure 3.5**). These results indicate that the intestinally expressed 7,8-dehydrogenase, DAF-36, is required for Δ^7- and $\Delta^{1,7}$-DA biosynthesis, whereas HSD-1 contributes to additional production of Δ^7-unsaturated DAs in the XXX cells. It thus appears that the biosynthesis of Δ^7- and $\Delta^{1,7}$-DA relies on partially redundant and tissue-specific pathways.

Biosynthesis of Different Ligands is Differentially Regulated:

Whereas the hsd-1 mutation did not significantly affected the relative abundance of $\Delta^{1,7}$- and Δ^7-DA, mutations of two other genes involved in DAF-12-ligand biosynthesis and regulation, the short-chain dehydrogenase, dhs-16 (Wollam et al., 2012), and the methyltransferase, strm-1 (Hannich et al., 2009), showed strongly altered ligand ratios. Analysis of the *dhs-16;daf-22* metabolome revealed greatly reduced production of Δ^7-DA, whereas $\Delta^{1,7}$-DA levels were reduced only slightly (**Figures 3.5 and B.3**). These results indicate

that $\Delta^{1,7}$- and Δ^{7}-DA may be derived from partially divergent biosynthetic pathways or that deletion of DHS-16 indirectly affects regulation of the $\Delta^{1,7}$-DA to Δ^{7}-DA ratio. Only trace quantities of 3α-OH-Δ^{7}-DA were detected in *dhs-16;daf-22* worms, indicating that production of both 3α-OH-Δ^{7}-DA and Δ^{7}-DA are DHS-16-dependent. Next, we characterized the DAF-12-ligand profile of strm-1 mutants (**Figure B.3**), which had previously been shown to produce elevated levels of DAF-12-ligands (Hannich et al., 2009). The methyltransferase, STRM-1, regulates DAF-12-ligand levels by converting cholesterol-derived intermediates of ligand biosynthesis into 4-methylated steroids, thereby rendering them unsuitable as ligand precursors (Hannich et al., 2009). NMR spectroscopy and SIM-GC/MS analyses revealed more than 100-fold increased levels of Δ^{7}-DA in strm-1 mutant metabolomes whereas $\Delta^{1,7}$-DA levels increased only about 7-fold compared to wild-type (**Figure 3.5**). These results provide further evidence for differential regulation of $\Delta^{1,7}$- and Δ^{7}-DA biosynthesis.

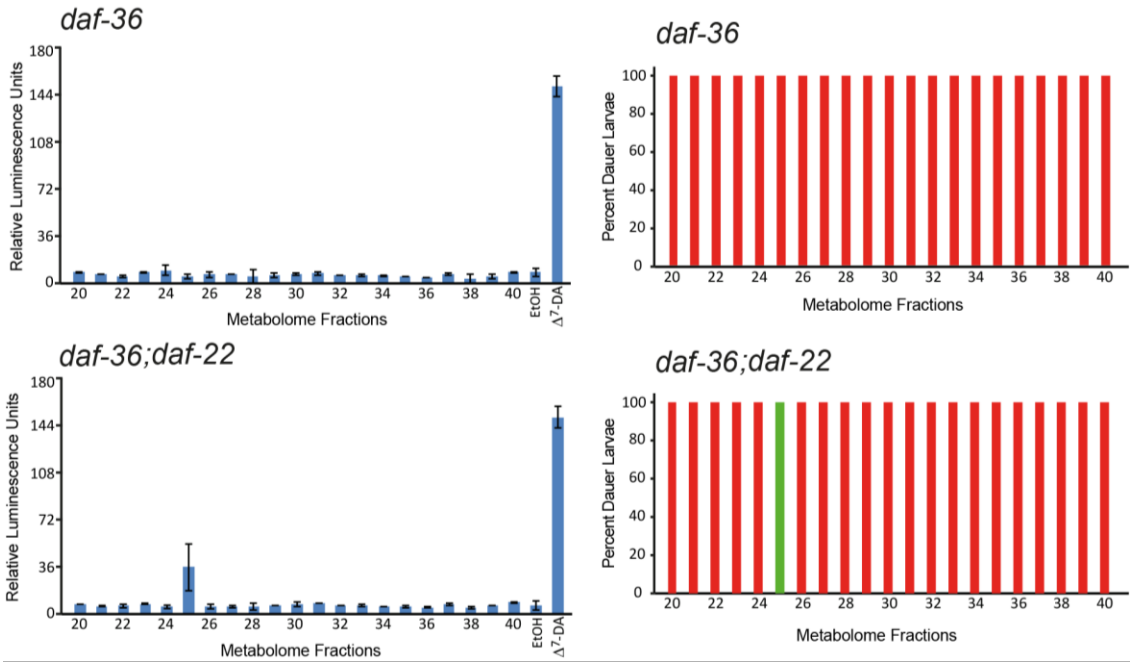

Figure 3.6. Bioactivity of hsd-1 metabolome fractions. Assessment of DAF-12 ligand content using the *in vitro* luciferase assay in HEK-293T cells (left) and the *in vivo daf-9(dh6)* dauer rescue (right) with metabolome fractions from **(Top)** *daf-36*, **(Bottom)** *daf-36;daf-22.*

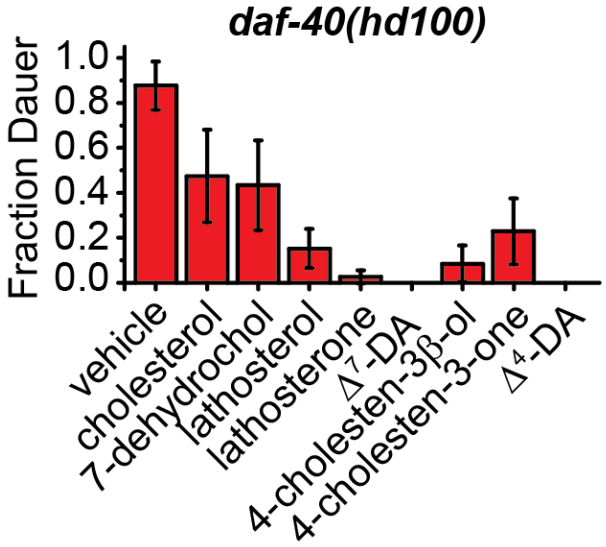

Figure 3.7. Sterol Supplementation Experiments Reveal Differences in *daf-40* from Other DA Synthetic Mutants. (A) Rescue of the Daf-c phenotypes of *daf-40(hd100)* mutants at 27°C with 33μM concentration of sterols. All compounds tested partially rescued, although only the DAs provided complete rescue (N=3, mean ± SEM). (Image Courtesy Josh Wollam).

Cytochrome P450 DAF-40 is involved in DA biosynthesis:

These results strengthened our original hypothesis that many of the enzymatic components of the DAF-12 ligand biosynthetic pathway still remain hidden. Therefore, to identify novel enzymes impacting DA biosynthesis, we conducted a genetic enhancer screen of the *daf-36(k114)* null allele, in which the ligand production is reduced but not abolished. The appearance of Mig (gonadal migration) and Daf-c (dauer constitutive) phenotypes at the normally permissive temperatures of 25°C were scored in previously reported genome-wide RNAi screens (**Figure B.4**). The enhancement of these phenotypes reflected greater loss of ligand-mediated DAF-12 activation suggesting changes in the ligand-biosynthetic pathway. From these screens, several loci that affect DA production were identified, one of which was a cytochrome P450, *T10B9.7/cyp-13a2*, and was named *daf-40* because of its role in *C. elegans* dauer formation.

The discovery of the novel dafachronic acids as described in the previous chapter led us to investigate where exactly DAF-40 acts in DA biosynthesis. For this purpose, sterol supplementation experiments were carried out, wherein phenotypic rescue was scored with the exogenous addition of predicted intermediates in the pathway. Intermediates that are downstream or parallel to the *daf-40* biosynthetic block should rescue whereas those lying upstream should not, a strategy used successfully to confirm the roles of *daf-36*, *dhs-16* and *daf-9* in DA pathways (Rottiers et al., 2006; Wollam et al., 2012; Motola et al., 2006). To our surprise, all sterol compounds partially rescued *daf-40* Daf-c phenotypes, although only the DAs themselves fully rescued (**Figure 3.10**). Sterol rescue experiments carried out using double mutants with *daf-36, dhs-16,* and *daf-9* showed the same rescue pattern as the single mutant, and not that of *daf-40* (**Figure B.5**). This sterol

rescue profile differs significantly from most other known DA biosynthetic mutants, suggesting that *daf-40* could be either upstream or parallel to known components, in a novel position or pathway.

Comparative Metabolomics Identifies Daf-40 Dependent DAF-12 Ligands:

To further understand the role of DAF-40 in the ligand biosynthetic pathway we proceeded to analyze the changes in the sterol metabolome in *daf-40* mutants. For this, we utilized a lipid fractionation approach. We hypothesized that fractionated lipid extracts from N2 wild-type animals should rescue *daf-40* mutant phenotypes, whereas corresponding fractions obtained from *daf-40* should not. Once again, we used the *daf-9*(dh6) rescue assay introduced in the previous chapter to identify fractions that contain DAF-12 ligands. In the WT lipid fractions, the three active regions described previously, rescued *daf-9(dh6)* animals. When these fractions were examined for their ability to rescue *daf-40(hd100),* an additional set of fractions, Region 1 - Fractions 14-19, also rescued *daf-40* but not *daf-9* mutants (**Figure 3.8**), presumably containing earlier DA intermediates as seen with rescues with candidate sterols.

Continuing the investigation of the DA profile in *daf-40* mutants we then prepared lipid extract fractions from *daf-40;daf-22* double mutants, once again to obtain larger number of DA-producing worms in the absence of the dauer pheromone. Similar to results from wild-type animals, several fractions derived from *daf-40:daf-22* animals rescued *daf-9* mutants, likely containing DAs (**Figure 3.8**). These results suggest that *daf-40* is not strictly required for DAF-12 ligand production and that residual activity is sufficient for rescue. Surprisingly, whereas the Region 3 fractions from *daf-22* efficiently rescued *daf-9* and *daf-40* mutants (**Figure B.6**), the corresponding fractions derived

from *daf-40;daf-22* animals fully rescued *daf-9* but could only partially rescue *daf-40* mutants. This finding that the region 3 rescuing activity is dependent on DAF-9 suggests these fractions contain 26-carboxylic acid modifications catalyzed by DAF-9. Presumably, *daf-9* mutants can directly use or efficiently convert compounds present in these *daf-40* fractions to bypass dauer, whereas *daf-40* animals cannot. A simple hypothesis is that DAF-40 acts on DA intermediates in these fractions that are products of DAF-9, or in a parallel pathway, but do not efficiently rescue dauer.

Consequently, we wanted to know how *daf-40(hd100)* mutants affect known sterol intermediates in the DA pathways and so their unfractionated sterol profile was examined by GC/MS/MS. Surprisingly little or no difference was seen in levels of known precursors of Δ^7-DA synthesis, including cholesterol, 7-dehydrocholesterol, lathosterol or lathosterone (**Figure 3.9**). However, Δ^7-DA levels were lower in daf-40 mutants relative to wild-type. Conversely, animals carrying an integrated daf-40::gfp overexpression construct contained elevated levels of Δ^7-DA (**Figure 3.9**).

Since the levels of the measured intermediates did not change, these observations suggest that DAF-40 is involved in an alternative pathway of Δ^7-DA production and we proceeded to analyze the active metabolite fractions by NMR spectroscopy in order to identify the metabolites responsible for the phenotypic rescue. Proton NMR spectra of the Region 1 *daf-40* rescuing metabolite fractions obtained from *daf-40;daf-22* worms (fractions 12-14) confirmed the presence of predicted precursor molecules including cholesterol, 7-dehydrocholesterol and lathosterol, in agreement with the initial sterol supplementation experiments (**Figure 3.10**). Due to extremely low abundance of the active components in Regions 2 and 3 these fractions had to be enriched by HPLC fractionation further to facilitate structure elucidation. While

the proton NMR spectra for HPLC-enriched active fractions from Region 2 revealed the presence of Δ^7-DA (**Figure 3.10**), the HPLC-enriched *daf-40* dependent Region 3 fractions contained 3α-hydroxy-Δ^7-DA (**Figure 3.10**). This compound was detected in higher concentrations in daf-40 mutants compared to wild-type, as confirmed by GC/MS analysis (**Figure 3.10**). The identification of 3α-hydroxy-Δ^7-DA as an endogenous DAF-12 ligand produced in *C. elegans* was described in the previous chapter, and this is specifically interesting due to the α-configuration of the hydroxyl group at the 3-position, reminiscent of mammalian bile acids. All previously characterized 3-hydroxylated steroids in *C. elegans* contain the 3β-configuration, as does cholesterol. *Daf-9* rescue experiments with 3α-hydroxy-Δ^7-DAs revealed that 3α-hydroxy-Δ^7-DA provides much more effective rescue than the 3β-isomer, albeit at higher doses than Δ^7-DA (**Figure 3.10**). 3α-hydroxy-Δ^7-DA also rescued the Daf-c phenotypes of daf-40. Interestingly, it failed to effectively rescue *daf-40;daf-9* double mutants, suggesting that both activities are required to convert this compound into a more potent ligand in vivo. Consistent with in vivo results, 3α-hydroxy-Δ^7-DA activated DAF-12 transcriptional activity in cell culture, but required significantly higher concentrations than Δ^7-DA itself (**Figure 3.10**). By contrast, 3α-hydroxy-Δ^7-DA did not appreciably activate DAF-12. In addition, high concentrations of 3α-hydroxy-Δ^7-DA, as well as the other DAs tested, rescued the reduced expression of the daf-12 target mir-241 in both the *daf-36* and *daf-40* mutant backgrounds, although *daf-40* mutants were not as efficiently rescued as *daf-36* (**Figure B.7**). Altogether these results support our finding that 3α-hydroxy-Δ^7-DA is a novel ligand for DAF-12, which, in these assays, is less potent than Δ^7 or $\Delta^{1,7}$-DA and suggests that DAF-40 acts on this compound to further convert it to a more potent ligand.

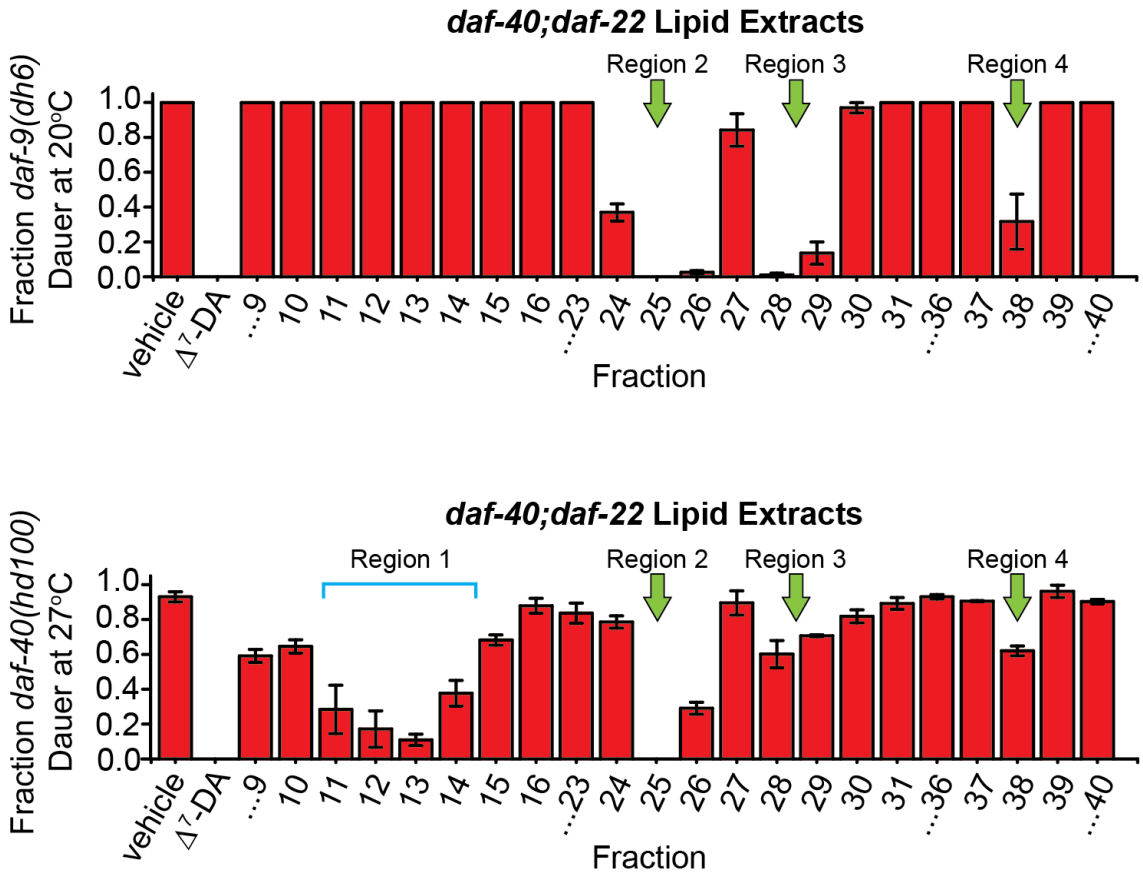

Figure 3.8. Rescue Experiments Suggest *daf-40* Functions in a Novel Way to Influence DAF-12 Activity. (Top) Fractionated lipid extracts from *daf-40;daf-22* double mutants rescue the Daf-c phenotypes of *daf-9(dh6)* mutants at 20°C. The fraction number reflects increasing polarity of the elution gradient, with an estimated 150 ng/μL sterol concentration per fraction. The control Δ^7-dafachronic acid, as well as several fractions rescue the animals to various extents (green arrows). No discernible changes are found from the pattern seen in *daf-22* rescues, demonstrating that DAs are still produced in the absence of *daf-40* (N=3, mean ± SD). (**Bottom)** *daf-40* dauer formation at 27°C is also rescued by fractions from *daf-40;daf-22* animals, as well as fractions 14-19 (Region 1). Rescue is not seen with Region 3 fractions 28-29, which efficiently rescue *daf-9*. These fractions potentially contain a precursor utilized by DAF-40 (N=3, mean ± SD). (Image Courtesy: Adam Antebi Lab).

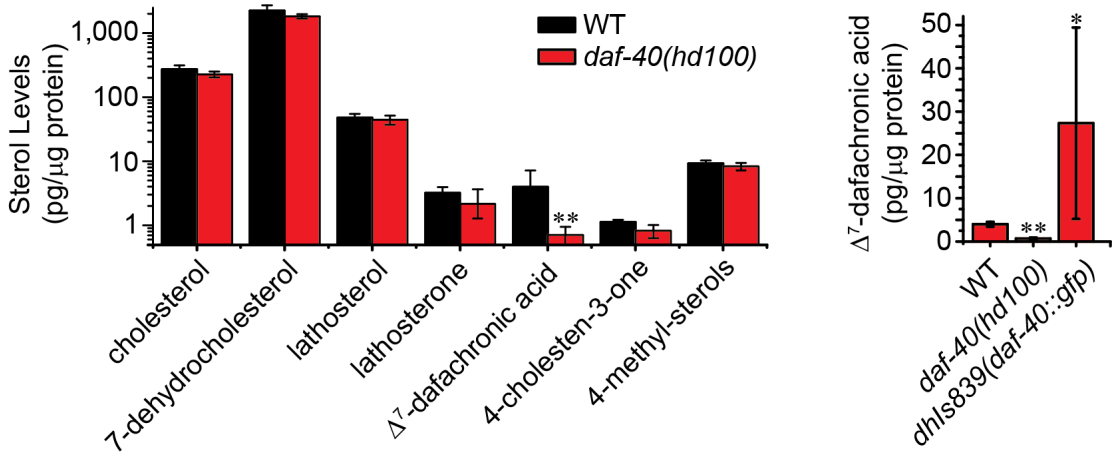

Figure 3.9. *daf-40* Mutant Animals are Deficient in Δ^7-Dafachronic Acid. (A) GC/MS/MS sterol analysis of L3 stage N2 wild-type and *daf-40(hd100)* animals at 20°C reveals that although levels of the proposed DA precursors are not changed, significantly lower levels of Δ^7-dafachronic acid are present in *daf-40* mutants (N≥9 ± SEM; ***P*<0.005). (B) Δ^7-dafachronic acid levels are reduced in *daf-40* mutants and elevated in animals expressing an integrated *dhIs839(daf-40::gfp)* overexpression construct (N≥4 ± SEM; ***P*<0.005, **P*<0.05). (Image Courtesy: Adam Antebi Lab).

Figure 3.10. NMR Analysis Reveals that DAF-40 Modulates Novel Dafachronic Acid Pathways. (A) Proton NMR spectra of the *daf-40;daf-22* Region 1 lipid fractions that rescue *daf-40* mutants reveal that these fractions contain the proposed Δ^7-DA precursors cholesterol, 7-dehydrocholesterol and lathosterol, consistent with previous sterol supplementation experiments. (B) NMR analysis of HPLC-enriched Region 3 fractions from *daf-40;daf-22* mutants, which contain potential DAF-40 activities, identified the presence of 3α-hydroxy-Δ^7-DA. (C) Additional GC/MS/MS analyses of crude lipid extracts confirmed that *daf-40* mutants contain elevated levels of 3-hydroxy-Δ^7-DA, suggesting it may act as a substrate of DAF-40 in a novel pathway of Δ^7-DA production (N=9, ****P*<0.0001). (Image Courtesy : Adam Antebi Lab) (D) Dose response experiments with 3α-hydroxy-Δ^7-DA. Only very high concentrations are able to rescue *daf-40;daf-9* double mutants, consistent with *daf-40* acting downstream or in parallel to *daf-9* (N=3, mean ± SEM). (E) Analysis of DAF-12 transcriptional activity in response to ligand activation in HEK293T cells. Provision of Δ^7-DA or 3α-hydroxy-Δ^7-DA activates the transcription of luciferase driven by the *mir-84* promoter (N=3, mean ± SEM).

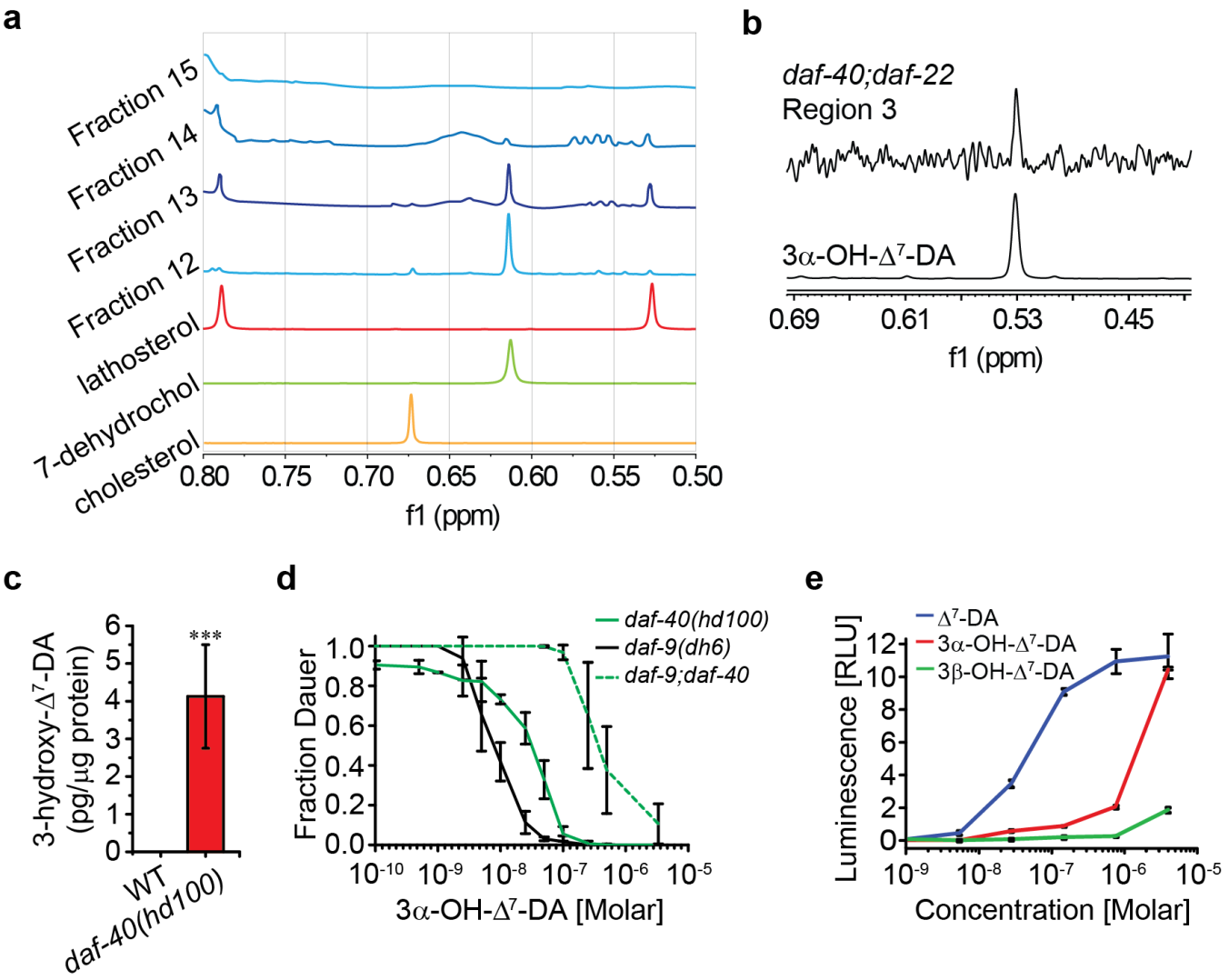
a
Fraction 15
Fraction 14
Fraction 13
Fraction 12
lathosterol
7-dehydrochol
cholesterol
0.80 0.75 0.70 0.65 0.60 0.55 0.50
f1 (ppm)
b
daf-40;daf-22
Region 3
3α-OH-Δ7-DA
0.69 0.61 0.53 0.45
f1 (ppm)
c
3-hydroxy-Δ7-DA (pg/μg protein)
***
WT
daf-40(hd100)
d
daf-40(hd100)
daf-9(dh6)
daf-9;daf-40
Fraction Dauer
3α-OH-Δ7-DA [Molar]
e
Δ7-DA
3α-OH-Δ7-DA
3β-OH-Δ7-DA
Luminescence [RLU]
Concentration [Molar]

DAF-40 Acts as a 3-α-Hydroxysterol Oxidase:

Based on our identification of 3α-hydroxy-Δ^7-DA in the sterol fractions that showed *daf-40* dependence, we hypothesized that DAF-40 contains 3-hydroxysteroid dehydrogenase activity, converting 3α-hydroxy-Δ^7-DA to the 3-keto form. This would explain the accumulation of 3α-hydroxy-Δ^7-DA and reduction of levels of Δ^7-DA in *daf-40* mutants. To determine the biochemical activity of DAF-40, we expressed the gene in cultured cells and assayed activities from isolated microsomes. Indeed, we observed that 3α-hydroxy-Δ^7-DA was converted to Δ^7-DA in the presence of DAF-40 (**Figure 3.11**). We therefore conclude that DAF-40 has 3-hydroxysteroid dehydrogenase activity, transforming 3α-hydroxyl substrates to their corresponding 3-ketone products.

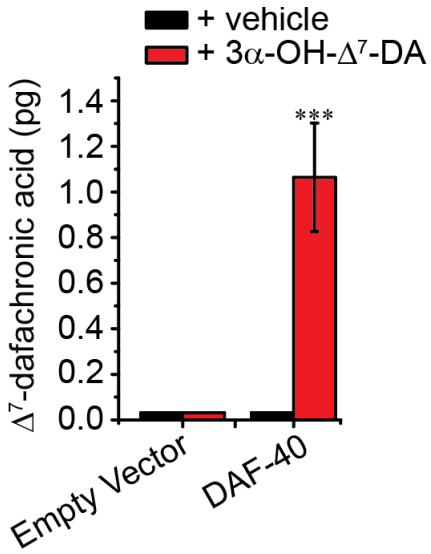

Figure 3.11. DAF-40 Acts as a 3-α-Hydroxysterol Oxidase. Enzyme assays reveal that DAF-40 acts as a 3-hydroxysteroid dehydrogenase to produce Δ^7-DA from 3α-hydroxy-Δ^7-DA (N=2, mean ± range) (Image Courtesy Josh Wollam).

Conclusions and Discussion:

Although it is well established that DAF-12 ligands are ultimately derived from dietary cholesterol, identification of $\Delta^{1,7}$-DA and 3α-OH-Δ^{7}-DA, and the absence of Δ^{4}-DA, as described in the previous chapter necessitated revision of DAF-12-ligand biosynthesis models. In this chapter, the author described the utilization of comparative metabolomics approaches towards the elucidation of steroid metabolism in *C. elegans*. These results indicate that DAF-36 as well as HSD-1 participate in the biosynthesis of Δ^{7}-DA and possibly $\Delta^{1,7}$-DA, whereas previously, HSD-1 had been assumed to function in Δ^{4}-DA biosynthesis. The finding that mutation of *dhs-16* affects Δ^{7}-DA much more strongly than $\Delta^{1,7}$-DA production suggests that, introduction of the 3-keto moiety in $\Delta^{1,7}$-DA may involve a different enzyme. Therefore, it appears that different DAF-12-ligands are produced via partially divergent biosynthetic pathways, which is also supported by the finding that in *strm-1* mutants Δ^{7}-DA production is increased to a much greater extent than that of $\Delta^{1,7}$-DA.

C. elegans offers a unique opportunity to study the role of tissue-specific NHR ligand biosynthesis for endocrine signaling in a simple model system. DAF-12-ligand biosynthetic enzymes link conserved insulin/IGF and TGF-β signaling to transcriptional regulation by DAF-12 (Wollam et al., 2012). The biosynthesis of multiple DAF-12-ligands via partially divergent pathways suggests that different ligands may serve different functions (**Figure 3.12**) (Arda et al., 2010). Notably, a recent study showed that DAF-12-ligand production in different worm tissues is interdependent, indicating that some DAF-12-ligands or ligand derivatives function as signaling molecules that trigger additional ligand production in tissues distal to the original site of ligand biosynthesis (Schaedel et al., 2012). The two neuron-like XXX cells appear to function as central regulators of organism-wide commitment to either

reproductive development or dauer (Gerisch and Antebi, 2004; Schaedel et al., 2012). Under favorable conditions, DAF-12-ligands produced in the XXX cells are thought to trigger abundant additional ligand biosynthesis in the hypodermis, locking in organism-wide commitment to reproductive adult development. Since the XXX cells are the primary sites of HSD-1 expression (Dumas et al., 2010; Patel et al., 2008), our finding that HSD-1 may contribute to Δ^7-DA biosynthesis supports a model in which XXX-produced Δ^7-DA (or derived 3α-OH-Δ^7-DA) triggers biosynthesis of large quantities of additional Δ^7-DA and $\Delta^{1,7}$-DA via *daf-36*, *dhs-16*, and hypodermal *daf-9* (**Figure 3.12**). Taken together, our identification of $\Delta^{1,7}$-DA, 3α-OH-Δ^7-DA, and Δ^0-DA as well as the differential production of these compounds in different mutant background indicates that several tissue specific components of the DAF-12-ligand biosynthetic pathway remain to be identified.

Subsequently, in a collaborative analysis of *C. elegans* sterol metabolites, utilizing a multidisciplinary approach the cytochrome P450 DAF-40 was characterized as a component of a novel branch of DAF-12 ligand biosynthesis influencing development and lifespan. *Daf-40* exhibits several unique features suggestive of a role in parallel to the previously proposed DA biosynthetic pathways. In contrast to most genes involved in DA production, *daf-40* mutant phenotypes were partially rescued by all proposed DA precursors, including cholesterol. In this regard it does not easily fit into the predicted model of DA synthesis, and suggests a novel role. Sterol profile analysis of *daf-40* mutants revealed significantly less Δ^7-DA, despite having normal levels of precursors, while animals overexpressing DAF-40 displayed elevated Δ^7-DA levels. Second, *daf-40;daf-22* lipid extract fractions were able to rescue *daf-9* null mutants but not *daf-40* animals, whereas fractions from wild-type or *daf-22* animals rescued both mutants. Rescuing activities in these

fractions included the novel 3α-OH-Δ^7-DA, suggesting this compound may be a DAF-40 substrate. Accordingly, *daf-40* mutants accumulate 3α-OH-Δ^7-DA. Finally, biochemical analysis of DAF-40 activity in cell culture demonstrates that it is able to convert 3α-OH-Δ^7-DA to Δ^7-DA and is one of the many missing components in the DA-biosynthesis pathway in *C. elegans* and probably other nematodes. It is also likely that DAF-40 has additional substrates and activities and future biochemical studies will reveal its specificity or promiscuity.

With the results described in Chapter 2 and Chapter 3, one can start hypothesizing about the roles that the different DAs play in *C. elegans* development and lifespan. While our initial characterization of these DAs has not uncovered strict functional differences, the difference in biological activity between these ligands is apparent (**Figure B.8**). It remains possible that 3α-OH-Δ^7-DA may influence sterol transport, act as an inhibitor, or be an alternate ligand mediating specific events. Further investigation into gene expression profiles of animals after treatment with these DAs should provide insight into functional differences, if they exist.

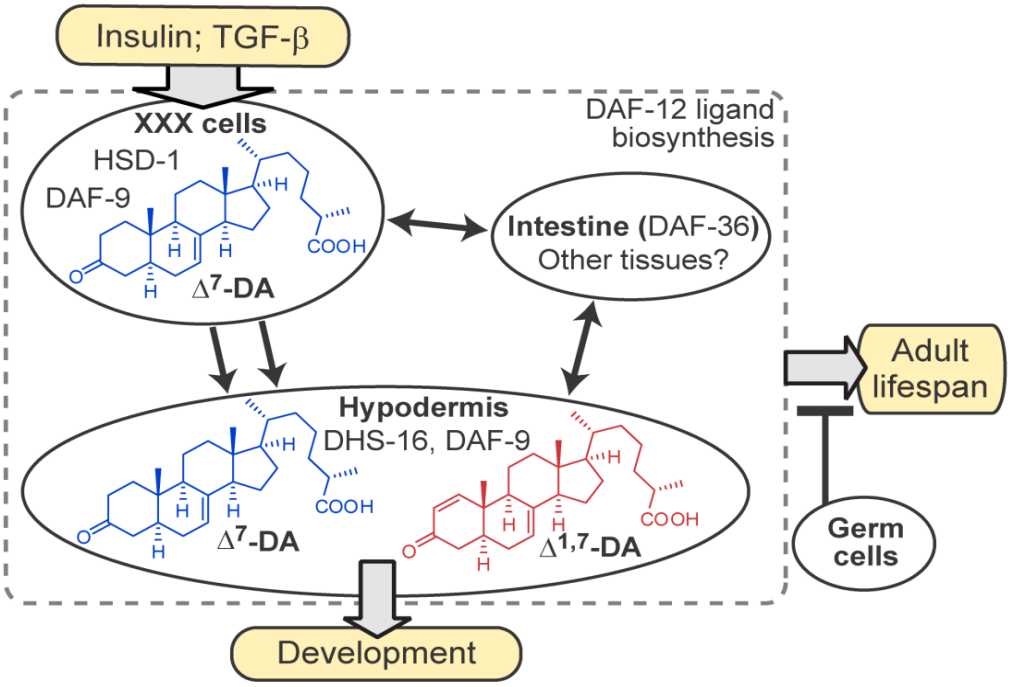

Figure 3.12. Model for biosynthesis of DAF-12-ligands that regulate development and lifespan (Schaedel et al., 2012; Yamawaki et al., 2010)**.** Enzymes in the XXX cells downstream of insulin and TGF-β signaling produce some Δ^7-DA, which triggers additional biosynthesis of DAF-12 ligands via upregulation of DAF-9 expression in the hypodermis, dependent on intestinally expressed DAF-36 and possibly other tissues. The lifespan-increasing effects of DAF-12 ligands depend on germ cell removal (Yamawaki et al., 2010).

REFERENCES

Arda, H.E., Taubert, S., MacNeil, L.T., Conine, C.C., Tsuda, B., Van Gilst, M., Sequerra, R., Doucette-Stamm, L., Yamamoto, K.R., and Walhout, A.J. (2010). Functional modularity of nuclear hormone receptors in a Caenorhabditis elegans metabolic gene regulatory network. Mol Syst Biol 6, 367.

Bethke, A., Fielenbach, N., Wang, Z., Mangelsdorf, D. J. & Antebi, A. (2009). Nuclear Hormone Receptor Regulation of MicroRNAs Controls Developmental Progression. Science *324*, 95-98.

Dumas, K.J., Guo, C., Wang, X., Burkhart, K.B., Adams, E.J., Alam, H., and Hu, P.J. (2010). Functional divergence of dafachronic acid pathways in the control of C. elegans development and lifespan. Dev Biol *340*, 605-612.

Fielenbach, N. & Antebi, A. (2008). C. elegans dauer formation and the molecular basis of plasticity. Genes & Dev *22*, 2149-2165.

Gerisch, B., Rottiers, V., Li, D., Motola, D.L., Cummins, C.L., Lehrach, H., Mangelsdorf, D.J.,and Antebi, A. (2007). A bile acid-like steroid modulates Caenorhabditis elegans lifespan through nuclear receptor signaling. Proc Natl Acad Sci U S A 104, 5014-5019.

Gerisch, B., Weitzel, C., Kober-Eisermann, C., Rottiers, V., and Antebi, A. (2001). A hormonal signaling pathway influencing C. elegans metabolism, reproductive development, and life span. Dev Cell 1, 841-851.

Hannich, J.T., Entchev, E.V., Mende, F., Boytchev, H., Martin, R., Zagoriy, V., Theumer, G.,Riezman, I., Riezman, H., Knolker, H.J., et al. (2009). Methylation of the sterol nucleus by STRM-1 regulates dauer larva formation in Caenorhabditis elegans. Dev Cell 16, 833-843.

Motola, D.L., Cummins, C.L., Rottiers, V., Sharma, K.K., Li, T., Li, Y., Suino-Powell, K., Xu, H.E., Auchus, R.J., Antebi, A., et al. (2006). Identification of ligands for DAF-12 that govern dauer formation and reproduction in C. elegans. Cell 124, 1209-1223.

Patel, D.S., Fang, L.L., Svy, D.K., Ruvkun, G., and Li, W. (2008). Genetic identification of HSD-1, a conserved steroidogenic enzyme that directs larval development in Caenorhabditis elegans. Development 135, 2239-2249.

Pungaliya, C., Srinivasan, J., Fox, B.W., Malik, R.U., Ludewig, A.H., Sternberg, P.W., and Schroeder, F.C. (2009). A shortcut to identifying small molecule signals that regulate behavior and development in Caenorhabditis elegans. Proc Natl Acad Sci USA 106, 7708-7713.

Rottiers, V., Motola, D.L., Gerisch, B., Cummins, C.L., Nishiwaki, K., Mangelsdorf, D.J., and Antebi, A. (2006). Hormonal control of C. elegans

dauer formation and life span by a Rieske-like oxygenase. Dev Cell 10, 473-482.

Schaedel, O.N., Gerisch, B., Antebi, A., and Sternberg, P.W. (2012). Hormonal Signal Amplification Mediates Environmental Conditions during Development and Controls an Irreversible Commitment to Adulthood. PLoS Biol 10, e1001306.

Shen, Y., Wollam, J., Magner, D., Karalay, O., and Antebi, A. (2012). A steroid receptor microRNA switch regulates life span in response to signals from the gonad. Science 338, 1472-1476.

Williams, T.W., Dumas, K.J., and Hu, P.J. (2010). EAK proteins: novel conserved regulators of C. elegans lifespan. Aging (Albany NY) 2, 742-747.

Wollam, J., and Antebi, A. (2011). Sterol regulation of metabolism, homeostasis, and development. Annu Rev Biochem 80, 885-916.

Wollam, J., Magner, D.B., Magomedova, L., Rass, E., Shen, Y., Rottiers, V., Habermann, B., Cummins, C.L., and Antebi, A. (2012). A Novel 3-Hydroxysteroid Dehydrogenase That Regulates Reproductive Development and Longevity. PLoS Biol 10, e1001305.

Wollam, J., Magomedova, L., Magner, D.B., Shen, Y., Rottiers, V., Motola, D.L., Mangelsdorf, D.J., Cummins, C.L., and Antebi, A. (2011). The Rieske oxygenase DAF-36 functions as a cholesterol 7-desaturase in steroidogenic pathways governing longevity. Aging Cell 10, 879-884.

Yamawaki, T.M., Berman, J.R., Suchanek-Kavipurapu, M., McCormick, M., Gaglia, M.M., Lee, S.J., and Kenyon, C. (2010). The somatic reproductive tissues of C. elegans promote longevity through steroid hormone signaling. PLoS Biol 8

Yoshiyama-Yanagawa, T., Enya, S., Shimada-Niwa, Y., Yaguchi, S., Haramoto, Y., Matsuya, T., Shiomi, K., Sasakura, Y., Takahashi, S., Asashima, M., et al. (2011). The conserved Rieske oxygenase DAF-36/Neverland is a novel cholesterol-metabolizing enzyme. J Biol Chem 286, 25756-25762.

Zhi, X., Zhou, X.E., Melcher, K., Motola, D.L., Gelmedin, V., Hawdon, J., Kliewer, S.A., Mangelsdorf, D.J., and Xu, H.E. (2012). Structural conservation of ligand binding reveals a bile acid-like signaling pathway in nematodes. J Biol Chem 287, 4894-4903.

CHAPTER 4

USING DIFFERENTIAL ANALYSIS BY 2D-NMR SPECTROSCOPY (DANS) TO INVESTIGATE TRYPTOPHAN METABOLISM IN *C.ELEGANS*: IDENTIFICATION OF DEATH FLUORESCENCE AND INVESTIGATION OF THE KYNURENINE PATHWAY

Introduction:

As introduced earlier, the simplicity of the model organism *C. elegans* provides unique opportunities to study biological pathways of metazoans. Ongoing *C. elegans* research continues to reveal intriguing phenotypes. One such example is the presence and function of “gut granules”, located abundantly in the intestinal cells of nematodes across the suborder Rhabditina (Chitwood and Chitwood, 1950). Because gut granules share functional similarities with lysosomes in their capacity for endocytosis and their acidic interior (Hermann et al., 2005; Clokey and Jacobsen, 1986) they are generally referred to as lysosome-related-organelles (LROs) (Hermann et al., 2005; Bernabucci et al., 2012), with similarity to the pigment containing melanosomes in mammals and eye pigment granules in Drosophila (Raposo and Marks, 2007). Notably, under ultraviolet light, gut granules emit blue fluorescence, with maximal intensity at 340/430 nm ($\lambda_{ex}/\lambda_{em}$) (**Figure 4.1**).

Lipofuscin is believed to accumulate with age in mammalian cells (Jung et al., 2007) and has frequently been used as biomarker for aging (Brunk et al., 2002; Jung et al., 2007, Terman et al., 1998). Consistent with this theory, blue fluorescence levels increase gradually with age in worm population cohorts (Garigan et al., 2002; Gerstbrein et al., 2005), but the presence of lipofuscin has not been verified in *C. elegans.* The composition of

lipofuscin is usually poorly defined and assumed to be somewhat variable, although autofluorescent properties are generally listed as its distinguishing characteristic (Jung et al., 2007). When excited by *in vitro* UV light, so-called lipofuscin emits blue fluorescent light, potentially due to the presence of Schiff bases (Fletcher et al., 1973; Klass et al., 1977), in addition, excitation of lipofuscin by UV *in vivo* results in peak fluorescence in the 540-640 nm (orange-yellow) range (Eldred et al., 1982). While these observations point towards lipofuscin as the fluorescent material in *C. elegans* intestine, biochemical composition of the *C. elegans* blue fluorescence has not been carried out.

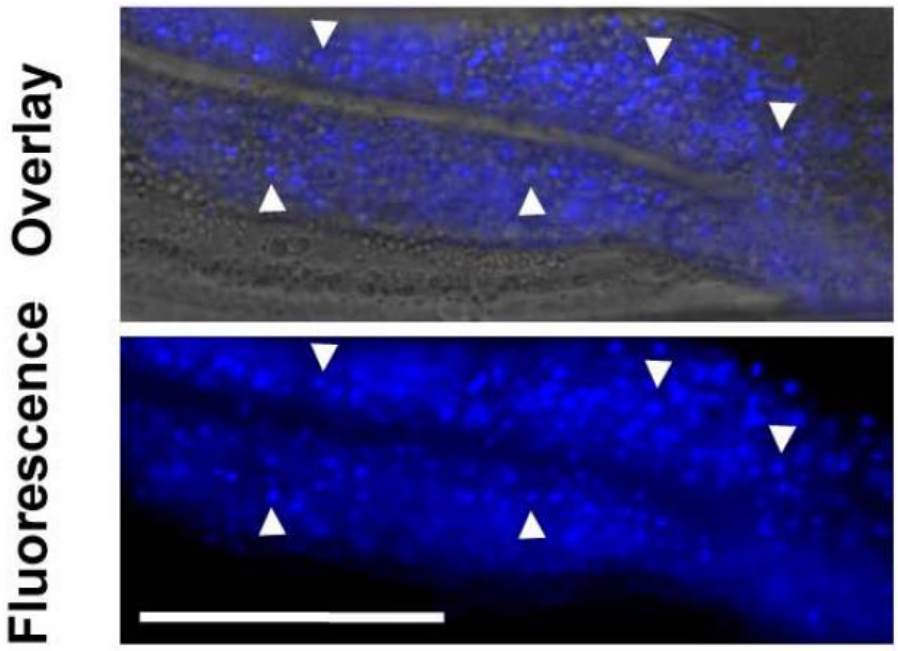

Figure 4.1. Gut granule fluorescence in *C. elegans*. Fluorescent gut granules (arrow heads) in intestinal cells of healthy, young adult *C. elegans. Bottom,* blue fluorescence observed through a DAPI filter. *Top*, brightfield and blue fluorescence images overlaid (Image courtesy – Cassandra Coburn).

A parallel and less popular idea about the origin of the blue fluorescence has been proposed from studies of *C. elegans* mutants with altered autofluorescence properties. Flu mutants have abnormal gut granule autofluorescence color and intensity (Siddiqui and Babu, 1980), and the, until recently unmapped, FLU genes have been hypothesized to function in tryptophan catabolism (Siddiqui and Babu, 1980). Metabolomics analysis of these mutants with respect to altered tryptophan catabolism has not been carried out.

In this study, the author describes how using Differential Analysis by 2D-NMR Spectroscopy the structural identity of the blue fluorescence in *C. elegans* was discovered and how this technique can be utilized to elucidate the tryptophan degradation pathway (aka kynurenine pathway) in *C. elegans.*

Blue fluorescence increases with death not stress:

This work was done in collaboration with Cassandra Coburn in Prof. David Gems' Lab at University College London, London.

Raised oxygen levels (40% O_2) increases lipofuscin levels in human fibroblasts (Terman et al., 1998) and so in order to investigate whether the blue fluorescence in *C. elegans* was indeed due to accumulation of lipofuscin in the gut granules, worms were exposed to normobaric hypoxia (90% O_2), and elevated iron levels. Both treatments significantly raised protein oxidative damage, but neither increased blue fluorescence levels **(Figure 4.2)**. This implies that *C. elegans* blue fluorescence is not a result of oxidative damage, suggesting that it is not lipofuscin.

Comparable to lipofuscin in mammals, mean fluorescence levels increase slowly with age in *C. elegans* population cohorts (Eldred et al., 1982; Garrigan et al., 2002), but population mean data does not address

inhomogeneity in the fluorescence of individual worms. This concern is addressed in a recent publication (Hermann et al., 2005) where it is reported that when individually analyzed, significant increase in *C. elegans* blue fluorescence levels is only seen in animals closer to death. To test this directly for the purpose of the present study, fluorescence levels of individually cultured, wild-type C. elegans *in situ* on nematode growth medium (NGM) agar plates were analyzed at intervals through their entire lifetime using a DAPI filter ($\lambda_{ex}/\lambda_{em}$ = 340/430 nm). Reduction of movement was considered the indicator of approaching of death and time-lapse imaging was used to capture fluorescence changes during death. This revealed that fluorescence levels in singular animals did not change significantly until immediately prior to death. Then, coinciding with the cessation of movement (i.e., death) a sudden and dramatic ~400% increase occurs in the fluorescence level **(Figure 4.3)**. This increase begins at ~2 h prior to death, and then fades by ~6 h after death **(Figure 4.3)**.

Blue fluorescent bursts are not specific to death from old age but could also be induced by killing younger worms, either using a heated worm pick on the agar adjacent to the worm or by freeze-thaw or low pH **(Figure 4.4)**. This observation was also conserved in the nematodes *C. briggsae* and *Pristionchus pacificus* **(Figure 4.4)**. Additionally, in both aged and killed worms, the distribution of fluorescence changed from punctate to diffuse during death, and eventually spread from the intestine to other tissues (**Figure 4.4**). This phenomenon was named *Death Fluorescence (*DF*)*.

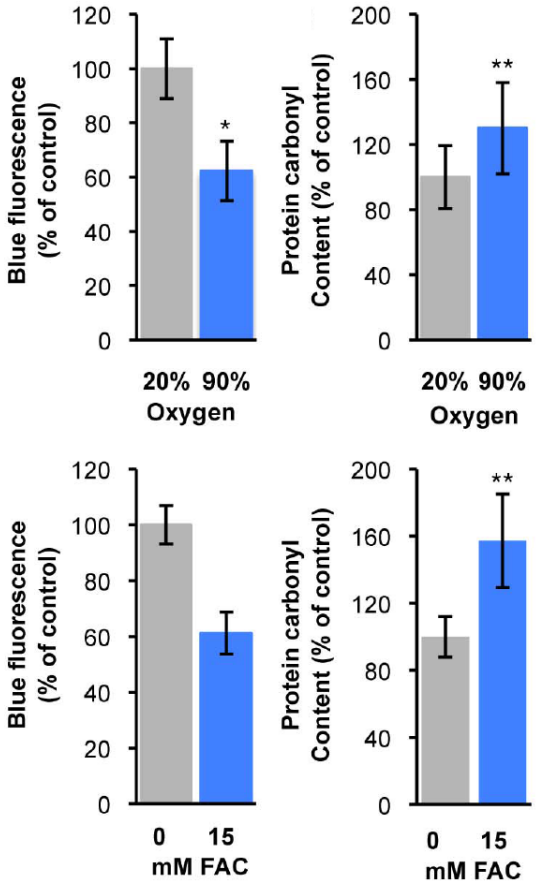

Figure 4.2. Molecular damage does not increase blue fluorescence. Hyperoxia (5-d exposure) and free iron (1-d exposure) increase protein oxidation, but not blue fluorescence. (Data courtesy Cassandra Coburn)

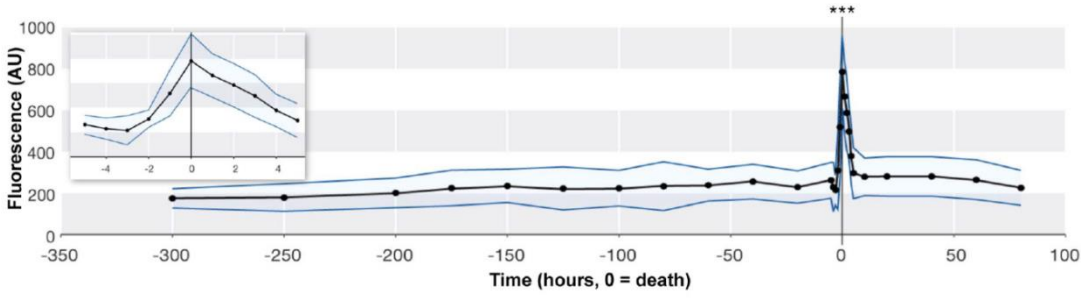

Figure 4.3. Blue fluorescence increases with death. Mean levels of fluorescence relative to time of death (black line), ± SD (blue lines) (Data courtesy Cassandra Coburn).

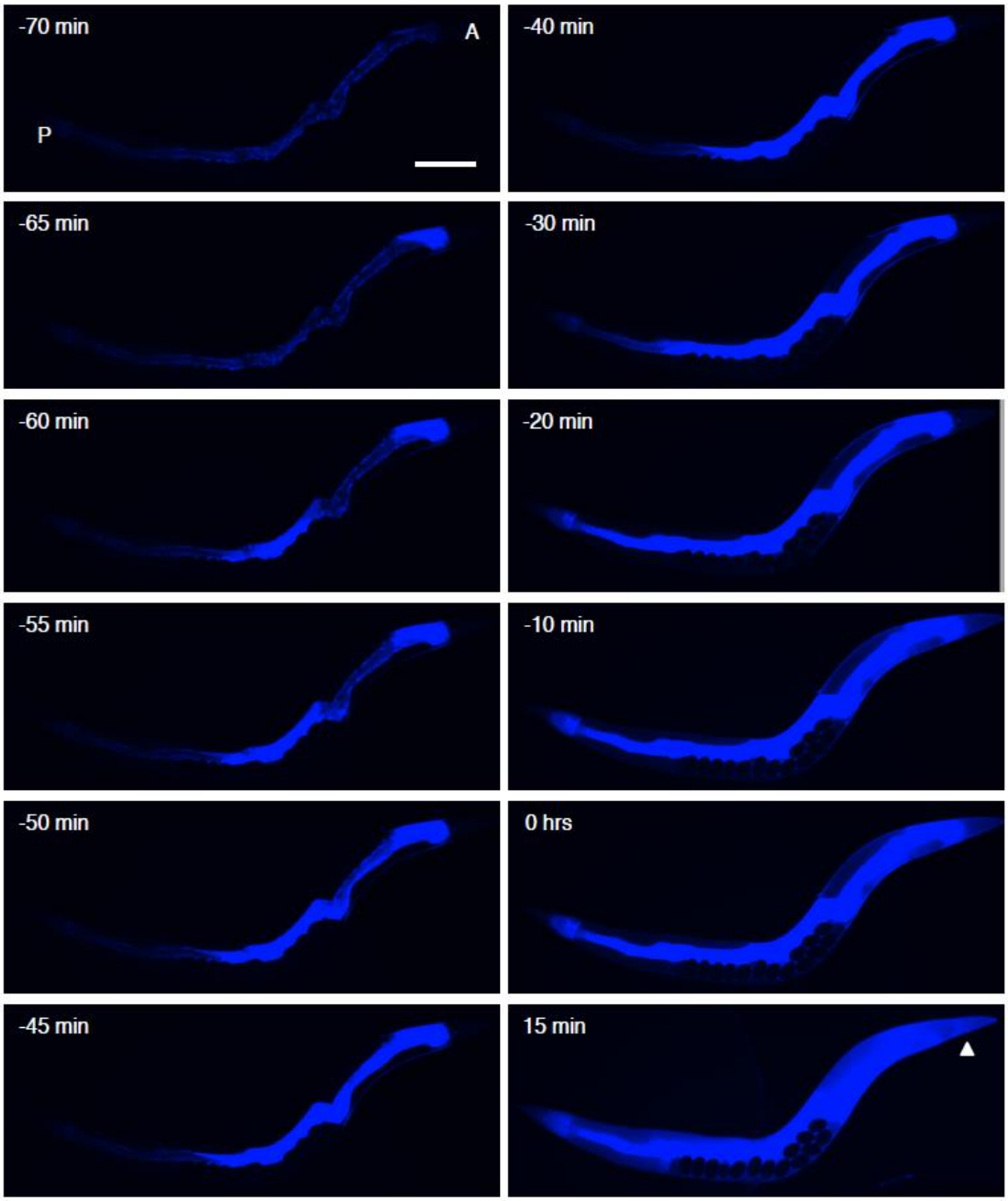

Figure 4.4. Visualization of DF. DF in young adult hermaphrodite killed with a heated wire. During DF the pattern of fluorescence changes from punctate to diffuse. A and P, anterior and posterior ends of intestine. Arrowheads, spread of DF from intestine to other tissues. Time, with respect to death. (Data courtesy Cassandra Coburn)

Comparative metabolomics reveals the chemical identity of death fluorescence (DF):

Once it was established that blue death fluorescence in *C. elegans* (being referred to as Death Fluorescence or DF for the rest of this chapter) is not generated by oxidative damage and is correlated with death and not aging, it seemed unlikely that lipofuscin was responsible. Therefore, we investigated the chemical identity of the blue fluorophore responsible for DF using Differential Analysis by 2D NMR Spectroscopy (DANS). As previously described, this comparative metabolomics approach allows identification of metabolites whose production is dependent on a specific genetic background without extensive chromatographic fractionation. For this comparison, we chose to compare the metabolome of wild-type *C. elegans* with that of the *glo-1 (zu437)* (gut granule loss 1) mutant strain which are deficient of gut granules (Hermann et al., 2005). *glo-1* animals showed significantly lower blue fluorescence both during life or death due to aging or thermal injury, suggesting that gut granule formation and DF are connected (**Figure 4.5**).

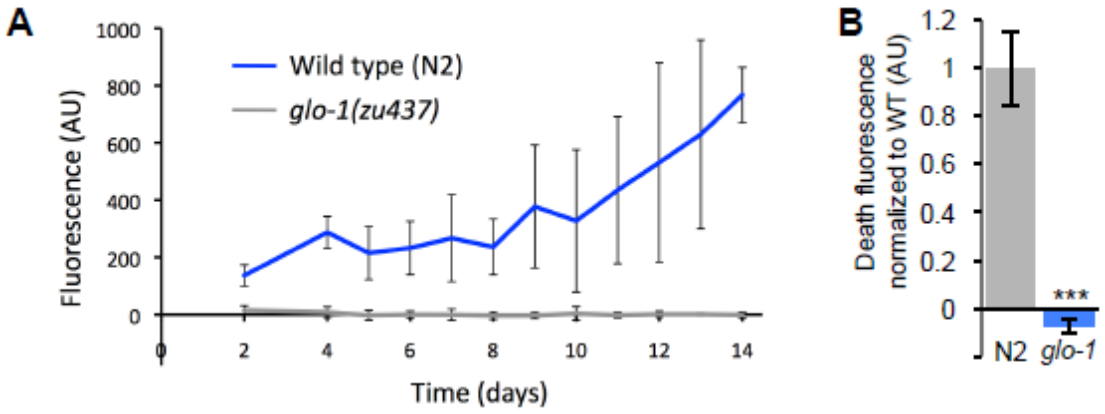

Figure 4.5. *glo-1* animals do not show gut granules or DF. *glo-1(zu437)* animals do not show an increase in blue fluorescence during aging (A) nor DF upon killing (B), making them a useful negative control for establishing the chemical source of gut granule fluorescence and DF. (Data courtesy Cassandra Coburn)

We first confirmed that blue fluorescence is present in whole-worm sonicates of wild-type animals, whereas sonicates of *glo-1(zu437)* mutants contained no blue fluorescence. After several purification steps, blue fluorescence remained present in the supernatant of wild-type worm homogenates (**Figure C.2**). The fluorophore also remained after protein precipitation through addition of 100% ethanol in the ratio 1:9 (Fig 3B), indicating that that the fluorophore is not proteinaceous. Gradient high performance liquid chromatography (HPLC) was then used to identify peaks at $\lambda_{ex}/\lambda_{em}$ 340/430 nm. Four peaks were present in the N2 samples but not in *glo-1(zu437)* or water controls (**Figure C.3**). The most intense peak eluted from the column within the polar-mobile phase, indicating that it had highly polar functional groups while the others were relatively less polar.

We then proceeded to acquire dqfCOSY spectra of the sonicates of wild-type and glo-1(zu437) worms. Comparison of the wild-type and *glo-1(zu437)* spectra showed significant differences in both the aliphatic and

aromatic regions (**Figures 4.6 - 4.9)**. These differences resulted from the presence of several groups of strong signals in the wild-type spectra that were absent or much attenuated in the *glo-1(zu437)* spectra. Detailed analysis of the fine structures of the differential signals indicated that the compounds absent in *glo-1(zu437)* mutants include three anthranilic acid moieties, an N-substituted indole, as well as four β-glucosyl units (**Figures 4.6 - 4.9)**. The chemical shift values of the anomeric protons in the four β-glucosyl moieties suggested that two of these are attached to anthranilic acid moieties forming two glucosyl esters, whereas the two remaining glucose units appeared to be part of N-glucosyl indoles. Furthermore, a characteristic downfield shift and additional *J*-splitting (**Figures 4.6 - 4.9)** of the protons in position 3 of two of the four glucose moieties indicated that anthranilic acid glucosyl ester (**angl#1**, **Figures 4.6 - 4.9**) and N-glucosyl indole (**iglu#1**) were both accompanied by the corresponding 3'-phosphorylated compounds (**angl#2** and **iglu#2**) (**Figure 4.9)**. These structural assignments were confirmed via high-resolution mass spectrometry and synthesis of authentic samples of anthranilic acid glucosyl ester and N-glucosylindole (Appendix C) (Roell and Rösler et al., 2011, Messaoudi et al., 2004).

Figure 4.6. NMR-based comparative metabolomics (DANS) applied to C. elegans wild type (N2) and *glo-1(zu437)*. Comparison of the aromatic regions of dqfCOSY 2D NMR spectra of wild type (N2, upper panel) and glo-1(zu437) (lower panel) sonicates reveals several groups of signals that are strongly downregulated in the glo-1(zu437) spectrum. These correspond to indole glucosides (black boxes) and fluorescent anthranilic acid derivatives (blue boxes).

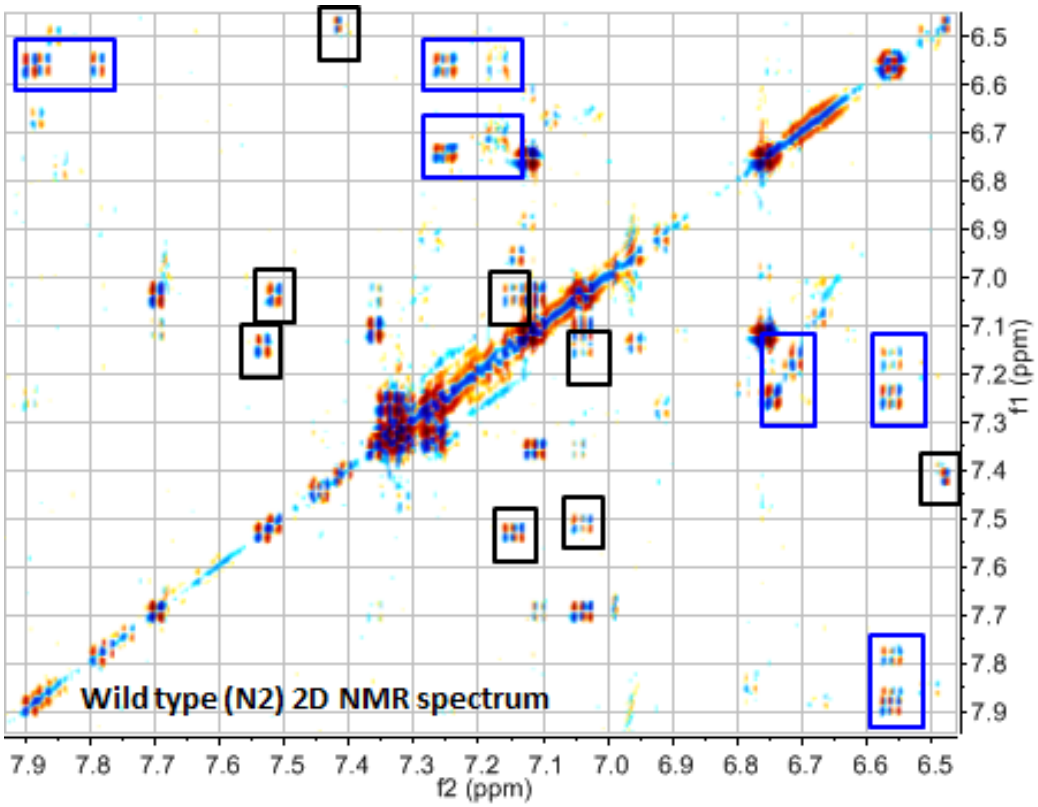
Wild type (N2) 2D NMR spectrum
f1 (ppm)
f2 (ppm)
6.5 6.6 6.7 6.8 6.9 7.0 7.1 7.2 7.3 7.4 7.5 7.6 7.7 7.8 7.9
7.9 7.8 7.7 7.6 7.5 7.4 7.3 7.2 7.1 7.0 6.9 6.8 6.7 6.6 6.5

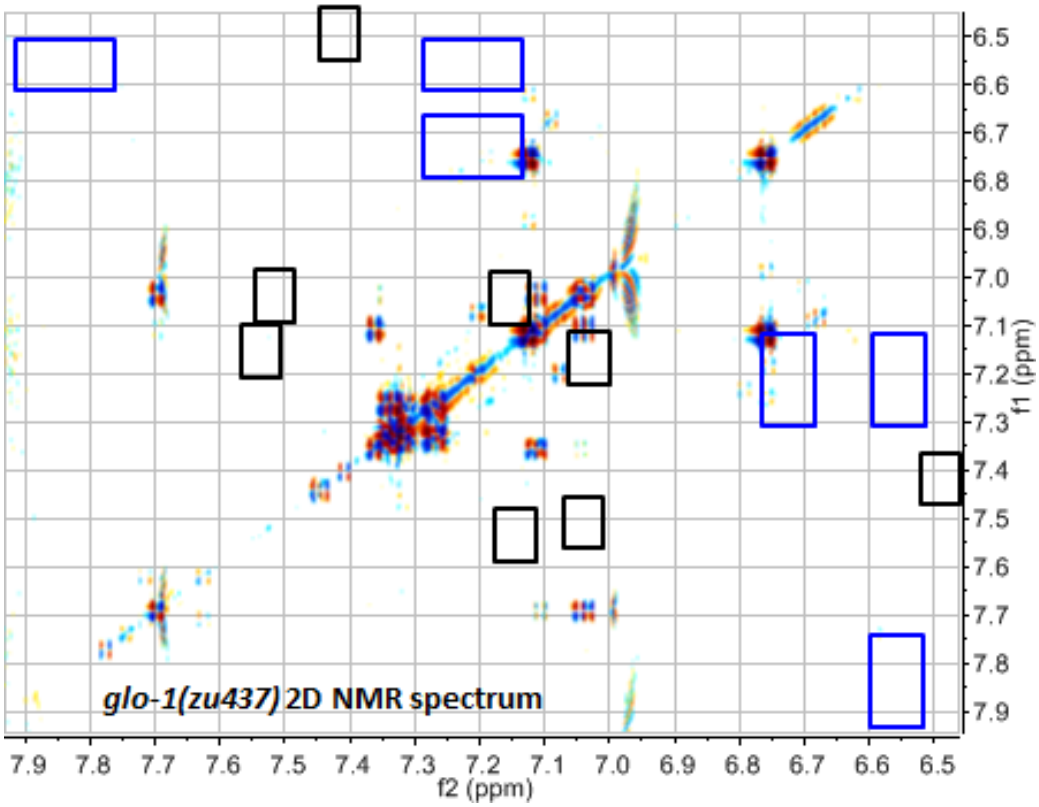
glo-1(zu437) 2D NMR spectrum
f1 (ppm)
f2 (ppm)
6.5 6.6 6.7 6.8 6.9 7.0 7.1 7.2 7.3 7.4 7.5 7.6 7.7 7.8 7.9
7.9 7.8 7.7 7.6 7.5 7.4 7.3 7.2 7.1 7.0 6.9 6.8 6.7 6.6 6.5

Figure 4.7. Biochemical identification of DF constituents - aliphatic region Comparison of 3.4-4.2 ppm region of the dqfCOSY spectrum (600 MHz, methanol-d_4) of N2 worm sonicates (**top)** and *glo-1* mutants (**bottom)** show cross-peaks representing several glucose moieties (black boxes). Crosspeaks at f2 = 4.12 ppm correspond to proton 3-H in angl#2 and show additional *J*-splitting due to coupling with ^{31}P of the adjacent phosphate group (double bordered boxes).

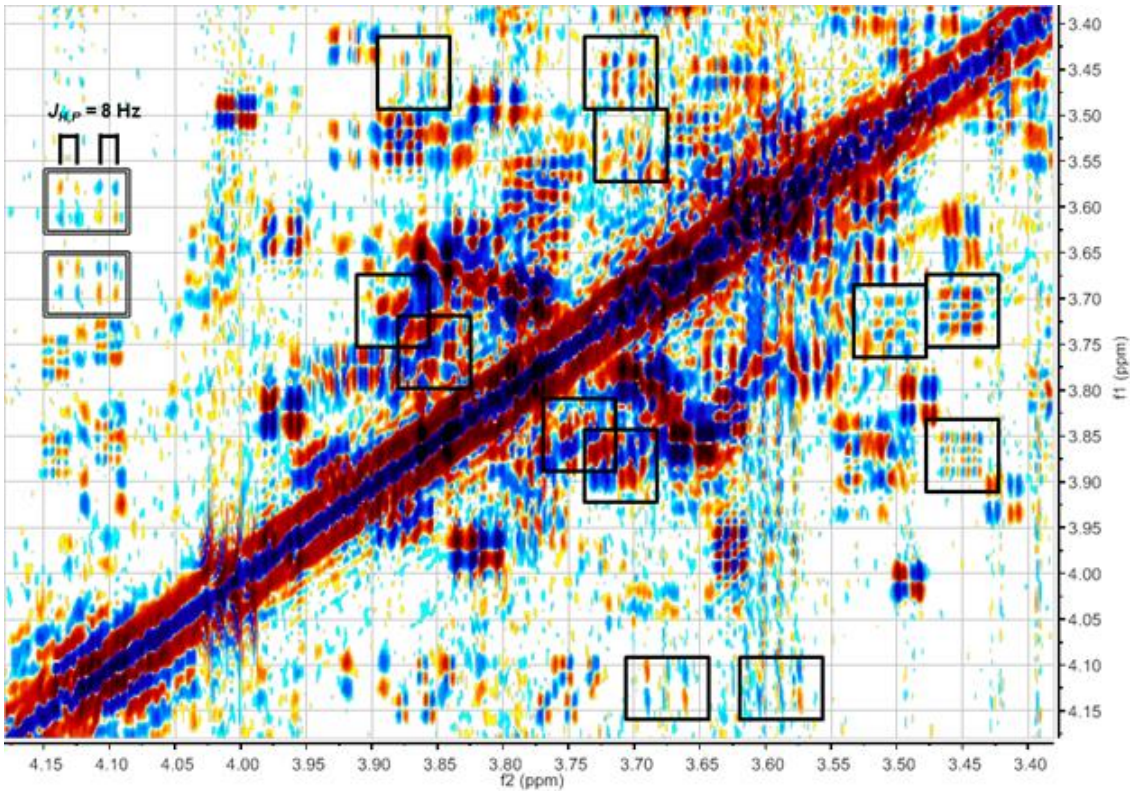
$J_{H,P}$ = 8 Hz
f2 (ppm)
f1 (ppm)

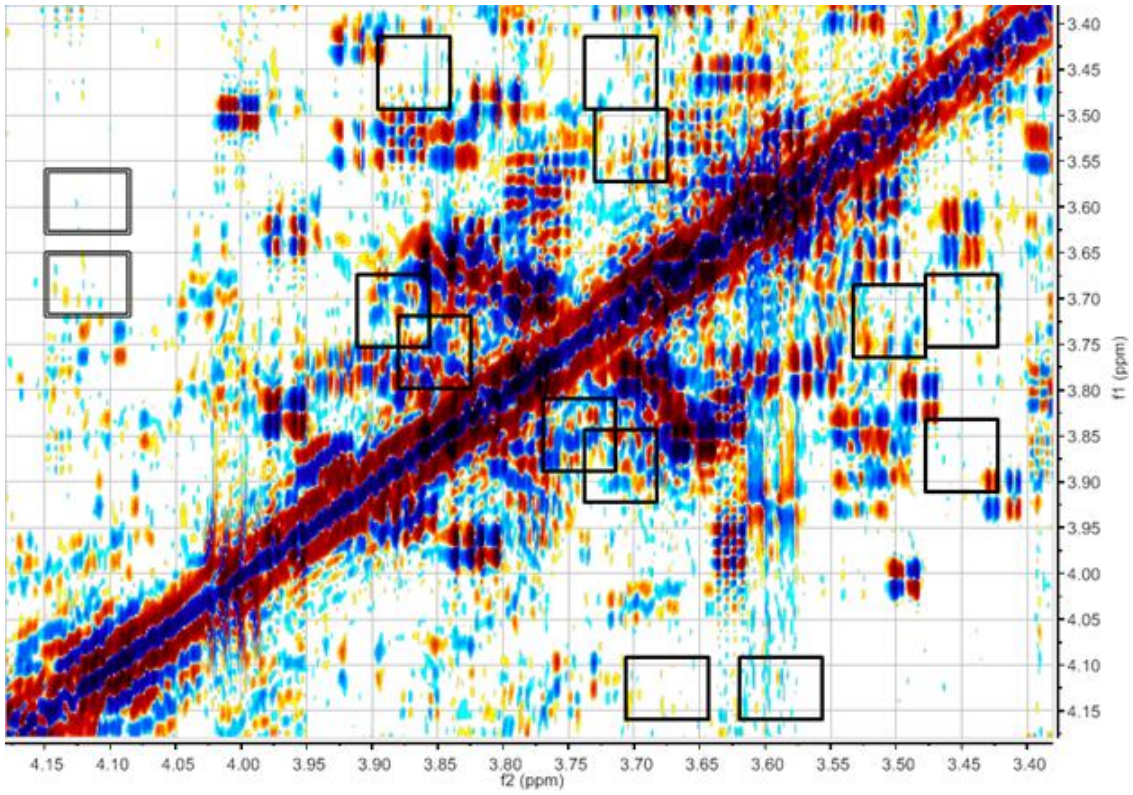
f2 (ppm)
f1 (ppm)

Figure 4.8. Biochemical identification of DF constituents – anomeric protons Section of the dqfCOSY spectrum (600 MHz, methanol-d_4) of N2 worm sonicates (**top)** and *glo-1* worm sonicates **(bottom)** showing crosspeaks for the anomeric protons of four glucose units. Two of these (red boxes) belong to the indole glucosides (iglu #1, iglu#2) and the other two (blue boxes) are part of the anthranilic acid glucosides (angl#1, angl#2) (**Figure 4.9)**.

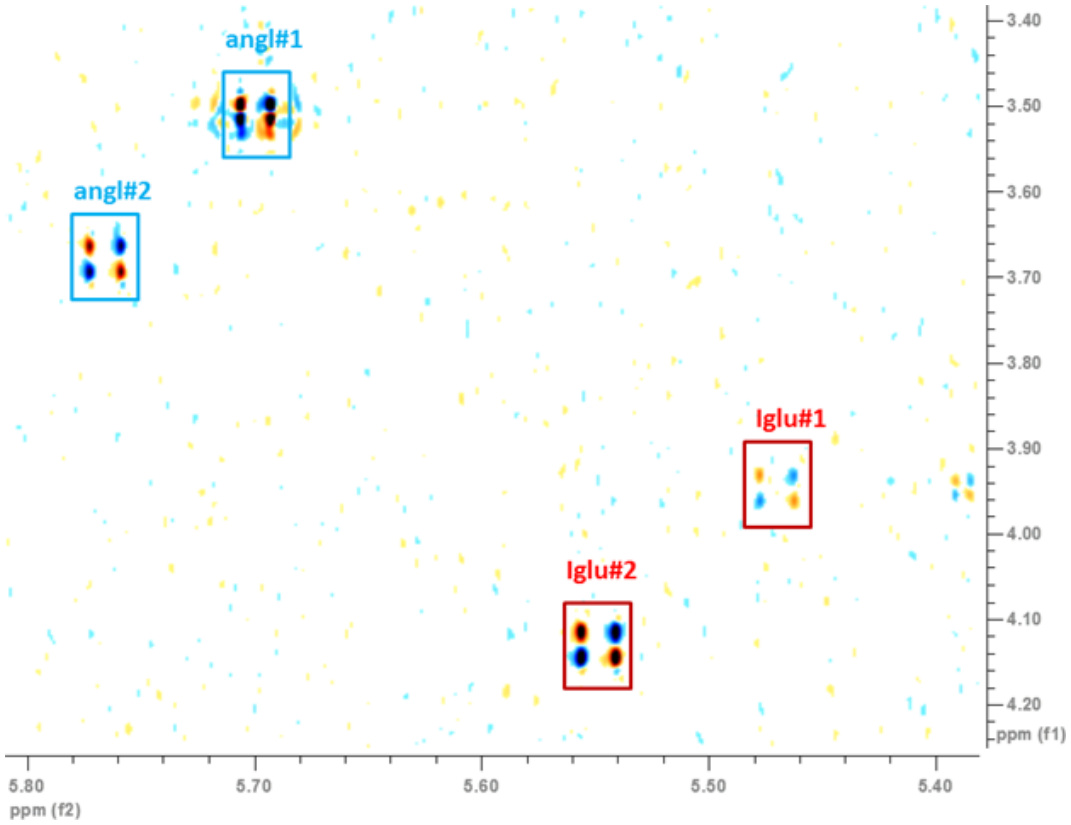
angl#1
angl#2
Iglu#1
Iglu#2
3.40
3.50
3.60
3.70
3.80
3.90
4.00
4.10
4.20
ppm (f1)
5.80
5.70
5.60
5.50
5.40
ppm (f2)

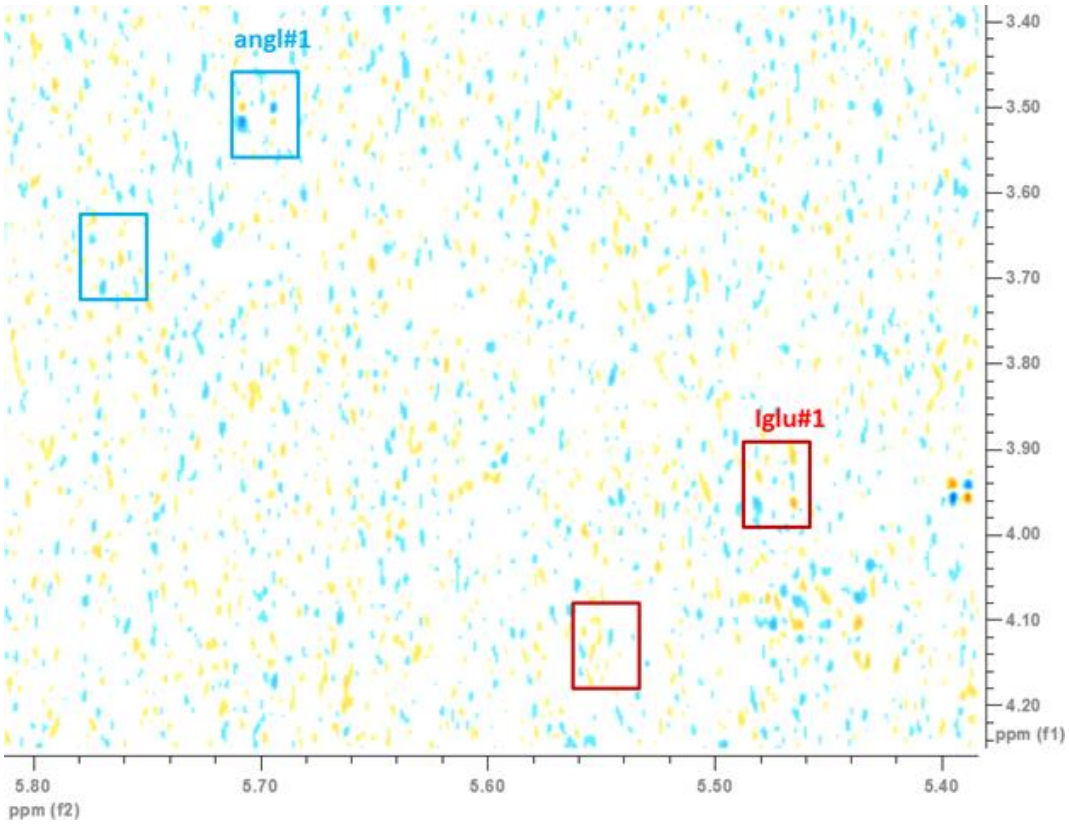
angl#1
Iglu#1
3.40
3.50
3.60
3.70
3.80
3.90
4.00
4.10
4.20
ppm (f1)
5.80
5.70
5.60
5.50
5.40
ppm (f2)

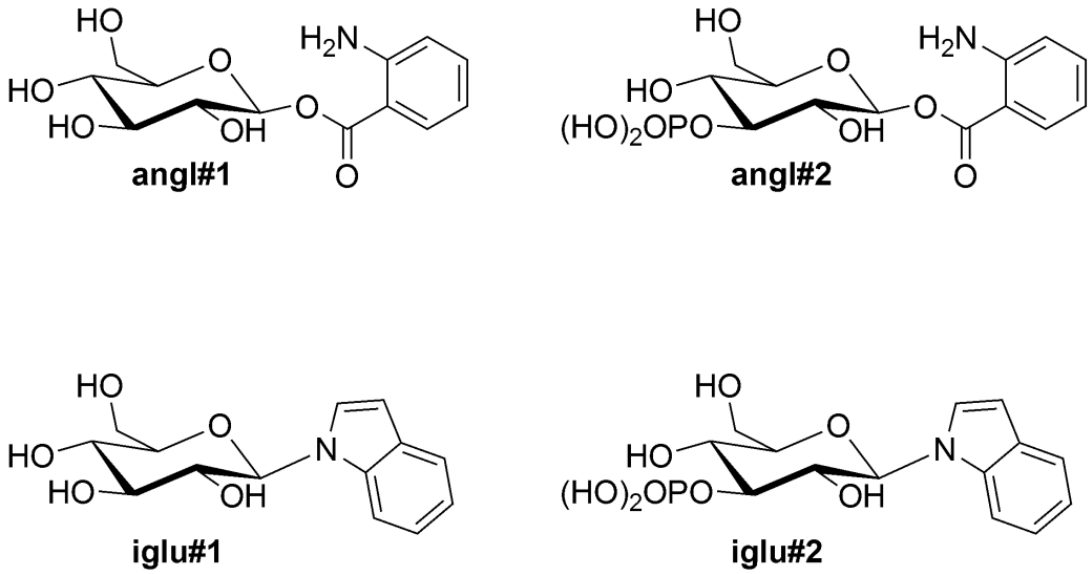

Figure 4.9. DANS analysis reveals *glo-1* dependent small molecules. Structures of *C. elegans* metabolites identified via DANS that are strongly downregulated in *glo-1(zu437)*.

Metabolite fractions obtained from N2 worm pellets grown in liquid cultures as described in Chapter 1 and 2 when exposed under UV showed blue fluorescence (**Figure C.4).** Proton NMR analysis of these fractions also confirmed that fluorescent fractions contained anthranilic acid moieties whereas glucosylated indoles were found in the non-fluorescent fractions (**Figure C.5**).

DF Arises from tryptophan via the kynurenine pathway:

The indole glucosides, iglu#1 and iglu#2, previously unreported in animals, did not emit blue fluorescence. AA is formed during catabolism of L-tryptophan via the kynurenine pathway (**Figure 4.10**) and has previously been observed in *C. elegans* (Rongvaux et al., 2003; van der Goot et al., 2012), but neither angl#1 nor angl#2 have previously been reported in animals.

Anthranilic acid (AA) derivatives show characteristic fluorescence at $\lambda_{ex}/\lambda_{em}$ 340/430 nm (Nakken et al., 1963), and their absence in the non-fluorescent sonicates of *glo-1(zu437)* mutant worms indicates that these compounds are responsible for the blue fluorescence observed in wild-type animals.

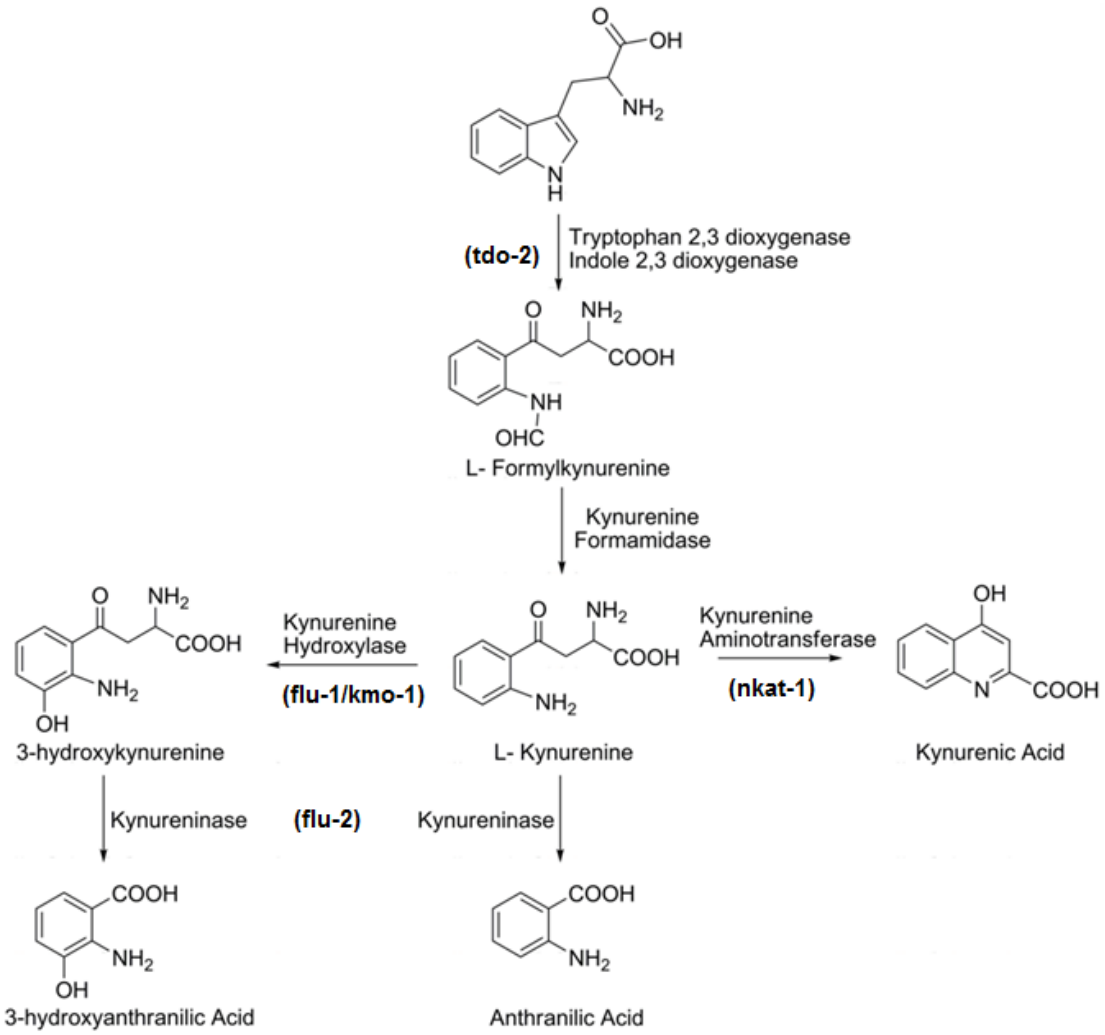

Figure 4.10. Kynurenine pathway in *C. elegans*. *C. elegans* genes known to be orthologous to mammalian genes in this pathway are shown in brackets and bold.

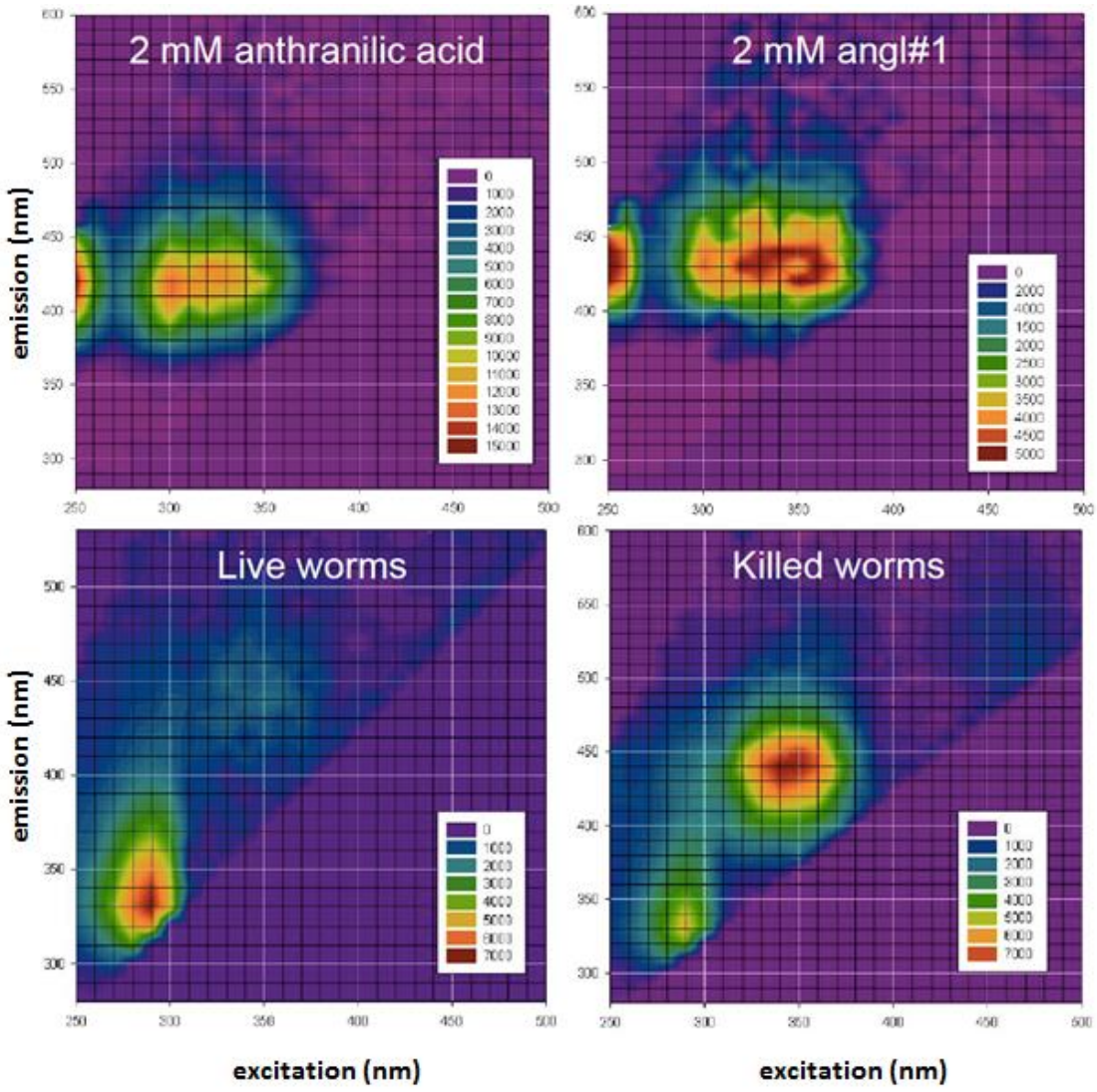

Figure 4.11. Fluorescence spectra for angl#1 (2 mM) and worm blue fluorescence are highly similar. Also shown is fluorescence of unconjugated anthranilic acid (2 mM). Data courtesy Filip Matthijssens (Bart Braeckman Lab, University of Ghent)

Moreover fluorescence spectra for angl#1 and worm blue fluorescence were identical (**Figure 4.11**). Additionally, the HPLC retention times of the identified AA derivatives match those of the fluorescent peaks detected in the initial HPLC analysis of the wild-type sonicates. Together, these data provide the structural evidence for the identification of anthranilic acid derivatives as fluorophores responsible for DF in nematodes.

To further verify this result, we used a genetic approach. The enzyme responsible for the first step in the conversion of Trp to AA is tryptophan 2,3-dioxygenase (TDO) encoded in *C. elegans* putatively by the gene *tdo-2* (C28H8.11). (Rongvaux, 2003; van der Goot, 2012). Treatment with *tdo-2* RNAi greatly reduced gut granule blue fluorescence and DF (freeze thaw) (**Figure C.6**). We further tested exogenous AA is sufficient to cause blue gut granule fluorescence. Indeed incubation of *tdo-2*-RNAi treated worms with 5 mM AA restored gut granule fluorescence to wild-type level (**Figure C.6**). We therefore concluded that gut granule fluorescence and DF emanate from AA.

Preliminary DANS analysis of the Flu mutants:

The identification of AA derivatives as DF fluorophores suggested that knowledge of tryptophan metabolism in *C. elegans* is incomplete. In particular, we were interested in the yet undetermined role of Flu mutants in the kynurenine pathway, one of the most highly conserved pathways across species. As noted earlier, several metabolites of this pathway have been implicated in various metabolic and degenerative disorders in mammals (**Figure 4.10**) and yet the first detailed investigation on the kynurenine pathway in *C. elegans* was reported only in 2012 (van der Goot et al., 2012). We therefore used DANS methodology to compare dqfCOSY spectra of metabolite extracts obtained from wild-type animals and from the four flu

mutants previously described. Our preliminary objective was to develop hypotheses about these genes' biosynthetic roles, based on observing changes in the global metabolomes of these mutants, which to date have not been cloned.

Comparison of wild-type and *flu-1* spectra showed significant differences in the aromatic region. *Flu-1* mutants have been reported to demonstrate significantly reduced kynurenine-3-hydroxylase activity (Siddiqui and Babu, 1980). Kynurenine 3-hydroxylase is responsible for the conversion of kynurenine into 3-hydroxy kynurenine or anthranilic acid to its 3-hydroxy counterpart (Babu et al., 1974). Therefore, *flu-1* mutants should have reduced levels of 3-hydroxy kynurenine (3-OH-Kyn) or 3-hydroxy anthranilic acid (3-OH-AA) and increased levels of l-kynurenine (Kyn) and AA. These changes are indeed evident when the *flu-1* and wild-type dqfCOSY spectra are analysed in a greater detail (**Figure 4.12**).

Figure 4.12. NMR-based comparative metabolomics (DANS) applied to C. elegans wild type (N2) and flu-1. Comparison of the aromatic regions of dqfCOSY 2D NMR spectra of wild type (N2, upper panel) and flu-1 (lower panel) sonicates reveals several groups of signals that are either strongly downregulated in the flu-1 spectrum (black boxes), or upregulated in the flu-1(red boxes) or remain unchanged (blue boxes).

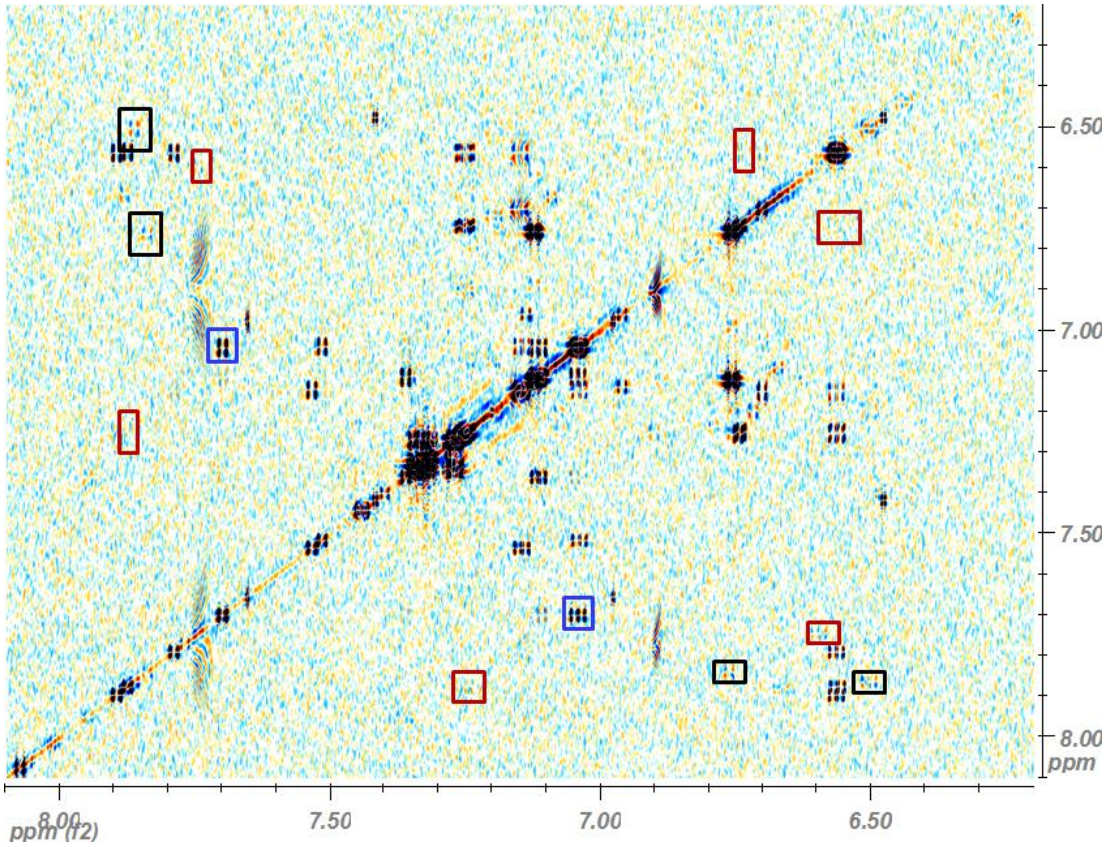
6.50
7.00
7.50
8.00
ppm
8.00
7.50
7.00
6.50
ppm (f2)

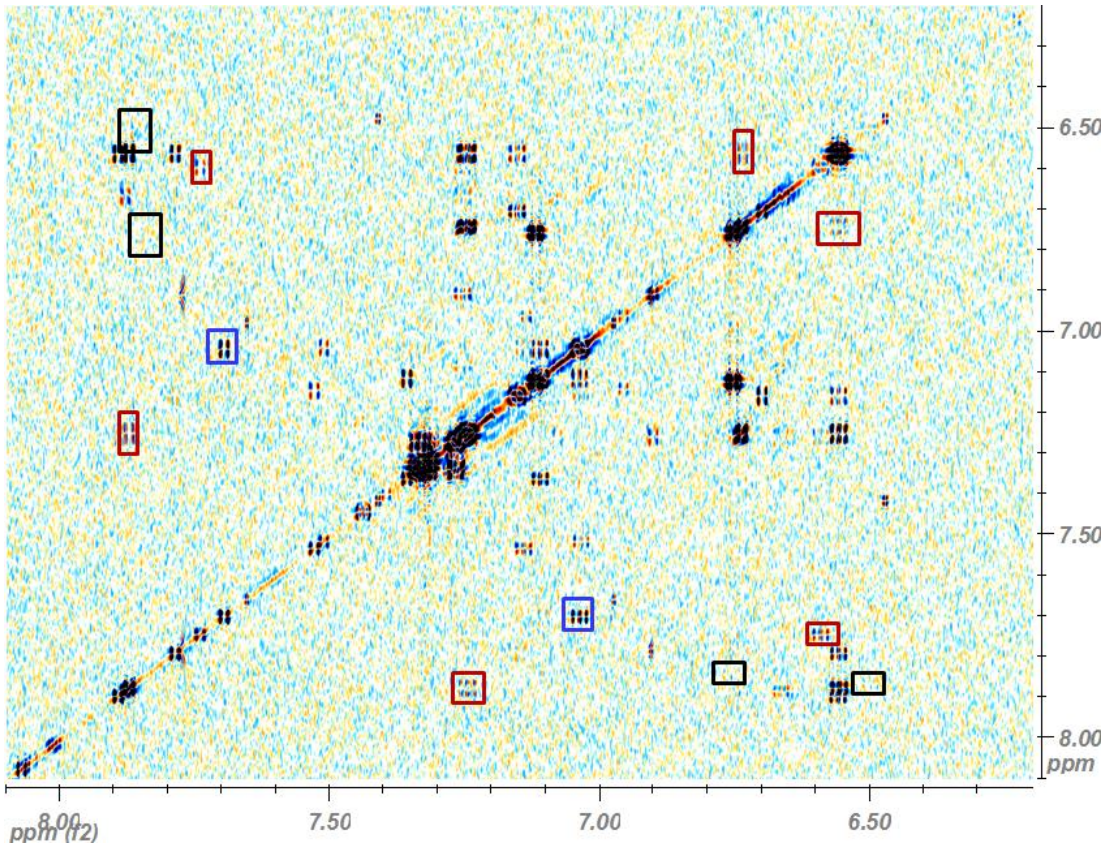
6.50
7.00
7.50
8.00
ppm
8.00
7.50
7.00
6.50
ppm (f2)

Flu-2 putatively encodes for the kynureninase enzyme which also uses kynurenine as a substrate converting it to anthranilic acid. Similarly, it can convert 3-OH-Kyn to 3-OH-AA. Our 2D-NMR spectroscopy based comparison of the *flu-2* metabolome to the wild-type metabolome, shows a striking difference. All of the cross peaks, earlier characterized to be derived from antranilic acid moieties were either absent or significantly downregulated. This suggests that the *flu-2* mutants contain a null mutation of the kynureninase gene and therefore has a blocked anthranilic acid production and conseqeuently an abnormal autofluorescence. (**Figure 4.13**). There are other differences between the two metabolomes but these differences have not been investigated to a greater detail and will be the subject of future studies.

Figure 4.13. NMR-based comparative metabolomics (DANS) applied to C. elegans wild type (N2) and flu-2. Comparison of the aromatic regions of dqfCOSY 2D NMR spectra of wild type (N2, upper panel) and flu-2 (lower panel) sonicates reveals several groups of signals that are either strongly downregulated in the flu-2 spectrum (black boxes), or upregulated in the flu-2(red boxes) or remain unchanged (blue boxes).

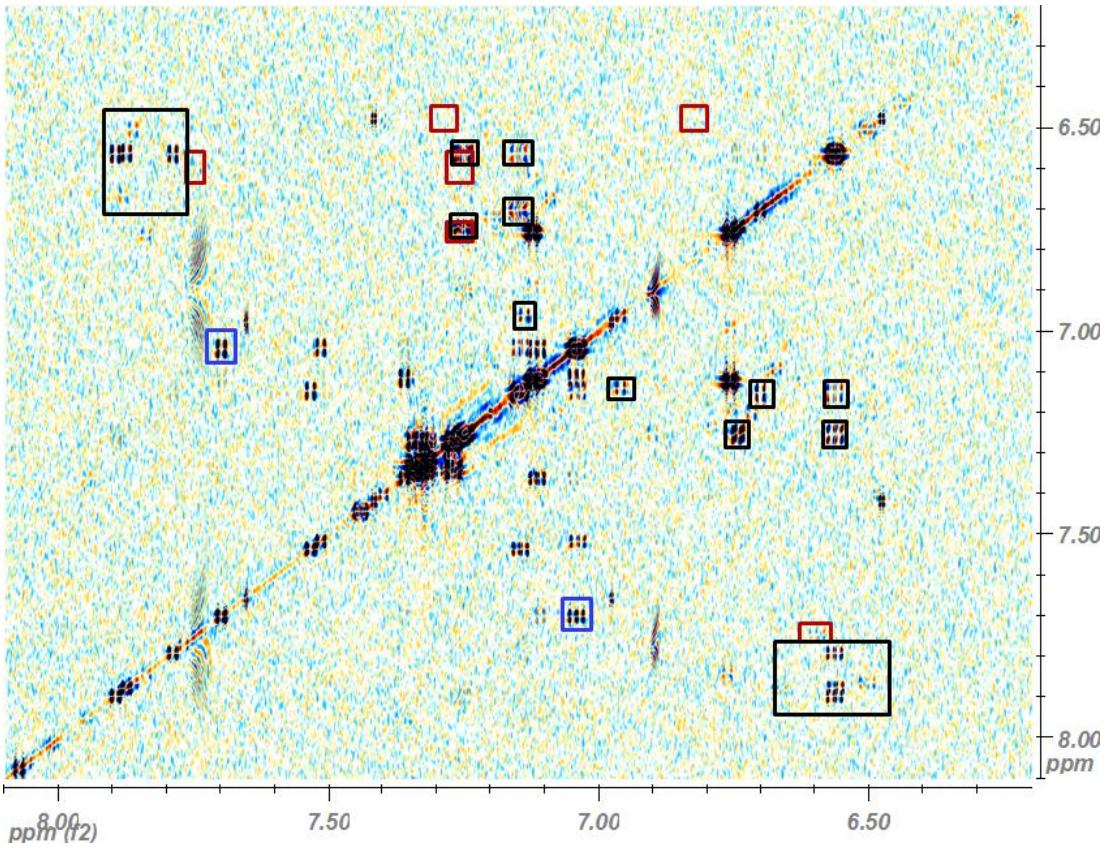
6.50
7.00
7.50
8.00
ppm
8.00
7.50
7.00
6.50
ppm (f2)

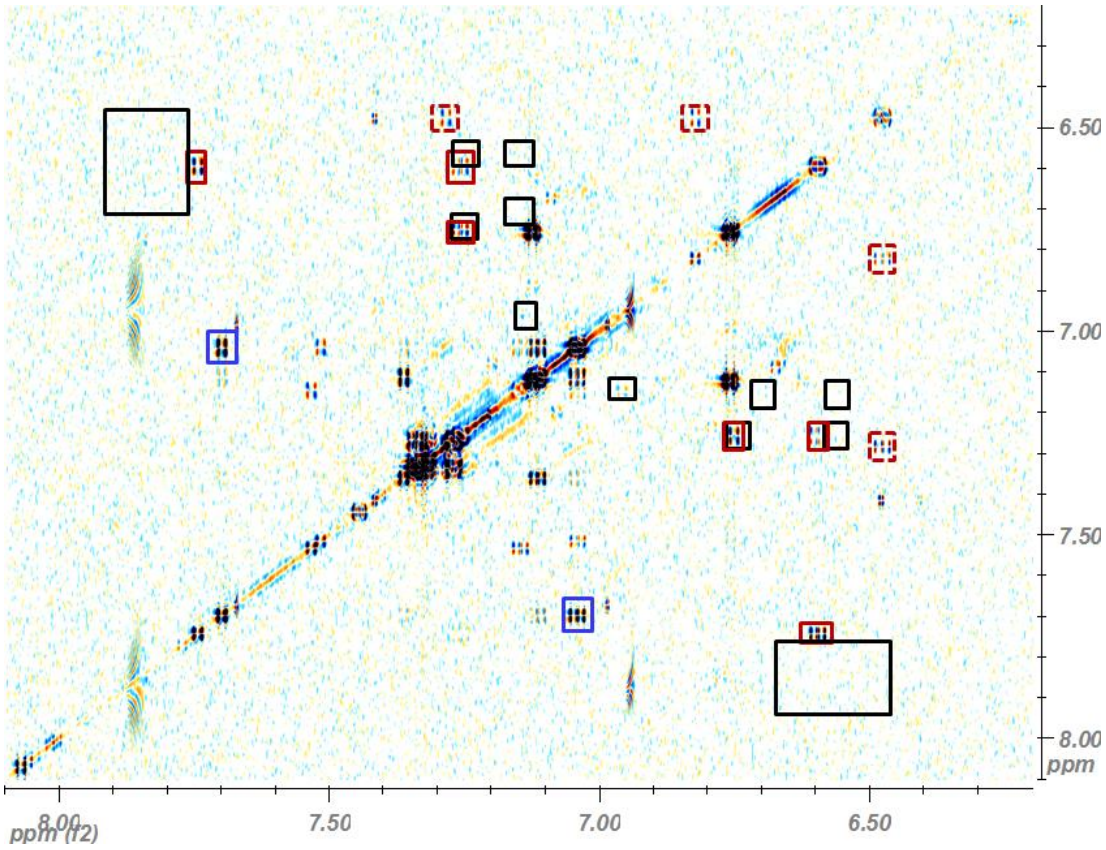
6.50
7.00
7.50
8.00
ppm
8.00
7.50
7.00
6.50
ppm (f2)

RNAi or mutation of flu-2 (putative kynureninase) also reduced DF, while inactivating kynurenine 3-monooxygenase by RNAi or flu-1 mutation raised DF, as expected according to the kynurenine pathway (**Figure 4.14**). These results along with our spectroscopic data support the putative enzymatic functions assigned to FLU-1 and FLU-2 and encourages further study on the tryptophan degradation pathway using the DANS methodology.

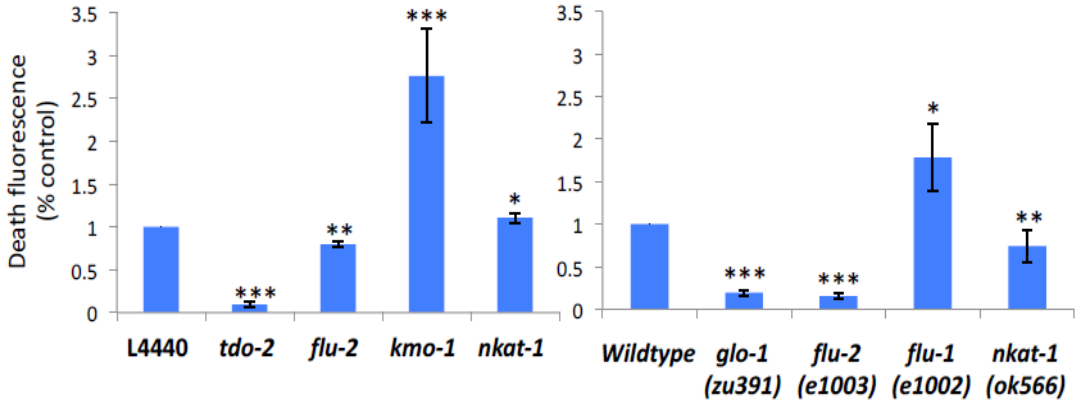

Figure 4.14. Kynurenine pathway genes affect DF levels. Effects of RNAi of kynurenine pathway genes on DF. Worms were killed by freeze thaw, and fluorescence measured in a plate reader (Appendix C) (Image Courtesy : Cassandra Coburn).

While flu-1 and flu-2 have been assigned a putative function in the tryptophan degradation pathway, the other two members of the Flu mutant family have not been connected to any phenotype or function except their altered fluorescence. We have started to analyze the differences in the metabolomes of flu-3 and flu-4 mutants from wild-type *C. elegans* (**Figures C.7 and C.8**) specifically investigating changes in the production of tryptophan catabolites. Comparison of the wild-type and flu-3 spectra reveals one distinct difference between the two metabolome. The signal at 6.53 and 7.82 ppm is strictly

present in N2 and absent in flu-3. Preliminary analyses of this crosspeak and comparison with commercial standards of metabolites from the Kynurenine Pathway suggest that this cross peak is derived from an anthranilic acid moiety. But interestingly other anthranilic acid moieties such as angl#1 and angl#2 are present in flu-3 suggesting a possible perturbation in the tryptophan degradation pathway and further analyses will reveal connections between these other differential cross peaks. but these differences have not been analyzed in greater detail.

Similar preliminary analysis of flu-4 spectra also show minor differences in the aromatic region of the metabolomes, although none among the AA derivatives suggesting that, flu-4 mutations do not perturb any of the known genes in the tryptophan catabolism and any changes arising in its autofluorescence is possibly a consequence of perturbations in another pathway.

Together these results show that our comparative metabolomics approach is extremely powerful for investigating the kynurenine pathway in C. elegans and based on these preliminary studies we can proceed towards fully characterizing all known and putative mutants implicated in the tryptophan degradation pathway to obtain a complete understanding of the downstream metabolites produced i.e. understanding gene function by looking at the metabolite profiles. The knowledge of these intermediates will not only help our understanding of tryptophan degradation but also complement our efforts to identify a novel ligand for the *C. elegans* aryl hydrocarbon receptor, ahr-1.

Conclusions and Discussion:

In this chapter, the author shows the utilization of Differential Analysis by 2D-NMR Spectroscopy technique to identify the chemical moieties involved in the striking blue fluorescence produced within the gut granules in nematodes. Coupled with biochemical and genetic techniques (Cassandra Coburn, University College London) and Fluorescence measurements (Filip Matthijssens, Bart Braeckman Lab, University of Ghent), this work explains how this blue gut granule fluorescence is actually associated with death and not aging, and thus defines a new phenomenon, that of “death fluorescence”. While previously it was proposed that the origin of this fluorescence is lipofuscin, a heterogenous protein degradation product mix, this study provides unambiguous spectroscopic evidence to confirm the role of tryptophan derived, anthranilic acid derivatives as the blue fluorophore.

The identification of these anthranilic acid derivatives was made possible by comparing metabolomes of WT and glo-1(zu437), a mutant strain defective in the biogenesis of gut granules and consequently deficient in gut granule fluorescence. The anthranilic acid glucosyl ester angl#1 and its corresponding 3-O-phosphorylated derivative angl#2 account for both death and gut granule-associated fluorescence. glo-1 mutants lack both forms of fluorescence and AA derivatives, and inhibition of the kynurenine pathway blocks both forms of fluorescence, establishing that this blue fluorescence is not lipofuscin. Whether lipofuscin accumulation occurs during aging in C. elegans remains an open question. However, our finding that blue fluorescence is not lipofuscin removes one reason for believing that aging in C. elegans is caused by accumulation of stochastic molecular damage. The kynurenine pathway that generates gut granule and DF is also involved in

mammalian neurodegeneration, and has recently been shown to regulate protein folding homeostasis in C. elegans (van der Goot et al., 2012).

One can explore several possibilities to explore the possibilities of roles of kynurenines in *C. elegans.* It is possible that AA derivatives may have some protective function. There is evidence that the kynurenine pathway is involved in immunity and tumuorogenesis (Opitz et al., 2011). AA can inhibit growth of bacterial pathogens (Sasaki et al., 2012) and 3-hydroxyanthranilic acid can induce cell death in lymphocytes (Piscianz et al., 2011). Alternatively the kynurenines may contribute to organismal death in some manner that is not self-evident. It has been found that in patients suffering from stroke, Huntington's disease chronic brain injury and depression, amongst other diseases, an increased AA to 3-HA ratio can be seen.

For this reason, we have started investigating the kynurenine pathway using DANS methodology and while comparison of the N2 metabolome with that of flu-1 and flu-2 confirms the putative role of these genes in the kynurenine pathway, similar comparison of the N2 and flu-3 metabolome provides preliminary evidence that there may exist other novel regulators of the tryptophan degradation pathway that has not been reported previously and this work will be continued in the Schroeder Lab.

Another direct consequence of this work is to look into the role of these tryptophan catabolites in other *C. elegans* pathways, e.g. as ligands of the transcription factor AHR-1(Opitz et al., 2011) or maybe as signaling molecules involved in protection against bacterial toxicity (Dan Kalman Lab, personal communication). Recent studies show that kynurenine is a putative endogenous ligand of AHR-1 in mammalian tissues (Opitz et al., 2011). There are numerous other studies which implicate several other tryptophan derivatives as endogenous activators of this ligand dependent transcription

factor and further study of the tryptophan degradation pathway in *C. elegans* will surely allow us to understand: 1) what are the endogenous ligands for *C. elegans* aryl hydrocarbon receptor encoded by ahr-1, 2) does the flu mutants and other kynurenine pathway mutants form a biosynthetic block to the production of these ligands and 3) do these same molecules bind the mammalian AhR ?

Other unanswered questions that remain is the need for glycosylation of the anthranilic acid moieties as well as the biological significance of gut granules. It has been previously reported that glycosylation is a technique that *C. elegans* uses to make toxic substances within its body more polar and therefore easily excretable (Bommarius B, et al., 2012; Stupp et al., 2011). While it does not seem likely in the case of AA derivatives, since they are largely confined within the animal, the reasons for glycosylation of the AA moieties and subsequent phosphorylation, still needs to be investigated. Similarly, while this work does provide a concrete evidence for the structural identity of death fluorescence, which originates in the gut granules, the actual biological significance of the gut granules still remains a mystery and future analysis of the glo family of mutants should reveal exciting insights to this end.

REFERENCES

Babu P. (1974). Biochemical genetics of Caenorhabditis elegans. Mol Gen Genet *135*, 39–44.

Bernabucci M., Notartomaso S., Zappulla C., Fazio F., Cannella M., et al. (2012). N-acetyl-cysteine causes analgesia by reinforcing the endogenous activation of type-2 metabotropic glutamate receptors. Mol Pain *8*, 77.

Bommarius B., Anyanful A., Izrayelit Y., Bhatt S., Cartwright E., et al. (2013). A Family of Indoles Regulate Virulence and Shiga Toxin Production in Pathogenic E. coli. PLoS One *8*(1), e54456.

Brunk U.T., Terman A. (2002). Lipofuscin: mechanisms of age-related accumulation and influence on cell function. Free Radic Biol Med *33*, 611–619.

Chitwood B. G., Chitwood M. B. (1950). An Introduction to Nematology. Baltimore: University Park Press.

Clokey G. V., Jacobson L. A. (1986). The autofluorescent “lipofuscin granules” in the intestinal cells of *Caenorhabditis elegans* are secondary lysosomes. *Mech. Ageing Dev 35,* 79–94.

Eldred G.E., Miller G.V., Stark W.S., Feeney-Burns L. (1982). Lipofuscin: resolution of discrepant fluorescence data. Science *216*, 757–759.

Fletcher B.L., Dillard C.J., Tappel A.L. (1973). Measurement of fluorescent lipid peroxidation products in biological systems and tissues. Anal Biochem *52*, 1–9.

Garigan D., Hsu A.L., Fraser A.G., Kamath R.S., Ahringer J., et al. (2002). Genetic analysis of tissue aging in Caenorhabditis elegans: a role for heat-shock factor and bacterial proliferation. Genetics *161*, 1101–1112.

Gerstbrein B., Stamatas G., Kollias N., Driscoll M. (2005). In vivo spectrofluorimetry reveals endogenous biomarkers that report healthspan and dietary restriction in Caenorhabditis elegans. Aging Cell *4*, 127–137.

Hermann G.J., Schroeder L.K., Hieb C.A., Kershner A.M., Rabbitts B.M., et al. (2005). Genetic analysis of lysosomal trafficking in Caenorhabditis elegans. Mol Biol Cell *16*, 3273–3288.

Jung T., Bader N., Grune T. (2007). Lipofuscin: formation, distribution, and metabolic consequences. Ann N Y Acad Sci *1119*, 97–111.

Klass M.R. (1977). Aging in the nematode Caenorhabditis elegans: major biological and environmental factors influencing life span. Mech Ageing Dev *6*, 413–429.

Messaoudi S., Sancelme M., Polard-Housset V., Aboab B., Moreau P., et al. (2004). Synthesis and biological evaluation of oxindoles and benzimidazolinones derivatives. Eur J Med Chem *39*, 453–458.

Nakken K.F. (1963). Quantitative fluorometric determination of anthranilic acid, 3-hydroxy-5-hydroxyanthranilic acid in urine. Scand J Clin Lab Invest *15*, 78–79.

Opitz C.A., Litzenburger U.M., Sahm F., Ott M., Tritschler I., et al. (2011). An endogenous tumour-promoting ligand of the human aryl hydrocarbon receptor. Nature. *478*, 197-203.

Piscianz E., Cuzzoni E., De Iudicibus S., Valencic E., Decorti G., et al. (2011). Differential action of 3-hydroxyanthranilic acid on viability and activation of stimulated lymphocytes. Int Immunopharmacol 11, 2242–2245.

Raposo G., Marks M. S. (2007). Melanosomes – dark organelles enlighten endosomal membrane transport. Nat Rev Mol Cell Biol*. 8* 786–797.

Roell D., Rosler T.W., Degen S., Matusch R., Baniahmad A. (2011). Antiandrogenic activity of anthranilic acid ester derivatives as novel lead structures to inhibit prostate cancer cell proliferation. Chem Biol Drug Des 77, 450–459.

Rongvaux A., Andris F., Van Gool F., Leo O. (2003). Reconstructing eukaryotic NAD metabolism. Bioessays *25*, 683–690.

Sasaki T., Mizuguchi S., Honda K. (2012). Growth inhibitory effects of anthranilic acid and its derivatives against Legionella pneumophila. J Biosci Bioeng *113*, 726–729.

Siddiqui S.S., Babu P. (1980). Kynurenine hydroxylase mutants of the nematode Caenorhabditis elegans. Mol Gen Genet *179*, 21–24.

Stupp G.S., von Reuss S.H., Izrayelit Y., Ajredini R., Schroeder F.C., Edison A.S. (2013). Chemical detoxification of small molecules by Caenorhabditis elegans. ACS Chem Biol *8*, 309-13.

Terman A., Brunk U.T. (1998). Ceroid/lipofuscin formation in cultured human fibroblasts: the role of oxidative stress and lysosomal proteolysis. Mech Ageing Dev *104*, 277–291.

Van der Goot A.T., Zhu W., Vazquez-Manrique R.P., Seinstra R.I., Dettmer K., et al. (2012). Delaying aging and the aging-associated decline in protein homeostasis by inhibition of tryptophan degradation. Proc Natl Acad Sci U S A 109: 14912–14917

CHAPTER 5

CONCLUSIONS AND OUTLOOK

Conclusions and impact of this work

While quantitative measurement of the impact of any scientific work requires multiple factors to be considered and is often corrupted with specific biases, one interesting way of evaluating scientific results could be by weighing not just the number of questions answered but also the number of new questions unearthed as a consequence of the investigation. Applying this metric to evaluate this study, one can come up with a plethora of questions regarding animal metabolism in general, all based on the results generated by this study.

The most important outcome of this work is the demonstration of a largely unbiased (by preconceptions about ligand structures) approach for the identification of endogenous small molecule ligands for NHRs. This is significant because NHRs, both historically and continually, have been important targets for therapeutic development (Shi, 2007) due to the possibility of perturbing their activity by small molecules. A systematic, unbiased approach to identify ligands and their biosynthetic machinery providing will reveal multiple new nodes that can be perturbed or fine-tuned for therapeutic purposes. Only 50% of mammalian NHRs have known ligands, and of these 50%, a majority have subsequently become therapeutic targets (Shi, 2007). While our understanding of the roles that NHRs play has continuously improved, the same cannot be said about our knowledge of their endogenous ligands. This work provides a novel approach to bridge this gap.

Specifically, this study has identified key components of the steroid biosynthetic machinery in *C. elegans* that are fascinating because of the unexpected nature of some of their structural features. The discovery of a Δ^1 steroid in *C. elegans* is the first example for such steroids in animals. This is especially interesting because of the already known significance of the Δ^1 double bond in synthetic ligands of mammalian NHRs (Counsell and Klimstra, 1962; Goulding and Flower, 2001) and calls for reinvestigation of mammalian NHR ligand pathways for the presence of this structural modification. In addition it will be of great interest to find the *C. elegans* enzyme that incorporates this double bond in the steroid A-ring, an enzymatic function previously unrecognized in animals. Questions such as tissue specificity and species specificity of this enzyme can then be asked.

Similarly, the identification of a 3-α-hydroxy steroid in *C. elegans*, a sterol auxotroph that utilizes exogenous cholesterol and other 3-β-hydroxy sterols as its primary sterol source, directs towards the existence of another previously unrecognized, steroid-metabolizing enzyme in *C. elegans*, and perhaps other metazoans. The subsequent characterization of the CYP450/DAF-40 as a regio-specific enzyme carrying out oxidation (and putatively other functions) at the 3 position of steroids underlines our original hypothesis that the identification of newer small molecules will lead to the identification of other novel components in pathway regulating the NHR DAF-12.

Together, these results will revitalize the interest of the *C. elegans* community in understanding NHR function and reinforce the idea that minute changes in the structure of a small-molecule can significantly change its overall function and subsequent physiological responses. We now have to ask whether there is a specific function of the additional unsaturation, how

structural changes at the ligand level are perceived and transduced to the transcription level i.e. are there ligand-specific co-activators or response elements, whether there are DAF-12 outputs affected differentially by the different identified ligands, and finally do these ligands bind to other NHRs in *C. elegans* and/or other nematodes?

In chapter 4, the chemical nature of the “death fluorescence” has been revealed. This blue fluorescence was earlier considered a consequence of age-related degradation products of proteins, and this work has confirmed that this is not the case: the blue death fluorescence is due to release of specific tryptophan catabolites. The discovery of anthranilic acid derivatives as fluorescent biomarker of death is therefore a significant discovery not just within the *C. elegans* community but the entire scientific community. Tryptophan degradation pathways have frequently been hypothesized to be correlated to aging and age-related diseases, (van der Goot and Nollen, 2013) and thus the finding that the production of a specific tryptophan catabolite is closely correlated with the onset of death is not a mere coincidence. More importantly, a number of questions have arisen from these results – why are anthranilic acid glucosylated, i.e. is it similar to glycosylation of toxic compounds and functions only as a transport mechanism, how and why is the *in-situ* production of anthranilic acid and its derivatives suddenly increased at death, and it will be interesting to ask whether this pathway is conserved in other animals and whether can we in fact visualize death in other living organisms as a function of the over production of a specific small molecule.

These and many other questions have arisen and will arise from this work and will be duly investigated either by other members of the Schroeder lab, our collaborators or other ‘metabonauts’ – chemists and biologists interested to investigate the metabolomic terrain of living systems.

Future Outlook - Comparative metabolomics-based analysis of essential biological pathways in higher organisms

As described in this dissertation, comparative metabolomics approaches utilizing 2D NMR-spectroscopy and LC/MS based methodology is extremely effective in understanding metabolic pathways in *C. elegans.* Parallel work from other members of the Schroeder Lab and its collaborators have confirmed the applicability of these techniques in microorganisms such as bacteria (Li et al., 2012) and fungi (Forseth et al., 2011), as well as other nematodes and *P. pacificus* (Bose et al., 2012). The key question now is how to move closer to our ultimate objective of elucidating small molecule-mediated signaling in higher organisms, so that it can help us provide more logical and more informative answers regarding biomedical questions that exist today asw well as new ones that may appear tomorrow. Encouraging in this respect, and challenging at the same time, is the knowledge that small molecules are involved in a significant portion of the signal transduction pathways that effect living systems, and that even today we have only uncovered or appreciated a small fraction of the structural and functional diversity they incorporate.

As developers of metabolomics approaches, to move forward without being distracted by the fascinating complexity of small molecule architecture, we then have to focus on two key aspects of biological research : biological systems (i.e. organisms) and biological processes (i.e. metabolic pathways). The Preface of this dissertation introduced the necessity and reasoning for using model organisms (Hulme and Whitesides, 2011). In this regard, as shown in this dissertation as well as other contemporary work, *C. elegans* provides an excellent platform to ask and answer key questions about animal biology, so much so, that Sydney Brenner called this organism “Nature’s gift to

science". However, like with all models, the use of *C. elegans*, despite its wide use as disease models, brings with it a certain set of limitations, especially the percentage of genetic overlap, which physiologically manifests as higher complexity in behavior, development and reaction to environmental responses. Therefore, looking at alternative models, especially vertebrate models such as puffer fish (*Fugu rubripes*) or frogs (*Xenopus* spp.) for specific pathways may become more beneficial. Of course if in the sudden discovery of a 'disruptive technology', propagation and genetic manipulation with mice (*Mus musculus*) becomes easier and cheaper, it would be the most ideal system to study small molecule signaling networks, mainly because of the easy interpolation of results and conclusions to the human model.

Of note is also the existence of a new nematode model based on the organism *Pristionchus pacificus*. Originally studied as a satellite model to *C. elegans*, work in recent years has catapulted this organism into the limelight, primarily because of its higher complexity of many signaling networks, which may be due to its more complex ecological interactions (Bento et al., 2010). *P. pacificus* has revealed fascinating examples of phenotypic plasticity that are regulated by conserved signaling pathways, in part based on small molecules. Coupled with its closer proximity (than *C. elegans*) to parasitic nematodes make this an exceptionally useful and plausible "next step" for *C. elegans* researchers to proceed. Specifically regarding the work described in this research, investigation of the steroid profile of *P. pacificus* is an obvious future direction, in particular the identification of the Ppa-endogenous DAF-12 ligands. Additionally, *P. pacificus* can also be the next frontier for investigating the tryptophan degradation pathway. We are already aware of the presence of a more evolved small-molecule bio-synthesis machinery in *P. Pacificus* (Bose et al., 2012) and it would be of course interesting to investigate the presence

or absence or structural modifications of the kynurenine pathway metabolite in this nematode.

The identification of novel steroids in this study will increase motivation towards investigating the presence of similar structural modifications and corresponding enzymes in higher organisms e.g. Δ^1 steroids, Δ^1 desaturase enzyme, a P450 that specifically oxidises 3-α-hydroxy steroids, and tissue-specific hormone production machinery. This work will encourage re-consideration of steroid bio-transformations and their relevance for NHR-hormone interactions.

The author of this dissertation has been fortunate to have worked with two central biological pathways that define key physiological responses in living systems across phyla. Both steroid hormone-dependent NHR regulation and the involvement of tryptophan catabolites in central processes such as immunity, degeneration and death are fields of research that require further in-depth analysis using multiple, distinct interdisciplinary approaches, and metabolomics will play an important role in these investigations. The results obtained in this study can be used as starting points to further investigate these processes in *C. elegans* and higher organisms.

One important example for a small molecule-regulated pathway that remains poorly understood is that of molting. As previously mentioned, *C. elegans* contains 283 orphan nuclear receptors, of which 14 have similarity to NHRs of higher animals, and among these at least two, NHR-23 and NHR-25, have been implicated in the process of molting (Taubert et al., 2010). Elucidation of ligand structures of these receptors will be extremely important. The approach developed by this study requires an efficient method to detect bioactivity within metabolite extracts, and mutant organisms that are deficient of production of the target compound. In both these aspects, studying the

molting phenomena poses great challenges especially since mutants associated with defects in molting or developmental timing are often sterile or of limited viability. However, RNAi-based silencing of molting genes may provide a way to address this challenge.

A direct consequence from this work has been the renewed interest within Schroeder lab on the tryptophan degradation pathway and the association of tryptophan metabolites with the Aryl Hydrocarbon Receptor. The author of this dissertation strongly believes that AhR will play a major role in medicine in the next decade, primarily for two reasons: 1) the recent discoveries that, although AhR was discovered originally as a mediator of xenobiotic responses, this transcription factor actually plays a major role in regulating development and immunity across species, and 2) the possibility that specific tryptophan derived metabolites serve as the endogenous ligands of AhR. Not least because of its association with AhR, the tryptophan degradation pathway has recently come to the forefront of biomedical research, with increasing number of results pointing towards the involvement of tryptophan catabolites in disease pathways such as neurodegeneration, tumorigenesis and several primary metabolic pathways. The discovery of novel endogenous, tryptophan-derived ligand for Ahr-1 in *C. elegans* could therefore have important implications. This work has only shown some preliminary results regarding the kynurenine pathway mutants in *C. elegans*, and based on these initial results one can definitely hypothesize that a more extensive analysis of this pathway will lead to the characterization of more novel components of this widely conserved pathway, including perhaps the presence of a previously unrecognized enzyme.

A third focus area for future studies on metabolomics concerns signaling processes that mediate interactions of different organisms. We can

identify endogenous metabolites produced by an organism as a consequence of environmental, genetic changes. Can we extrapolate this and find out more about species cross-talk, host-pathogen interactions and symbiotic relationships among living systems. Humans have tried and are still trying to overcome barriers caused by language using our other sensory perceptions. Is this possible in a molecular level? There are already examples where organisms have been found “listening in” to the conversations of other organisms and using it to their benefit, and almost always this is because of the existence of receptors or sensory organs that detect a specific kind of small molecule. Can we then, use our metabolomics approaches to tap into these conversations, held in a universally accepted language based on small molecules?

REFERENCES

Bento, G., Ogawa, A., and Sommer, R.J. (2010). Co-option of the hormone-signalling module dafachronic acid-DAF-12 in nematode evolution. Nature 466, 494-7.

Bose, N., Ogawa, A., von Reuss, S.H., Yim, J.J., Ragsdale, E.J., Sommer, R.J., and Schroeder, F.C. (2012). Complex small-molecule architectures regulate phenotypic plasticity in a nematode. Angew Chem Int Ed Engl 50,12438-43.

Brenner, S. (2003). Nobel lecture. Nature's gift to science. Biosci Rep 23, 225–237.

Counsell, R.E., and Klimstra, P.D. (1962). Anabolic Agents: Derivatives of 2-Halo 5alpha-Androst-1-Ene. J Med Pharm Chem *91*, 477-483.

Forseth, R.R., Fox, E.M., Chung, D., Howlett, B.J., Keller, N.P., and Schroeder F.C. (2011). Identification of cryptic products of the gliotoxin gene cluster using NMR-based comparative metabolomics and a model for gliotoxin biosynthesis. J Am Chem Soc 133, 9678-81.

Goulding, N.J. and Flower, R.J. (2001). Glucocorticoids (Milestones in Drug Therapy). BirkHouser Publishing House.

Hulme, S.E., and Whitesides, G.M. (2011). Chemistry and the worm: Caenorhabditis elegans as a platform for integrating chemical and biological research. Angew Chem Int Ed Engl *50*, 4774-4807.

Li, B., Forseth, R.R., Bowers A.A., Schroeder F.C., and Walsh CT. (2012) A backup plan for self-protection: S-methylation of holomycin biosynthetic intermediates in Streptomyces clavuligerus. Chembiochem *13*, 2521-6.

Motola, D.L., Cummins, C.L., Rottiers, V., Sharma, K.K., Li, T., Li, Y. et al. (2006). Identification of ligands for DAF-12 that govern dauer formation and reproduction in C. elegans. Cell *124*, 1209-1223.

Shi Y. (2006). Orphan Nuclear Receptors in Drug Discovery. Drug Discov Today 12, 440-445.

Taubert, S., Ward, J.D., and Yamamoto, K.R. (2010). Nuclear hormone receptors in nematodes: evolution and function. Mol Cell Endocrinol 334, 49-55.

van der Goot, A.T., and Nollen, E.A.A. (2013). Tryptophan metabolism: entering the field of aging and age-related pathologies. Trends Mol Med *19*, 336 – 344.

Wollam, J., and Antebi, A. (2011). Sterol regulation of metabolism, homeostasis, and development. Annu Rev Biochem *80*, 885-916.

APPENDIX A

1. *C. elegans* Strains and Maintenance

Nematode stocks were maintained on Nematode Growth Medium (NGM) plates made with Bacto agar (BD Biosciences) and seeded with bacteria (*E. coli* strain OP50) at 20 °C (http://www.wormbook.org/). The following *C. elegans* strains were used: wild type (N2, Bristol), *daf-22(m130), daf-22(ok693), daf-9(dh6), daf-9(dh6);daf-12(rh411rh61), hsd-1(mg345), glp-1(e2141), glp-1(e2141)*;*daf-36(k114)*. Compound mutants were constructed using standard techniques. Worms were grown at 20 °C for at least two generations under replete growth conditions prior to growing in liquid cultures.

2. Liquid Cultures

Worms from four 10 cm NGM agar plates were washed using M9-medium into a 100 mL S-complete medium pre-culture where they were grown for four days at 22 °C on a rotary shaker. Concentrated bacteria derived from 1 L of *E. coli* OP50 culture was added as food at days one and three. Subsequently, the pre-culture was divided equally into sixteen 500 mL Erlenmeyer flask containing 100 mL of S-complete medium on day 4, which was then grown for an additional 5 days at 22 °C on a rotary shaker and fed with concentrated bacteria *ad lib*. The cultures were harvested on day 5 and centrifuged to separate the supernatant media and worm pellets. At harvest, liquid cultures contained approximately 80% L1-L3 worms. The worm pellets were stored at -20 °C until used for further analyses.

3. Preparation of Metabolome Extracts

The frozen worm pellets were added to pre-cooled (-78 °C) 200 mL of methanol in a Waring laboratory blender and blended until no chunks remained. Methanol was evaporated *in vacuo* at 20 °C and the residue resuspended in 300 mL of water. The resulting suspension was then frozen using a dry ice-acetone bath and lyophilized. The lyophilized residue was crushed to a fine powder using a mortar and pestle over 8 g granular sodium chloride. The powder was then extracted twice with 250 mL of 9:1 ethyl acetate:ethanol mixture over 12 h. The resulting yellow-brown suspension was filtered and the filtrate evaporated *in vacuo* at room temperature to produce the worm pellet metabolome extract used for chromatographic separations.

All synthetic samples were synthesized in collaboration with Joshua Judkins (Frank Schroeder Lab) and will be reported in detail elsewhere.

4. NMR Spectroscopic Instrumentation and Analysis

NMR spectra were recorded on a Varian 900 MHz NMR spectrometer (899.9 MHz for 1H, 226.7 MHz for ^{13}C) equipped with a 5 mm 1H ($^{13}C/^{15}N$) cryogenic probe, a Varian INOVA 600 MHz NMR spectrometer (600 MHz for 1H, 151 MHz for ^{13}C) equipped with an HCN indirect detection probe, and a Varian INOVA 500 MHz NMR spectrometer (500 MHz for ^{1}H, 125 MHz for ^{13}C) equipped with an DBG broadband probe. Each spectrum was manually phased, baseline corrected and calibrated to solvent peaks ($CHCl_3$ singlet at 7.26 ppm; CHD_2OD quintet at 3.31 ppm). Non-gradient phase-cycled dqfCOSY spectra were acquired using the following parameters: 0.8 s acquisition time, 500-900 complex increments, 16-64 scans per increment.

Obtained dqfCOSY spectra were zero-filled to 8k-16k × 4k and a cosine bell-shaped window function was applied in both dimensions before Fourier transformation. NMR spectra were processed using Varian VNMR, MestreLabs' MestReC, and MNova software packages. Dynamic range of the resulting spectra ranged from 300:1 to 500:1. For example, coupling constants could be determined for characteristic steroidal crosspeaks from dqfCOSY spectra containing as little as 5 µg $\Delta^{1,7}$-DA in a 2.5 mg enriched metabolome fraction.

5. daf-9(dh6) **Dauer Rescue Assay**

Plate based assay: Metabolome fractions were resuspended in ethanol, mixed with 40 µL of 5 x concentrated OP50 bacteria (from an overnight culture in LB media) and plated on 3 cm plates containing 3 mL NGM agar without added cholesterol. For rescue, ~100 eggs from a 4-8 hour egg lay were transferred onto the bacterial lawn, and scored for dauer arrest at 27 °C after 60 h. For rescue experiments with synthetic steroids (0.1 nM – 500 nM tested), 10 µL compounds in ethanol (or ethanol alone) were mixed with 40 µL 5X concentrated OP50 bacteria and plated. Final concentrations include the total volume of agar (3 mL). 100 nM Δ^7-DA was used as positive control.

Liquid Culture based assay: Individual metabolome fractions were dried *in vacuo* and resuspended in 500 µL EtOH. 20-25 gravid *daf-9(dh6)* adults were picked onto three 6 cm NGM agar plates seeded with OP50 containing 25 µL of 10 µM Δ^7-DA each and allowed to grow for three days. On the third day each of the plates were washed with M9 and treated with alkaline hypochlorite solution to isolate eggs from gravid adults. Isolated eggs were allowed to hatch in S-complete media without food, overnight. 100 µl of the resulting

synchronized L1 suspension was added to 400 µl of HB101 seeded S-complete media and 5 µl of ethanol or metabolome fraction or ethanol solution of synthetic ligands (1.25 nM – 200 nM tested) per well of a 12 well plate. Wells were examined after 48 and 72 h and scored for dauers, recovered animals and intermediate worms with molting defects and/or mig phenotypes. For active metabolome fractions, additional assays using smaller amounts were conducted.

Data obtained from both plate based and liquid culture assays are comparable. All figures in Chapter 1 and Appendix A are representative of data from plate based assays.

6. Luciferase Assay for DAF-12 Transcriptional Activation

Luciferase assays to determine transcriptional activation of DAF-12 were performed as described earlier (Bethke et al., 2009). Briefly, HEK-293T cells were seeded and transfected in 96-well plates with (pr well) 30 ng transcription factor vector, 30 ng of gfp expression vector, 30 ng of luciferase reporter, and 5 ng β-galactosidase expression vector using the calcium phosphate precipitate method. Ethanol or ethanol solutions of ligands (synthetic DAs, 1 nM – 3125 nM tested and metabolome fractions) were added 8h after transfection and the luciferase and β-galactosidase activities were measured by a Synergy 2 Biotek LC Luminometer, 16 h after compound addition. 100 nM Δ^7-DA was used as positive control. Data was processed using GEN5 software. Individual fractions were dried *in vacuo* and resuspended in 500 µL EtOH. 1 µL per 100 µL of media solution was added to each well.

7. Alphascreen Assay for Direct Binding of DAF-12 Ligand Candidates

Direct binding of ligand candidates to DAF-12 was assessed by measuring ligand dependent interaction between a heterologously expressed DAF-12 construct and the mammalian co-activator peptide, SRC1-4, in Alphascreen assays (Perkin Elmer). An N-terminally GST-6xHis-tagged DAF-12 construct (amino acids 281-753, which includes most of the hinge region and the entire LBD) was purified from BL21 (DE3) cells (Sigma) using a GT sepharose column followed by a size exclusion column. Purified DAF-12 (25 nM final concentration) and biotinylated SRC1-4 (synthetic biotin-QKPTSGPQTPQAQQKSLLQQLLTE obtained from Anaspec, used at 50 nM final concentration), were incubated separately in plastic tubes for 20 min with Ni^{2+} chelate acceptor beads (for DAF-12) or streptavidin donor beads (for SRC1-4, 25 µg/mL final concentration, Perkin Elmer, Cat. No - 6760619C). They were then combined with subsequent addition of ligand candidates or ethanol (stored in glass vials) to obtain a final volume of 20 µL, and incubated for 60 min in white, low volume, 384 well Optiplates (Perkin Elmer). The plates were then read using a Synergy 2 Biotek LC luminometer using the manufacturer's Alphascreen detection protocol. All solutions were made using assay buffer containing 25 mM HEPES (pH 7.4) and 100 mM NaCl. Cholesterol and heptadecanoic acid, assayed at 1 µM concentration as additional negative controls, gave no signal (Figure S3C). Addition of CHAPS (40 µM) did not significantly affect assay results, whereas addition of 0.01% BSA reduced signal. All incubations were carried out at room temperature in the dark. Figure 4H shows combined data derived from at least independent experiments (each N = 4 or higher) run on three or more different days.

8. GC/MS Instrumentation and Sample Preparation

GC/MS analysis was carried out with an Agilent Technologies 6890N Network GC system with a DB-5MS+DG column (25 µm, 30 m x 0.25 mm) operating in split-less mode, connected to a JEOL JMS-GCmateII mass spectrometer. (For details about GC conditions, see Extended Experimental Procedures). Methylation of 3-keto-DAs: synthetic standards or 1-10 % of active metabolome fractions were evaporated *in vacuo* and resuspended in toluene:methanol (500 µL, 3:2), followed by the drop-wise addition of trimethylsilyldiazomethane (120 µL, 2 M solution in Et_2O) with stirring. The reaction was stirred at room temperature for 30 min, quenched with acetic acid, evaporated *in vacuo,* and resuspended in dichloromethane (30-200 µL). Of this solution, 1-5 µL were injected per GC/MS analysis. Silylation of 3-hydroxy-DAs: Synthetic standards or 1-10 % of active fractions were evaporated *in vacuo* and a mixture (100 µL) of 3% 1-(trimethylsilyl)imidazole (TMSIM) in *N*-methyl-*N*-(trimethylsilyl)trifluoroacetamide (MSTFA) was added with stirring at 80 °C for 45 min. The reaction mixture was evaporated *in vacuo* and resuspended in dichloromethane (30-200 µL). Of this solution, 1-5 µL were injected per GC/MS run.

9. HPLC Enrichment Protocol

Metabolome fractions derived from the Combiflash® method described above were evaporated *in vacuo*, resuspended in 250 µL of methanol and submitted to HPLC, using an Agilent 1100 Series HPLC system equipped with an Agilent Eclipse XDB C-18® column (25 cm x 9.4 mm, 5 µm particle diameter). A 0.1% acetic acid in water (aqueous) – 9:1 acetonitrile : methanol (organic) solvent system was used, starting with 70% organic solvent for 3 min, which was increased linearly to 100% over a period of 20 min and continued at 100%

organic solvent for 2 min. One minute fractions were collected using a Teledyne ISCO Foxy 200 X-Y Fraction Collector® connected to the HPLC from 12 to 36 min. Collected fractions were individually evaporated *in vacuo* for further analysis.

10. Life Span Assay

Life span assays were performed in Percival I-36NL incubators at 20 °C. After alkaline hypochlorite treatment and two generations of growth, animals were raised at 25 °C, and sterile young adult animals were placed onto NGM plates seeded with 10X concentrated *E. coli* OP50, containing 100 nM dafachronic acid or ethanol vehicle control. Every fourth day, animals were transferred to new NGM plates with freshly added dafachronic acid or vehicle control. Activity of dafachronic acid in each batch of plates was confirmed by assessing the ability of dafachronic acid to rescue *daf-9(dh6)* dauer arrest, compared to vehicle control. Animal viability was assessed visually or with gentle prodding. GraphPad Prism (GraphPad Software, La Jolla, CA) was used for data representation and statistical analysis. These experiments were carried out by Josh Wollam (Adam Antebi Lab, MPI Cologne) and Kathlyn J. Dumas (Patrick Hu Lab, Univ. of Michigan).

11. GC/MS Method

GC conditions: Injector was kept at 240 °C and 1 mL/min He flow was maintained. Initial column temperature was at 120 °C for 1.4 min, then increased to 320 °C at a rate of 7 °C/min, and maintained at 320 °C for 10 min.

MS conditions: Electron impact ionization (EI) operated at 70 eV. For synthetic samples (high concentrations, >100 ng/µL), MS was first operated in scanning

mode for a mass range of *m/z* 35-500 for 3-keto-DA methyl ester and 3-keto-steroids, and *m/z* 35-650 for 3-OH-DA TMS derivatives to select for the most abundant fragment ions for each compound. For low concentrations (<5 ng/µL) of synthetic samples and metabolome fractions, MS was operated in Selective Ion Monitoring (SIM) mode and the following ions were selectively observed: *m/z* = 428, 271, 229 (Δ^7-DA); 426, 269, 227 ($\Delta^{1,7}$-DA); 430, 398, 231 (Δ^0-DA); 428, 305, 229, 124 (Δ^4-DA); 545, 470, 255 (3α- and 3β-OH-Δ^7-DA); 384, 261, 229 (4-cholesten-3-one).

12. Quantification of DAs from Metabolome Fractions via SIM-GC/MS

GC/MS Data was analyzed using Shrader Analytical and Consulting Laboratories, Inc.'s TSSPro 3.0 software package. Quantification of DAs was performed by integration of GC/MS peaks from the following ion traces: *m/z* = 428 (Δ^7-DA); 426 ($\Delta^{1,7}$-DA); 231 (Δ^0-DA); 428 (Δ^4-DA); 255 (3α- and 3β-OH-Δ^7-DA). Dafachronic acid concentrations were calculated using response factors determined from synthetic standards. Mass spectrometer response was roughly linear (<5% error) for amounts of 10 pg to 5 ng per compound injection.

Figure A.1. Biological activity of metabolite fractions obtained from *C. elegans.* Assessment of DAF-12 transcriptional activation in the *in vitro* luciferase assay in HEK-293T cells (left) and dauer rescue activity in *daf-9(dh6)* worms (right) with metabolome fractions obtained from **(a)** wild type **(b)** *daf-22* animals. These data show that *daf-9(dh6)* dauer rescue activity is generally higher in *daf-22* mutant metabolome fractions. **(c)** DIC images of *daf-9(dh6)* worms showing different phenotypes scored in the dauer rescue assay. Dauer (top left), adult recovered (top right), intermediate phenotypes showing molting defects (bottom left, arrows point to incompletely shed cuticle from previous molt), fully recovered late L4 (bottom center), and intermediate phenotypes showing incomplete gonad migration (bottom right). Yellow lines indicate gonadal shape in shown mig phenotypes.

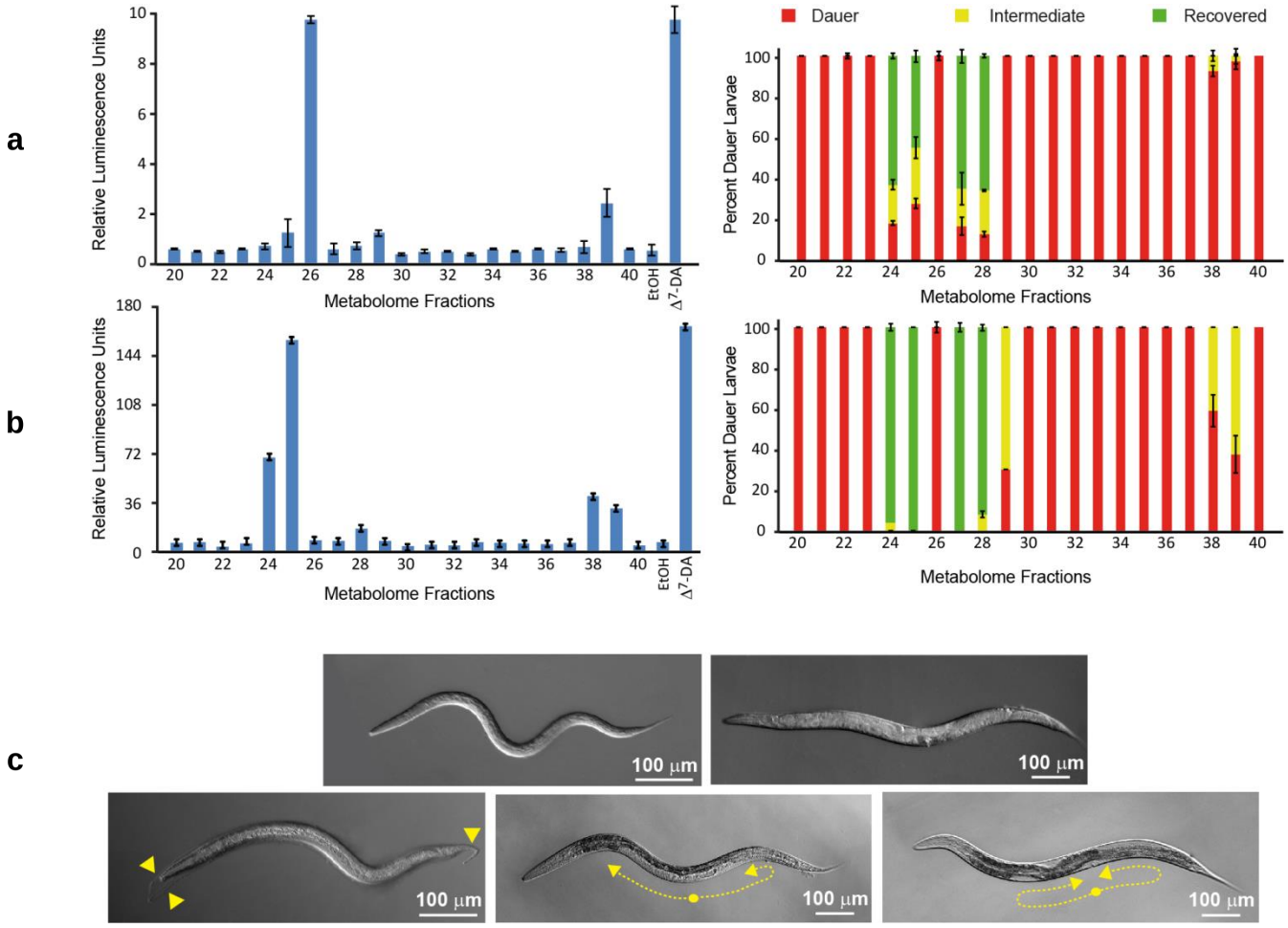
a
b
c
Relative Luminescence Units
Metabolome Fractions
EtOH
Δ7-DA
Dauer
Intermediate
Recovered
Percent Dauer Larvae
100 μm

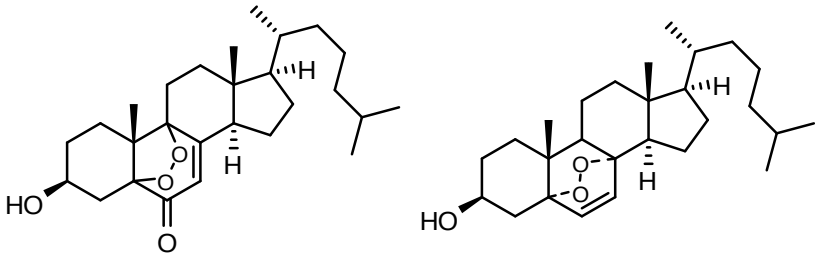

Figure A.2. *daf-9* independent sterols in metabolome fractions. Structures of major epidioxy sterol derivatives that elute with Δ^7 and $\Delta^{1,7}$-DAs in active fractions but can also be observed in corresponding inactive *daf-9;daf-12* fractions.

Figure A.3. Identification of $\Delta^{1,7}$-DA in active region I. Sections of dqfCOSY spectra (600 MHz, $CDCl_3$) used for identification of $\Delta^{1,7}$-DA in *C. elegans*. **(a)** Natural $\Delta^{1,7}$-DA in HPLC-enriched fraction 25-6 **(Figure 2.5)** from *daf-22* mutant. **(b)** Synthetic $\Delta^{1,7}$-DA. Characteristic crosspeaks are boxed blue.

a

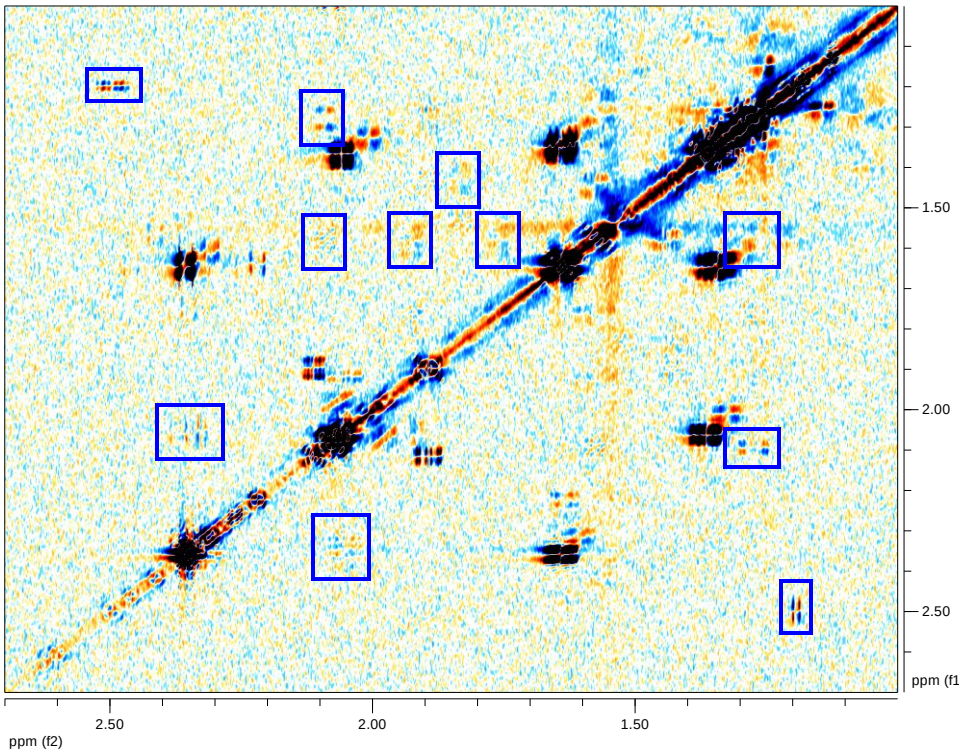
1.50
2.00
2.50
ppm (f1
2.50
2.00
1.50
ppm (f2)

b

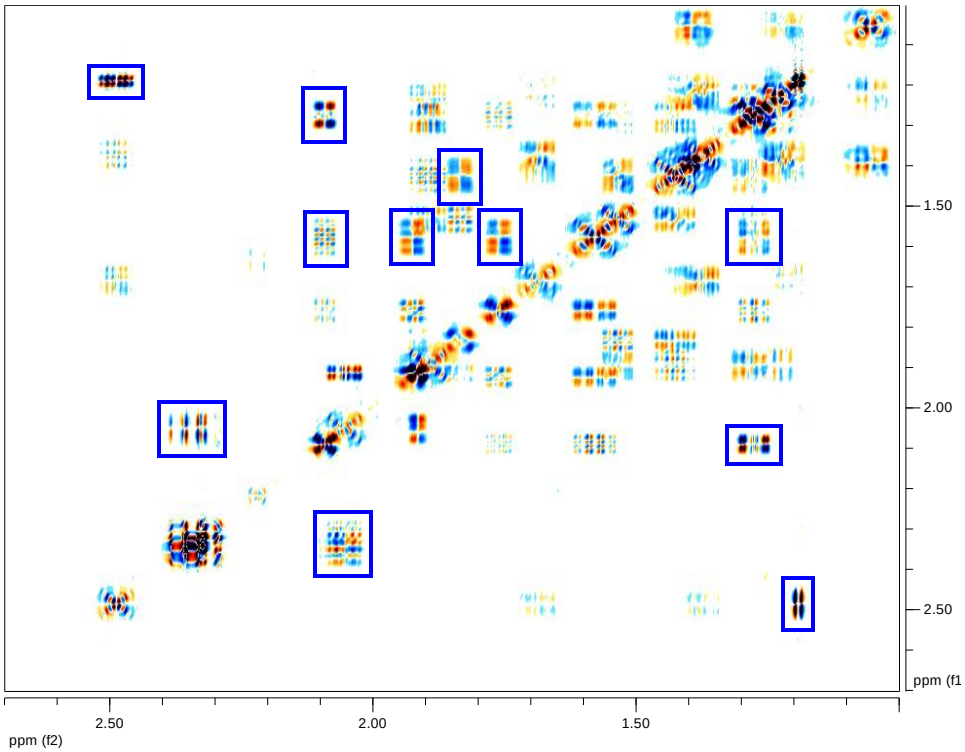
1.50
2.00
2.50
ppm (f1
2.50
2.00
1.50
ppm (f2)

Figure A.4. Identification of of Δ^7-DA in active region I. Sections of dqfCOSY spectra (600 MHz, $CDCl_3$) confirming presence of Δ^7-DA in *C. elegans*. **(a)** Natural Δ^7-DA in HPLC-enriched fraction 25-8 from *daf-22* mutant **(Figure 2.5)**. **(b)** Synthetic Δ^7-DA. Characteristic crosspeaks are boxed blue.

a

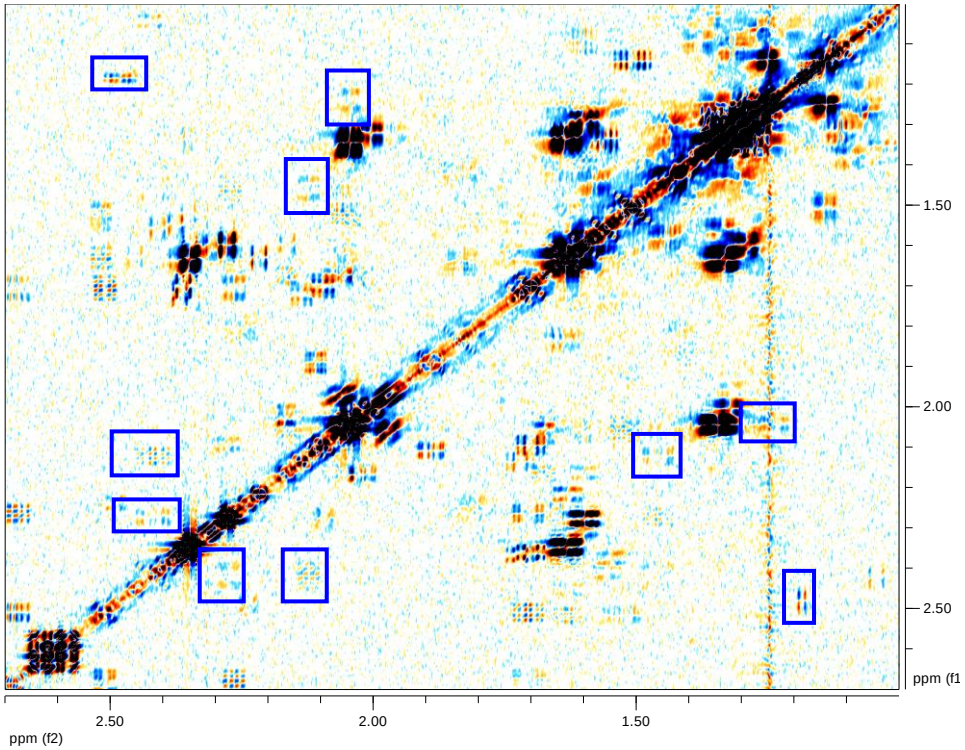
1.50
2.00
2.50
ppm (f1
2.50
2.00
1.50
ppm (f2)

b

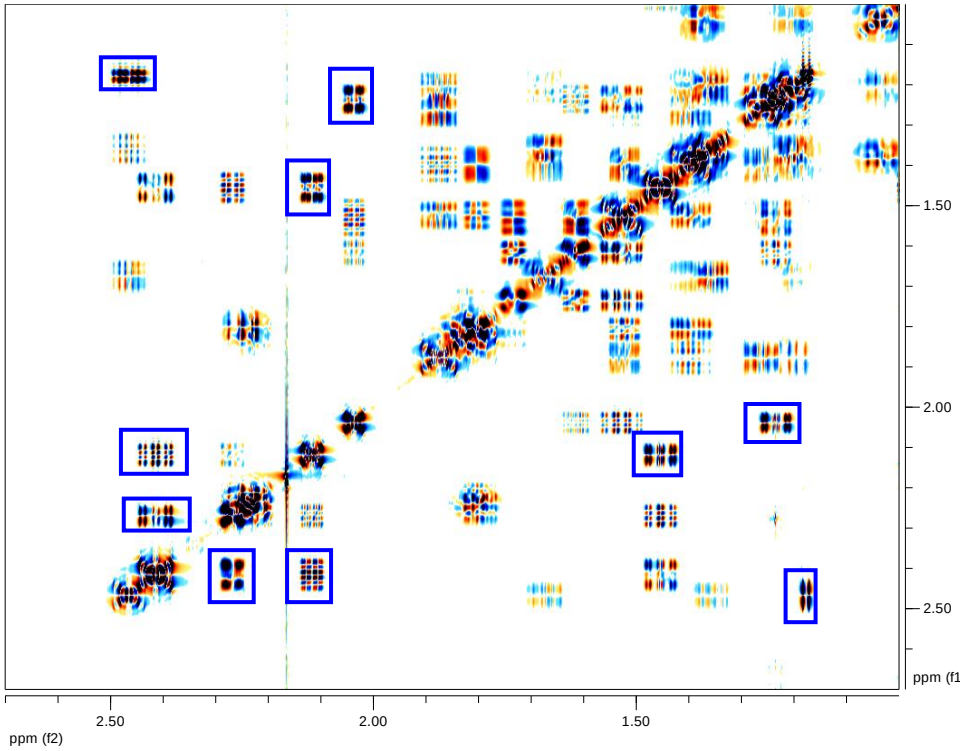
1.50
2.00
2.50
ppm (f1
2.50
2.00
1.50
ppm (f2)

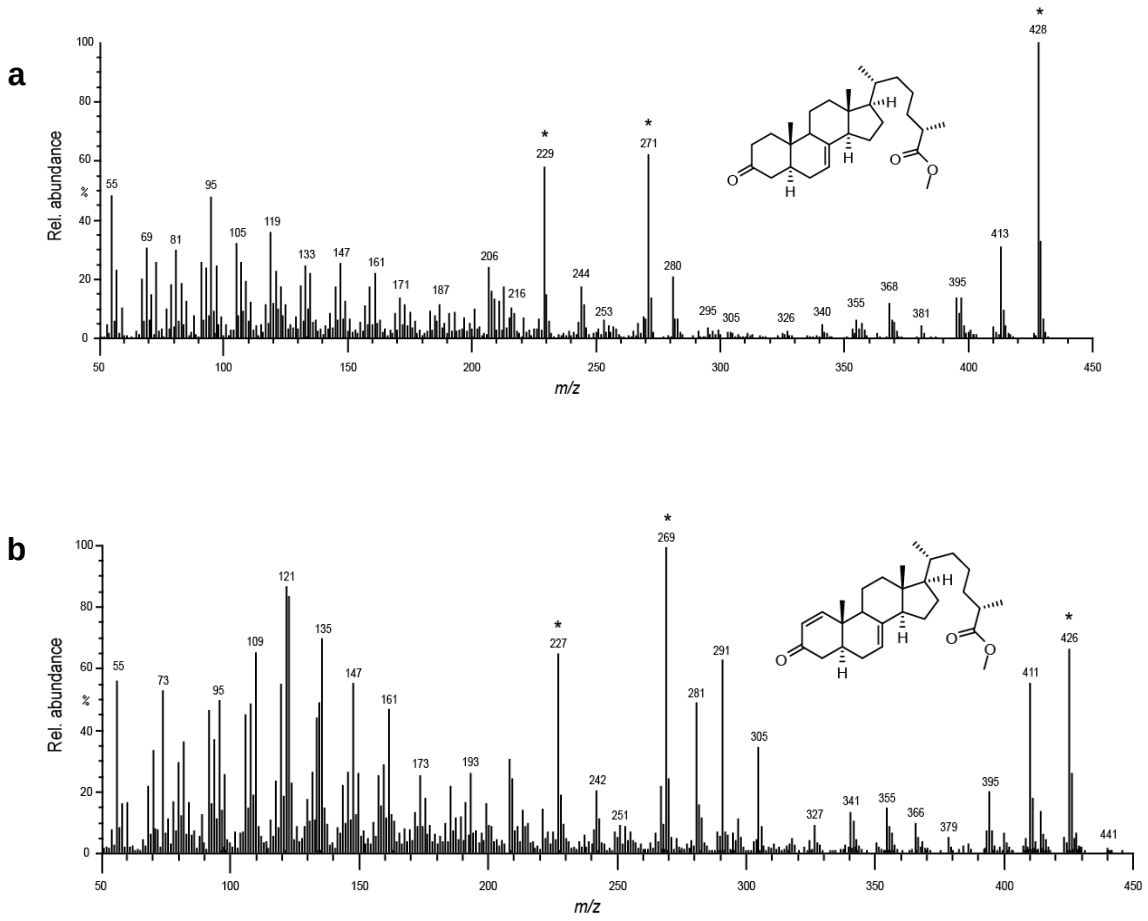

Figure A.5.EI-MS for methyl esters of DAs in active region I. EI-MS for methyl esters of **(a)** Δ^7-DA and **(b)** $\Delta^{1,7}$-DA. (*) Indicates the ion fragments subsequently used for SIM-GC/MS analyses of these compounds in metabolome fractions.

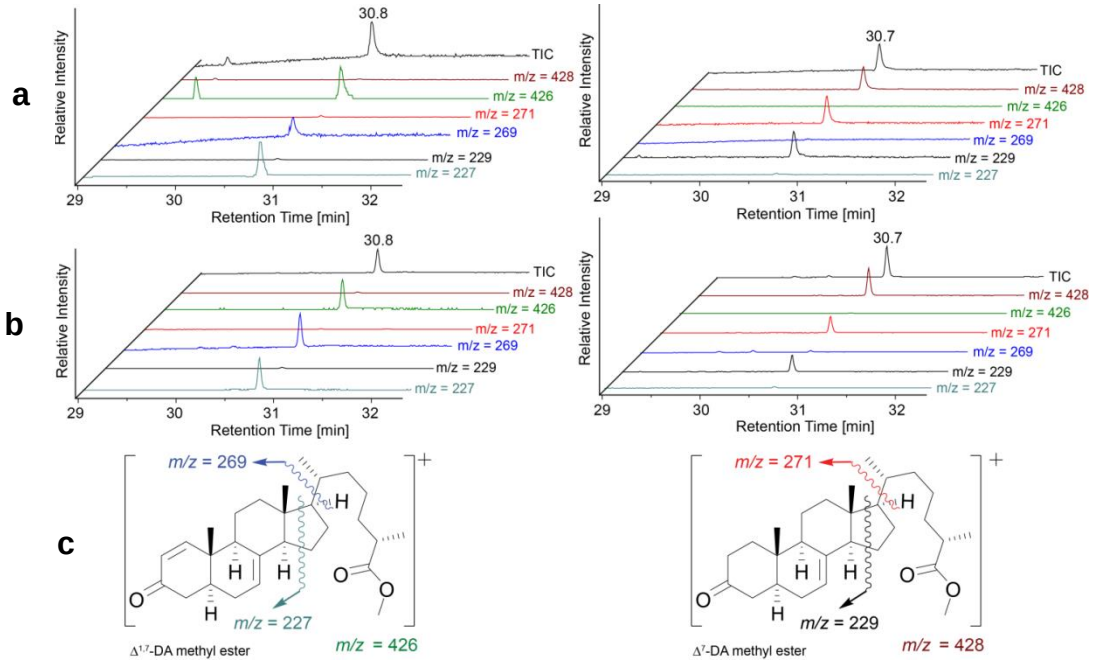

Figure A.6. SIM-GC/MS analyses of DAs in active region I. SIM-GC/MS analyses showing characteristic fragment ion traces for methyl esters of **(a)** natural $\Delta^{1,7}$-DA (left), natural Δ^{7}-DA (right) in HPLC-enriched fractions 25-6 and 25-8 respectively from *daf-22*, **(b)** synthetic $\Delta^{1,7}$-DA (left), and synthetic Δ^{7}-DA (right). **(c)** Characteristic EI-MS fragments of $\Delta^{1,7}$-DA methyl ester (left) and Δ^{7}-DA methyl ester (right)

Figure A.7. EI-MS for standard 3-OH-Δ^7-DA TMS derivatives. (*) Indicates the ion fragments subsequently used for SIM-GC/MS identification of these compounds in natural samples. **(a)** 3α-OH-Δ^7-DA **(b)** 3β-OH-Δ^7-DA. The red box indicates the ion fragment *m/z* = 213 that have been implicated in a previous publication[4] as belonging to a putative DAF-12 ligand.

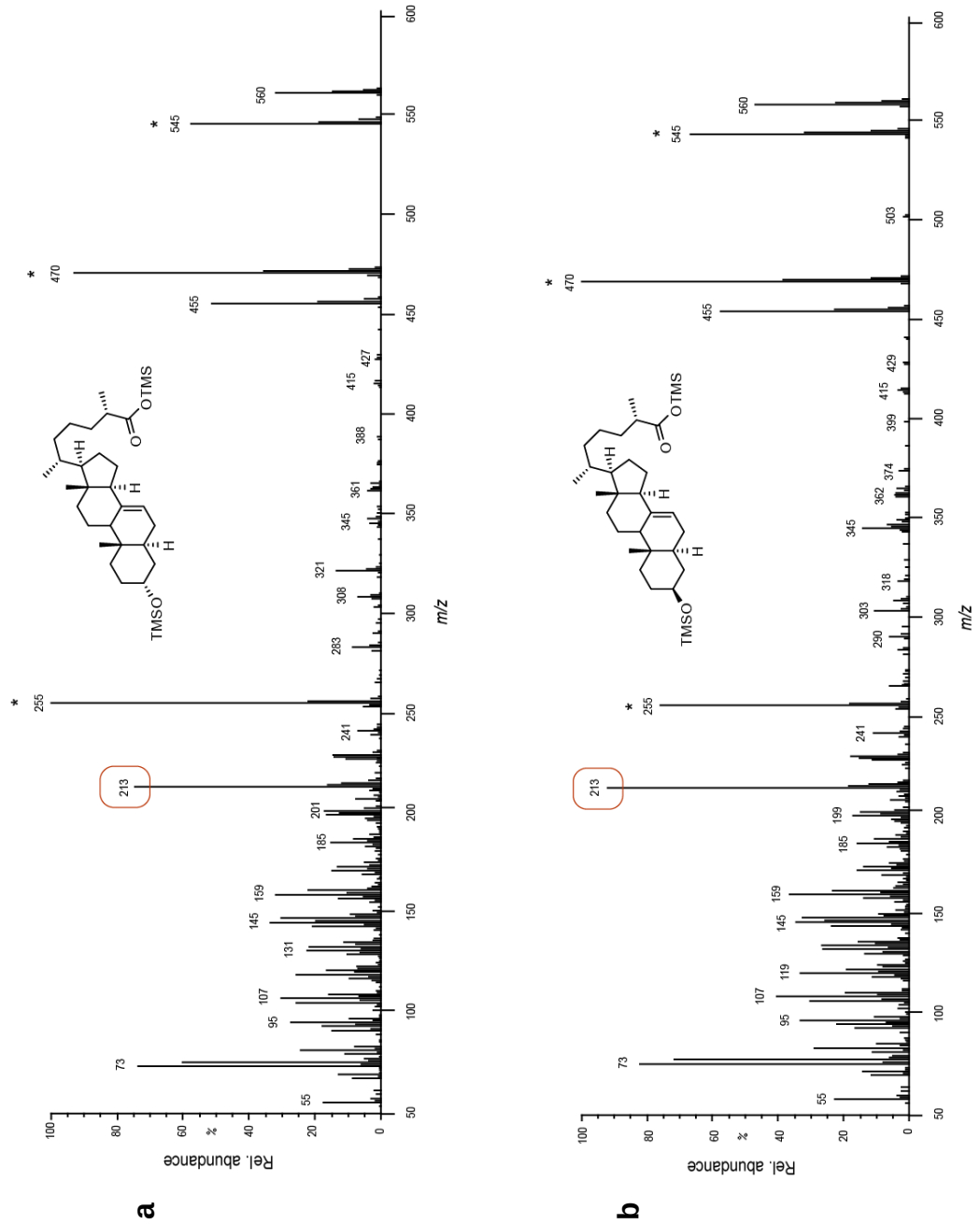
a
b
Rel. abundance
m/z
TMSO
OTMS
213
255
470
545
560
455
503

Figure A.8. Identification of 3α-OH-Δ^7-DA in active region II. SIM-GC/MS analysis showing characteristic fragment ion traces for TMS derivative of 3α-OH-Δ^7-DA. **(a)** Natural 3α-OH-Δ^7-DA in HPLC-enriched fraction from active region II. **(b)** Synthetic 3α-OH-Δ^7-DA. **(c)** Characteristic EI-MS fragments of 3α-OH-Δ^7-DA TMS derivative shown in (e) and (f). **(d)** GC/MS total ion chromatograms (TIC) of synthetic 3α-OH-Δ^7-DA, synthetic 3β-OH-Δ^7-DA, and natural 3-OH-Δ^7-DA TMS derivatives. The GC retention times for the natural compound matches precisely with that of synthetic 3α-OH-Δ^7-DA and is distinctly different from that of the 3β-isomer. (*) indicates small amounts of impurities in the synthetic 3β-OH-Δ^7-DA sample.

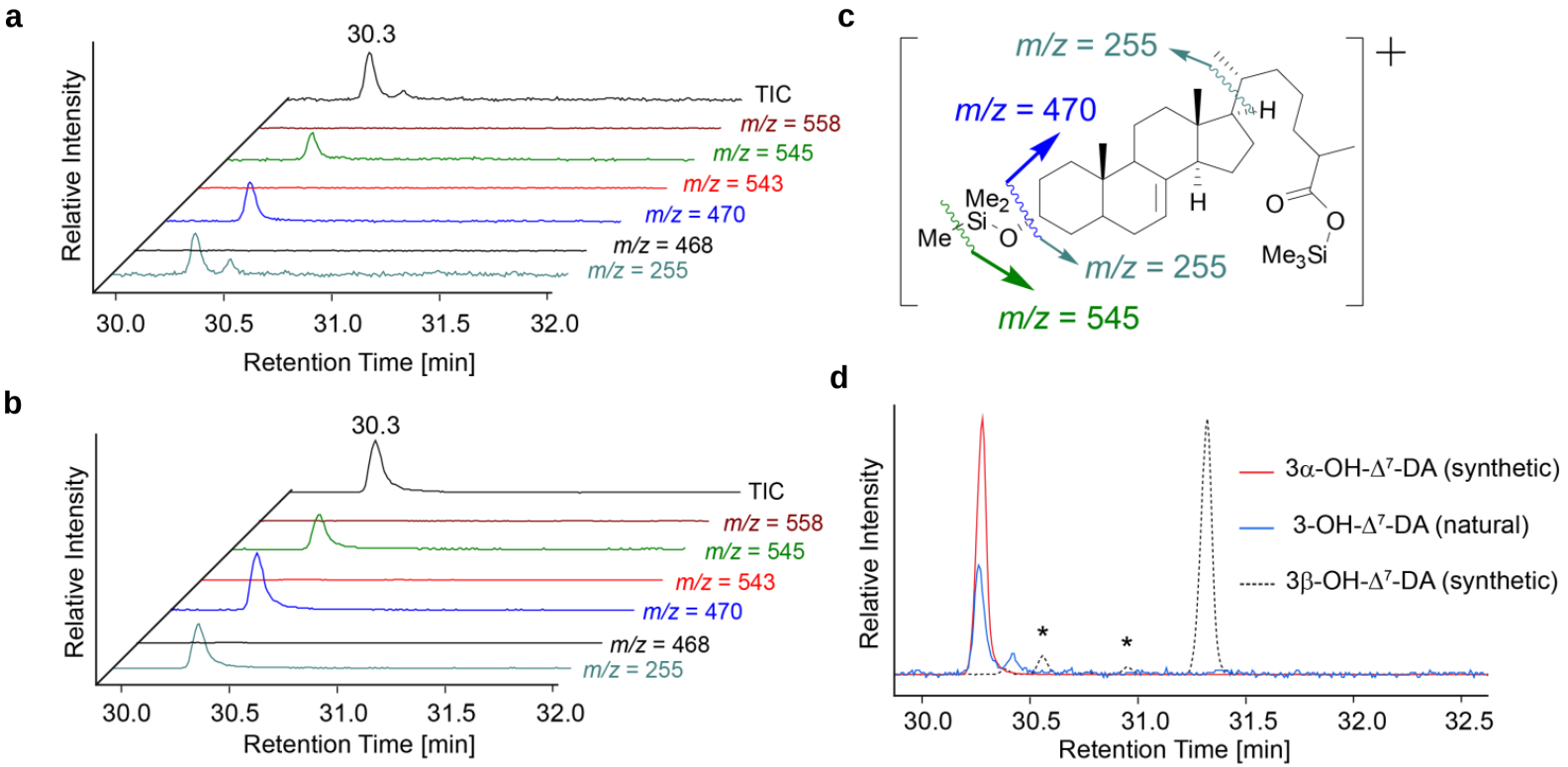
a
30.3
TIC
m/z = 558
m/z = 545
m/z = 543
m/z = 470
m/z = 468
m/z = 255
Relative Intensity
30.0
30.5
31.0
31.5
32.0
Retention Time [min]
b
30.3
TIC
m/z = 558
m/z = 545
m/z = 543
m/z = 470
m/z = 468
m/z = 255
Relative Intensity
30.0
30.5
31.0
31.5
32.0
Retention Time [min]
c
m/z = 255
m/z = 470
H
Me2
Si
Me
O
H
O
O
Me3Si
m/z = 255
m/z = 545
d
Relative Intensity
3α-OH-Δ7-DA (synthetic)
3-OH-Δ7-DA (natural)
3β-OH-Δ7-DA (synthetic)
*
*
30.0
30.5
31.0
31.5
32.0
32.5
Retention Time [min]

Figure A.9. Bioactivity of synthetic DAs. (a) Lifespan extension due to the loss of the germline-deficient *glp-1* mutants is not affected by the addition of 100 nM of the most abundant DAF-12 ligands, Δ^{7}- and $\Delta^{1,7}$-DA. **(b)** DAF-12-ligand candidates produced signal in the Alphascreen assay only in the presence of SRC1-4 peptide. **(c)** 500 nM cholesterol and heptadecanoic acid did not produce any signal in the Alphascreen assay.

a

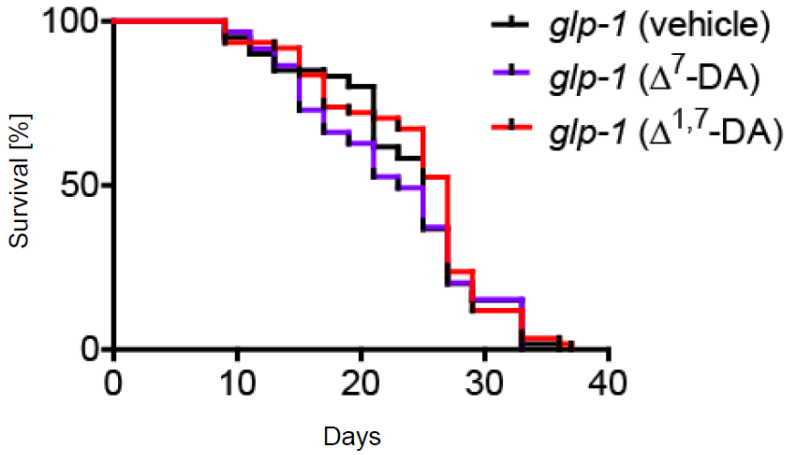
100
50
0
Survival [%]
0
10
20
30
40
Days
glp-1 (vehicle)
glp-1 (Δ7-DA)
glp-1 (Δ1,7-DA)

b

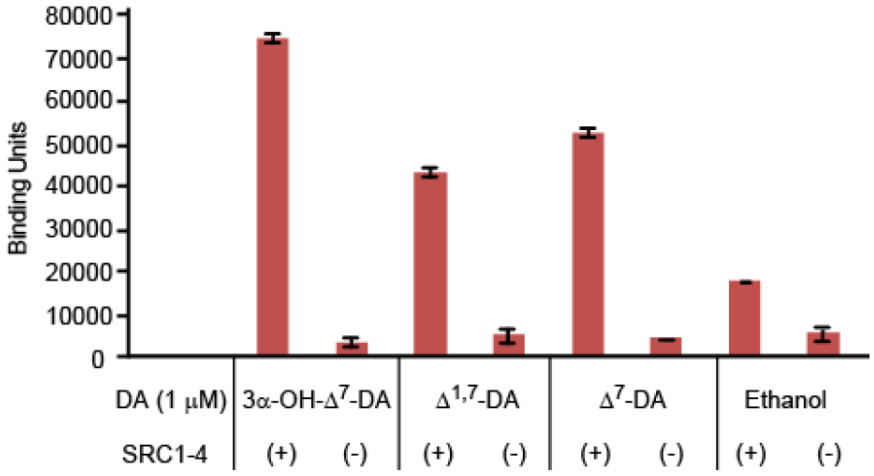
80000
70000
60000
50000
40000
30000
20000
10000
0
Binding Units
DA (1 μM)
3α-OH-Δ7-DA
Δ1,7-DA
Δ7-DA
Ethanol
SRC1-4
(+)
(-)
(+)
(-)
(+)
(-)
(+)
(-)

c

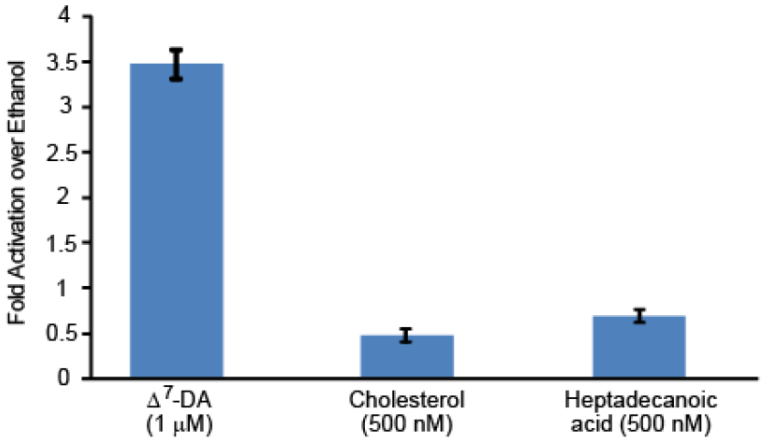
4
3.5
3
2.5
2
1.5
1
0.5
0
Fold Activation over Ethanol
Δ7-DA
(1 μM)
Cholesterol
(500 nM)
Heptadecanoic
acid (500 nM)

Figure A.10. SIM-GC/MS analysis did not reveal Δ^4-DA as a significant *C. elegans* metabolite. (a) EI-MS for Δ^4-DA methyl ester. (*) Indicates the ion fragments subsequently used for SIM-GC/MS analysis of this compound in natural samples. **(b)** SIM-GC/MS total ion chromatograms (TIC) of synthetic Δ^4-DA methyl ester, 1% injection of methylated inactive fraction 26 from *daf-22* to which trace amounts of synthetic Δ^4-DA (100 ng, ~20-fold less than Δ^7-, $\Delta^{1,7}$-DAs in active metabolome fractions) had been added, and 100% injection of a methylated and HPLC-enriched natural fraction matching the LC retention time of synthetic Δ^4-DA**.**

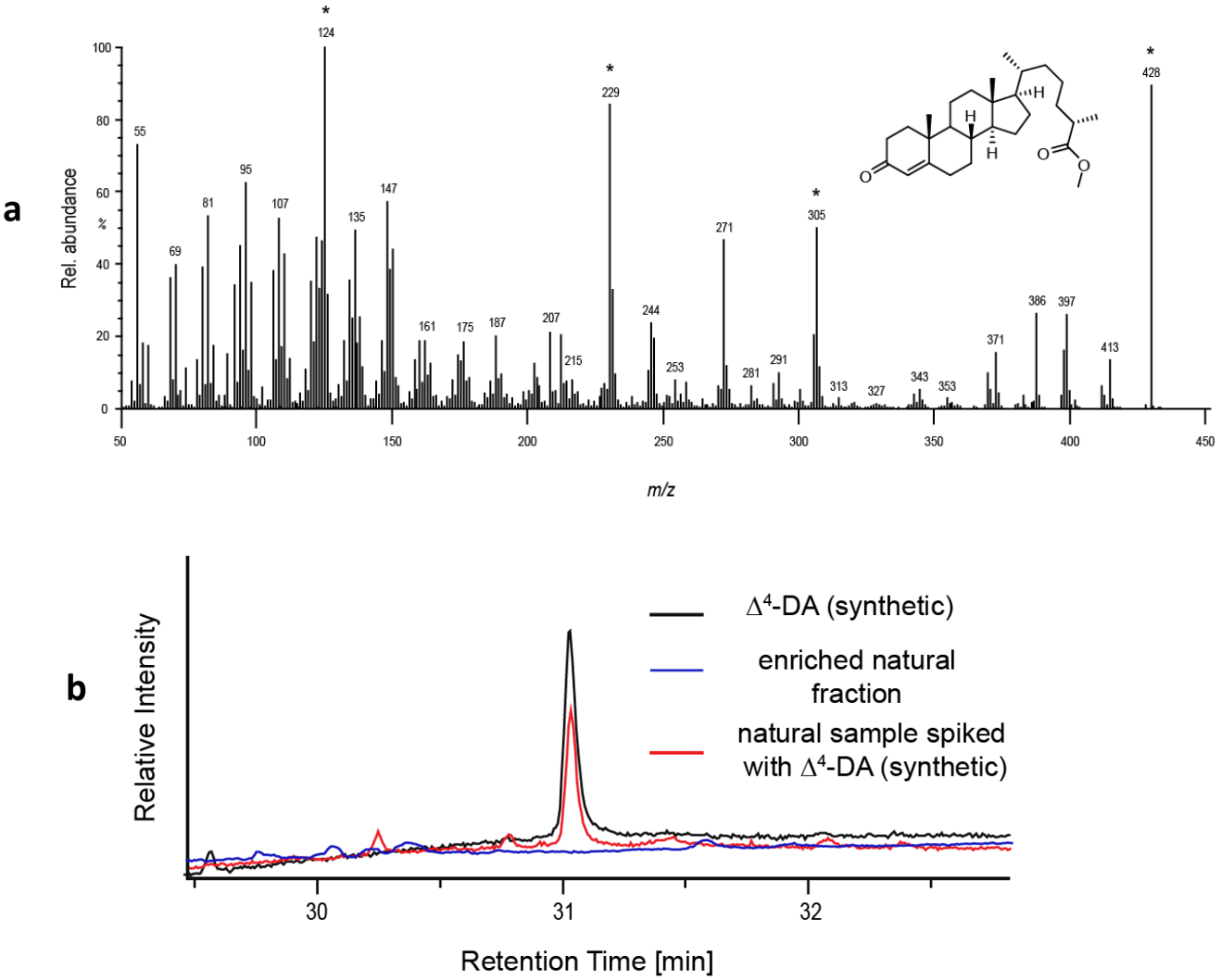
a
Rel. abundance
%
m/z
55
69
81
95
107
124
135
147
161
175
187
207
215
229
244
253
271
281
291
305
313
327
343
353
371
386
397
413
428
b
Relative Intensity
Δ4-DA (synthetic)
enriched natural fraction
natural sample spiked with Δ4-DA (synthetic)
Retention Time [min]

Figure A.11. Identification of 4-cholesten-3-one and lathosterone from *daf-22*. Sections of dqfCOSY spectra (600 MHz, $CDCl_3$) confirming presence of 4-cholesten-3-one in *C. elegans*. **(a)** 4-Cholesten-3-one in enriched natural fraction from *daf-22*. **(b)** Synthetic 4-cholesten-3-one. Characteristic crosspeaks are boxed blue.

a

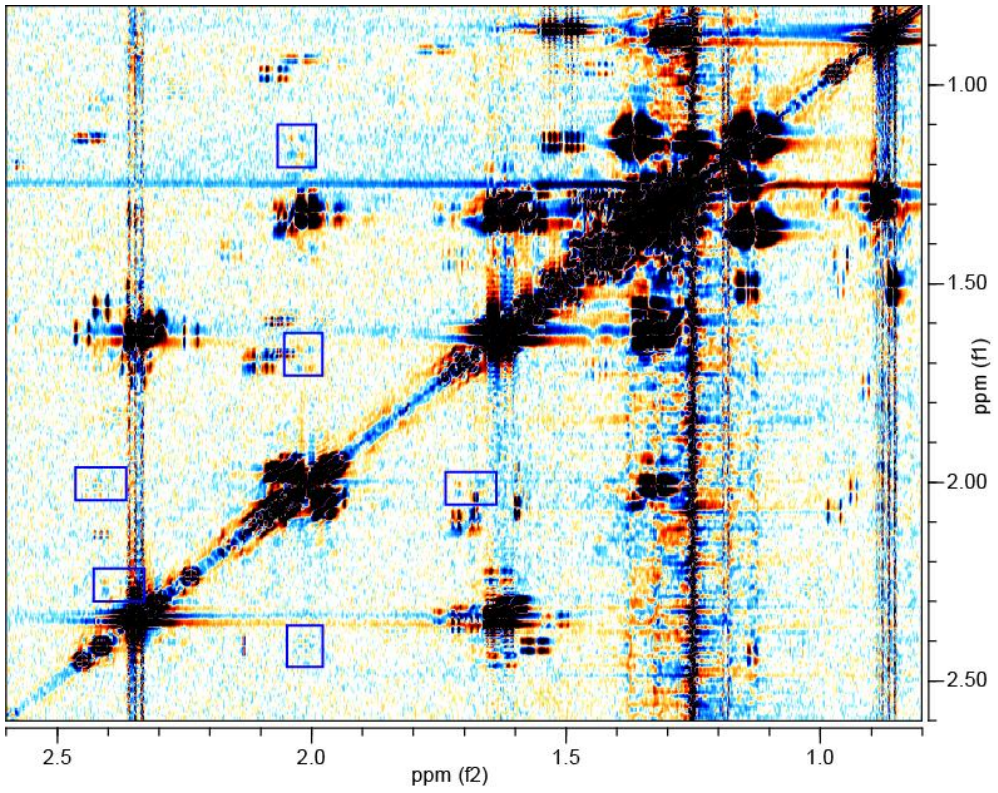
1.00
1.50
2.00
2.50
ppm (f1)
2.5
2.0
1.5
1.0
ppm (f2)

b

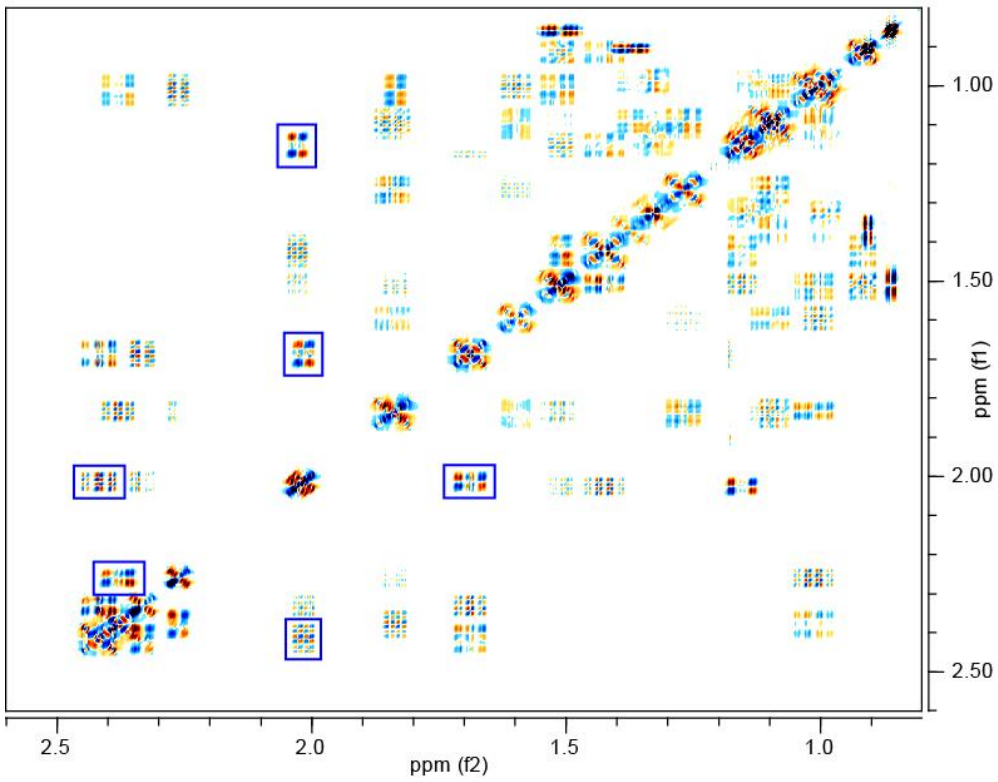
1.00
1.50
2.00
2.50
ppm (f1)
2.5
2.0
1.5
1.0
ppm (f2)

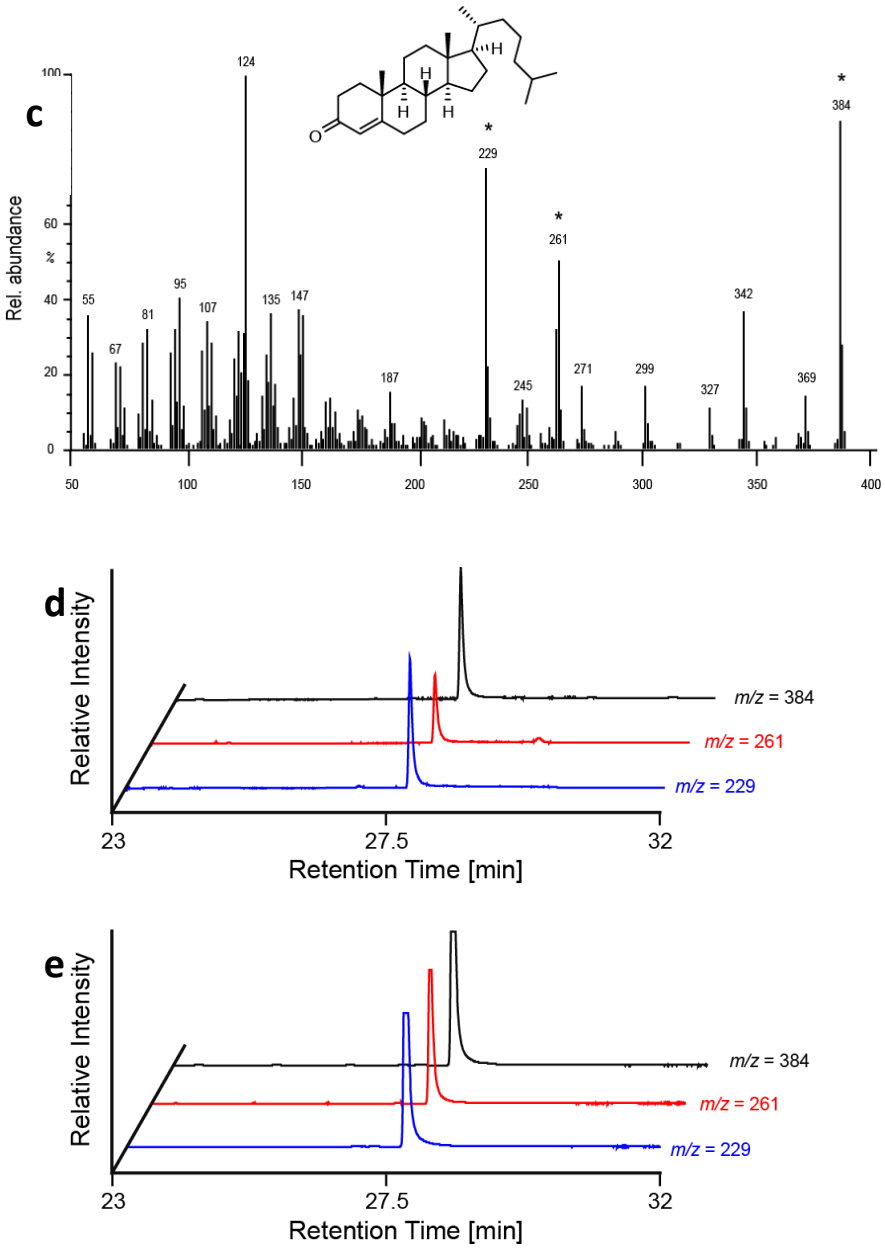

Figure A.11. Identification of 4-cholesten-3-one and lathosterone from *daf-22*. (c) EI-MS for 4-cholesten-3one. (*) Indicates the ion fragments subsequently used for SIM-GC/MS analysis of this compound in natural samples. SIM-GC/MS analysis showing characteristic fragment ion traces for **(d)** enriched natural fraction from *daf-22* containing 4-cholesten-3-one and **(e)** synthetic 4-cholesten-3-one.

Figure A.11. Identification of 4-cholesten-3-one and lathosterone from *daf-22*. Sections of dqfCOSY spectra (600 MHz, $CDCl_3$) confirming presence of lathosterone in *C. elegans*. **(f)** Lathosterone in enriched natural fraction from *daf-22*. **(g)** Synthetic lathosterone. Characteristic crosspeaks are boxed blue.

f

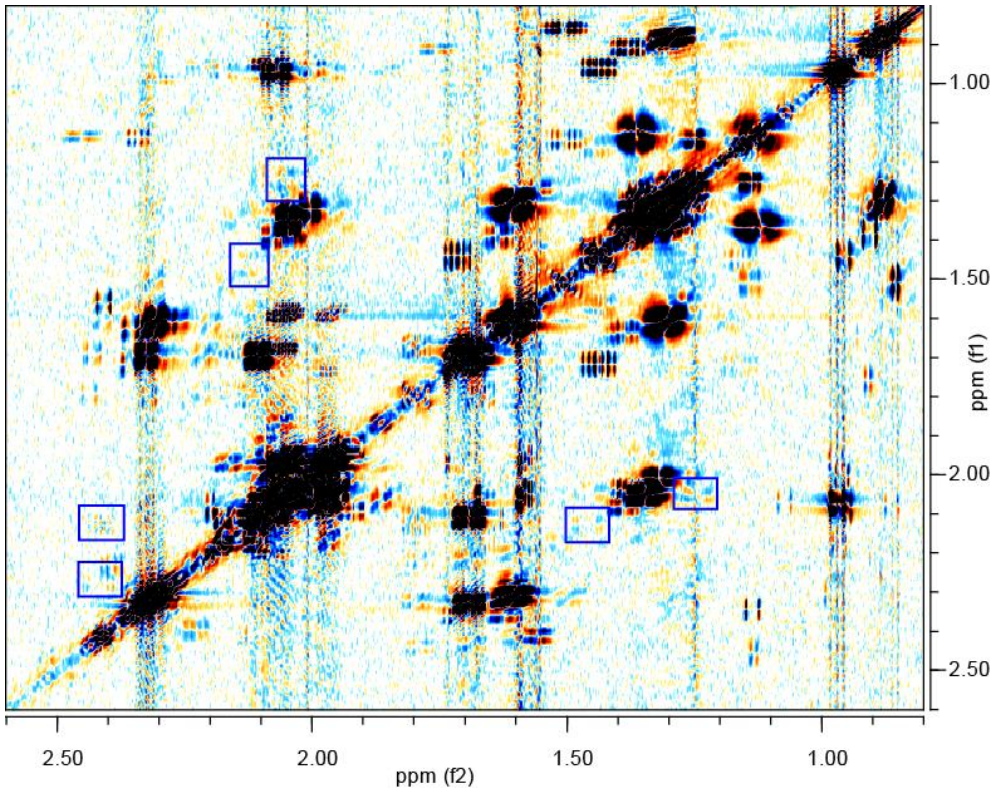
1.00
1.50
2.00
2.50
ppm (f1)
2.50
2.00
1.50
1.00
ppm (f2)

g

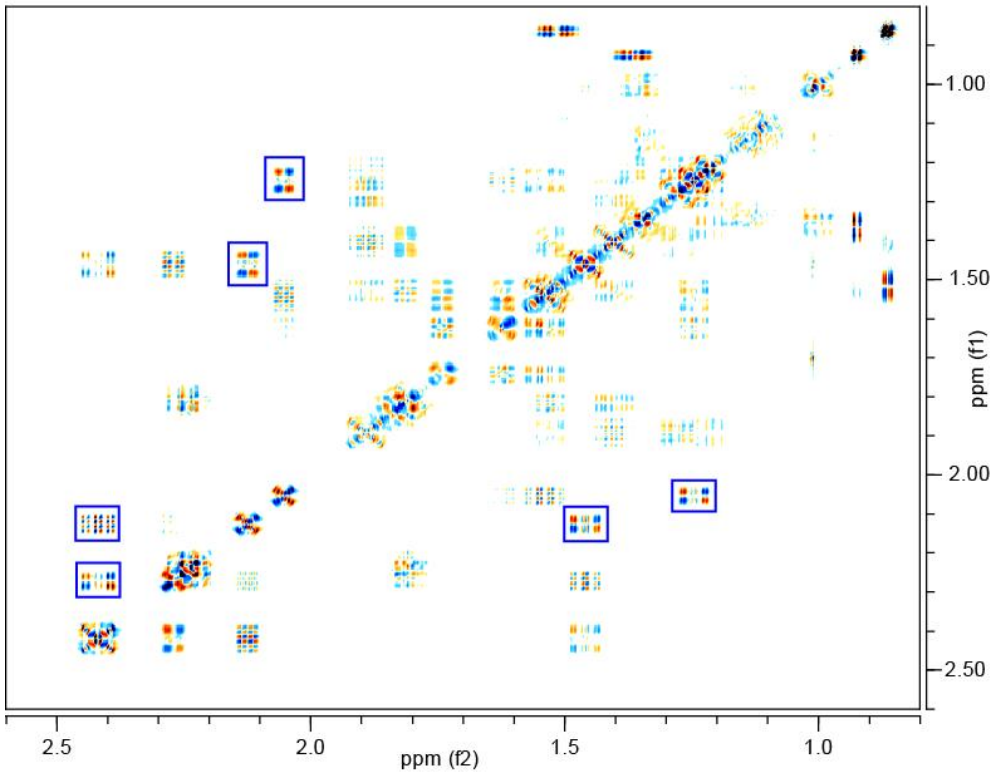
1.00
1.50
2.00
2.50
ppm (f1)
2.5
2.0
1.5
1.0
ppm (f2)

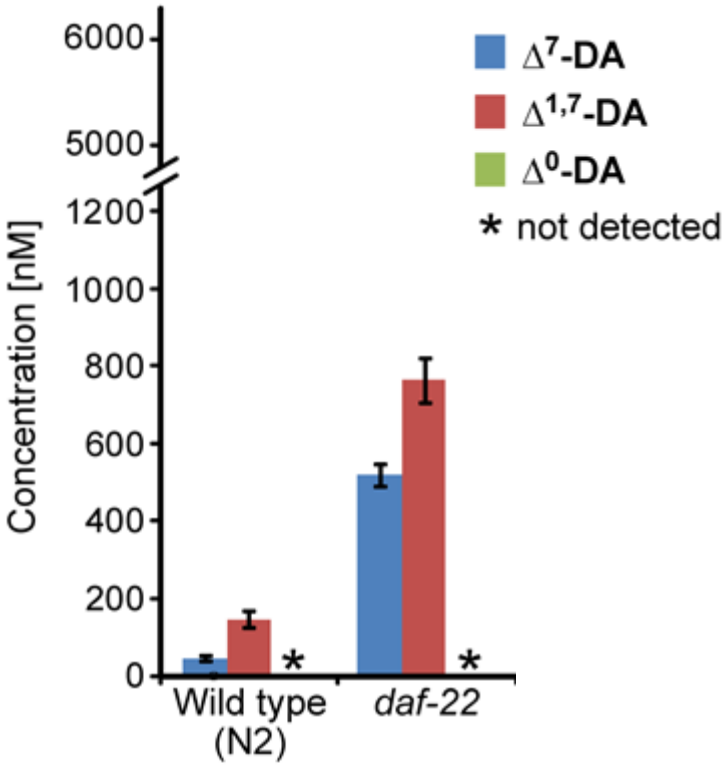

Figure A.12. Endogenous concentrations of DAs. *In vivo* concentrations of Δ^7-DA, $\Delta^{1,7}$-DA, and Δ^0-DA derived from SIM-GC/MS-based quantification in wild-type (N2), *daf-22*, and steroid metabolism mutants (error bars, SD).

Table A.1. EC_{50} values of synthetic DAs for luciferase, Alphascreen and dauer rescue assays as well as HPLC retention times for synthetic DAs.

Compound	EC_{50} (nM) for luciferase assay (in vitro)	EC_{50} (nM) for Alphascreen assay (in vitro)	EC_{50} (nM) for daf-9(dh6) dauer rescue assay (in vivo)	HPLC retention time ranges (mins)
$\Delta^{1,7}$-DA	146	15	2	20.5-20.9
Δ^{7}-DA	39	6	3	20.9-21.5
Δ^{0}-DA	411	not determined	19	24-25
3α-OH-Δ^{7}-DA	240	200	6	21-22
3β-OH-Δ^{7}-DA	not determined	not determined	22	18-19

Spectroscopic Data

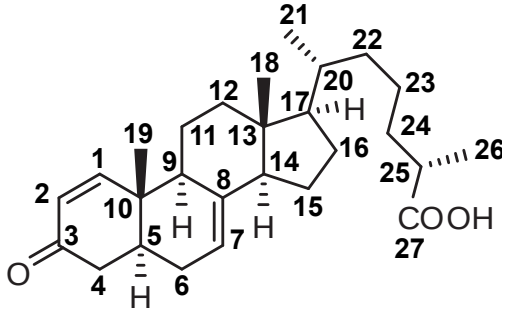

$\Delta^{1,7}$-Dafachronic acid

Table A.2 NMR Spectroscopic Data of $\Delta^{1,7}$-DA. ^{1}H (600 MHz), ^{13}C (151 MHz), and HMBC NMR spectroscopic data for $\Delta^{1,7}$-DA in $CDCl_3$. Chemical shifts were referenced to ($C\underline{H}Cl_3$) = 7.26 ppm and ($\underline{C}DCl_3$) = 77.16 ppm.

Carbon No.	δ (ppm)	Proton No.	δ (ppm)	J (Hz)	HMBC Correlations
1	157.3	1-H	7.01	$J_{1,2}$=10	C-10, C-9, C-5, C-3
2	127.1	2-H	5.89		C-10, C-4
3	199.8	----	----	----	----
4	40.1	4-H_α	2.34		C-3, C-10
		4-H_β	2.34		C-3, C-10
5	39.6	5-H	2.05		
6	28.7	6-H_α	1.89-1.94		C-8
		6-H_β	1.89-1.94		
7	117.8	7-H	5.25		
8	138.8	----	----	----	----
9	45.2	9-H	1.93		
10	39.6	----	----	----	----
11	21.5	11-H_α	1.76		
		11-H_β	1.58		
12	39.2	12-H_α	1.27		
		12-H_β	2.09		
13	43.5	----	----	----	----
14	55.1	14-H	1.83		
15	23.0	15-H_α	1.53		
		15-H_β	1.42		
16	27.8	16-H_α	1.89		
		16-H_β	1.28		
17	55.9	17-H	1.82		
18	11.9	18-H	0.57	----	C-12, C-13, C-14, C-17
19	12.6	19-H	0.95	----	C-1, C-10, C-5, C-9
20	36.1	20-H	1.38		
21	18.7	21-H	0.93	$J_{21,22}$=6.4	
22	35.7	22-H_α	1.05		
		22-H_β	1.39		
23	23.9	23-H_α	1.21		
		23-H_β	1.39		
24	34.0	24-H_α	1.37		
		24-H_β	1.68		
25	38.9	25-H	2.48	$J_{25,26}$=6.9	C-23, C-24, C-27
26	17.0	26-H	1.19		C-25, C-27, C-24
27	179.3	----	----	----	----

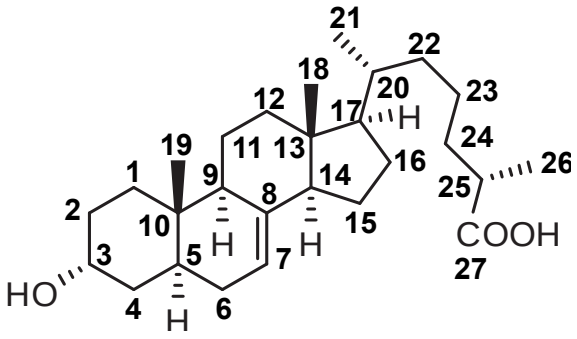

3α-OH-Δ^7-Dafachronic acid

Table A.3. NMR Spectroscopic Data of 3α-OH-Δ^7-DA. ^{1}H (600 MHz), ^{13}C (151 MHz), and HMBC NMR spectroscopic data for 3α-OH-Δ^7-DA in $CDCl_3$. Chemical shifts were referenced to ($C\underline{H}Cl_3$) = 7.26 ppm and ($\underline{C}DCl_3$) = 77.16 ppm.

Carbon No.	δ(ppm)	Proton No.	δ (ppm)	*J* (Hz)	HMBC Correlations
1	31.9	1-H□	1.43		C-3
		1-H□	1.55		C-3, C-5
2	28.7	2-H□	1.4-1.63		
		2-H□	1.4-1.63		
3	66.4	3-H	4.07	$J_{3\text{-}2}$= 8.7, $J_{3\text{-}4}$= 3.5	
4	35.4	4-H□	1.40-1.52		
		4-H□	1.40-1.52		
5	34.6	5-H	1.74	----	C-10
6	29.5	6-H□	1.67-1.72		
		6-H□	1.67-1.72		
7	117.5	7-H	5.17		
8	139.6	----	----	----	----
9	49.4	9-H	1.75		
10	34.7	----	----	----	----
11	21.2	11-H□	1.58		
		11-H□	1.43		
12	39.5	12-H□	1.24		
		12-H□	2.02		
13	43.4	----	----	----	----
14	55.0	14-H	1.80		
15	22.9	15-H□	1.53		C-8
		15-H□	1.39		
16	29.6	16-H□	1.86		
		16-H□	1.25		
17	55.9	17-H	1.20		
18	11.9	18-H	0.53		C-12, C-13, C-14, C17
19	12.0	19-H	0.77		C-1, C-10, C-5, C-9
20	36.0	20-H	1.36		
21	18.9	21-H	0.92	$J_{21\text{-}20}$ = 6.5	C-20, C-17, C-22
22	35.7	22-H□	1.38		
		22-H□	1.05		
23	23.7	23-H□	1.20		
		23-H□	1.36		
24	34.0	24-H□	1.37		
		24-H□	1.66		
25	38.8	25-H	2.49	$J_{25\text{-}26}$ = 7.0	C-23, C-24, C-27
26	17.0	26-H	1.19		C-24, C-25, C-27
27	179.0	----	----	----	----

NMR Spectra of Synthetic Compounds

^{1}H NMR Spectrum (600 MHz, $CDCl_3$) of (25*S*)-$\Delta^{1,7}$-Dafachronic Acid

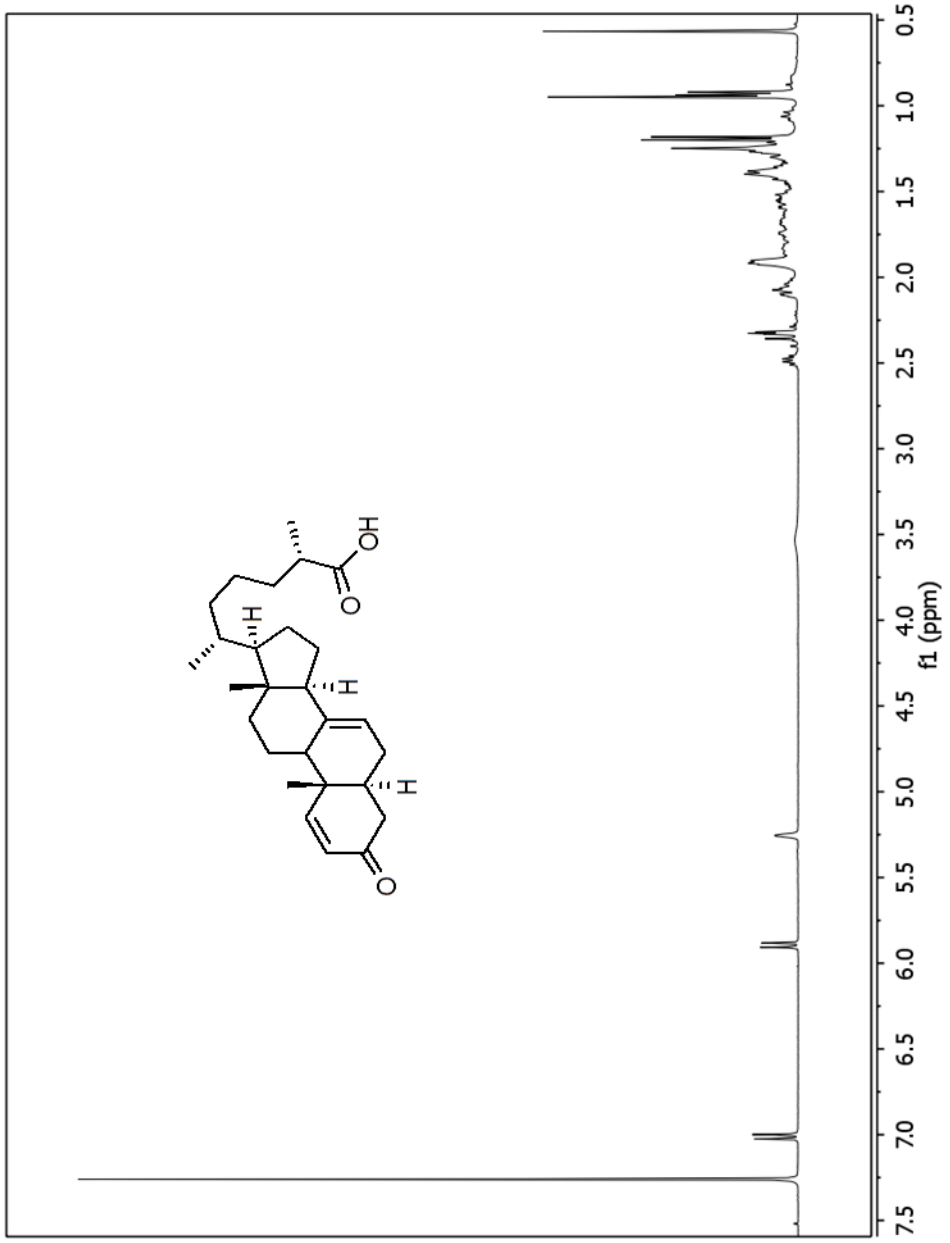

dqfCOSY Spectrum (600 MHz, $CDCl_3$) of (25*S*)-$\Delta^{1,7}$-Dafachronic Acid

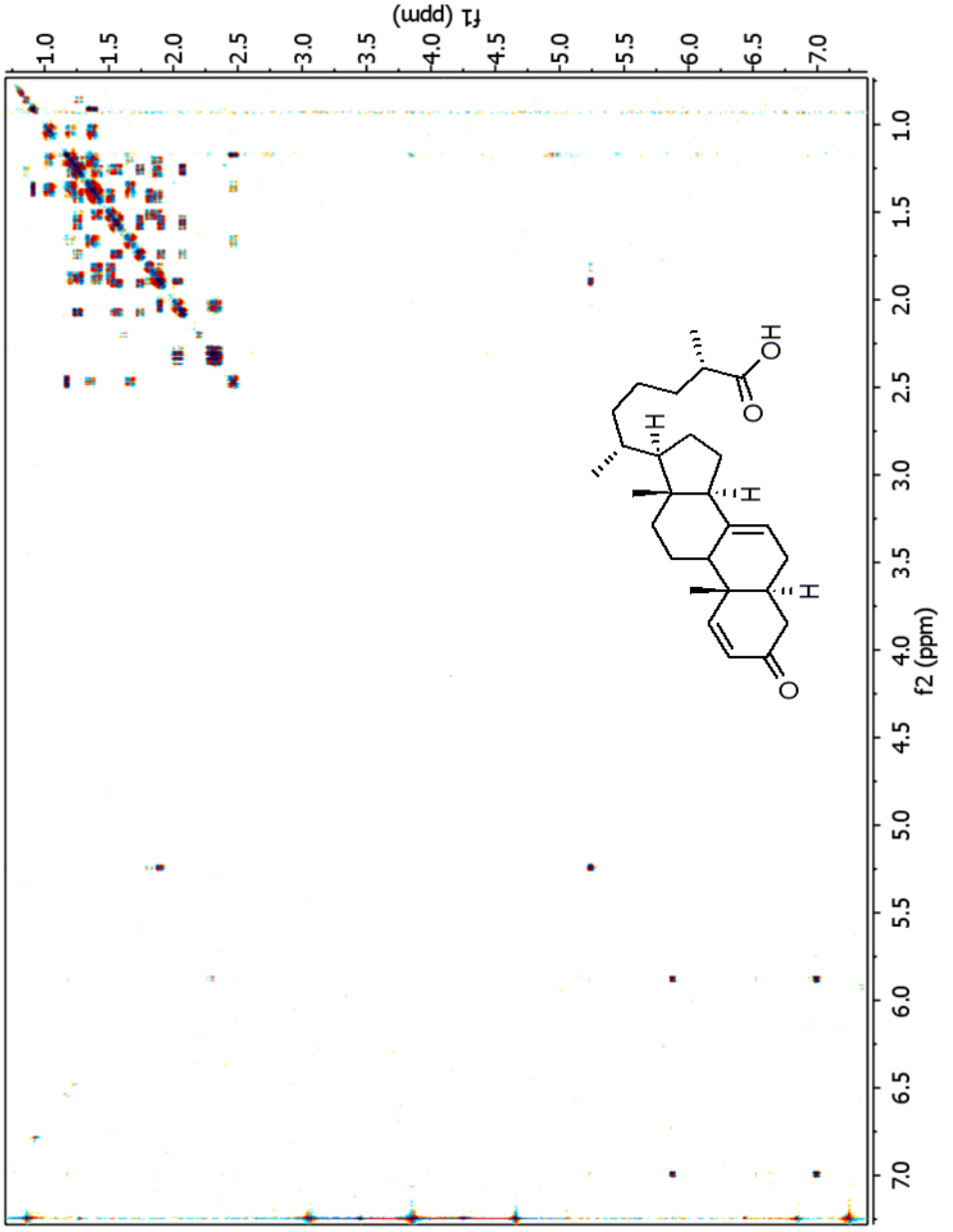

HMQC Spectrum (600 MHz for ^{1}H, 151 MHz for ^{13}C, $CDCl_3$) of (25*S*)-$\Delta^{1,7}$-Dafachronic Acid

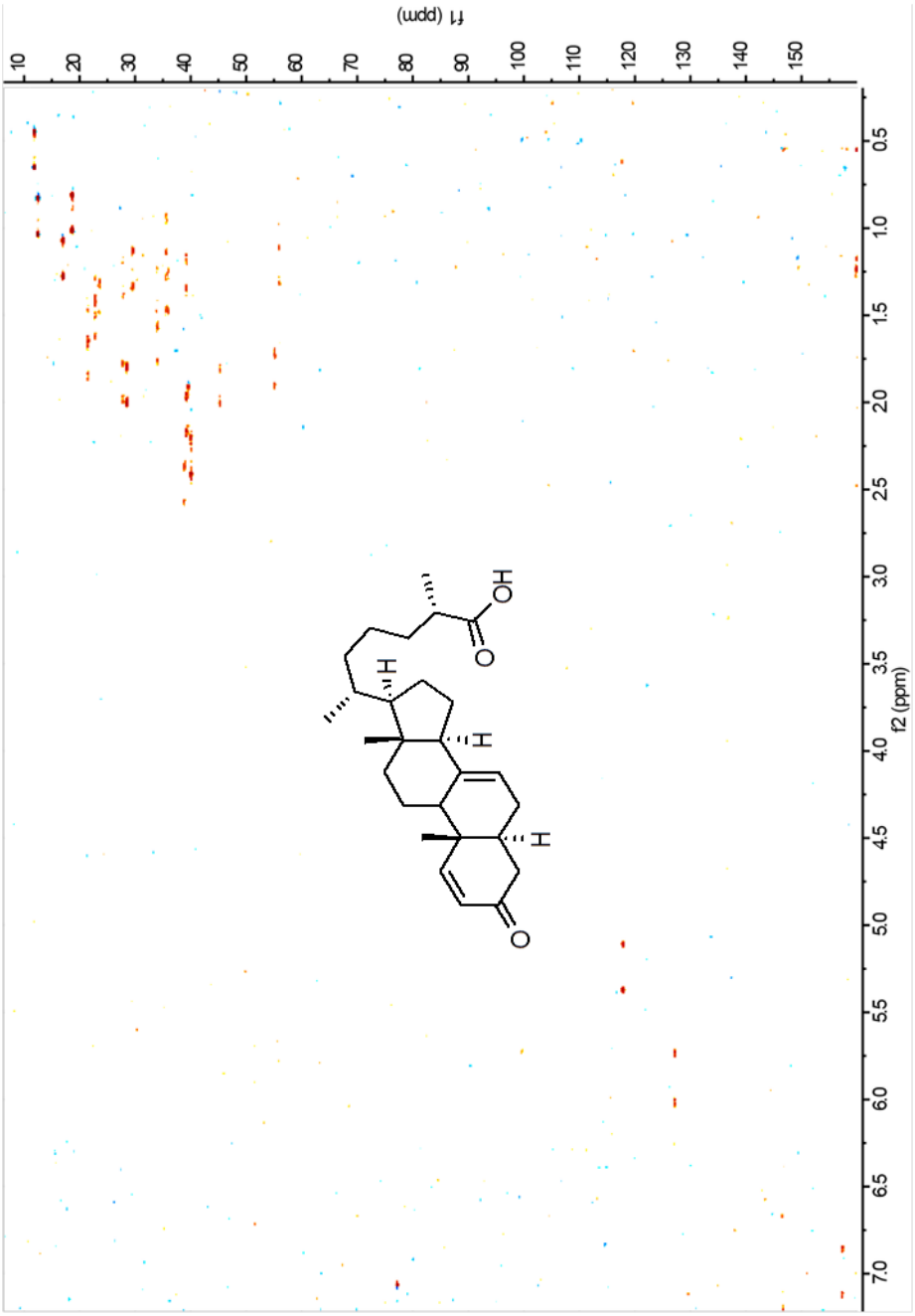

HMBC Spectrum (600 MHz for ^{1}H, 151 MHz for ^{13}C, $CDCl_3$) of (25*S*)-$\Delta^{1,7}$-Dafachronic Acid

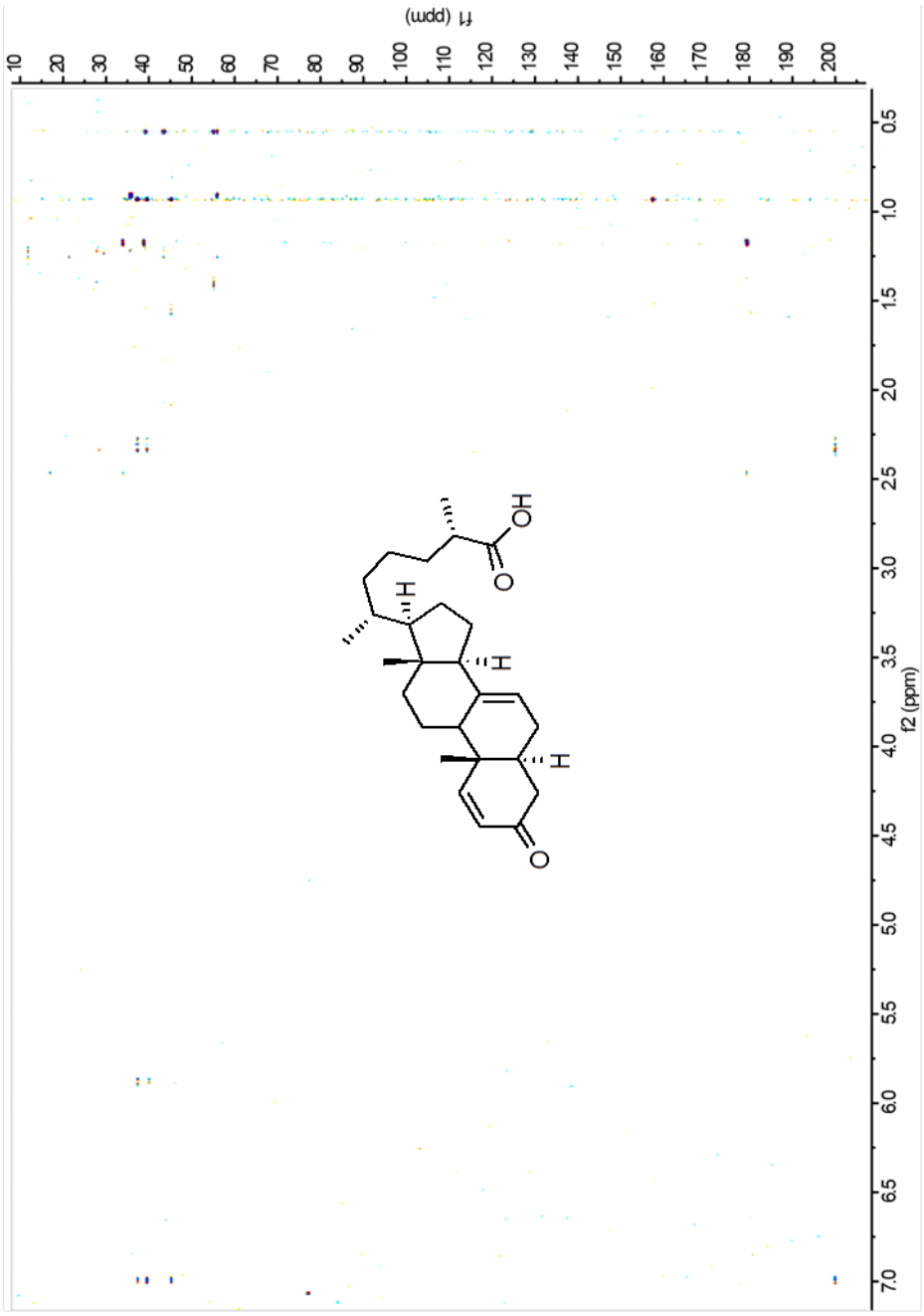

^{1}H NMR Spectrum (600 MHz, $CDCl_3$) of 3α-OH-(25*S*)-Δ^7-Dafachronic Acid

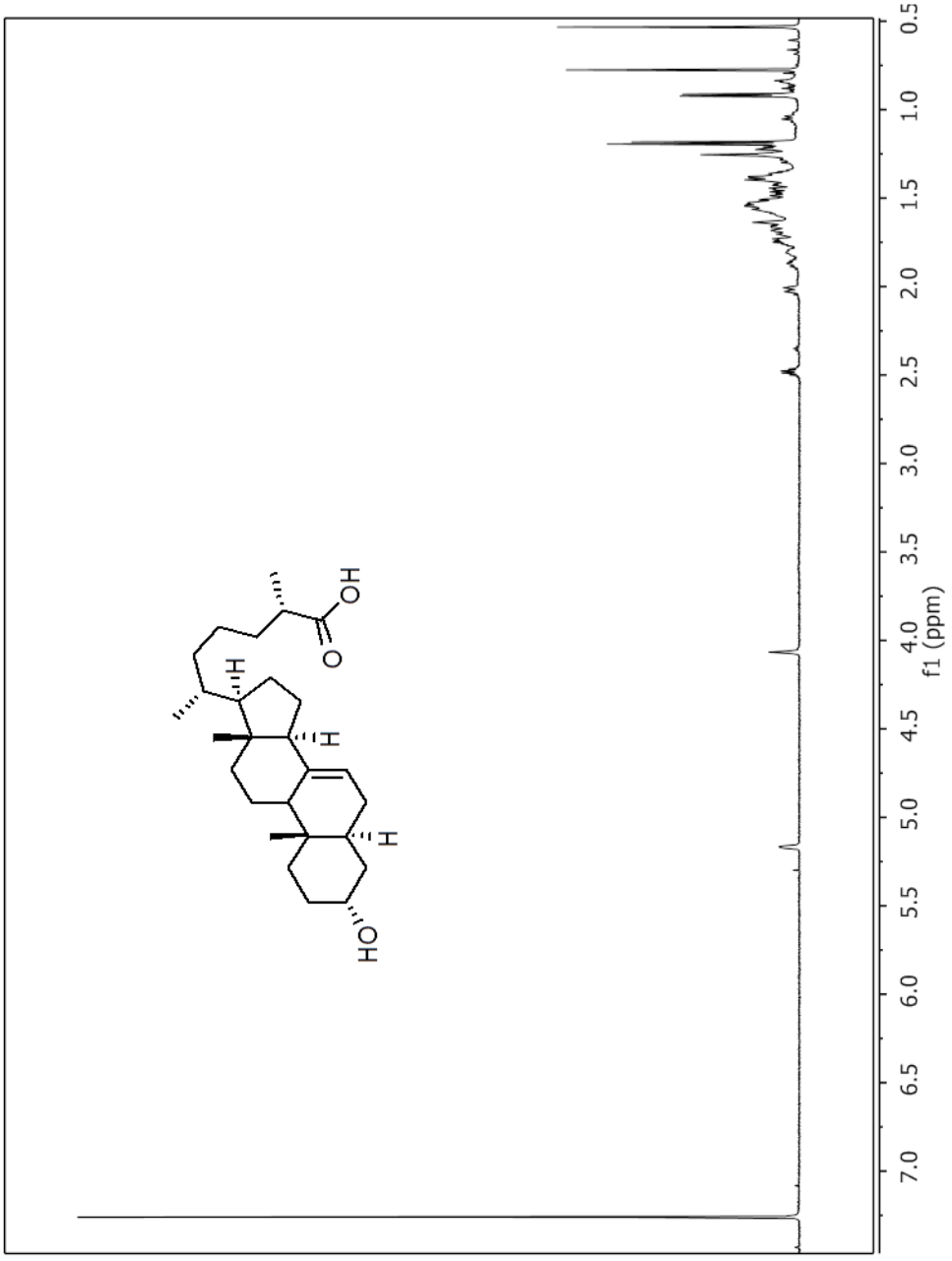

dqfCOSY Spectrum (600 MHz, $CDCl_3$) of 3α-OH-(25*S*)-Δ^7-Dafachronic Acid

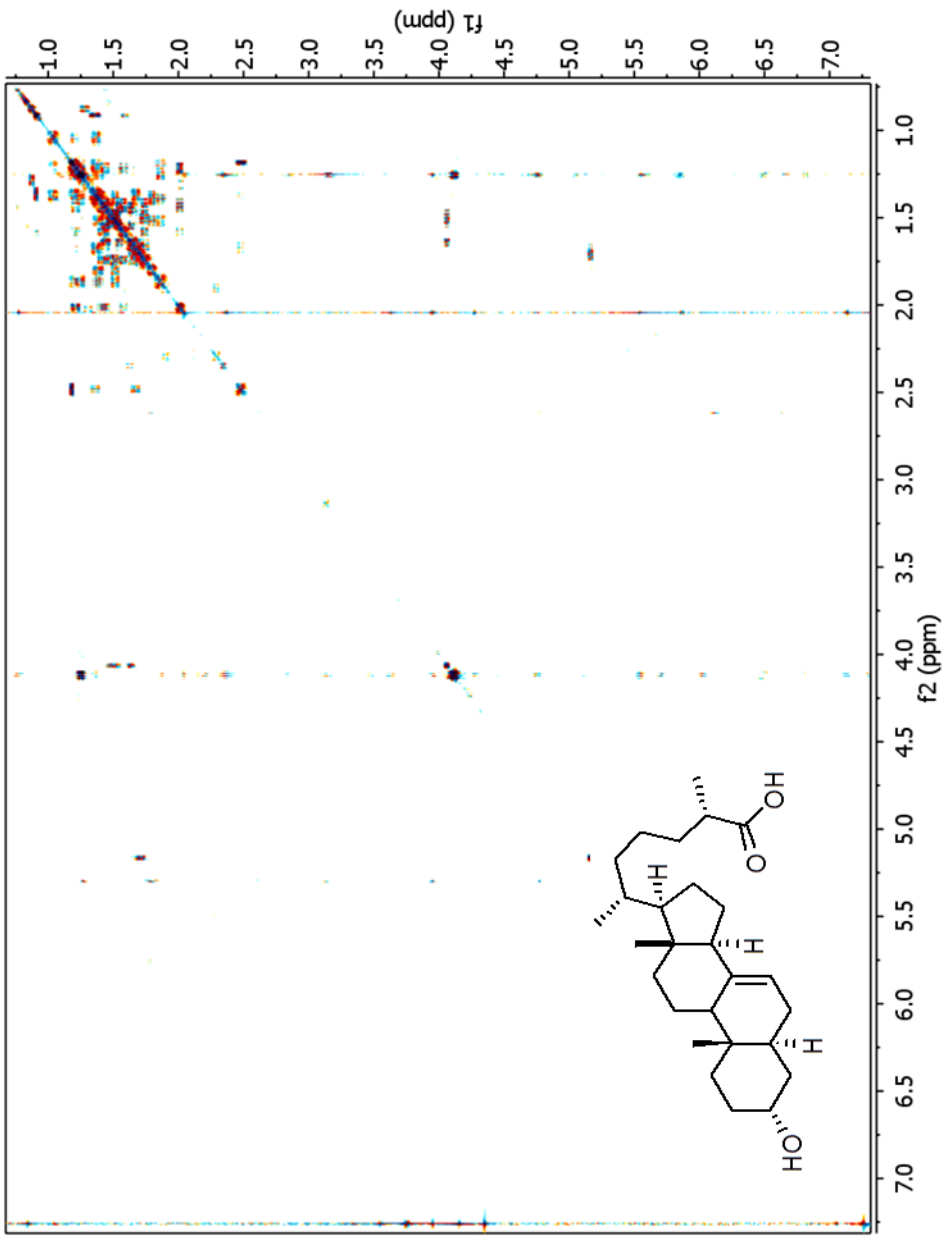

HMQC Spectrum (600 MHz for ^{1}H, 151 MHz for ^{13}C, $CDCl_3$) of 3α-OH-(25*S*)-Δ^{7}-Dafachronic Acid

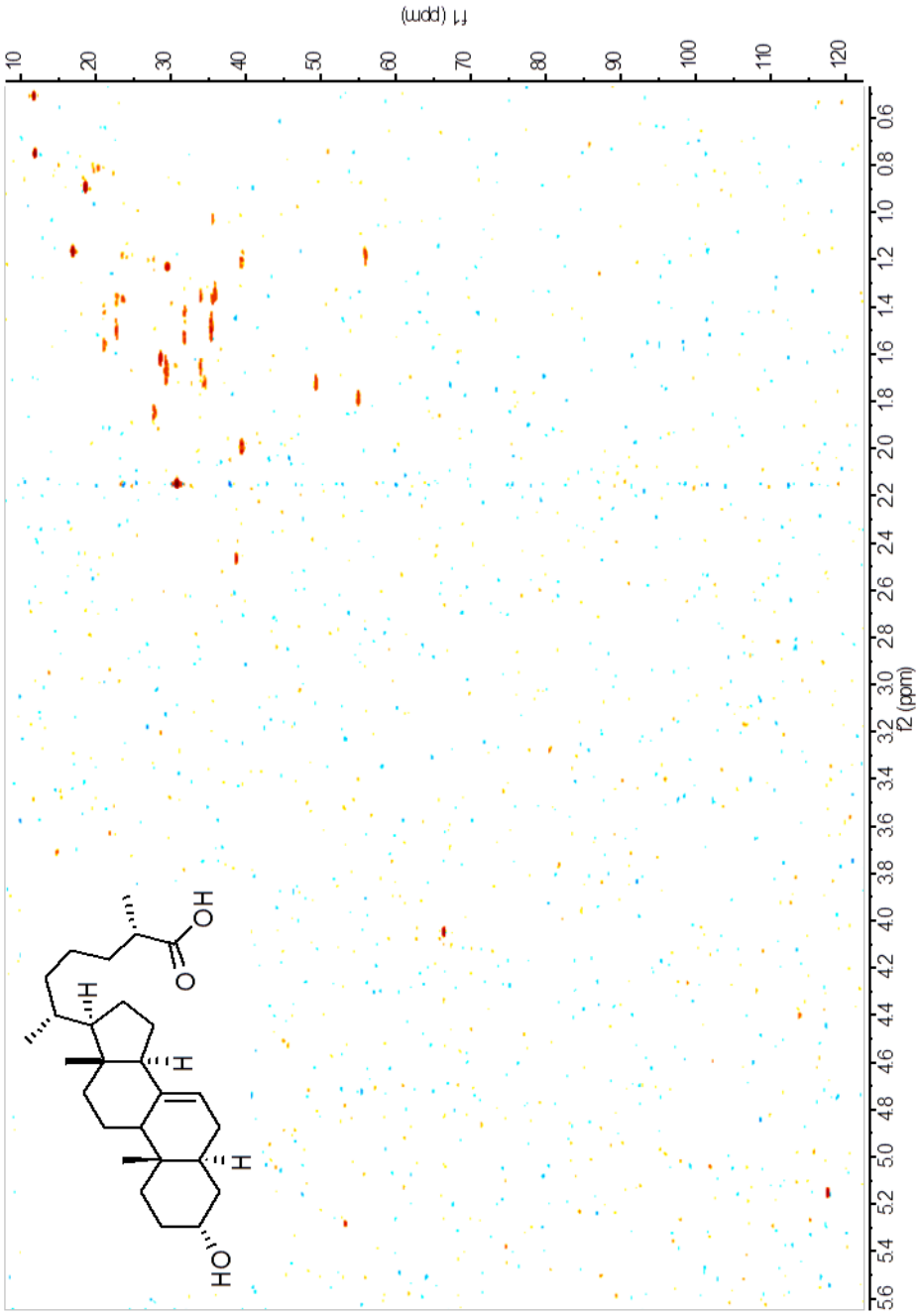

REFERENCES

Bethke, A., Fielenbach, N., Wang, Z., Mangelsdorf, D.J., and Antebi, A. (2009). Nuclear hormone receptor regulation of microRNAs controls developmental progression. Science *324*,95-98.

Motola, D.L., Cummins, C.L., Rottiers, V., Sharma, K.K., Li, T., Li, Y., Suino-Powell, K., Xu, H.E., Auchus, R.J., Antebi, A.*, et al.* (2006). Identification of ligands for DAF-12 that govern dauer formation and reproduction in C. elegans. Cell *124*, 1209-1223.

Wollam, J., Magner, D.B., Magomedova, L., Rass, E., Shen, Y., Rottiers, V., Habermann, B., Cummins, C.L., and Antebi, A. (2012). A Novel 3-Hydroxysteroid Dehydrogenase That Regulates Reproductive Development and Longevity. PLoS Biol *10*, e1001305.

Xu H.E., Stanley T.B., Montana V.G., Lambert M.H., Shearer B.G, Cobb J.E.,. McKee D.D., Galardi C.M., Plunket K.D., Nolte R.T., Parks D.J., Moore J.T., Kliewer S.A., Willson T.M., Stimmel J.B. (2002). Structural basis for antagonist-mediated recruitment of nuclear co-repressors. Nature 415, 813-7.

APPENDIX B

1. *C. elegans* Strains and Maintenance

Nematode stocks were maintained on Nematode Growth Medium (NGM) plates made with Bacto agar (BD Biosciences) and seeded with bacteria (*E. coli* strain OP50) at 20 °C (http://www.wormbook.org/). The following *C. elegans* strains were used: wild type (N2, Bristol), *daf-22(m130), daf-22(ok693), daf-9(dh6), daf-9(dh6);daf-12(rh411rh61), hsd-1(mg345), hsd-1(mg433), hsd-1(mg433);daf-22(ok693), daf-36(k114), daf-36(k114);daf-22(ok693), dhs-16(tm1890);daf-22(m130), strm-1(tm1781), glp-1(e2141), glp-1(e2141)*;*daf-36(k114), daf-40(hd100), daf-36(k114);daf-9(k182), daf-40(hd100);daf-12(rh61rh411), daf-40(hd100);daf-36(k114), daf-40(hd100);dhs-16(tm1890),), daf-40(hd100);daf-9(dh6), daf-40(hd100);daf-2(e1368), daf-40(hd100);daf-22(m130),* and *dhIs839(Pdaf-40::daf-40::gfp;coel::rfp).*

Compound mutants were constructed using standard techniques. Worms were grown at 20 °C for at least two generations under replete growth conditions prior to growing in liquid cultures.

2. Liquid Cultures

Worms from four 10 cm NGM agar plates were washed using M9-medium into a 100 mL S-complete medium pre-culture where they were grown for four days at 22 °C on a rotary shaker. Concentrated bacteria derived from 1 L of *E. coli* OP50 culture was added as food at days one and three. Subsequently, the pre-culture was divided equally into sixteen 500 mL Erlenmeyer flask containing 100 mL of S-complete medium on day 4, which was then grown for an additional 5 days at 22 °C on a rotary shaker and fed with concentrated

bacteria *ad lib*. The cultures were harvested on day 5 and centrifuged to separate the supernatant media and worm pellets. At harvest, liquid cultures contained approximately 80% L1-L3 worms. The worm pellets were stored at -20 °C until used for further analyses.

3. Preparation of Metabolome Extracts

For NMR studies. The frozen worm pellets were added to pre-cooled (-78 °C) 200 mL of methanol in a Waring laboratory blender and blended until no chunks remained. Methanol was evaporated *in vacuo* at 20 °C and the residue resuspended in 300 mL of water. The resulting suspension was then frozen using a dry ice-acetone bath and lyophilized. The lyophilized residue was crushed to a fine powder by a mortar and pestle using ~8 g granular sodium chloride. The powder was then extracted twice with 250 mL of 9:1 ethyl acetate:ethanol mixture over 12 h. The resulting yellow-brown suspension was filtered and the filtrate evaporated *in vacuo* at room temperature to produce the worm pellet metabolome extract used for chromatographic separations.

C. elegans Lipid Extracts for GC/MS/MS. This methodology was used for preparing GC samples in the Adam Antebi Lab. Worms were grown on 10 cm NGM agar plates seeded with OP50 bacteria at 20°C. Gravid adults were bleached and the resulting embryos transferred to 2-3 additional 10 cm plates. Two to three successive rounds of growth and lysis were performed. For the final round, worms were grown until the L3 stage, harvested, frozen in liquid nitrogen and stored at -80 °C. Thawed worms were homogenized by sonication or with an Emulsi-flex C-5 homogenizer (Avestin), and total lipids

(plus 1 μg cholesterol-d_7 and 5β-cholanic acid) were extracted with 2:1 chloroform:methanol. The resulting chloroform layer was dried under argon

All synthetic samples for these experiments were synthesized in collaboration with Josh Judkins and their synthesis will be described in detail elsewhere.

4. NMR Spectroscopic Instrumentation and Analysis

NMR spectra were recorded on a Varian 900 MHz NMR spectrometer (899.9 MHz for 1H, 226.7 MHz for ^{13}C) equipped with a 5 mm 1H ($^{13}C/^{15}N$) cryogenic probe, a Varian INOVA 600 MHz NMR spectrometer (600 MHz for 1H, 151 MHz for ^{13}C) equipped with an HCN indirect detection probe, and a Varian INOVA 500 MHz NMR spectrometer (500 MHz for ^{1}H, 125 MHz for ^{13}C) equipped with an DBG broadband probe. Each spectrum was manually phased, baseline corrected and calibrated to solvent peaks ($CHCl_3$ singlet at 7.26 ppm; CHD_2OD quintet at 3.31 ppm). Non-gradient phase-cycled dqfCOSY spectra were acquired using the following parameters: 0.8 s acquisition time, 500-900 complex increments, 16-64 scans per increment. Obtained dqfCOSY spectra were zero-filled to 8k-16k × 4k and a cosine bell-shaped window function was applied in both dimensions before Fourier transformation. NMR spectra were processed using Varian VNMR, MestreLabs' MestReC, and MNova software packages. Dynamic range of the resulting spectra ranged from 300:1 to 500:1. For example, coupling constants could be determined for characteristic steroidal crosspeaks from dqfCOSY spectra containing as little as 5 μg $\Delta^{1,7}$-DA in a 2.5 mg enriched metabolome fraction.

5. daf-9(dh6) **Dauer Rescue Assay**

Plate based assay: Metabolome fractions were resuspended in ethanol, mixed with 40 µL of 5 x concentrated OP50 bacteria (from an overnight culture in LB media) and plated on 3 cm plates containing 3 mL NGM agar without added cholesterol. For rescue, ~100 eggs from a 4-8 hour egg lay were transferred onto the bacterial lawn, and scored for dauer arrest at 27 °C after 60 h. For rescue experiments with synthetic steroids (0.1 nM – 500 nM tested), 10 µL compounds in ethanol (or ethanol alone) were mixed with 40 µL 5X concentrated OP50 bacteria and plated. Final concentrations include the total volume of agar (3 mL). 100 nM Δ^7-DA was used as positive control.

Liquid Culture based assay: Individual metabolome fractions were dried *in vacuo* and resuspended in 500 µL EtOH. 20-25 gravid *daf-9(dh6)* adults were picked onto three 6 cm NGM agar plates seeded with OP50 containing 25 µL of 10 µM Δ^7-DA each and allowed to grow for three days. On the third day each of the plates were washed with M9 and treated with alkaline hypochlorite solution to isolate eggs from gravid adults. Isolated eggs were allowed to hatch in S-complete media without food, overnight. 100 µl of the resulting synchronized L1 suspension was added to 400 µl of HB101 seeded S-complete media and 5 µl of ethanol or metabolome fraction or ethanol solution of synthetic ligands (1.25 nM – 200 nM tested) per well of a 12 well plate. Wells were examined after 48 and 72 h and scored for dauers, recovered animals and intermediate worms with molting defects and/or mig phenotypes. For active metabolome fractions, additional assays using smaller amounts were conducted.

6. Luciferase Assay for DAF-12 Transcriptional Activation

Luciferase assays to determine transcriptional activation of DAF-12 were performed as described earlier (Bethke et al., 2009). Briefly, HEK-293T cells were seeded and transfected in 96-well plates with (pr well) 30 ng transcription factor vector, 30 ng of gfp expression vector, 30 ng of luciferase reporter, and 5 ng β-galactosidase expression vector using the calcium phosphate precipitate method. Ethanol or ethanol solutions of ligands (synthetic DAs, 1 nM – 3125 nM tested and metabolome fractions) were added 8h after transfection and the luciferase and β-galactosidase activities were measured by a Synergy 2 Biotek LC Luminometer, 16 h after compound addition. 100 nM Δ^7-DA was used as positive control. Data was processed using GEN5 software. Individual fractions were dried *in vacuo* and resuspended in 500 µL EtOH. 1 µL per 100 µL of media solution was added to each well.

8. Biochemical experiments

These experiments were carried out in collaboration with Josh Wollam (Adam Antebi Lab, MPI Cologne).

Isolation of Microsomes. Isolation of microsomes from HEK293T cells was performed as described (Bozidis et al 2007). Cells were grown in T-75 flasks and transfected with vector only or FLAG-tagged DAF-40. Expression of DAF-40 was verified by immunoblot, using anti-FLAG antibodies (Sigma). Microsomal fractions were resuspended in 0.1 M KPO_4 buffer, pH 7.4, containing 1 mM EDTA and 20 % glycerol, and stored at -80 °C.

Microsomal Incubations. Microsomes were thawed on ice and brought to 80 µg/mL in 0.1 M KPO_4 buffer, pH 7.4, containing 1 mM EDTA, 0.5 pmol purified

recombinant human cytochrome P450 reductase, and 0.1 % hematin. Substrates were added at 100 µM in 0.25 mL total volume, pre-incubated for 5 minutes at 37 °C, and reacted with 1 mM NAD for 16 hours at 37 °C. Reactions were processed by extracting twice with 1 mL MTBE, combining the top layers and drying under argon. 0.25 µg of cholesterol-d_7 or 5β-cholanic acid was added as an internal standard for extractions.

Sterol Supplementation Experiments. Metabolite extract fractions were resuspended in ethanol, mixed with 40 µL 5X concentrated OP50 bacteria and plated on 3 cm plates containing 3 mL NGM agar without added cholesterol. For rescue, ~100 embryos from a 4-8 hour egg lay were transferred onto the bacterial lawn and scored for dauer arrest at 27°C after 48 hours. For experiments with pure steroids, 10 µL compounds in ethanol (or ethanol alone) were mixed with 40 µL 5X concentrated OP50 bacteria and plated. Final concentrations include the total volume of agar (3 mL). Dauer arrest was scored after 60 hours at 20 °C and after 48 hours at 25 °C and 27 °C.

qRT-PCR. MicroRNA detection was accomplished using a protocol modified from a previous report (Chen et al.). Briefly, total RNA was purified from L3 stage larvae using TRIzol (Invitrogen) and the miRNeasy kit (Qiagen). TaqMan MicroRNA Reverse Transcription kit (Applied Biosystems) was used to generate cDNA with microRNA-specific primers. qRT-PCR was performed with Power SYBR Green master mix (Applied Biosystems) according to the manufacturer's instructions. Sno-RNA U18 was used as an internal control for microRNA detection.

9. HPLC Enrichment Protocol

Metabolome fractions derived from the Combiflash® method described above were evaporated *in vacuo*, resuspended in 250 µL of methanol and submitted to HPLC, using an Agilent 1100 Series HPLC system equipped with an Agilent Eclipse XDB C-18® column (25 cm x 9.4 mm, 5 µm particle diameter). A 0.1% acetic acid in water (aqueous) – 9:1 acetonitrile : methanol (organic) solvent system was used, starting with 70% organic solvent for 3 min, which was increased linearly to 100% over a period of 20 min and continued at 100% organic solvent for 2 min. One minute fractions were collected using a Teledyne ISCO Foxy 200 X-Y Fraction Collector® connected to the HPLC from 12 to 36 min. Collected fractions were individually evaporated *in vacuo* for further analysis.

10. GC/MS Instrumentation and Sample Preparation

GC/MS analysis was carried out with an Agilent Technologies 6890N Network GC system with a DB-5MS+DG column (25 µm, 30 m x 0.25 mm) operating in split-less mode, connected to a JEOL JMS-GCmateII mass spectrometer. (For details about GC conditions, see Extended Experimental Procedures). Methylation of 3-keto-DAs: synthetic standards or 1-10 % of active metabolome fractions were evaporated *in vacuo* and resuspended in toluene:methanol (500 µL, 3:2), followed by the drop-wise addition of trimethylsilyldiazomethane (120 µL, 2 M solution in Et_2O) with stirring. The reaction was stirred at room temperature for 30 min, quenched with acetic acid, evaporated *in vacuo,* and resuspended in dichloromethane (30-200 µL). Of this solution, 1-5 µL were injected per GC/MS analysis. Silylation of 3-hydroxy-DAs: Synthetic standards or 1-10 % of active fractions were evaporated *in vacuo* and a mixture (100 µL) of 3% 1-(trimethylsilyl)imidazole

(TMSIM) in *N*-methyl-*N*-(trimethylsilyl)trifluoroacetamide (MSTFA) was added with stirring at 80 °C for 45 min. The reaction mixture was evaporated *in vacuo* and resuspended in dichloromethane (30-200 µL). Of this solution, 1-5 µL were injected per GC/MS run.

11. GC/MS Method

GC conditions: Injector was kept at 240 °C and 1 mL/min He flow was maintained. Initial column temperature was at 120 °C for 1.4 min, then increased to 320 °C at a rate of 7 °C/min, and maintained at 320 °C for 10 min.

MS conditions: Electron impact ionization (EI) operated at 70 eV. For synthetic samples (high concentrations, >100 ng/µL), MS was first operated in scanning mode for a mass range of *m/z* 35-500 for 3-keto-DA methyl ester and 3-keto-steroids, and *m/z* 35-650 for 3-OH-DA TMS derivatives to select for the most abundant fragment ions for each compound. For low concentrations (<5 ng/µL) of synthetic samples and metabolome fractions, MS was operated in Selective Ion Monitoring (SIM) mode and the following ions were selectively observed: *m/z* = 428, 271, 229 (Δ^7-DA); 426, 269, 227 ($\Delta^{1,7}$-DA); 430, 398, 231 (Δ^0-DA); 428, 305, 229, 124 (Δ^4-DA); 545, 470, 255 (3□- and 3□-OH-Δ^7-DA); 384, 261, 229 (4-cholesten-3-one).

12. Quantification of DAs from Metabolome Fractions via SIM-GC/MS

GC/MS Data was analyzed using Shrader Analytical and Consulting Laboratories, Inc.'s TSSPro 3.0 software package. Quantification of DAs was performed by integration of GC/MS peaks from the following ion traces: *m/z* = 428 (Δ^7-DA); 426 ($\Delta^{1,7}$-DA); 231 (Δ^0-DA); 428 (Δ^4-DA); 255 (3□- and 3□-OH-Δ^7-DA). Dafachronic acid concentrations were calculated using response

factors determined from synthetic standards. Mass spectrometer response was roughly linear (<5% error) for amounts of 10 pg to 5 ng per compound injection.

13. GC/MS/MS Analysis

These experiments were carried out by Daniel Magner (Adam Antebi Lab, MPI Cologne) Samples were analyzed by GC/MS/MS on a 7000A Triple Quadrupole GC/MS instrument (Agilent Technologies) equipped with an ESI source and an HP-5MS column. Briefly, lipid extracts were spiked with cholesterol-d_7 or 5β-cholanic acid as internal standards, derivitized with an activated *N*-Methyl-*N*-(trimethylsilyl)trifluoroacetamide (MSTFA)/NH_4I mixture followed by Fluka III silylation mixture (for sterols) or with trimethylsilyldiazomethane (for bile acids), and analyzed in MRM mode. The following transitions were observed: 5β-cholanic acid (*m/z* 374.3→264.0) and Δ^7-dafachronic acid (*m/z* 428.3→229.1). Data was normalized to total protein content, as determined by Bradford Assay.

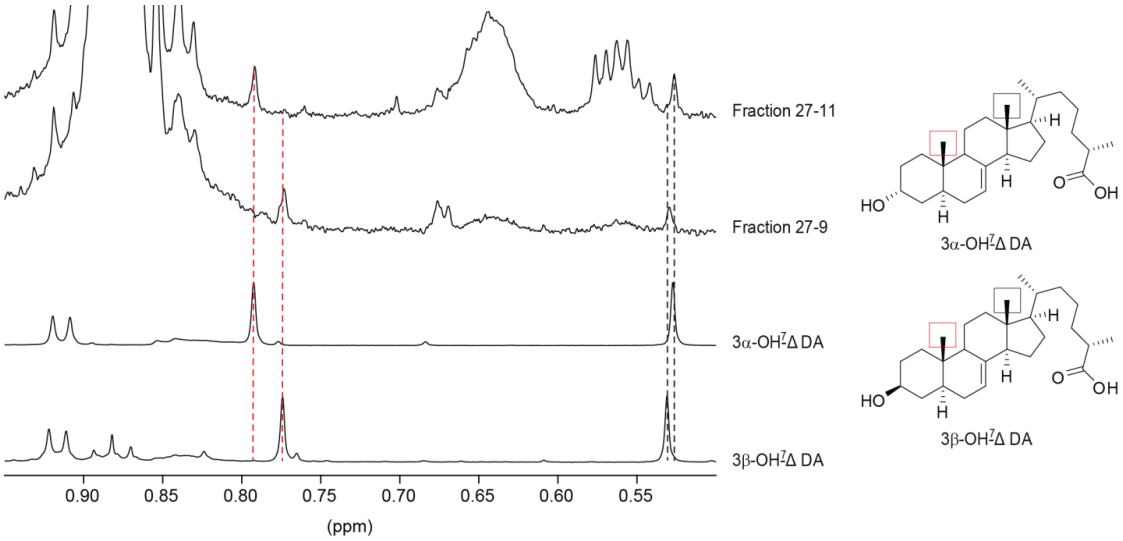

Figure B.1. Detection of 3β-OH-Δ^7-DA in active region II of *hsd-1;daf-22*. Comparison of representative sections of ^{1}H-NMR spectra of active HPLC-enriched fractions from *hsd-1;daf-22* active region II with synthetic 3α-OH-Δ^7-DA and 3β-OH-Δ^7-DA reveals the presence of 3α-OH-Δ^7-DA in fraction 27-11 and 3β-OH-Δ^7-DA in fraction 27-9 in roughly equal amounts.

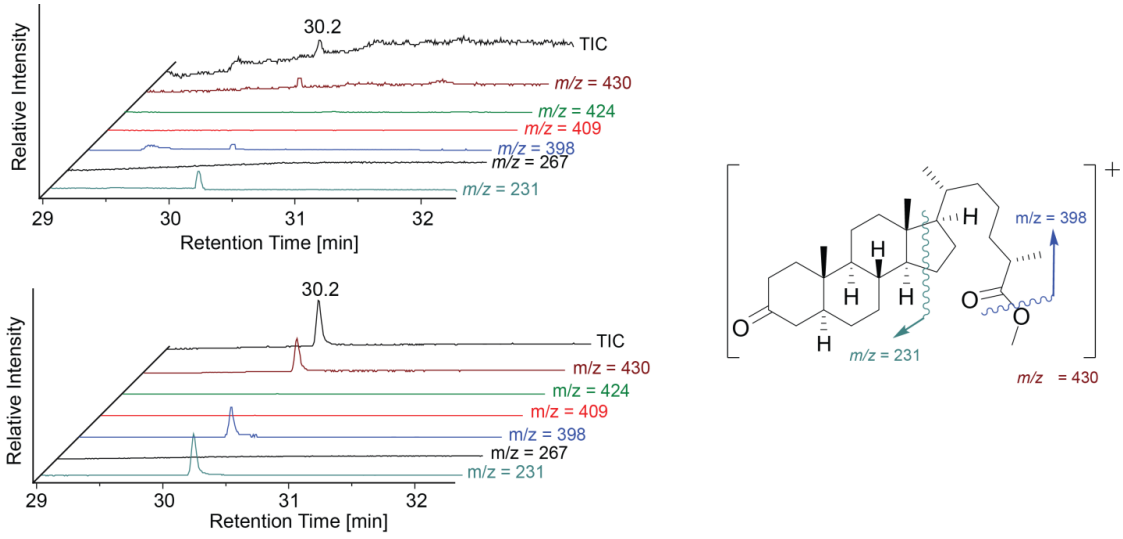

Figure B.2. Confirmation of the presence of Δ^0-DA in active region I of *daf-36;daf-22*. SIM-GC/MS analysis showing characteristic fragment ion traces for Δ^0-DA methyl ester. **(a)** Natural Δ^0-DA in metabolome fraction 25 from *daf-36;daf-22* mutant. **(b)** Synthetic Δ^0-DA. **(c)** Characteristic EI-MS fragments of Δ^0-DA methyl ester shown in (a) and (b).

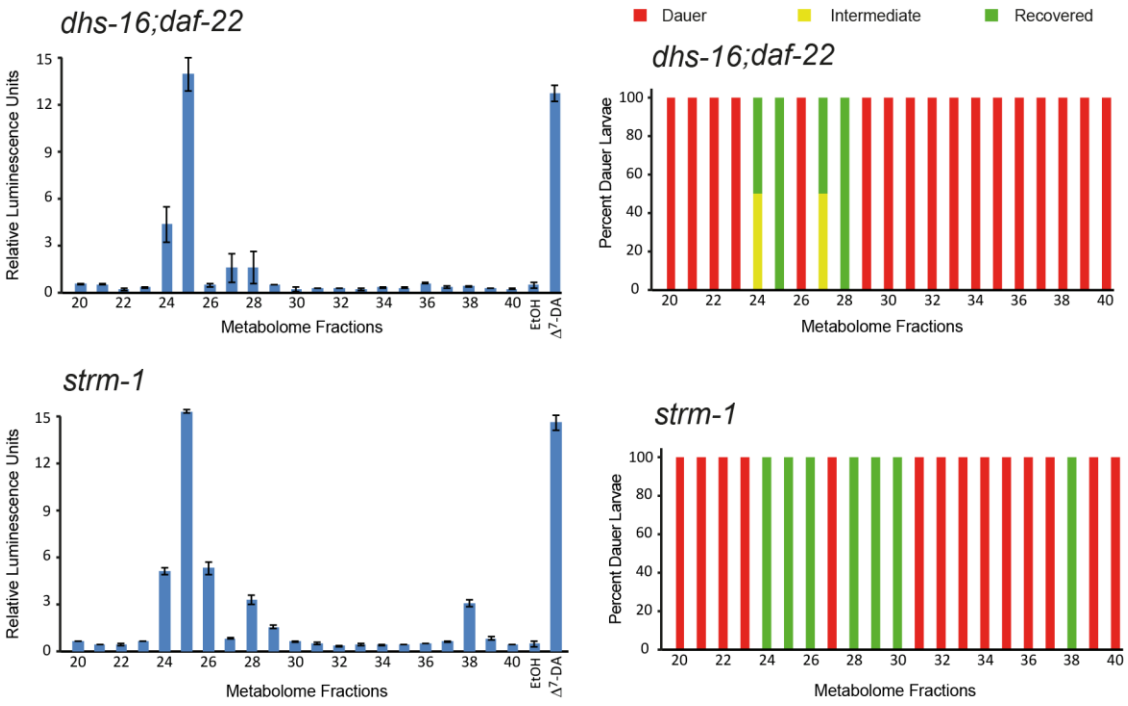

Figure B.3. Bioactivity of mutant metabolome fractions. Assessment of DAF-12 ligand content using the *in vitro* luciferase assay in HEK-293T cells (left) and the *in vivo daf-9(dh6)* dauer rescue (right) with metabolome fractions from (**top)** *dhs-16;daf-22* and **(bottom)** *strm-1*.

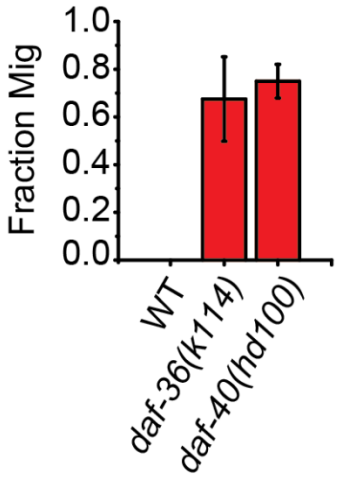

Figure B.4. *daf-40* Phenotypes and Regulation are Consistent with a Role in DA Production. *daf-40(hd100)* mutants show gonadal Mig phenotypes on NGM without added cholesterol (Image Courtesy – Josh Wollam).

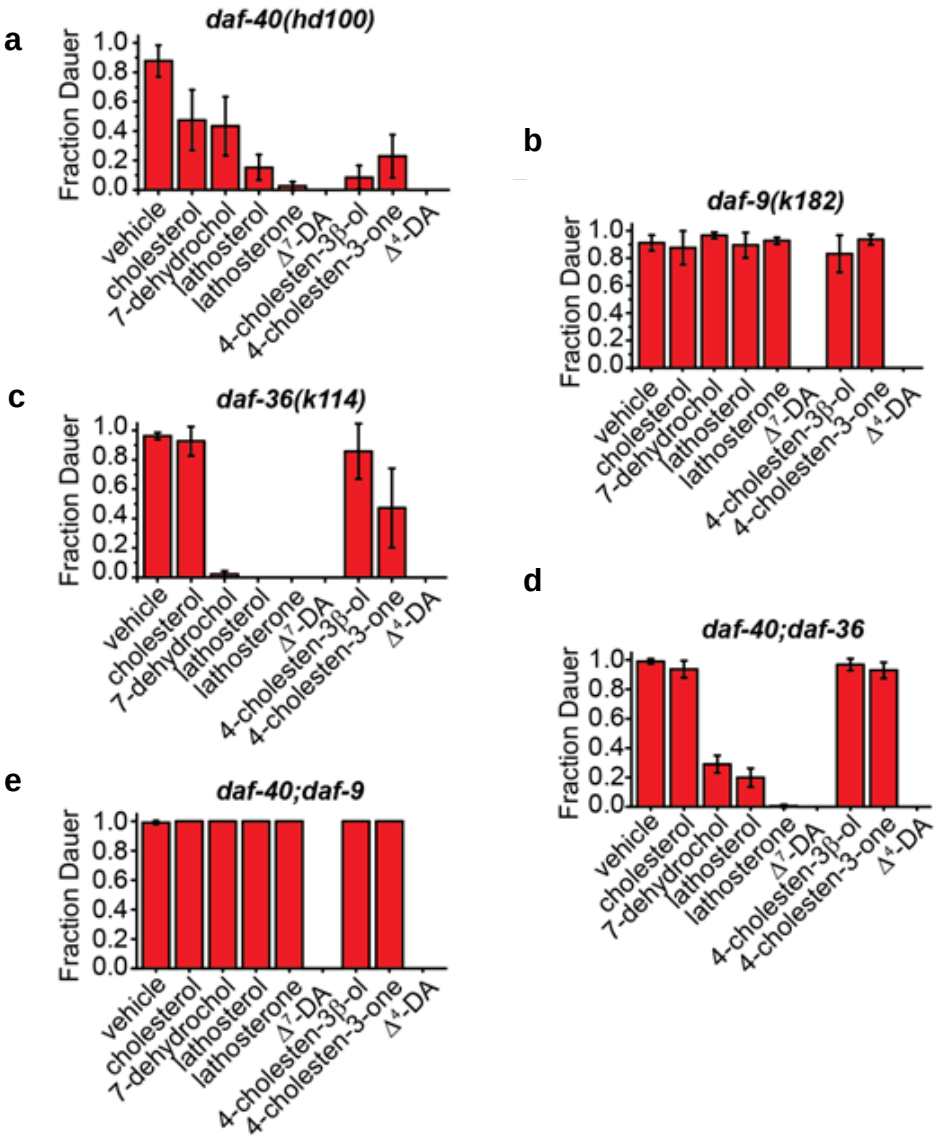

Figure B.5. Sterol Supplementation Experiments Reveal Differences in *daf-40* from Other DA Synthetic Mutants. (A) Rescue of the Daf-c phenotypes of *daf-40(hd100)* mutants at 27 °C with 33 μM concentration of sterols. All compounds tested partially rescued, although only the DAs provided complete rescue (N=3, mean ± SEM). (B) Rescue of the *daf-9(k182)* hypomorphic allele is seen only with the DAs. (C) *daf-36(k114)* null mutants are rescued by 7-dehydrocholesterol (7-dehydrochol) and proposed downstream compounds (N=3, mean ± SEM). (D) *daf-40;daf-36* double mutants are rescued by 7-dehydrocholesterol and downstream compounds but not by cholesterol (N=2, mean ± range), similar to *daf-36* single mutant. (E) *daf-40;daf-9(k182)* double mutants are 100% Daf-c, and are only rescued by the DAs, similar to the *daf-9* single mutant (N=2, mean ± range). (Image Courtesy Josh Wollam).

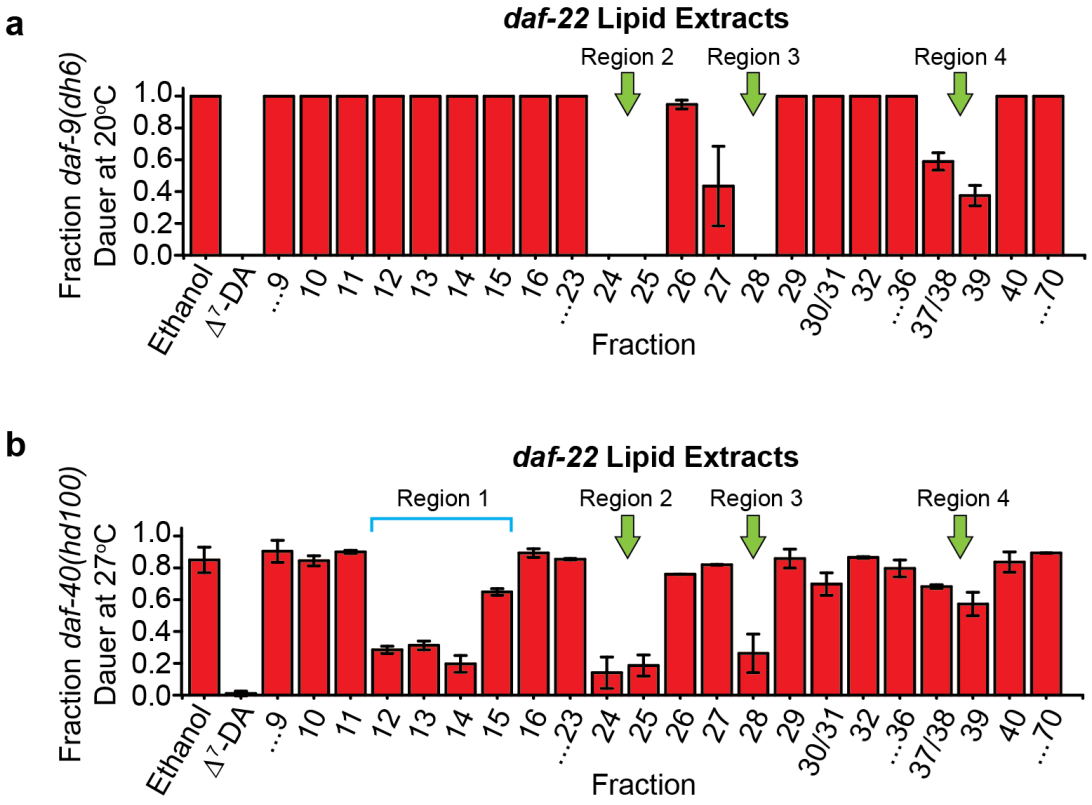

Figure B.6. Rescue Experiments with Fractionated *daf-22* Nematode Lipid Extracts. (A) Fractionated lipid extracts from *daf-22(m130)* rescue the Daf-c phenotypes of *daf-9(dh6)* mutants at 20°C. The fraction number reflects increasing polarity of the elution gradient, with an estimated 150 ng/μL sterol concentration per fraction. The control Δ^7-dafachronic acid, as well as several fractions (Region 2: 24-25, Region 3: 27-28, Region 4: 37-39) rescue the animals to various extents (green arrows). This is a similar pattern of rescue as by wild-type extracts, but with increased efficacy, corresponding with increased DA levels found in *daf-22* mutants (N=3, mean ± SD). (B) The same fractions also rescue *daf-40(hd100)* Daf-c phenotypes at 27°C, as well as fractions 14-19 (Region 1) which contain cholesterol and other proposed DA precursors (labeled with a blue line) (N=3, mean ± SD). (Image Courtesy: Josh Wollam).

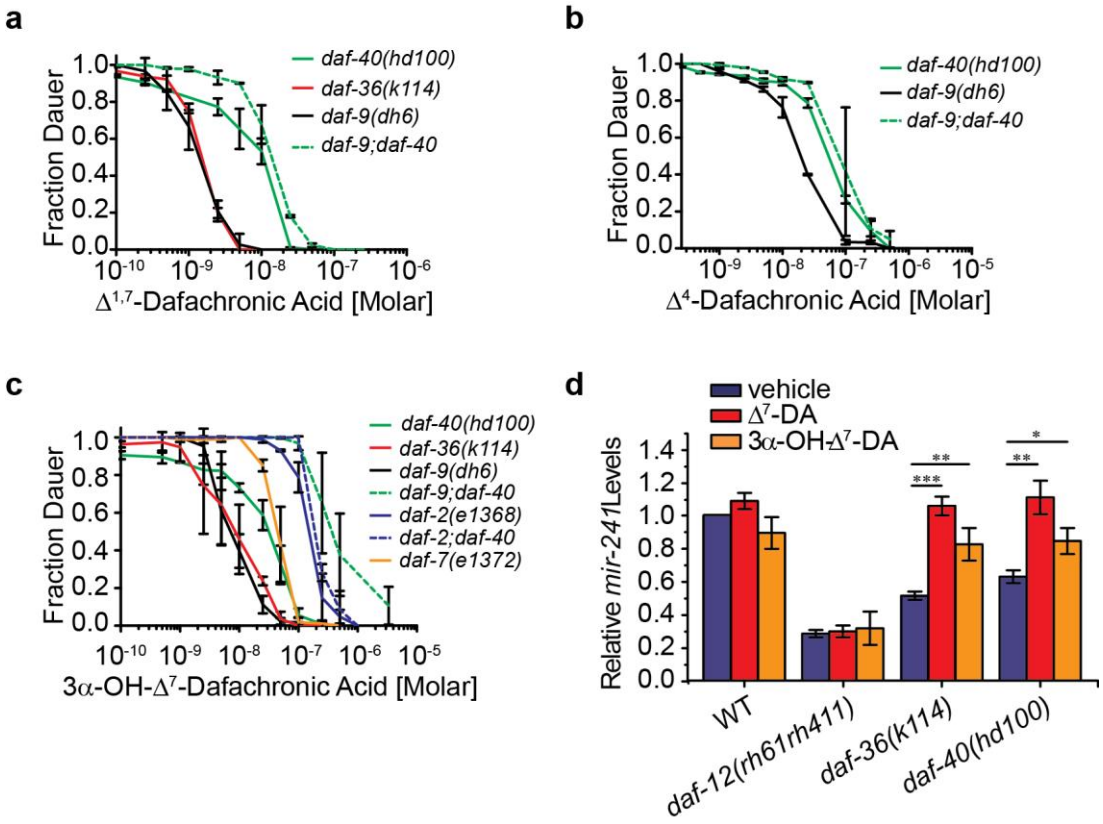

Figure B.7. *daf-40* Mutants are Less Responsive to DA Supplementation. (A) Dose response experiments with the recently identified $\Delta^{1,7}$-dafachronic acid show a similar trend to Δ^{7}-dafachronic acid, as increased concentrations are required to rescue *daf-40(hd100)* dauer formation at 27°C compared to *daf-9(dh6)* mutants. (B) *daf-40* mutants displayed a similarly reduced response of upon Δ^{4}-dafachronic acid. (C) Although the newly identified 3α-hydroxy-Δ^{7}-dafachronic acid shows slightly reduced ability to rescue *daf-9* and *daf-40* dauer formation, *daf-9;daf-40* double mutants show a dramatically reduced response. (D) qPCR analysis of the DAF-12 target gene *mir-241* reveals that supplementation with high concentrations of Δ^{7}-DA or 3α-hydroxy-Δ^{7}-DA rescues reduced expression seen in the *daf-36* and *daf-40* mutant backgrounds (100 nM, N≥4, mean ± SD, **P*<0.01, ***P*<0.001, ****P*<0.0001). (Image Courtesy Josh Wollam).

Figure B.8. Rescue Experiments with Fractionated Nematode Lipid Extracts Identify *daf-9* Dependent Dafachronic Acid Activities. (A) Chromatographic separations of lipid extracts from wild-type (WT) animals were fed to *daf-9(dh6)* null mutants and animals were analyzed for rescue of Daf-c phenotypes at 20°C. The fraction number reflects increasing polarity of the elution gradient, with an estimated 150 ng/□L sterol concentration per fraction. The control □^{7}-dafachronic acid, as well as several fractions (Region 2: 25-26, Region 3: 28-29, Region 4: 38-39) rescue the animals to various extents (green arrows) (N=2 ± range). (B) The same wild-type fractions also rescue *daf-40(hd100)* Daf-c phenotypes at 27°C, as well as fractions 14-19 (Region 1) which contain cholesterol and other proposed DA precursors (labeled with a blue line) (N=2 ± range). (C) *daf-9(dh6)* mutants are not rescued by fractions from *daf-9(dh6);daf-12(rh61rh411),* suggesting the wild-type activities are *daf-9* dependent DAF-12 ligands (N=2 ± range). (D) Earlier fractions from *daf-9;daf-12* mutants still rescue *daf-40* mutants (blue line), suggesting those activities are not *daf-9* dependent, consistent with the presence of cholesterol metabolite DA precursors (N=2 ± range). (Image Courtesy Josh Wollam).

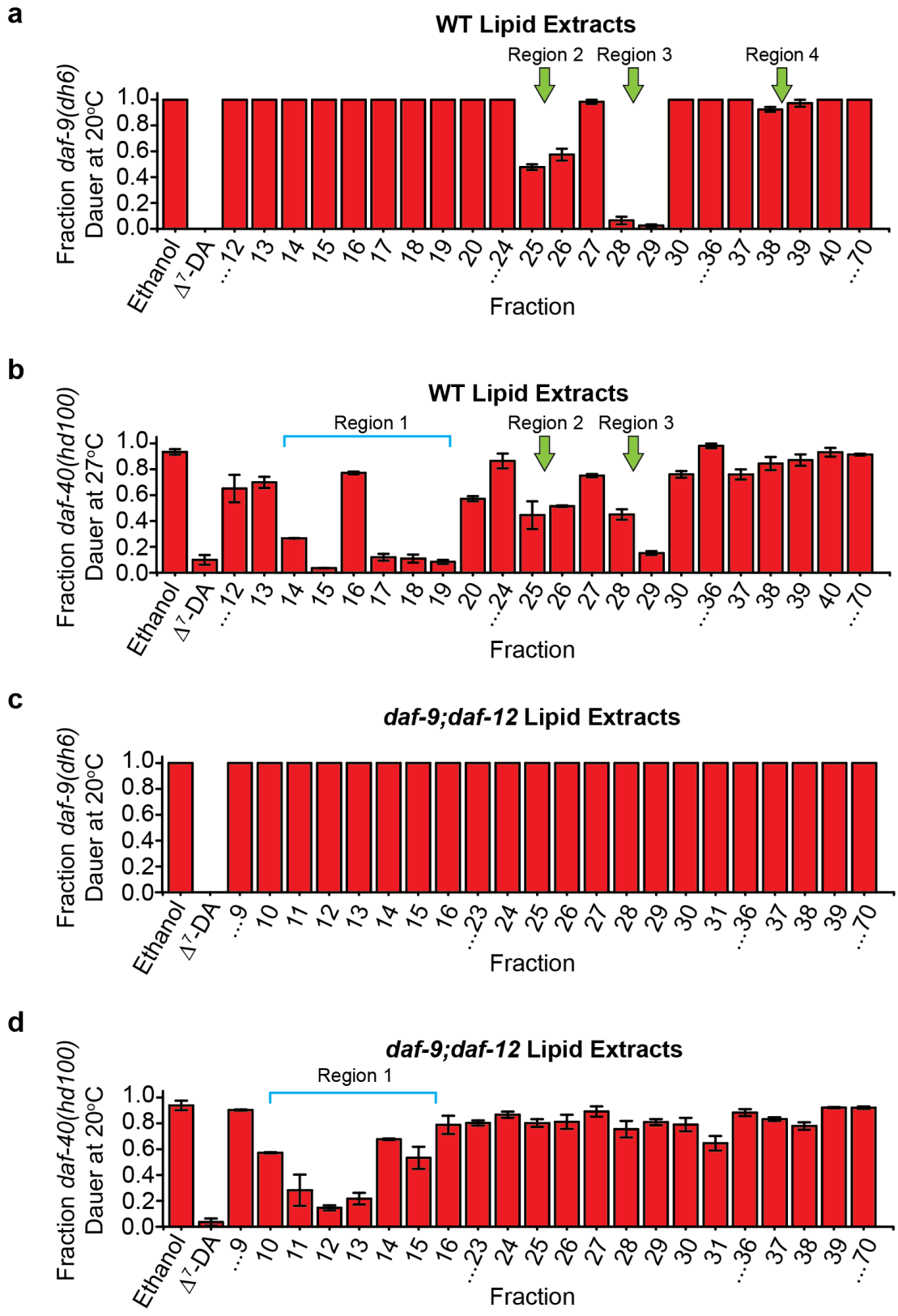
a
WT Lipid Extracts
Region 2
Region 3
Region 4
Fraction daf-9(dh6) Dauer at 20°C
1.0
0.8
0.6
0.4
0.2
0.0
Ethanol
Δ7-DA
...12
13
14
15
16
17
18
19
20
...24
25
26
27
28
29
30
...36
37
38
39
40
...70
Fraction
b
WT Lipid Extracts
Region 1
Region 2
Region 3
Fraction daf-40(hd100) Dauer at 27°C
1.0
0.8
0.6
0.4
0.2
0.0
Ethanol
Δ7-DA
...12
13
14
15
16
17
18
19
20
...24
25
26
27
28
29
30
...36
37
38
39
40
...70
Fraction
c
daf-9;daf-12 Lipid Extracts
Fraction daf-9(dh6) Dauer at 20°C
1.0
0.8
0.6
0.4
0.2
0.0
Ethanol
Δ7-DA
...9
10
11
12
13
14
15
16
...23
24
25
26
27
28
29
30
31
...36
37
38
39
...70
Fraction
d
daf-9;daf-12 Lipid Extracts
Region 1
Fraction daf-40(hd100) Dauer at 20°C
1.0
0.8
0.6
0.4
0.2
0.0
Ethanol
Δ7-DA
...9
10
11
12
13
14
15
16
...23
24
25
26
27
28
29
30
31
...36
37
38
39
...70
Fraction

REFERENCES

Bethke, A., Fielenbach, N., Wang, Z., Mangelsdorf, D.J., and Antebi, A. (2009). Nuclear hormone receptor regulation of microRNAs controls developmental progression. Science *324*, 95-98.

Bozidis, P., Williamson, C. D. & Colberg-Poley, A. M. (2007). Isolation of Endoplasmic Reticulum, Mitochondria, and Mitochondria-Associated Membrane Fractions from Transfected Cells and from Human Cytomegalovirus-Infected Primary Fibroblasts. *Curr Protoc Cell Biol* Chapter 3, Unit 3 27, doi:10.1002/0471143030.cb0327s37.

Chen, C. *et al.* (2005). Real-time quantification of microRNAs by stem-loop RT-PCR. *Nucleic Acids Res* 33, e179.

Motola, D.L., Cummins, C.L., Rottiers, V., Sharma, K.K., Li, T., Li, Y., Suino-Powell, K., Xu, H.E., Auchus, R.J., Antebi, A.*, et al.* (2006). Identification of ligands for DAF-12 that govern dauer formation and reproduction in C. elegans. Cell *124*, 1209-1223.

Wollam, J., Magner, D.B., Magomedova, L., Rass, E., Shen, Y., Rottiers, V., Habermann, B., Cummins, C.L., and Antebi, A. (2012). A Novel 3-Hydroxysteroid Dehydrogenase That Regulates Reproductive Development and Longevity. PLoS Biol *10*, e1001305.

APPENDIX C

1. *C. elegans* Strains and Maintenance

Nematode stocks were maintained on Nematode Growth Medium (NGM) plates made with Bacto agar (BD Biosciences) and seeded with bacteria (*E. coli* strain OP50) at 20 °C (http://www.wormbook.org/). The following *C. elegans* strains were used: wild type (N2, Bristol), *glo-1(zu437), flu-1(e1002), flu-2(1003), flu-3(e1001), flu-4(1004), nkat-1(ok566)*. Worms were grown at 20 °C for at least two generations under replete growth conditions prior to growing in liquid cultures.

2. Liquid Cultures

Worms from four 10 cm NGM agar plates were washed using M9-medium into a 100 mL S-complete medium pre-culture where they were grown for four days at 22 °C on a rotary shaker. Concentrated bacteria derived from 1 L of *E. coli* OP50 culture was added as food at days one and three. Subsequently, the pre-culture was divided equally into sixteen 500 mL Erlenmeyer flask containing 100 mL of S-complete medium on day 4, which was then grown for an additional 5 days at 22 °C on a rotary shaker and fed with concentrated bacteria *ad lib*. The cultures were harvested on day 5 and centrifuged to separate the supernatant media and worm pellets. At harvest, liquid cultures contained approximately 80% L1-L3 worms. The worm pellets were stored at -20 °C until used for further analyses.

3. C. elegans Stress and Killing Assays, RNAi and Supplementation experiments

These experiments were carried out by Cassandra Coburn and other colleagues at David Gems' Lab, University College London.

Hyperoxia treatment. Young N2 adults were placed in either 90% O2 or air at 25uC for 5 d on 10 mM FUdR (fluorodeoxyuridine), OP50 seeded NGM plates.

Iron treatment. 15 mM ferric ammonium citrate (FAC) plates were prepared as previously described (Valentini et al., 2011). Young N2 adults were placed on fresh NGM or FAC plates for 24 h prior to fluorescence and carbonyl measurements.

Worms were killed in three ways, detailed below, all of which result in bursts of blue fluorescence of similar magnitude. Heat killing was used to observe DF dynamics in individual animals in situ on NGM plates. This approach allows lethal stress to be applied near the head or tail, and allows observation of spatial changes in fluorescence, but is relatively difficult to quantitate. Killing by oxidative stress was used for higher resolution microscopy for which it was necessary to view worms under cover slips. Freeze-thaw assays of worms in microtitre plates were used for accurate quantitation of DF to compare genotypes cohorts of worms, and for acquisition of whole spectrum excitation/emission scans.

Heat killing. Here fluorescence of individual animals was measured in situ on NGM plates after killing with a heated worm pick, fitted with a platinum wire (0.3 mm diameter). The wire was flame heated immediately prior to use, and

then placed briefly (~1 s) on the agar immediately adjacent to the worm (~0.1–0.2 mm away), and usually near the head end.

Exposure to tert-butylhydroperoxide. Worms were exposed to 0.726 M (or 7%) t-BOOH, diluted in M9, for 5 min. Following exposure, worms were moved to a 2% agarose pad for time-lapse imaging. Worms were imaged at 100X magnification, on a Nikon Eclipse TE2000-U inverted fluorescence microscope equipped with an excitation monochromator (Polychrome IV, TILL Photonics) and a high-speed monochromatic camera (Sensi-Cam, Cooke). Fluorescence emissions were monitored at 460 nm after 4 ms excitation at 360 nm. Images were captured every 10 s. Image capture and quantitative measurements were performed using the TILLvisION software package (TILL Photonics). Traces were plotted in Microsoft Excel.

Freeze-thaw. Approximately 45 or 50 1-d adults worms per placed per condition in 150 mL M9 plus 0.2% levamisole in a V-shaped 96-well plate (Greiner Bio-One, Frickenhausen, Germany). The plate was then centrifuged at 1,500 rpm for 1 min and frozen at 280 °C for 15 min. The plate was then incubated at 42 °C in an Infinite 200 PRO plate-reader running Magellan software (Tecan Group Ltd., Switzerland) and blue fluorescence measurements were acquired every 30 s for 30 min and for each well, using λ_{ex}/ λ_{em} 340±9/435±20 nm. A peak in fluorescence intensity occurred at, 7–10 min marking the release of gut granule AA into the cytosol, and giving a readout of total AA fluorescence. Relative AA fluorescence was calculated as the difference between the initial minimum and subsequent peak fluorescence intensities for each well, normalized to the N2 control. To account for variation in worm size between conditions (genetic background or RNAi treatment),

relative AA fluorescence was then divided by a size factor. This size factor was obtained by imaging 30 worms by DIC microscopy at 106for each condition, measuring intestinal cross-sectional area and normalizing it to the control (N2) intestinal cross-sectional area.

RNAi. The flu-2, kmo-1, nkat-1, and tdo-2 clones were acquired from the Ahringer library, and the inserts confirmed by DNA sequencing. E. coli HT115 were transformed with the clone and fed to animals as described (Kamath RS, Martinez-Campos M, Zipperlen P, Fraser AG, Ahringer J (2001) Effectiveness of specific RNA-mediated interference through ingested doublestranded RNA in Caenorhabditis elegans. Genome Biol 2: RESEARCH0002).

Anthranilic Acid Supplementation. A 55 mM stock of anthranilic acid (Sigma) was prepared by dissolving AA solid in PBS at 55 °C and then diluted further in PBS. Worms were incubated in AA solution for 3 h at 20 °C in a 96-well microtitre plate with constant shaking.

4. Measurement of DF by Fluorescence spectroscopy and Microfluorimetry

These experiments were carried out by Cassandra Coburn and other members of the David Gems' Lab at UCL) and Filip Matthijssens (Bart P. Braeckman Lab, University of Ghent).

Worms were either imaged in situ on NGM plates or anaesthetized on agar pads on glass slides. Images were acquired using an Orca digital camera (Hamamatsu) and a Leica DMRXA2 microscope. Blue fluorescence was observed through a DAPI filter cube ($\lambda_{ex}/\lambda_{em}$ 300–400 nm/410–510 nm) (ET DAPI, set 49000, Chroma). Green fluorescent protein (GFP) fluorescence was

observed through a GFP filter, ($\lambda_{ex}/\lambda_{em}$ 450–490 nm/500–550 nm) (Endow GFP Bandpass, 41017 Chroma). Images were acquired using the application Volocity Acquisition (Improvision, Perkin-Elmer). Fluorescence was quantified by manually tracing around worm peripheries using an Intuos graphics tablet (Wacom), and measuring mean pixel density using Volocity Quantitation. Worm fluorescence was estimated as the mean pixel density of the worm image area minus the pixel density of the image background.

Time-lapse photography. Wild-type (N2) L4 hermaphrodites were cultured individually (one per plate) on NGM agar plates with E. coli OP50 and 10 mM FUdR (Gandhi et al., 1980). Worms were individually photographed in situ on the plates every 1–2 d until death and beyond as described below. Nematodes were placed on ice for 10 min prior to photography to induce stillness. Nematode viability phenotype was scored daily as described (Herndon et al., 2002).

Single-animal vermiculture. This was performed as previously described (Pincus et al., 2011). Fluorescence was measured under both DAPI and GFP filters, as before, and under a TRITC filter ($\lambda_{ex}/\lambda_{em}$ 530–560 nm/585–645 nm, TRITC 41002b, Chroma)

Whole-Spectrum Excitation Emission Scans. Synchronous populations of L4 animals were transferred to NGM plates seeded with E. coli OP50 and containing 50 mM FUdR (24uC). One-day-old adults were then rinsed off the plates and washed using S buffer. For each strain, three replicate aliquots of 100 ml worm suspensions were loaded in black microtiter plates (Greiner). Aliquots resulted in ,1 mg alkali-extracted protein, determined by standard

BCA assay (ThermoScientific). The 10-nm step fluorescence emission spectra of living worm suspensions were measured upon excitation at 250–450 nm (10 nm intervals) using a microplate reader (Spectramax Gemini XS, Molecular Devices). Worms were then killed by freeze-thaw and fluorescence measurements repeated. All data shown are averages of three technical replicates, corrected by a blank measurement, and normalized by protein content of the worm suspensions.

5. Preparation of Metabolome Extracts

Whole worm sonicates were prepared in dH_2O from large heterogeneous populations grown on NGM plates. Sonication was performed in repeated cycles of 1 min followed by a 30 s pause for cooling in a ‘‘Bioruptor’’ water bath sonicator (Diagenode) until samples were homogenously clouded. Samples were spun down at 4 °C at 14,000 rpm for 15 min, and the supernatant extracted. Cold 100% ethanol was added in 1:9 sample: ethanol ratio and left at 220uC overnight. Samples were spun down again as above. The remaining supernatant was taken. Samples were then evaporated in vacuum at room temperature. For NMR-spectroscopic analysis, the residues were dissolved in 200–600 mL of methanol-d4. Following NMR-spectroscopic analysis, samples were evaporated to dryness, resuspended in 500 mL methanol, centrifuged, and 1–30 mL aliquots were used for HPLC/MS analysis.

6. Analytical Instrumentation and Procedures

NMR spectroscopy: NMR spectra were recorded on a Varian INOVA 600 NMR (600 MHz for ^{1}H, 151 MHz for ^{13}C) and INOVA 400 NMR (400 MHz for ^{1}H, 100

MHz for ^{13}C) instruments. Non-gradient phase-cycled dqfCOSY spectra were acquired using the following parameters: 0.6 s acquisition time, 500-900 complex increments, 8-32 scans per increment. Gradient and non-gradient HSQC[AD], HMQC, and HMBC[AD] spectra were acquired with these parameters: 0.25 s acquisition time, 300-600 increments, 8-32 scans per increment. $^{1}H,^{13}C$-HMBC spectra were optimized for $J_{H,C}$ = 6 Hz. Susceptibility-matched NMR tubes (Shigemi) were used for sample amounts smaller than 2 mg. NMR spectra were processed using Varian VNMR, MestreLabs, MestReC, and Mnova software packages.

HPLC-MS: HPLC-MS was performed using an Agilent 1100 Series HPLC system equipped with a Varian Pursuit XRs-3-C18 column (4.6 x 250 mm, 5 µm particle diameter) connected to a Quattro II spectrometer (Micromass/Waters) A water (containing 0.1% acetic acid) – acetonitrile (also containing 0.1% acetic acid) solvent gradient was used at a flow rate of 0.7 ml/min, starting with an acetonitrile content of 5% for 15 min which was increased to 35% over a period of 20 min and subsequently to 95% over a period of 5 min and continued at 95% for 6 min. Metabolite extracts were analyzed by positive and negative electrospray ionization-MS. High resolution HPLC-MS was performed using a Waters nanoACQUITY UPLC System equipped with a Waters Acquity UPLC HSS C-18 column (2.1 x 100 mm, 1.8 µm particle diameter) connected to a Xevo G2 QTof Mass Spectrometer.

7. Synthesis of angl#1 (β-D-glucosyl anthranilic acid ester)

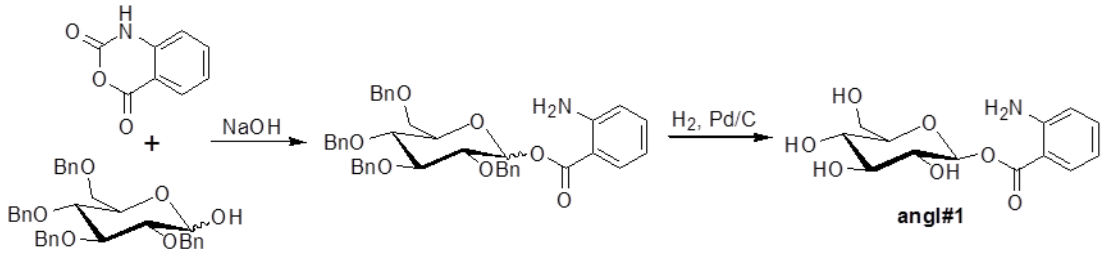

Adapting a previously described procedure (Roell et al., 2011), a catalytic amount (about 1 mg, 0.025 mmol) of sodium hydroxide was added to a solution of 75 mg (0.462 mmol) of isatoic anhydride (Sigma-Aldrich, I12808) and 250 mg (0.462 mmol) of 2,3,4,6-tetra-*O*-benzyl-D-glucopyranose (Sigma-Aldrich, 86730) in 4 mL dioxane. The reaction mixture was stirred and heated gradually until moderate evolution of CO_2 occurred (75-90 °C). This temperature was maintained until gas evolution ceased (2 h) and the mixture was cooled and diluted with 6 ml of water. Crude 2,3,4,6-tetra-*O*-benzyl-D-glucosyl anthranilic acid ester, containing both the α and β isomers, separated out as an immiscible oil and was extracted with methylene chloride (yield 255 mg, 84%). To deprotect the glucose moiety, this mixture of products was dissolved in ethyl acetate (10 mL) to which 10 % palladium on activated carbon (28 mg) was added, and the resulting suspension was stirred under a hydrogen atmosphere for 24 h. Subsequently, the reaction vessel was flushed with argon, and the reaction mixture was filtered over Celite and the filtrate evaporated to dryness *in vacuo*. An 10-mg sample of pure angl#1 was isolated from the mixture of α- and β-isomers by silica gel column chromatography using 20% ethyl acetate and hexane.

A sample of iglu#1 was synthesized as described previously (Messaoudi et al., 2004).

8. Compound names

All newly identified *C. elegans* metabolites were named using their four letter **"**SMID"s (Small Molecule IDentifiers), e.g. "iglu#2" or "angl#1". The SMID database (www.smid-db.org) is an electronic resource maintained by Frank Schroeder and Lukas Mueller at the Boyce Thompson Institute in collaboration with Paul Sternberg and WormBase (www.wormbase.org). This database catalogues *C. elegans* small molecules, assigns a unique four-letter SMID, and for each compound lists other names and abbreviations used in the literature.

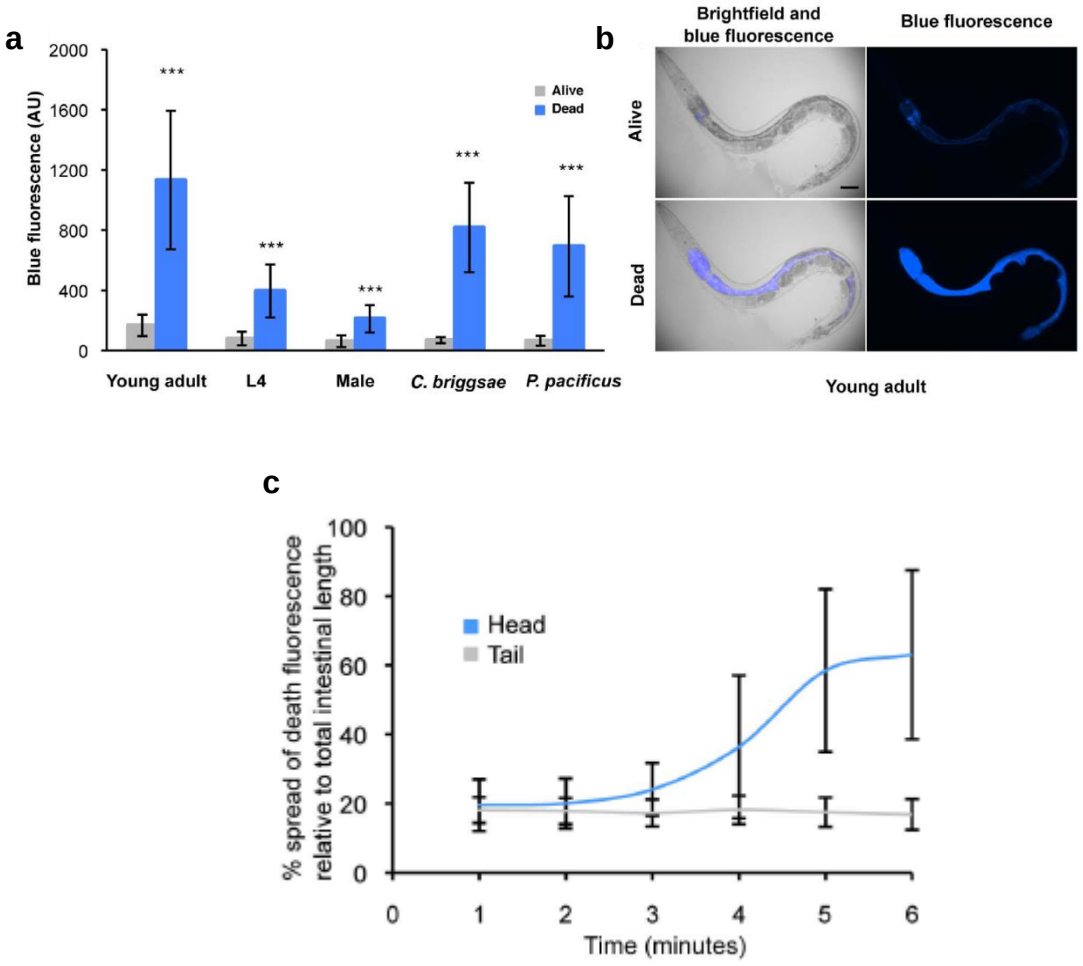

Figure C.1. DF is induced by different methods of killing and seen in other nematodes. (A) DF induced by hot pick killing in young WT adult, L4 and male *C. elegans* as well as in other nematodes species *C. briggsae* and *P. pacificus.* (B) Typical fluorescence increase in young adult worm killed by a hot pick (C) Fluorescence increases in an anterior to posterior wave and DF will not propagate on the other way. (Image Courtesy: Cassandra Coburn)

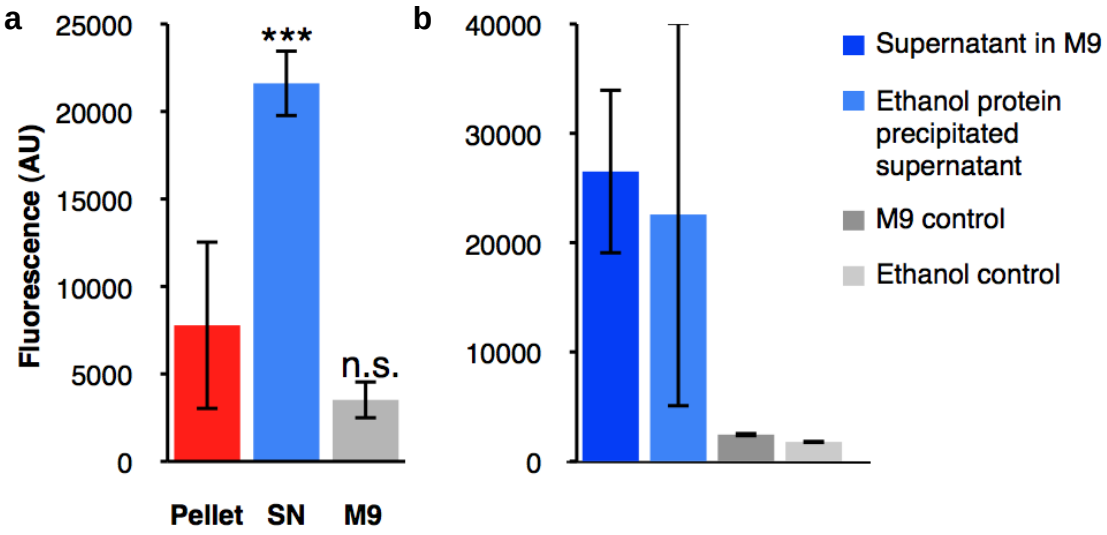

Figure C.2. Blue fluorescence is unlikely to be proteinaceous. (A) Fluorescence can be isolated to the supernatant of a homogenate and remains even after removal of protein (B). Data is mean of three (A) or two (B) biological replicates, error bars ± SD. (Image courtesy: Cassandra Coburn)

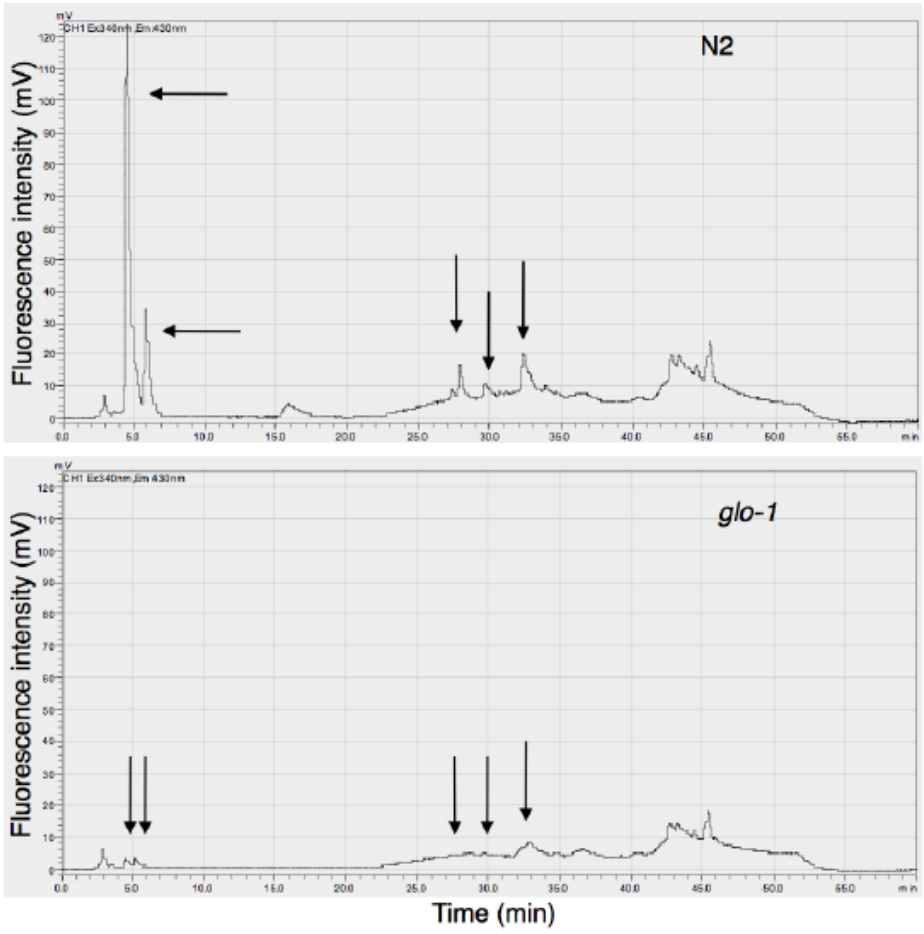

Figure C.3. Extracts from *glo-1* animals do not contain fluorescent molecules at 340/430. HPLC chromatogram reveals four peaks present in N2 but not in *glo-1* animals

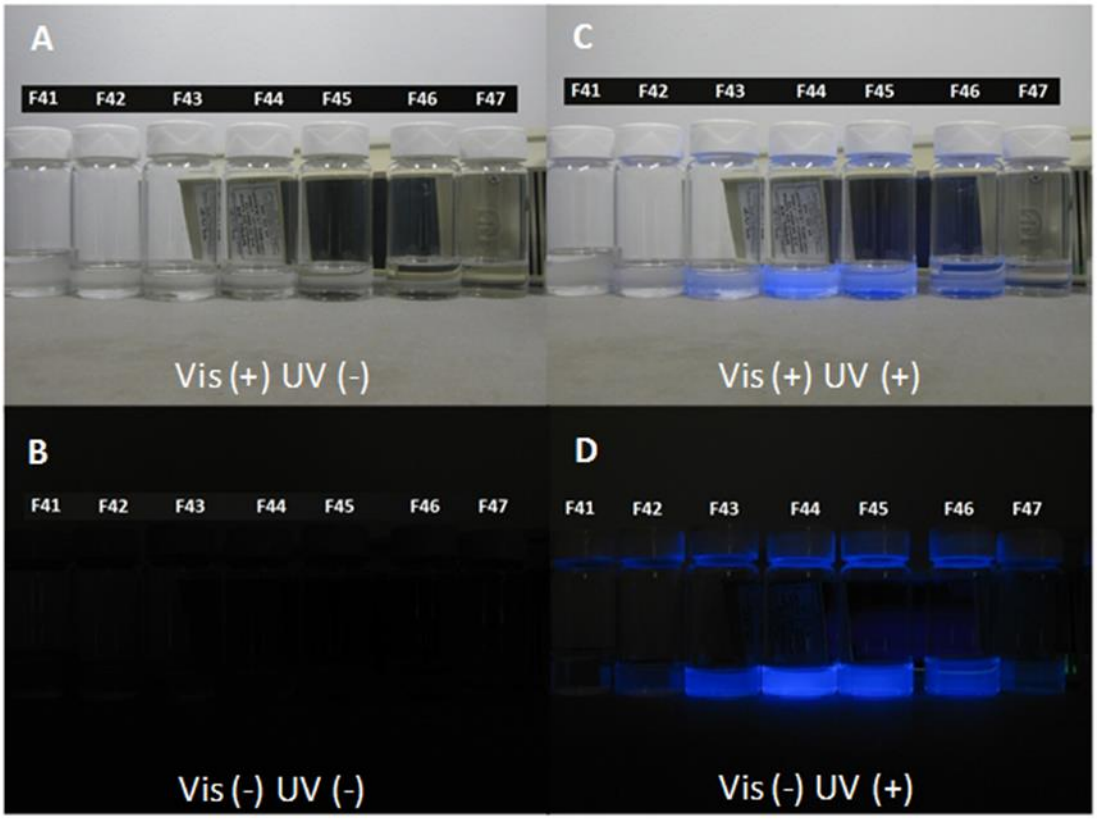

Figure C.4. Metabolite extracts from N2 worms show blue fluorescence.

Figure C.5. Proton NMR spectra of metabolite fractions show anthranilic acid moieties. Metabolite extracts from N2 worms showing blue fluorescence contain aromatic peaks corresponding to anthranilic acid moieties (blue boxes). Non-fluorescent fractions in the similar polarity range contain glucosylated indole compounds.

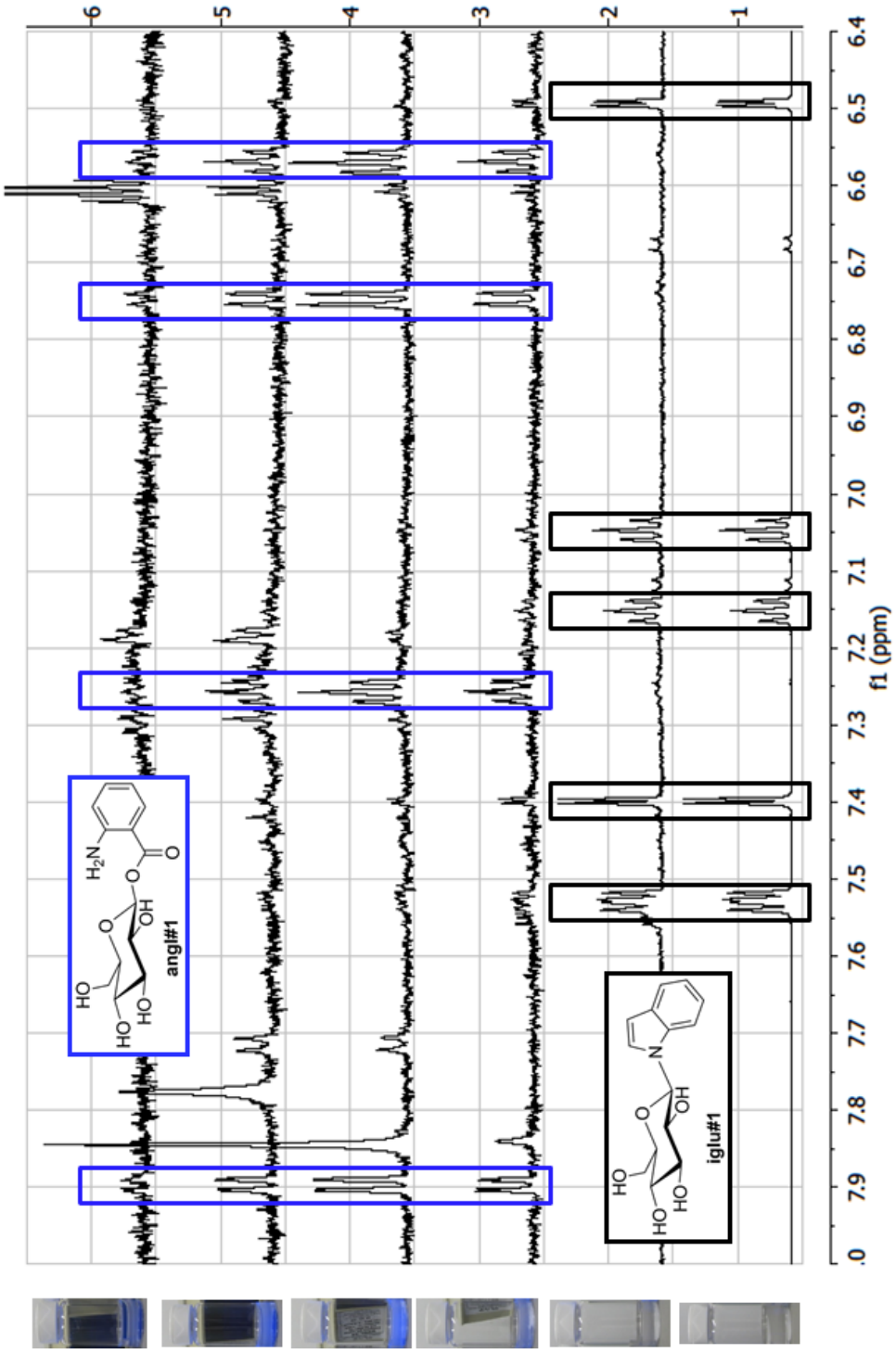
6
5
4
3
2
1
6.4
6.5
6.6
6.7
6.8
6.9
7.0
7.1
7.2
f1 (ppm)
7.3
7.4
7.5
7.6
7.7
7.8
7.9
.0
H_2N
O
O
OH
HO
HO
HO
angl#1
N
O
OH
HO
HO
HO
iglu#1

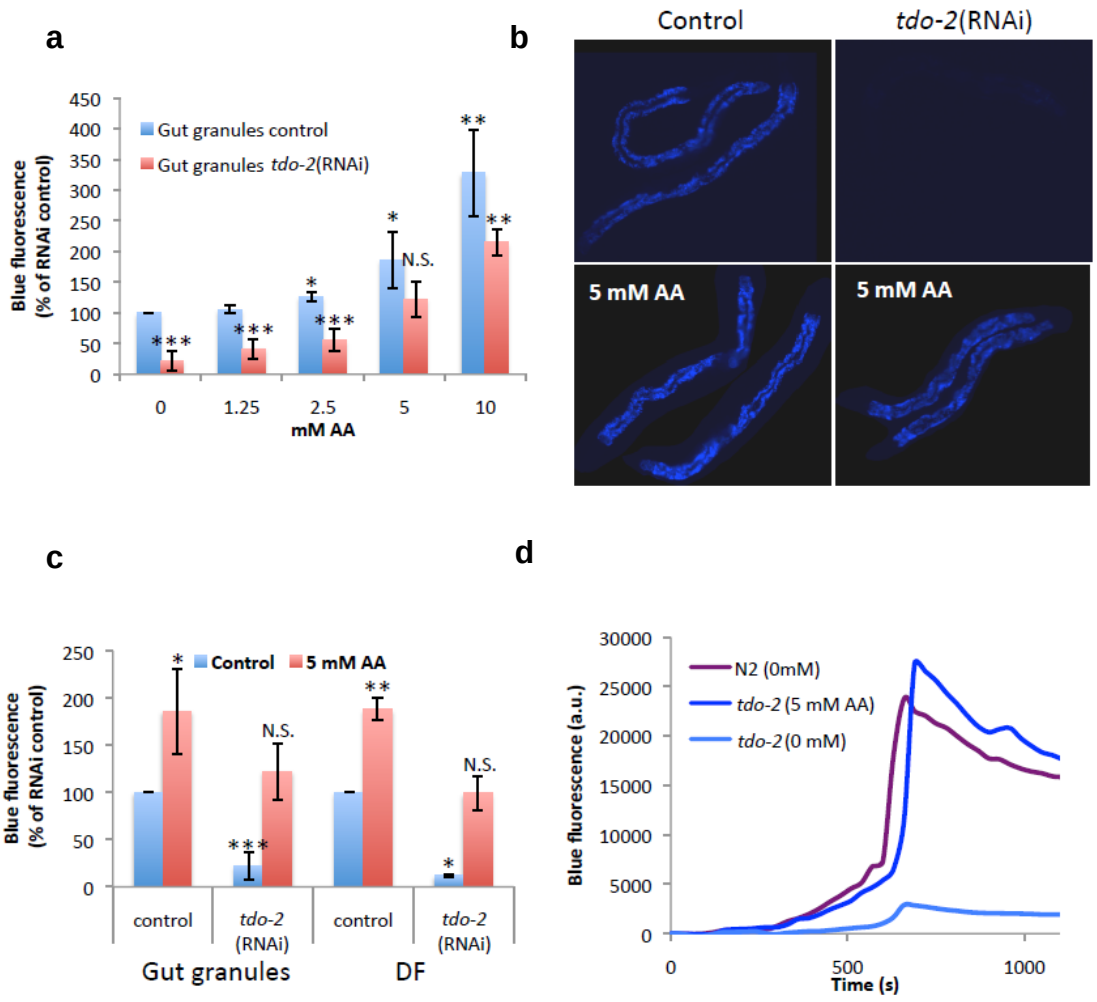

Figure C.6. Anthranilic acid supplementation rescues gut granule fluorescence and DF. (**A**) Effect on gut granule fluorescence of incubation in a range of AA concentrations. 5 mM AA gives fluorescence levels similar to wild type, (**B**) Epifluorescence microscopy reveals restoration of gut granule fluorescence by incubation in 5 mM AA (**C**) Effects of *tdo-2*(RNAi) and AA supplementation on peak DF (**D**) Similar kinetics of DF in control worms and tdo-2(RNAi) worms with AA-replenished gut granules, even though only the former can synthesize AA. image courtesy : Cassandra Coburn.

Figure C.7. NMR-based comparative metabolomics (DANS) applied to C. elegans wild type (N2) and flu-3. Comparison of the aromatic regions of dqfCOSY 2D NMR spectra of wild type (N2, upper panel) and flu-3 (lower panel) sonicates reveals that a specific kind of anthranilic acid moiety (black boxes) are absent in flu-3 mutants. Other anthranilic acid derivative cross peaks (red boxes) are unchanged or in some cases down regulated. Several other cross peaks remain unchanged (blue boxes).

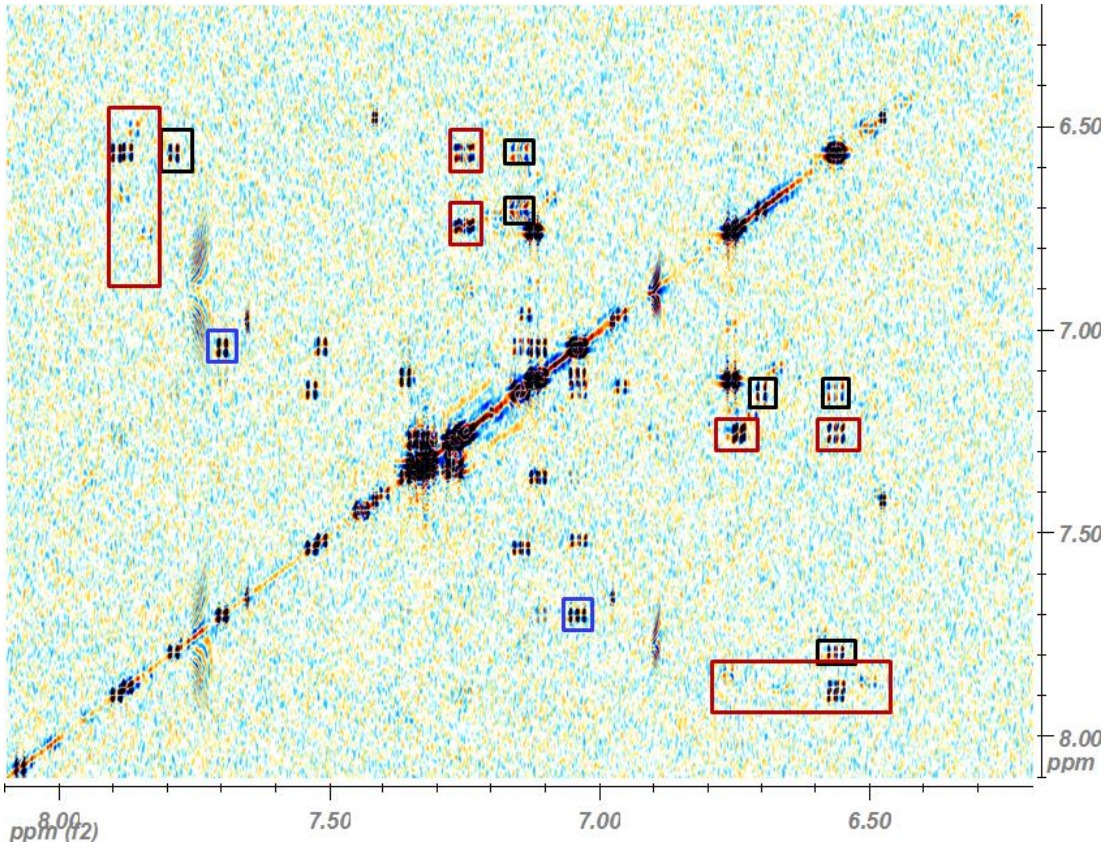
6.50
7.00
7.50
8.00
ppm
8.00
7.50
7.00
6.50
ppm (f2)

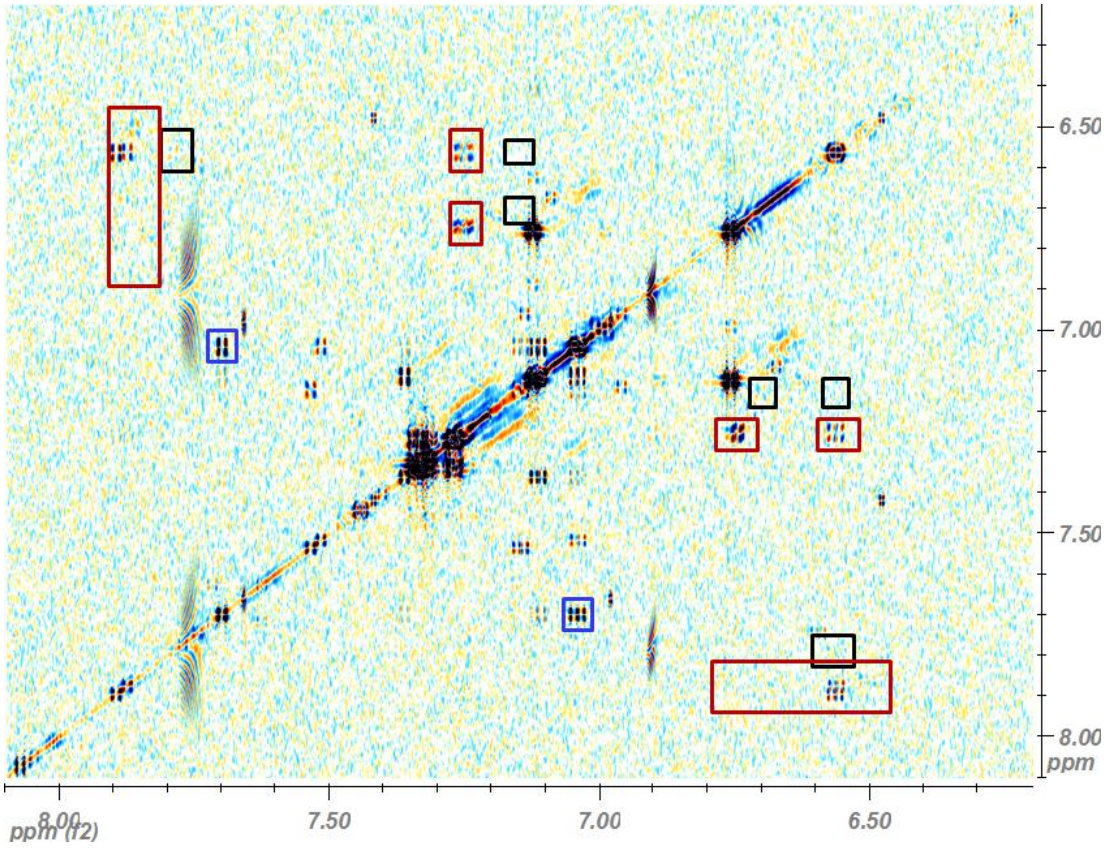
6.50
7.00
7.50
8.00
ppm
8.00
7.50
7.00
6.50
ppm (f2)

Figure C.8. NMR-based comparative metabolomics (DANS) applied to C. elegans wild type (N2) and flu-4. Comparison of the aromatic regions of dqfCOSY 2D NMR spectra of wild type (N2, upper panel) and flu-4 (lower panel) sonicates reveals several groups of signals that are either strongly downregulated in the flu-4 spectrum (black boxes), or upregulated in the flu-4(red boxes) or remain unchanged (blue boxes).

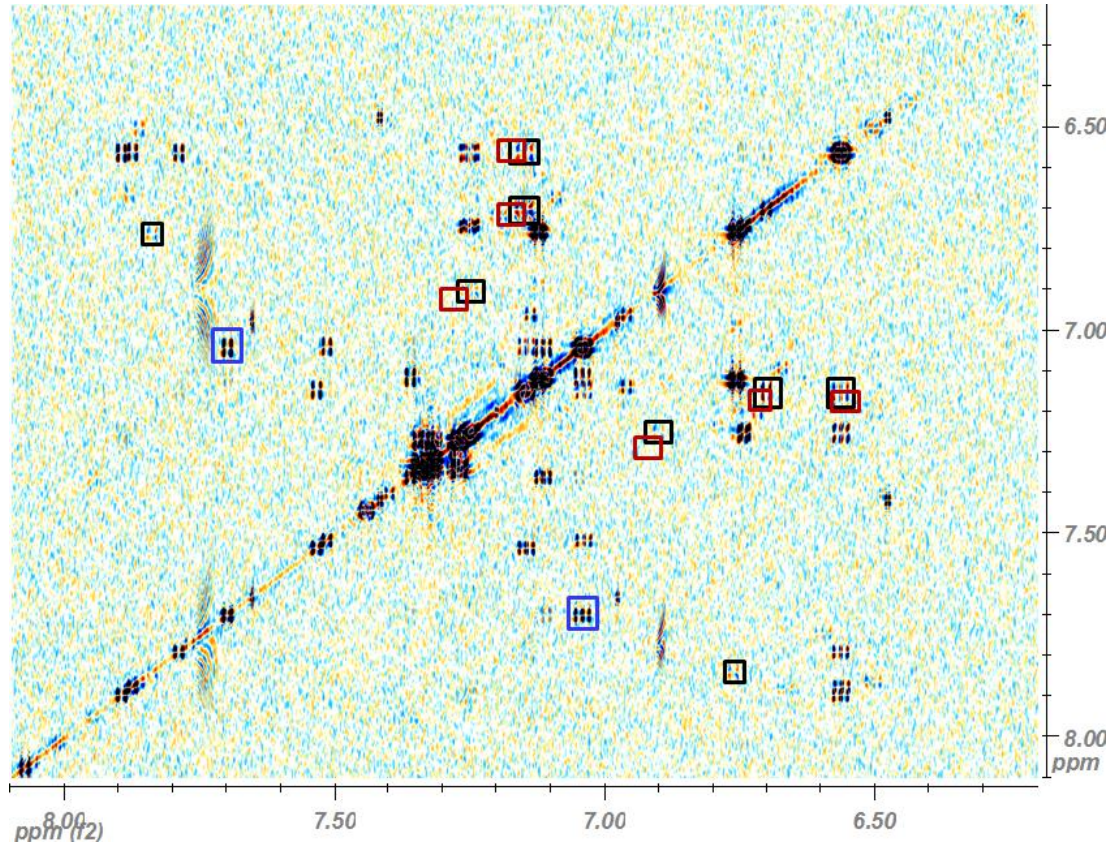
6.50
7.00
7.50
8.00
ppm
8.00
ppm (f2)
7.50
7.00
6.50

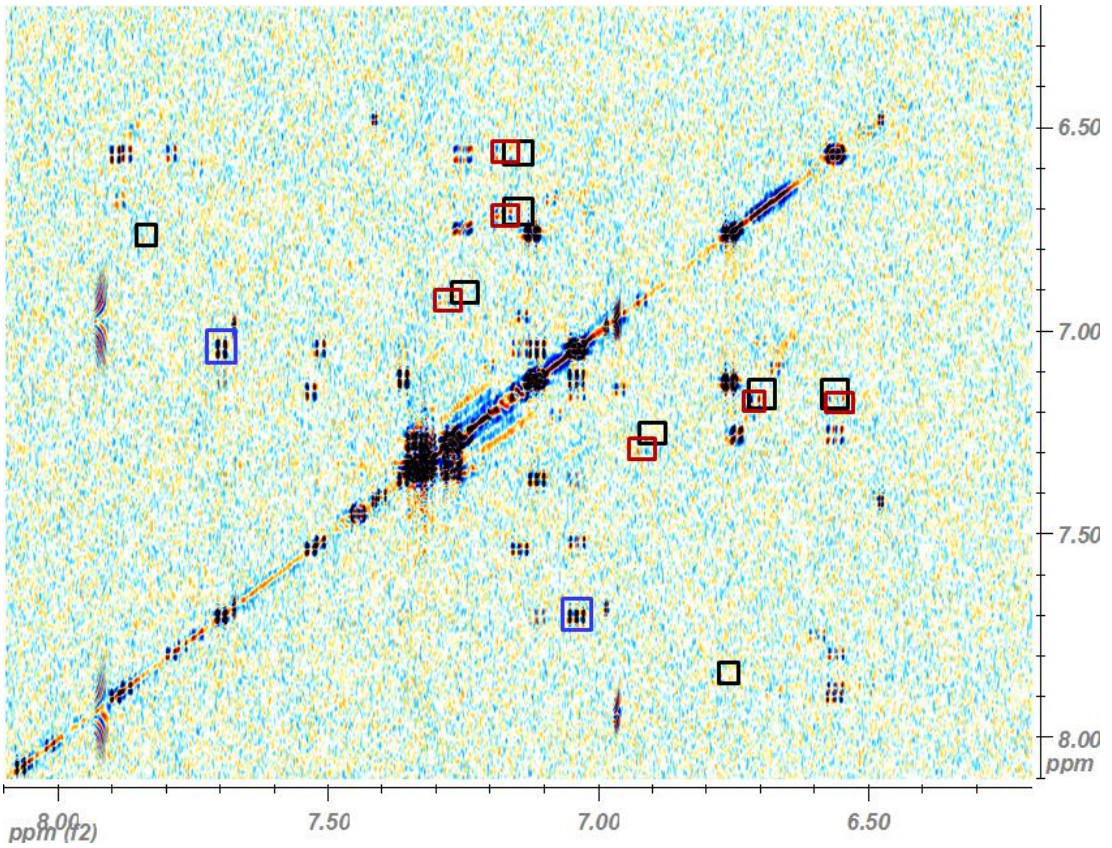
6.50
7.00
7.50
8.00
ppm
8.00
ppm (f2)
7.50
7.00
6.50

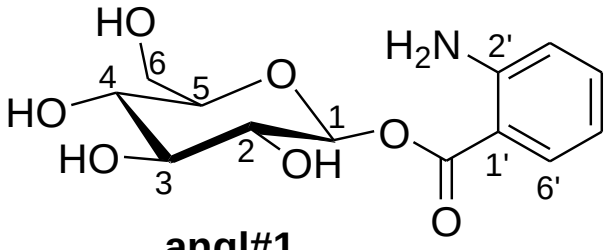

angl#1

Table C.1. ^{1}H (600 MHz), ^{13}C (151 MHz), and HMBC NMR spectroscopic data for angl #1 in methanol-d_4. Chemical shifts were referenced to ($CD_2\underline{H}OD$) = 3.31 ppm and ($\underline{C}D_2HOD$) = 49.05 ppm.

Position	angl#1 δ ^{13}C [ppm]	angl#1 δ ^{1}H [ppm]	angl#2[1] δ ^{1}H [ppm]	angl#1 coupling constants [Hz]	angl#1 HMBC correlations
1	95.2	5.70	5.77	$J_{1,2''}$ = 7.8	C-2, C-3, C-4, C-5, C-1'-COO
2	73.8	3.50	3.67		C-1, C-3
3	77.8	3.47	4.11 ($J_{H,P}$ = 8Hz)		C-2, C-4
4	70.8	3.40	3.59		C-5
5	78.5	3.44			C-1, C-4
6a	62.1	3.86		$J_{6a,6b}$ = 12.1, $J_{5,6a}$ = 5.2	C-4, C-5
6b		3.70		$J_{5,6b}$ = 2.1	C-4, C-5
1'-COO	167.8				
1′	109.8				
2′	153.1				
3′	117.5	6.75		$J_{3,4}$ = 8.5, $J_{3,5}$ = 1.1	C-1', C-5', C-1'-COO
4′	135.5	7.26		$J_{4,5}$ = 7.1, $J_{4,6}$ = 1.7	C-2', C-6'
5′	116.1	6.57		$J_{5,6}$ = 8.2	C-1', C-3'
6′	132.1	7.89			C-2', C-4', C-1'-COO

[1]Characteristic ^{1}H NMR signals of angl#2.

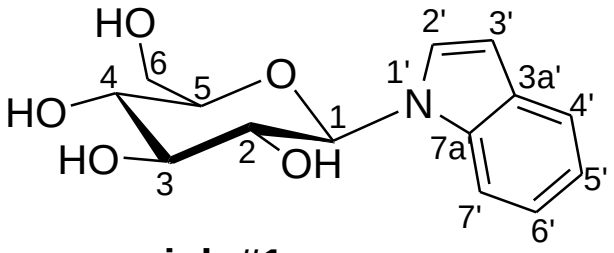

iglu#1

Table C.2. ^{1}H (600 MHz), ^{13}C (151 MHz), and HMBC NMR spectroscopic data for iglu #1 in methanol-d_4. Chemical shifts were referenced to ($CD_2\underline{H}OD$) = 3.31 ppm and ($\underline{C}D_2HOD$) = 49.05 ppm.

Position	iglu#1 δ ^{13}C [ppm]	iglu#1 δ^{1}H [ppm]	iglu#2[1] δ ^{1}H [ppm]	iglu#1 ^{1}H-^{1}H-coupling constants [Hz]	iglu#1 HMBC correlations
1	86.5	5.46	5.55	$J_{1,2}$ = 9.0	C-2, C-3, C-5, C-2', C-7a'
2	73.4	3.94	4.12	$J_{2,3}$ = 9.0,	C-1, C-3
3	78.9	3.60	4.24($J_{H,P}$ = 8Hz)	$J_{3,4}$ = 9.0	C-2, C-4
4	71.2	3.50	3.68	$J_{4,5}$ = 9.0	C-3, C-5, C-6
5	80.4	3.58		$J_{5,6a}$ = 5.8	C-1, C-3, C-6
6a	62.5	3.70		$J_{6a,6b}$ = 12.1	C-4, C-5
6b		3.88		$J_{5,6b}$ = 2.2	C-4, C-5
2′	126.2	7.40		$J_{2',3'}$ = 3.3	C-1(weak), C-3', C-3a', C-7'(weak), C-7a'
3′	103.2	6.49			C-2', C-3a', C-4' (weak), C-7a' (weak)
3a′	130.3				
4′	121.3	7.52		$J_{4',5'}$ = 8.0,	C-3', C-6', C-7a'
5′	120.7	7.05		$J_{5',6'}$ = 7.4, $J_{3,5}$ = 1.1,	C-3a', C-7'
6′	122.4	7.15		$J_{6',7'}$ = 8.0, $J_{4',6'}$ = 1.0	C-4', C-7a'
7′	111.2	7.54			C-3a', C-5'
7a′	137.8				

[1]Characteristic ^{1}H NMR signals of iglu#2.

Table C.3. High-resolution MS data for previously unreported *C. elegans* metabolites angl#1, angl#2, iglu#1, and iglu#2, acquired using negative-ion electrospray ionization (ESI^-).

Compound	**Ion**	**Ion formula**	**Calculated m/z**	**Observed m/z**
angl#1	$[M-H]^-$	$C_{13}H_{16}NO_7^-$	298.0932	298.0910
angl#2	$[M-H]^-$	$C_{13}H_{17}NO_{10}P^-$	378.0596	378.0600
iglu#1	$[M-H]^-$	$C_{14}H_{16}NO_5^-$	278.1034	278.1071
iglu#2	$[M-H]^-$	$C_{14}H_{17}NO_8P^-$	358.0697	358.0701

NMR Spectra of angl#1

^{1}H NMR Spectrum (600 MHz, CD_3OD) of ang#1

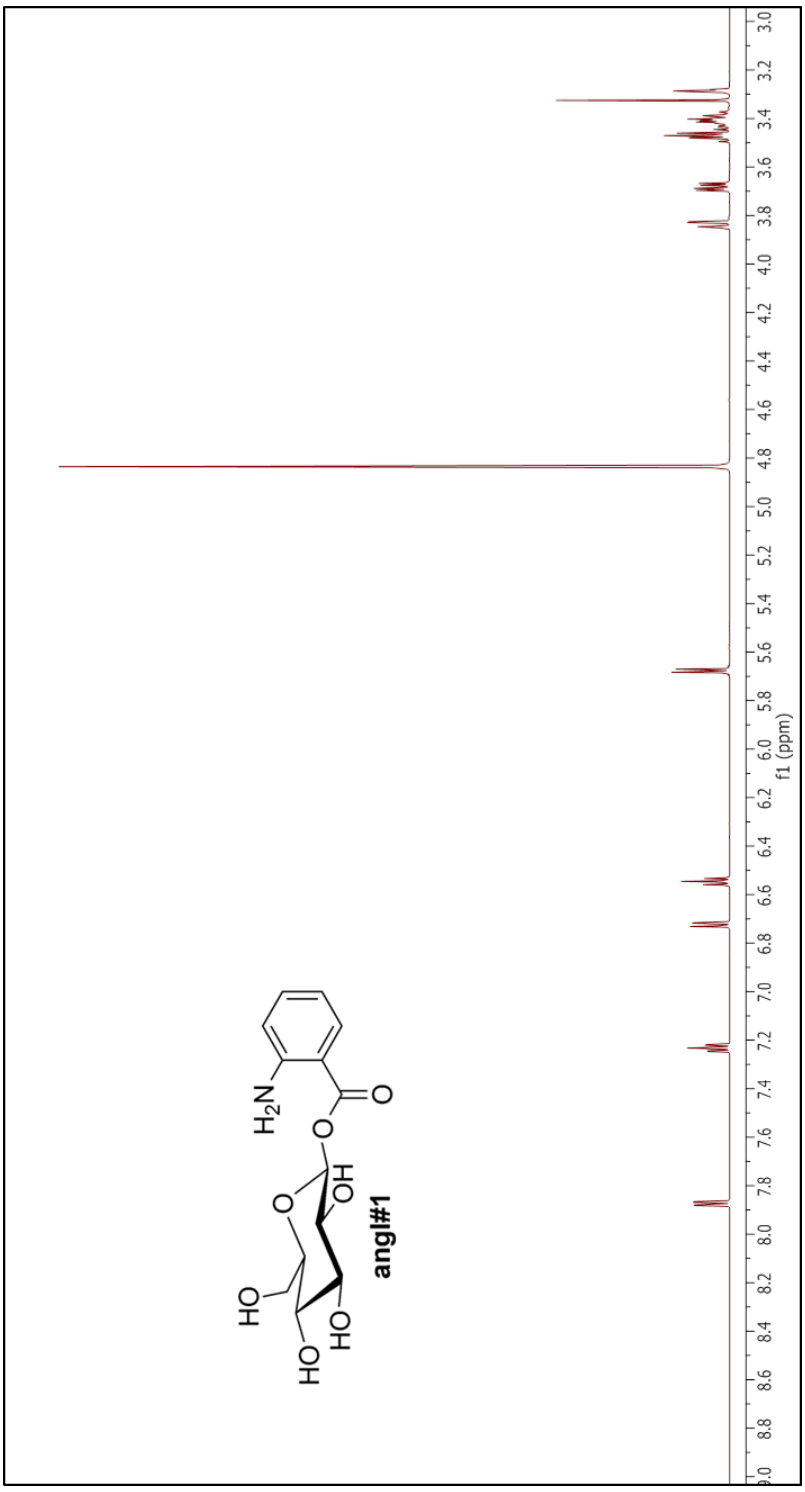

dqfCOSY Spectrum (600 MHz, CD_3OD) of ang#1

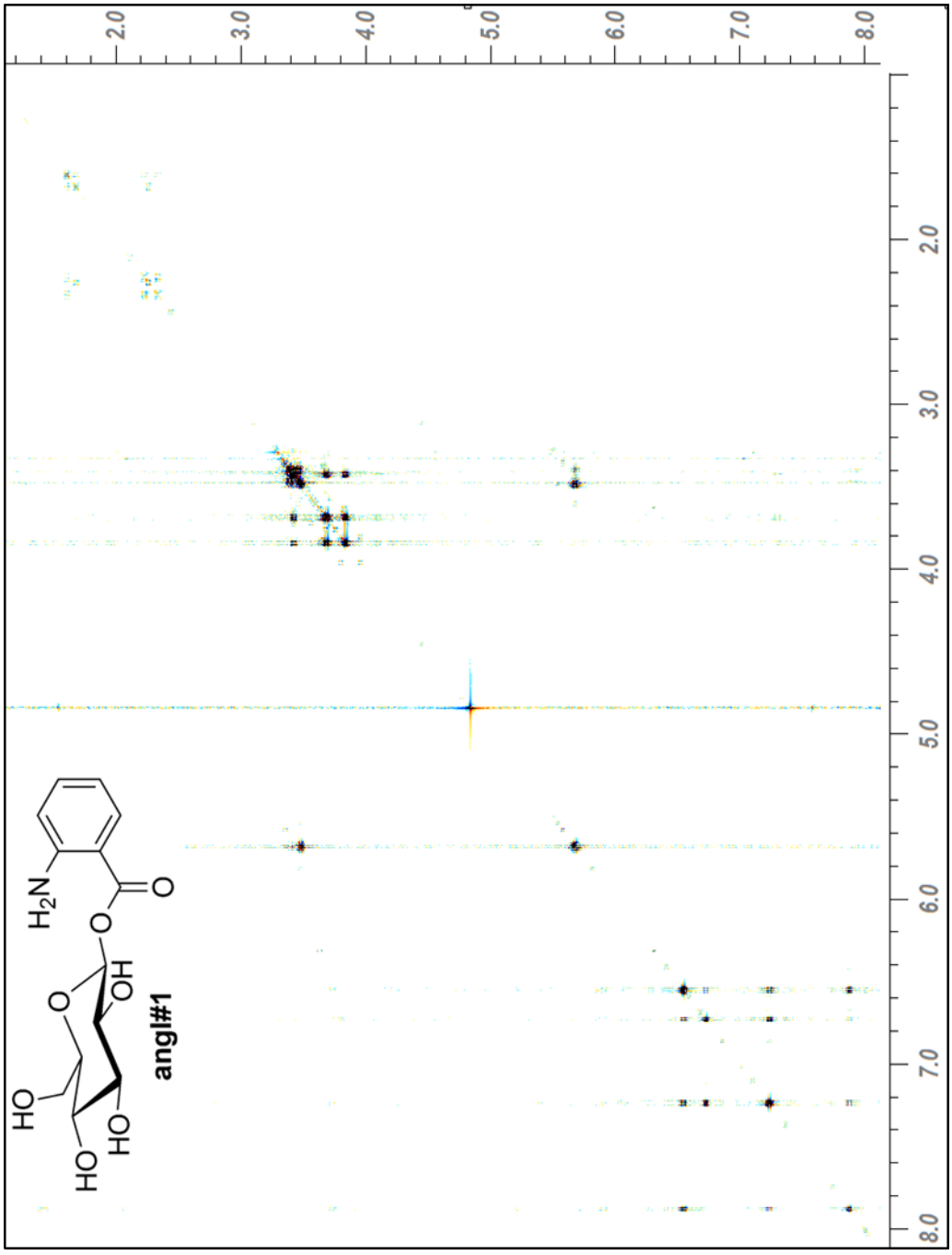

HMBC Spectrum (600 MHz for ^{1}H, 151 MHz for ^{13}C, CD_3OD) of ang#1

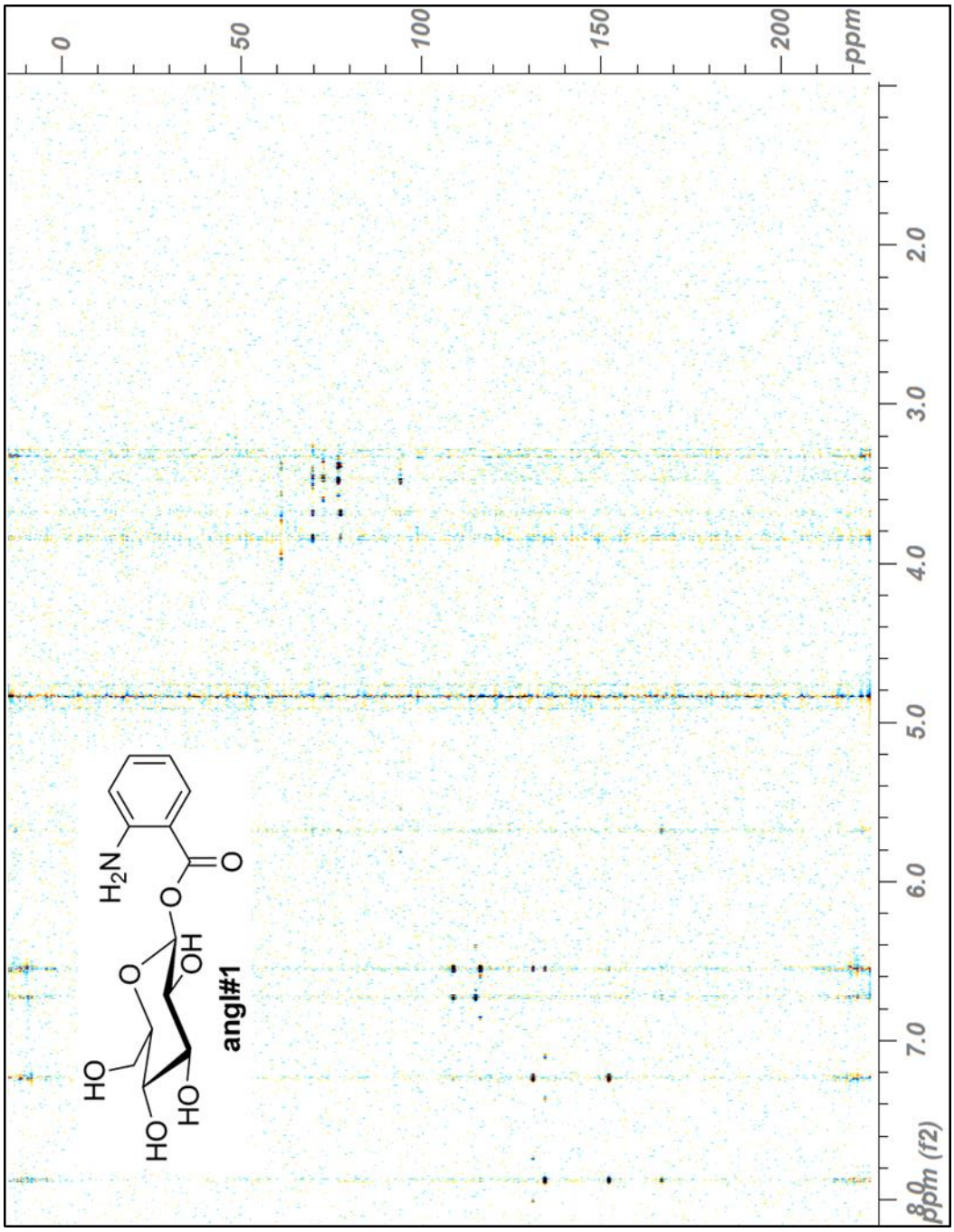

HMQC Spectrum (600 MHz for ^{1}H, 151 MHz for ^{13}C, CD_3OD) of ang#1

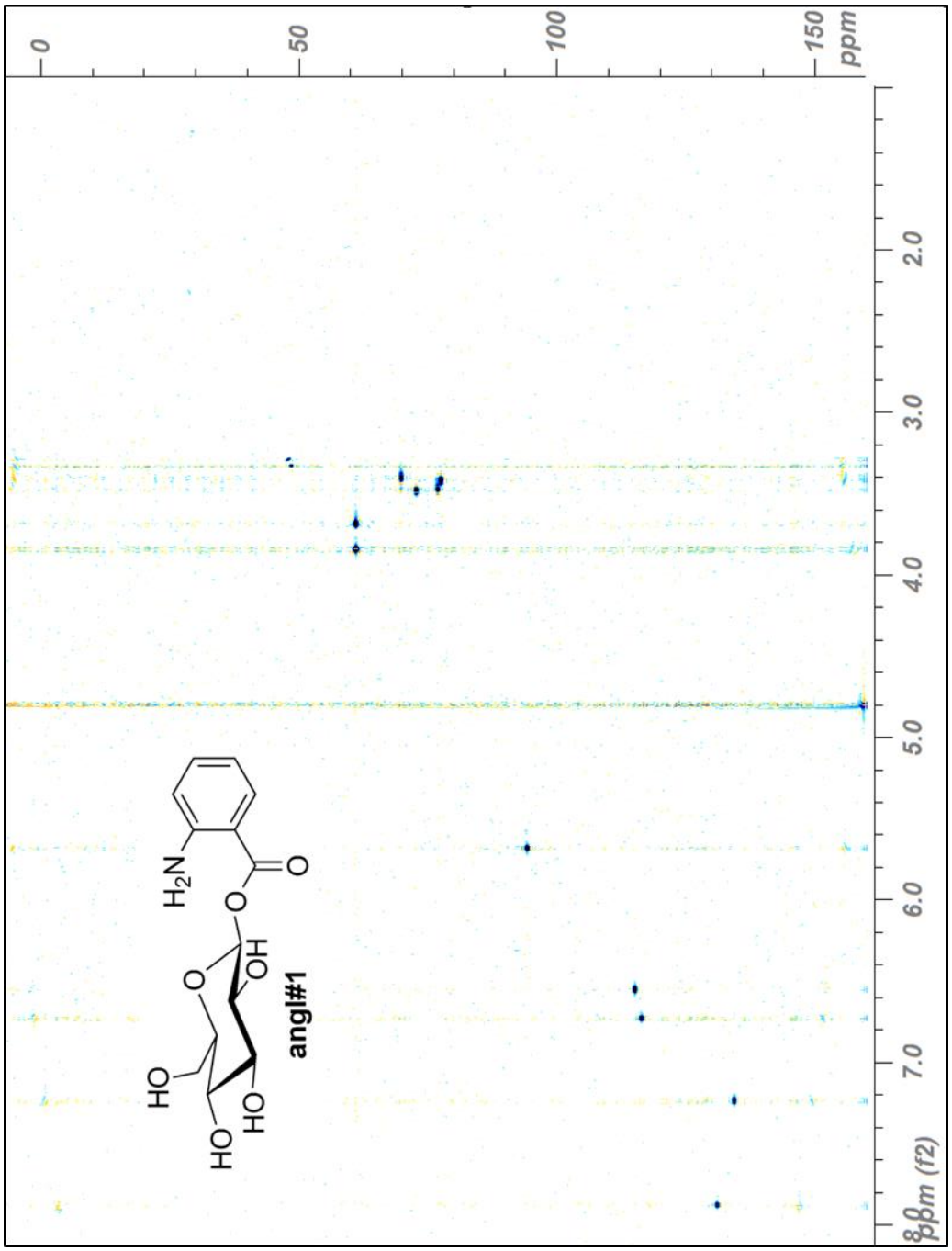

REFERENCES

Gandhi, S., Santelli, J., Mitchell, D.H., Stiles, J.W., Sanadi, D.R. (1980). A simple method for maintaining large, aging populations of Caenorhabditis elegans. Mech Ageing Dev 12, 137–150.

Herndon, L.A., Schmeissner, P.J., Dudaronek, J.M., Brown, P.A., Listner, K.M., et al. (2002). Stochastic and genetic factors influence tissue-specific decline in ageing C. elegans. Nature 419, 808–814.

Messaoudi, S., Sancelme, M., Polard-Housset, V.r., Aboab, B., Moreau, P., and Prudhomme, M. (2004). Synthesis and biological evaluation of oxindoles and benzimidazolinones derivatives. European journal of medicinal chemistry *39*, 453-458.

Pincus, Z., Smith-Vikos, T., Slack, F.J. (2011). MicroRNA predictors of longevity in Caenorhabditis elegans. PLoS Genet 7: e1002306.

Roell, D, Rosler, T.W., Degen, S., Matusch, R., Baniahmad, A. (2011) Antiandrogenic activity of anthranilic acid ester derivatives as novel lead structures to inhibit prostate cancer cell proliferation. Chem Biol Drug Des 77, 450–459.

Valentini, S., Cabreiro, F., Ackerman, D., Alam, M.M., Kunze, M.B., et al. (2012). Manipulation of in vivo iron levels can alter resistance to oxidative stress without affecting ageing in the nematode C. elegans. Mech Ageing Dev 133, 282–290.